UNIVERSITY OF ALBERTA

SEMI-DISTRIBUTED HYDROLOGIC MODELING USING REMOTELY SENSED DATA AND GIS

by

GETU FANA BIFTU ©

A thesis submitted to the Faculty of Graduate Studies and Research
in partial fulfillment of the requirements for the degree of
Doctor of Philosophy

in

WATER RESOURCES ENGINEERING

DEPARTMENT OF CIVIL AND ENVIRONMENTAL ENGINEERING

Edmonton, Alberta
Fall, 1998

National Library
of Canada

Acquisitions and
Bibliographic Services

395 Wellington Street
Ottawa ON K1A 0N4
Canada

Bibliothèque nationale
du Canada

Acquisitions et
services bibliographiques

395, rue Wellington
Ottawa ON K1A 0N4
Canada

Your file Votre référence

Our file Notre référence

The author has granted a non-exclusive licence allowing the National Library of Canada to reproduce, loan, distribute or sell copies of this thesis in microform, paper or electronic formats.

The author retains ownership of the copyright in this thesis. Neither the thesis nor substantial extracts from it may be printed or otherwise reproduced without the author's permission.

L'auteur a accordé une licence non exclusive permettant à la Bibliothèque nationale du Canada de reproduire, prêter, distribuer ou vendre des copies de cette thèse sous la forme de microfiche/film, de reproduction sur papier ou sur format électronique.

L'auteur conserve la propriété du droit d'auteur qui protège cette thèse. Ni la thèse ni des extraits substantiels de celle-ci ne doivent être imprimés ou autrement reproduits sans son autorisation.

0-612-34736-2

Canada

UNIVERSITY OF ALBERTA

Library Release Form

Name of Author:	Getu Fana Biftu
Title of Thesis:	Semi-distributed Hydrologic Modeling using Remotely Sensed data and GIS
Degree:	Doctor of Philosophy
Year this Degree Granted:	1998

Permission is hereby granted to the University of Alberta Library to reproduce single copies of this thesis and to lend or sell such copies for private, scholarly, or scientific research purposes only.

The author reserves all other publication and other rights in association with the copyright in the thesis, and except as hereinbefore provided, neither the thesis nor any substantial portion thereof may be printed or otherwise reproduced in any material form whatever without the author's prior written permission.

Getu Fana Biftu
Addis Ababa University
Faculty of Technology
P.O. Box 385
Addis Ababa, Ethiopia.

Dated: 18/09/98

UNIVERSITY OF ALBERTA

Faculty of Graduate Studies and Research

The undersigned certify that they have read, and recommend to the Faculty of Graduate Studies and Research for acceptance, a thesis entitled *SEMI-DISTRIBUTED HYDROLOGIC MODELING USING REMOTELY SENSED DATA AND GIS* submitted by GETU FANA BIFTU in partial fulfillment of the requirements for the degree of DOCTOR OF PHILOSOPHY in WATER RESOURCES ENGINEERING.

Gan Thian Yew

Dr. Thian Yew Gan (Supervisor)

Dr. Upmanu Lall (External Examiner)

F E Hicks

Dr. Faye E. Hicks

Dr. Peter M. Steffler

Kevin Biggar

Dr. Kevin W. Biggar

Martin Sharp

Dr. Martin J. Sharp

Date: 9/16/1998

Abstract

A semi-distributed, physically based hydrologic model (called DPHM-RS) is designed to take advantage of distributed hydrologic information retrieved from various space platforms and topographic information processed from Digital Terrain Elevation Data (DTED). DPHM-RS was applied to the Paddle River Basin of central Alberta which was characterized by 5 sub-basins with each sub-basin having its own land cover types and terrain features. Input data to the model included meteorological data collected from 2 meteorological towers set up at the study site, field soil moisture data, topographic information derived from DTED, and distributed hydrologic information retrieved from NOAA-AVHRR, Landsat-TM, and Radarsat SAR data.

DPHM-RS was calibrated with the data of summer, 1996 and validated with data of summer, 1997 and 1998. Excellent agreements between simulated and observed runoff at the basin outlet, energy fluxes and surface temperature demonstrated that DPHM-RS is capable of modeling basin-scale hydrologic processes. This is further confirmed by logical differences in the actual evapotranspiration (ET) simulated for different land covers and by sensible temporal variations of soil moisture simulated for each sub-basin.

Given that in many aspects the performance of DPHM-RS is creditable, the ET component is used, the two-source model, to assess two popular ET models, the Penman-Menteith equation and the modified Penman equation of Granger and Gray (1989) for non-saturated surface. Based on the ET simulated for several land use classes, it seems that the closed canopy assumption of Penman-Menteith is applicable to coniferous forest

and agricultural lands but not to mixed forest and pasturelands of the Canadian Prairies. The modified Penman model is generally applicable under dry environment but could estimate ET that is biased under cloudy, rainy days and wet environment.

From 6 scenes of Radarsat SAR images acquired for the Paddle River Basin, and 1350 soil moisture samples collected in the same days from 9 selected sites of the Basin, we demonstrated the feasibility of retrieving near-surface soil moisture from Radarsat SAR images using a linear regression and the theoretical integration equation model (IEM) of Fung et al. (1992). From these data, we also found that for a single land use, the relationship between the cross-correlation of soil moisture and inter-site distance breaks down at a distance of about 250 m.

Acknowledgements

First, I thank God, for my strength and my refuge, who has been and ever present help.

I would like to express my unreserved gratitude to my supervisor Dr. Thian Yaw Gan for his guidance, input and constant source of inspiration that led to many fruitful discussions and experience. I am grateful for the time he has sacrificed to correct my manuscripts and thesis. It has been a very prolific experience working with him. For all he has done, I am truly thankful.

My gratitude goes out to Professor N. Rajaratnam, Professor F. Hicks, and Professor P. Steffler for their constant encouragement throughout the course of my study.

I should express my sincere appreciation to Mr. S. Lovell for his assistance in equipment assembling required for fieldwork and Mr. P. Fedun for his help with computing facilities of Water Resources Section. Fellow graduate students in the Water Resources program have been friendly and supportive. I also thank my friends Abebaw Belay, Eshetu Tesfaye, and other fellow students at the University of Alberta for their different levels of help and encouragement.

Financial support from the University of Alberta, Canadian center for Remote Sensing through EODS program, and Alberta Environment and Protection is gratefully acknowledged. I also thank Terry Pultz of CCRS for re-processing the radiometric correction of some of the Radarsat SAR images.

Last, but not least I would like to thank my parents, brothers and sisters for the support and encouragement they provided me across many thousand miles that separates us. To my wife Fasika, thank you for your moral support, patient and understanding throughout my program. Thanks are due to my daughter Iyarusalem, and my son Joel for providing me with many joyful moments, love and their sacrifice.

Table of Contents

Chapter 1 Introduction, Literature Review, Research Objectives, and Site Description 1

1.1 Introduction.. 1
1.2 Literature Review of Hydrologic models 3
    1.2.1 Hydrologic Modeling using System Theory..4
    1.2.2 Conceptual Hydrologic Models..4
    1.2.3 Distributed Hydrologic Models..5
    1.2.4 Precipitation..7
    1.2.5 Snow Cover Mapping and Snow Water Equivalent..8
    1.2.6 Soil Moisture..9
    1.2.7 Surface Temperature..9
    1.2.8 Vegetation Index and Land Cover Types..10
    1.2.9 Surface Albedo..10
1.3 Research Objectives..11
1.4 Organization of Thesis..12
1.5 Study Site Description..13
1.6 Miscellaneous..14
References..15

Chapter 2 Semi-distributed, physically based, hydrologic modeling using Remotely sensed data and GIS, I. Model development 23

2.1 Introduction 23
2.2 Model components of DPHM-RS..26
    2.2.1 Interception..26
    2.2.2 Evapotranspiration..28
        2.2.2.1 Net Radiation..28
            2.2.2.1.1 Short Wave Radiation..29
            2.2.2.1.2 Long Wave Radiation..29

2.2.2.2 Sensible and Latent Heat Fluxes....................................30
2.2.2.2.1 Energy Balance Above Canopy....................................31
2.2.2.2.2 Energy Balance Within Canopy Height....................................33
2.2.2.2.3 Energy Balance at Soil Surface....................................35
2.2.2.3 Evaporation for Each Sub-basin....................................37
2.2.3 Soil Moisture Component....................................37
2.2.3.1 Capillary fringe lies Within the Transmission Zone....................................37
2.2.3.2 Capillary Fringe lies Within the Active Layer....................................38
2.2.4 Saturated subsurface flow....................................39
2.2.5 Surface runoff....................................41
2.2.6 Channel routing....................................42
2.2.7 Snowmelt models....................................44
2.2.7.1 The surface energy balance model....................................45
2.2.7.2 Modified degree-day method....................................46
2.3 Division of a river basin into sub-basins....................................47
2.4 Calibration of model parameters....................................48
2.5 Summary....................................49
References....................................50
List of symbols....................................58

Chapter 3 Semi-distributed, physically based, hydrologic modeling using Remotely sensed data and GIS, II. Application to the Paddle River Basin, Alberta 73
3.1 Introduction....................................73
3.2 Data description....................................75
3.2.1 Meteorological data 75
3.2.2 Soil data....................................76
3.2.3 Topographic data....................................76
3.2.4 Vegetation index....................................77
3.2.5 Land cover classes....................................78

3.2.6 Surface Albedo...78
3.2.7 Surface temperature...81
3.2.8 Streamflow...82
3.2.9 Throughfall coefficient...83
3.3 Parameter estimation...83
3.4 Discussion of the results...85
3.4.1. Model calibration and validation...85
3.4.1.1 Runoff at basin outlet...86
3.4.1.2 Net radiation...87
3.4.1.3 Surface temperature...89
3.4.1.4 Soil moisture...89
3.4.2. Effect of land cover on water and energy fluxes...90
3.5 Application of TOPMODEL to Paddle River Basin...91
3.5 Summary and conclusions...94
References...97

Chapter 4 Evapotranspiration from a watershed with mixed land-use classes 154

4.1 Introduction...154
4.2 Research objectives...156
4.3 The Penman-Monteith Equation...156
4.4 The two-source model...157
4.5 Modified Penman method...157
4.6 Description of data...160
4.7 Discussion of Results...160
4.7.1 Penman-Monteith (PM) model versus two-source model...160
4.7.2 Modified Penman model versus two-source model...161
4.7.2.1 A further look at relative evaporation...163
4.8 Summary and conclusions... 165
References...167

Chapter 5 Retrieving near-surface soil moisture from Radarsat SAR data 177

5.1 Introduction........177

5.2 Research objectives........178

5.3 Research methodology........179

  5.4.3 Soil moisture data collection........180

  5.3.2 Satellite data processing and analysis........180

5.4 Discussion of Results........183

  5.4.1 Regression analysis........183

  5.4.2 The Integral Equation Model........185

  5.4.3 Spatial variability of soil moisture........188

5.6 Summary and conclusions........190

References........192

Chapter 6 Summary, conclusions and recommendations for future works ...209

References........212

Appendix 213

  A1 Infiltration capacity........213

  A2 Exfiltration capacity........215

  A3 Solution of evaporation equation........216

References........218

List of Tables

Table 2.1 Summary and comparison of the general characteristics of some distributed and semi-distributed hydrological models....64

Table 2.2 Parameters of the DPHM-RS model....65

Table 3.1 Data requirements for applying DPHM-RS to the Paddle River Basin....103

Table 3.2 Analysis of an Hubalta Soil Profile, the major soil group of the Paddle River Basin....104

Table 3.3 NOAA-AVHRR radiance conversion parameters....105

Table 3.4 Normalized difference vegetation Index (NDVI) from NOAA-AVHRR data acquired in 1996 and 1997 for different land covers (averaged over the Paddle River Basin)....106

Table 3.5 Relationships between NDVI and Leaf Area Index (LAI) for different land use classes....107

Table 3.6 Percentage of different land cover classes for each sub-basin of the Paddle River Basin....108

Table 3.7 LANDSAT TM-5 radiance parameters....109

Table 3.8 Surface Albedo for different land cover classes in each sub-basin for each land cover of the whole Paddle River Basin for July 31, August 7, 1996, July 25 and August 26, 1997....110

Table 3.9 Average surface temperature derived from NOAA-AVHRR data of 1996 and 1997 for different land covers of the Paddle River Basin....111

Table 3.10 Surface temperature for different land cover classes in each sub-basin for August 7, 1996 and averaged for each land cover of the whole Paddle River Basin for August 7, July 31, 1996 and July25, August 26, 1997....112

Table 3.11 Throughfall coefficients, δ, for various land cover types....113

Table 3.12 Model parameters derived from field observations, past studies and model clibration....114

Table 3.13 Cross-correlation coefficient of daily rainfall data recorded at seven climatic stations located within and around the Paddle River Basin....115

Table 3.14 Comparison of skin temperature, T_s, simulated by DPHM-RS against skin temperature derived from NOAA-AVHRR and Landsat-TM data....116

Table 3.15 Parameter sets used in TOPMODEL....117

Table 4.1 Regression statistics for Penman-Monteith model and modified Penman model as compared to two-source model for different land cover types....170

Table 5.1 Description of the six Radarsat SAR images acquired at descending orbit over the Paddle River Basin....197

Table 5.2 Summary of the calibration and validation results of the regression model and IEM given on Figure 5.7....198

List of Figures

Figure 2.1 Flow chart of DPHM-RS model for each sub-basin.........................66

Figure 2.2 Water balance scheme of a canopy...67

Figure 2.3 Energy balance of the boundary layer that is at a reference height above ground...68

Figure 2.4 A land surface and its air column...69

Figure 2.5 A schematic diagram of the energy fluxes of the two source model for the vegetation canopy, the soil surface, and the air column above canopy 70

Figure 2.6 Conceptual representation of soil infiltration between the active layer, transmission zone and ground water zone for each sub-basin...71

Figure 2.7 The average response function per unit rainfall excess for sub-basin based on the kinematic wave theory and eight flow directions...72

Figure 3.1 Location map, meteorological stations, stream gauging station, and the response function for each of the 5 sub-basins of the Paddle River Basin...118

Figure 3.2 Typical plots of meteorological data measured at the Paddle River Basin for four days...119

Figure 3.3 Average soil group for the Paddle River Basin 121

Figure 3.4 Mean elevations of Paddle River Basin derived from Digital Terrain Elevation data...122

Figure 3.5 Flow direction for surface runoff from Paddle River Basin derived from Digital Terrain Elevation data..................................123

Figure 3.6 Topographic-soil index for Paddle River Basin derived from Digital Terrain Elevation data...124

Figure 3.7 Normalized Difference Vegetation Index (NDVI) derived from NOAA-AVHRR Image for Paddle River Basin (1996).....................125

Figure 3.8 Land use classification for Paddle River Basin retrieved from

Landsat TM image of August 7, 1996……127

Figure 3.9 Surface Albedo for Paddle River Basin retrieved from Landsat TM image of August 7, 1996……128

Figure 3.10 Surface temperature for Paddle River Basin retrieved from Landsat TM image of August 7, 1996……129

Figure 3.11 Stream flow for Paddle River Basin as recorded at the stream gauging station near Anselmo (No. 07BB011)……130

Figure 3.12 A simple regression between throughfall coefficient, δ, and leaf area index based on actual field measurements of several researchers……132

Figure 3.13 Comparison of rainfall data measured at two rain gauges installed 15 Km apart in the Paddle River Basin……133

Figure 3.14 Location of meteorological stations with respect to the Paddle River Basin……134

Figure 3.15 Comparison of runoff observed at the outlet of the Paddle River Basin with runoff simulated by DPHM-RS ((a)-(c)) and TOPMODEL ((d)-(f)) at both calibration and validation periods……135

Figure 3.16 Net radiation simulated by DHPM-RS based on surface albedo retrieved from Landast TM data, model simulated surface temperature, and measured solar radiation and air temperature for (a) caliberation period of summer, 1996, and (b) validation period of summer, 1997……136

Figure 3.17 Correction for the effect of cloud cover based on the measured shortwave radiation: (a) the effect of cloud cover on the measured shortwave radiation when compared to the net radiation; (b) a proposed envelop (R_s(max) to the daily measured shortwave radiation; (c) a regression approach to compute the fraction of cloud cover; (d) simulated net radiation after correction for cloud cover effect based on (c)……137

Figure 3.18 Comparison of model simulated surface temperature retrieved from remotely sensed data (either NOAA-AVHRR or Landsat TM) for various land cover types……139

Figure 3.19 Evapotranspiration, surface temperature, canopy temperature, soil moisture, and sensible and latent energy fluxes simulated by DPHM-RS during calibration period..140

Figure 3.20 Evapotranspiration, surface temperature, canopy temperature, soil moisture, and sensible and latent energy fluxes simulated by DPHM-RS during validation period..147

Figure 4.1 Comparison of actual evapotranspiration estimated by two-source and Penman-Motheith models..171

Figure 4.2 Comparison of actual evapotranspiration estimated by two-source and modified Penman models with relative evaporation computed using expression established by Granger and Gray (1989)................172

Figure 4.3 Plot of relative evaporation against relative drying power derived from two-source model output data versus Granger and Gray (1989)..173

Figure 4.4 Relationship between relative evaporation, G and relative drying power, D derived based on actual evaporation simulated by two-source model for hourly data of summer of 1996 and the corresponding curve derived by Granger and Gray (1989) using daily water balance..174

Figure 4.5 Comparison of actual evapotranspiration estimated by two-source and modified Penman models with relative evaporation computed using expression established by Biftu and Gan (1998) based on two-source model out put (calibration period)..............................175

Figure 4.6 Actual evaporation simulated by modified Penman model as compared to two-source model during validation period using hourly data of summer of 1997..176

Figure 5.1 Location map and field soil sampling sites of Paddle River Basin, Alberta..199

Figure 5.2 Photographs of three land cover types of Paddle River Basin from which soil moisture data was collected.........................200

Figure 5.3 The six raw Radarsat SAR images acquired for Paddle

River Basin, Alberta. 201

Figure 5.4. Field soil moisture data collected from different land cover types for September of 1996..202

Figure 5.5 Changes of the average gravimetric soil moisture content among the nine sampling sites for three days of August 1997............203

Figure 5.6 Plots showing the regression of observed soil moisture data (α and β are regression coefficients) with Radarsat SAR backscattering values for the six individual days and for the combined data of 1996 and 1997....................................204

Figure 5.7 Four sets of calibration and validation results for the regression model and IEM comparing the retrieved (based on Radarsat SAR data) versus observed soil moisture: (a) 1996 data used for calibration and 1997 data for validation; (b) 1997 data used for calibration and 1996 data for validation; (c) Both 1996 and 1997 data used for calibration, no validation; and (d) Average values of model parameters obtained in (a) and (b) used for retrieving soil moisture from backscatter values for 1996 and 1997...205

Figure 5.8 Sensitivity of the backscattering coefficient, σ^o to surface rms height σ for Radarsat satellite configuration (set correlation length L=10cm) using, (a) Gaussian correlation function and S1 beam (ϕ=23.3°), (b) Gaussian correlation function and S2 beam (ϕ=27.7°), (c) exponential correlation function and S1 beam (ϕ=23.3°), (d) exponential correlation function and S2 beam (ϕ=27.7°)...206

Figure 5.9 Sensitivity of the backscattering coefficient, σ^o to the correlation length L for Radarsat satellite configuration (set rms height σ=0.6cm) using, (a) Gaussian correlation function and S1 beam (ϕ=23.3°), (b) Gaussian correlation function and S2 beam (ϕ=27.7°), (c) exponential correlation function and S1 beam (ϕ=23.3°), (d) exponential correlation function and S2 beam (ϕ=27.7°)..........206

Figure 5.10 Spatial semi-variogram of (a) 1996 measured soil moisture of all 9 sites, and (b) Radarsat backscatters σ^o for one agricultural site of Paddle River Basin..........207

Chapter 1

Introduction, Literature Review, Research Objectives, and Site Description

1.1 Introduction

Water is one of the most fundamental substances to the existence of life and also the most prevalent in the earth-atmosphere system. It has a unique position in our planet as eloquently stated by Engman and Gurney (1991):

> 'Certainly the existence of abundant water in all three phases (solid, liquid, and gaseous) in the environment provides one of the most distinctive characteristics of the Earth compared with other planets of the solar system.'

Knowledge of the general laws governing the distribution and movement of water - the water cycle - is of practical importance for the rational use and protection of water resources. Fundamental questions such as, "Where does water come from?", "How much water is available?", "How come we never run out of water?", resulted in the evolution of a field of study called hydrology. Hydrology deals with the continual circulation, distribution, and interactions of water in the atmosphere, on the surface of the earth, and in the ground. On a global scale, the concept of the water cycle is straightforward. The solar energy causes liquid water to evaporate from oceans, rivers, and lakes as water vapor, which then rises with warm air currents till it reaches the cooler layer of the atmosphere where it condenses. The condensed water droplets often adhere to dust particles and grow to a stage where the falling velocity exceeds the updraft. Depending on the air temperature and other climatic factors, the droplets will fall as rain, snow, sleet or hail. Precipitation that reaches the earth's surface can either enter the ground via infiltration, contribute to surface streams and lakes as runoff, or return to the atmosphere as water vapor by evapotranspiration. The surface runoff can either percolate into the ground, or flow back to sea and oceans, and evaporates to complete the hydrologic cycle.

Moving from the global to smaller spatial scales, e.g., continental, regional, and local scales, the complexity and variabilities of hydrologic processes grow enormously. Even for the same climatic regime, the notorious variability of rainfall in time (season) and in space causes its occurrence to be very difficult to predict. On the land surface, the timing and amount of streamflow depend on the precipitation, wind, air temperature, terrain features, vegetation cover, soil types and other factors. In addition, land surface processes also exert a feedback on atmospheric processes. For example, the uneven heating of the earth's surface causes diurnal phenomena such as land and sea breezes which result in the redistribution of heat and moisture. The feedbacks between the atmosphere and the land surface vary over a wide range of spatial and temporal scales.

With the progress of human civilization, this feedback mechanism is modified by human actions. Man intrudes the natural water environment by building many huge hydraulic structures such as dams to store excess surface water as water supply for agricultural, residential, or industrial uses. Land use changes due to agriculture practices, afforestation, deforestation, building of mammoth reservoirs, drainage of wetlands could result in soil erosion, excessive evaporation, and the decrease of runoff and soil moisture in some regions. Lately, climatic warming caused by the effect of pumping greenhouse gases, especially CO_2, to the atmosphere is of major concern to both politicians and scientists. Because of feedback, climate change exerts an impact on the quantity and quality of regional water resources.

Numerous studies have been conducted on the impact of climate change on our water resources (e.g., Lattenmaier and Gan, 1990; Lattenmaier *et al.*, 1997). Often such studies are based on the simulations of hydrologic models under 2×CO2 climate scenarios projected by several general circulation models (GCM). The results are often subjected to errors since there is a mismatch of scale between GCMs of global scale and hydrologic models of local to regional scale. Furthermore, the reliability of climate scenarios projected by GCMs generally decreases with space and time scales, partly because of the coarse resolutions of GCMs and partly because climate variability increases as scale decreases.

Some land surface parameterization schemes have been developed to bridge the gap between large-scale atmospheric processes modeled by GCMs and land surface processes (e.g., Sellers *et al.*, 1986; Dickinson and Kennedy, 1991, Wood *et al.*, 1992). It is our intention to develop a hydrologic model that will eventually lead to a land surface scheme useful for climate related studies on our water resources.

1.2 Literature Review of Hydrologic Models

The necessity for estimating river flows from measurable causative factors, principally rainfall, has perhaps provided the most important driving force in developing hydrology as a discipline of science. As early as the late seventeenth century a little known French scientist, Pierre Perrauault (Dooge, 1959), quantitatively showed that rainfall and snowmelt were sufficient to maintain the flow in the river Seine. This contradicted the classic belief that water originating in the earth's interior provided a substantial component of streamflow. Two centuries later, Mulvaney (Dooge, 1973) attempted to relate the storm peak of river flow with rainfall records by what is now known as the 'rational method' that still finds application in the design of urban storm drainage networks in many parts of the world. Since then, a plethora of models have been developed for different purposes, mainly to simulate and forecast runoff from watersheds. The following provides a brief discussion of the classes of models developed through time.

1.2.1 Hydrologic Modeling using System Theory

Sherman (1932), who postulated the concept of unit hydrograph for a catchment, established the first instance to system theory. Later Clark (1945) refined Sherman's idea to the instantaneous unit hydrograph, which opened up the floodgates of systems approach from other disciplines to hydrological research. Regrettably, but understandably, the techniques and models carried over from other disciplines like communication and electrical engineering were quite inappropriate and often reflect the classic black box syndrome. As a result, prior to model inter-comparison studies instigated by WMO (1975), practical hydrologists were usually bewildered and often poorly served by the proliferation of techniques and models suggested for river flow forecasting. Regardless of these unfortunate difficulties, the development of systems concepts in hydrology was firmly established by the pioneering work of Snyder (1955), Nash (1957), Eagleson *et al.* (1965) and many others.

Following these inspirational leads, further work on system-theoretic, rainfall-runoff modeling continued unabated and resulted in many useful extensions and generalizations such as the nonlinear Volterra models introduced by Amorocho and Orlob (1961), the parallel assemblage of cascades of linear reservoir proposed by Diskin (1964), the discrete analogue reservoir models of O'Connor (1976), and the concept of the geomorphological unit hydrograph proposed by Rodriguez-Iturbe and Valdes (1979).

1.2.2 Conceptual Hydrologic Models

Conceptual rainfall-runoff (CRR) models were introduced in hydrology to improve the black box, system theoretical approach which depends mainly on some general, yet flexible relationships between input and output data without much physics within the system. Conceptual models are generally designed to account for the soil moisture phase of the hydrologic cycle at basin scale. The primary approach is to transform rainfall to streamflow through a number of interconnected mathematical functions, each representing a certain component of the hydrologic cycle (e.g., Crawford and Linsley, 1966; Burnash *et al.*, 1973). CRR models have generally been a very useful and successful approach in simulating runoff from catchments in different parts of the world for the last three decades (WMO, 1975, 1992). However, because the basin-scale hydrologic processes are lumped at a point, CRR ignores the spatial variability of meteorological variables. So CCR are limited in assessing the effect of land use and other changes in basin hydrology (e.g., Abbott, 1972; Gan and Biftu, 1996). Their applicability is limited to areas where runoff has been measured for some years and to places where no significant changes in catchment conditions have occurred over the period of simulation since model parameters that are calibrated, not measured, are assumed to remain constant.

1.2.3 Distributed Hydrologic Models

As a result of civilization and industrialization, men have upset the equilibrium of many aspects of our environment, including the water cycle. Recently environment protection, sustainable development and climate change are becoming issues of major concern to nations all across the world. Besides the emission of greenhouse gases to the atmosphere, politicians and scientists are also interested in the implications of land use changes, agricultural practices, afforestation or deforestation, building of mammoth reservoirs to our environment and to the world climate. NASA of USA has been monitoring our environment through its global earth observation program (EOS). Many scientists are also using various models to simulate the potential impact of various anthropogenic actions to our mother earth. Impact of land use changes are manifested through hydrological processes such as evaporation, runoff and soil moisture which all vary spatially.

Therefore in order to effectively study the impact of land-use changes, surface water and groundwater exploitation, climate changes, and subsurface migration of industrial and agricultural chemicals, on our river basins, there has been a trend towards developing fully distributed, physically based hydrologic models. For the last two decades, different causal models have been built with an attempt to fill in the gap of lumped models. A good example is the SHE model (European Hydrological System-Systeme Hydrologique Europeen) (Abbott *et al.*, 1986) which unfortunately has little real world applications since its data requirements often far exceed what is available.

As an improvement to lumped conceptual models, Amerman (1965) developed an extension of lumped, non-linear synthesis model based on 'unit source' areas in which the catchment is broken down into a system of sub-areas of relatively homogeneous soils, topography and land use. A similar approach, known as 'hydrological response zones', was adopted by England and Stephenson (1970) to account for spatial variability across the watershed. However these models do not allow for the interaction between sub-areas and the resulting runoff was estimated by summing up the contributions from the individual elements. Beven and Kirkby (1979) also developed a physically based model which takes into account the distributed effects of channel network topology and dynamic contributing areas. Based on the concept of unit sources proposed by Amerman (1965), semi-distributed hydrologic models have evolved recently as spatially distributed hydrologic data become more readily available through remote sensing (e.g., HYDROTEL of Fortin *et al.*, 1986; WATFLOOD of Kouwen, 1988; TOPMODEL of Beven *et al.*, 1987; and SLURP model of Kite, 1995).

Without spatially distributed hydrologic information retrievable from many space platforms launched in recent years, distributed or semi-distributed hydrologic models would have little or no practical application. Remotely sensed data, initially collected from truck mounted and airborne sensors and later from space platforms, have been used for wide ranges of applications in water resources problems. Kite and Pietroniro (1996) provide an excellent review of the current uses of remotely sensed data in various processes of a hydrologic model and indicate the likely future development in this aspect. Studies also indicated potential benefits of using satellite data on the mitigation of flood damage, improved planning of hydropower production, and irrigation (e.g., Castruccio *et al.*, 1980; Rango, 1980).

Even though there is potential to retrieve spatially distributed hydrologic information from satellite data, other than mapping of land cover and snow extent, the current use of remotely sensed data in hydrologic modeling is very limited. According to Kite and Pietroniro (1996), reasons for limited use of remotely sensed information in hydrologic models are (1) a lack of universally applicable operational methods for deriving hydrological variables from remotely sensed data, (2) lack of hydrological models that can utilize remotely sensed information at different resolutions from different platforms, and (3) lack of appropriate education and training.

It is our goal to develop a hydrologic model suitable for the routine use of remotely sensed data from different space platforms such as NOAA-AVHRR, Landsat TM, and Radarsat SAR. In the model, the amount of details to be considered for various hydrologic processes will depend on the data available and the limit of scientific knowledge in basin hydrology. The model will be designed to maximize the applicability of spatially distributed hydrologic information retrievable from the above space platforms. In addition, the model will accommodate topographic information to be derived from digital terrain elevation data (DTED) or from digital elevation model (DEM) using a raster or a vector geographic information system (GIS). Brief review of various hydrological variables that have been retrieved from space platforms and applied in hydrologic models for the past two decades are given below.

1.2.4 Precipitation

Precipitation is an important hydrological variable that is notoriously variable spatially. Satellites such as the Geosynchronous weather satellite system, GOES, have been used for operational monitoring of weather data, cloud cover, atmospheric temperature profiles, real-time storm movement, and severe storm warning. From the infrared and visible images of GOES, Scofield (1983) used the bi-spectral method to estimate hourly rainfall for convective systems. Pietroniro *et al.* (1989, 1991) used surface temperature derived from Meteosat satellite to estimate rainfall for a monthly water balance model. The NOAA of USA (NOAA, 1993) established a Nile forecasting system in Cairo, Egypt, based on an input of rainfall for every 30-min from the geostationary Meteosat satellite at a grid resolution of 5.5 km. Space-borne microwave techniques are also promising for measuring rainfall directly, as there is a strong interaction between raindrops and microwaves. Wilheit *et al.* (1977) demonstrated the use of a radiative transfer model to estimate the higher rainfall rates using the 19.35 GHz data of Nimbus-5, ESMR. Maneghini *et al.* (1983) and Goldhirsh (1988) proposed the use of space-borne radar for estimating rainfall rates. Future space programs such as the EOS of NASA would undoubtedly have a great potential for estimating precipitation from satellite data.

1.2.5 Snow Cover Mapping and Snow Water Equivalent

In middle and high latitudes such as in Canada, snowfall is an important component of precipitation particularly during winter time. To estimate the snowmelt runoff it is necessary to determine the snow water equivalent and snow cover extents of snowpacks. However, ground based measurements such as snow course data are never sufficient to accurately quantify the amount of snow, especially in mountainous catchments. In this aspect, remote sensing becomes a viable tool for us to obtain some of the variables.

Areal distributions of snow have been derived from different sensors in the visible band of NOAA-AVHRR (e.g., Carroll and Allen, 1988; Kite, 1989), Landsat TM and GOES satellites (e.g., Holroyd *et al.*, 1989). Recently, active microwave, Synthetic Aperture Radar, SAR data from airborne (Donald *et al.*, 1992) and spaceborne platform of ERS-1 (Hallikainen *et al.*, 1994; Haefner *et al.*, 1994; Rott and Nagler, 1994) have been used to map the areal snow extent for different mountainous catchments. There is also a possibility to map the spatial extent of snow cover from the Radarsat SAR satellite.

In addition to the areal extent of snow, it is important to know the snow water equivalent (SWE) of the snowpack to estimate the runoff from melting snow. Passive microwave data have been used to estimate SWE under different land cover conditions (Chang *et al.* 1982, 1991; Hall *et al.*, 1982; Goodison *et al.*, 1990; Gan, 1996). Researchers have shown that SWE can be derived from the brightness temperature of the Special Sensor Microwave/Imager (SSM/I) of the Defence Meteorological Satellite Program (DMSP) satellite at 18 and 37 GHz.

1.2.6 Soil Moisture

Soil moisture is the part of precipitation that is temporarily stored in a shallow topsoil layer of the earth's surface. It plays a major and interactive role with other hydrologic processes such as streamflow, infiltration, evaporation and ground water recharge. However, soil moisture is highly variable spatially because of the inhomogeneity of soil properties, topography, land cover and the non-uniformity of input from rainfall. Therefore ground measurements alone are rarely representative of the average soil moisture condition for heterogeneous catchments. On the other hand, remotely sensed data have great potential for providing areal estimates of soil moisture, particularly in the microwave range. Schmugge *et al.* (1980) and Engman (1990) provide a comprehensive summary of remote sensing approaches for measuring soil moisture.

Although a substantial amount of research has been performed to retrieve soil moisture from remotely sensed data, especially from passive and active microwave data, the direct application of remotely sensed soil moisture data in hydrologic models is still at an early stage. Existing hydrologic models are rarely designed to make direct use of soil moisture information retrieved from remotely sensed data. Recently Pietroniro *et al.* (1993) attempted to incorporate remotely sensed soil moisture directly into a hydrological model. Current studies with active microwave sensors showed that the C-band radar operating in VV or HH polarization at 10^{o}-20^{o} incidence angle would be ideal for soil moisture estimation from radar backscatter values. With the success of several space platforms like ERS-1, JERS, and Radarsat SAR, there is a great opportunity to estimate and map near-surface soil moisture at fine resolutions, e.g., 10-100m. Such soil moisture data can be used in hydrologic models to either initialize the soil moisture variable (at the beginning of simulation) or to update its status as simulation progresses.

1.2.7 Surface Temperature

Surface temperature is an important variable for estimating the energy flux emitted by the ground surface. The latent and sensible heat fluxes emitted by the soil surface depend highly on the surface temperature.As a result, evaporation from the soil surface is directly related to its skin temperature. During the last three decades, satellite thermal infrared measurements have been used to estimate sea and land surface temperature. McClain *et al.* (1983) provided an extensive literature review on the theory and application of infrared remote sensing to obtain sea surface temperature. Using NOAA-AVHRR data, Price (1984) established a relationship to estimate spatial land surface temperature from two thermal infrared channels (10.9 and 11.8 μm). Schott and Volchok (1985) and others retrieved surface temperature from Landsat TM band with reasonable accuracy.

1.2.8 Vegetation Index and Land Cover Types

Running *et al.* (1986) identified the area of leaves above a given ground surface area, called the leaf area index (LAI), as a the single most important variable for quantifying energy and water flux exchange by plant canopies over land surfaces. As a result, the LAI estimated from ground measurement or satellite data has been used in different hydrologic models for estimating transpiration, actual evaporation and interception of water by the canopy (e.g., Kite and Kouwen, 1992; Kite, 1995; Kite and Spence, 1995). Specifically, LAI retrieved from the visible and infrared band of the NOAA-AVHRR sensor has been used to derive stomatal indices of vegetation cover. Land cover types over watersheds can also be retrieved from Landsat TM sensor at a higher resolution than NOAA-AVHRR data (e.g., Pietroniro *et al.*, 1995; Emaruchi, 1998).

1.2.9 Surface Albedo

The net energy received at the earth surface depends upon the surface albedo or surface reflectivity. Field measurement of surface albedo is only meaningful for basins with fairly uniform/ homogeneous terrain features (Brest and Goward, 1987). As a result satellite measurement is the only practical means to estimate surface albedo especially for heterogeneous catchments and areas that are relatively inaccessible. Duguay and LeDrew (1991) used Landsat TM data to retrieve spatially distributed surface albedo for different land cover types. Stuttard *et al.* (1994) used refelectance values from channels 1 and 2 of NOAA-AVHRR to estimate surface albedo for bare soil land cover in the Kenyan Rift Valley area.

1.3 Research Objectives

This study attempts to achieve three objectives. The primary objective is:

(1) To develop a semi-distributed hydrologic model that is not as intensive computationally as a fully distributed model, yet (i) capable of effectively assimilating spatially distributed, hydrologic information retrieved from remotely sensed data of various resolutions in modeling basin-scale hydrologic processes; (ii) can adequately account for the catchment terrain features through the topographic information derived from digital terrain elevation data (DTED) using a GIS; (iii) is flexible to operate at various temporal scales ranging from a fraction of an hour to daily or even longer time scales; (iv) is an effective tool for hydrologic impact studies of land use changes such as agricultural practices, afforestation, and deforestation; and (v) can be further developed to a land surface parameterization scheme linking large-scale atmospheric processes modeled by mesoscale atmospheric models and/or general circulation models, GCMs, with land surface processes for climate impact studies.

The assessment of the semi-distributed model developed is based on its application to the Paddle River Basin (265 km^2) of Central Alberta and in terms of hydrologic variables such as streamflow, surface/skin temperature, surface albedo, near surface soil moisture, evpotranspiration. Ground based data used for model application and assessment are the hourly streamflow data of Water Survey Canada, hydroclimatic data collected by two meteorological towers set up on the study site, and soil moisture data. Similarly, remotely sensed data used are taken from the NOAA-AVHRR, Landsat TM, and Radarsat SAR satellites.

The two secondary objectives are:

(2) to evaluate evapotranspiration (ET) estimated by the complicated two-source model that is based on canopy cover and energy dynamics with ET estimated by two simpler algorithms for a number of land use covers in the Canadian Prairies; and

(3) to assess the feasibility of retrieving near-surface (5-10 cm deep) soil moisture of agricultural/ranch lands in the Canadian Prairies (Paddle River Basin) using regression and theoretical model from Radarsat SAR data.

1.4 Organization of Thesis

Chapter 1 gives an overview of the general background of scientific achievements in applied hydrology and remote sensing, particularly in the area of hydrologic models and their applications. Chapter 2 describes in detail the development of a semi-distributed, physically based hydrologic model using remotely sensed data and geographic information system (GIS), called DPHM-RS. In Chapter 3, DPHM-RS is applied to Paddle River Basin of Central Alberta using topographic information derived from Digital Terrain Elevation Data (DTED) of the USGS Defense Mapping Agency (DMA), spatial hydrologic data retrieved from satellites, and meteorological data collected on the study site. DPHM-RS, calibrated with data collected for the summer of 1996 (July 24 to August 29, 1996), was validated against data collected for the summer of 1997 (July 16 to September 26, 1997) and the spring of 1998 (May 1 to June 30). In addition, the TOPMODEL (Beven and Kirkby, 1979) is applied to Paddle River Basin over the same period of time as a comparison to DPHM-RS model.

Chapter 4 compares the actual evapotranspiration estimated from algorithms - the Penman-Monteith equation, the modified Penman equation for non saturated surface, and the two-source model - for different land covers using hourly data collected in the summer of 1996. Based on 1350 soil moisture samples collected from nine selected sites in the Paddle River Basin, and six scenes of Radarsat SAR data, Chapter 5 demonstrates the feasibility of retrieving surface soil moisture (5-10cm depth) from Radarsat SAR data using a linear regression model and the theoretical integral equation model (IEM) of Fung *et al.* (1992). In Chapter 5 a sensitivity analysis of the surface parameters of IEM is also performed using Gaussian and exponential correlation functions. In addition the spatial correlations of soil moisture and Radarsat backscatters with respect to inter-site distances were investigated. Finally, summary, concluding remarks, and recommendations for further work are outlined in Chapter 6.

1.5 Study Site Description

The study site, the Paddle River Basin (central latitude and longitude of 53° 52' N. and 115° 32' W., respectively) of Central Alberta with a catchment area of 265 km^2, lies within the western edge of the Alberta Plains with an elevation ranging from 750 to 1000 m amsl. The climate of the study area is in the "short, cool summer" koeppen climatic zone (Longley, 1968). The mean temperature varies from -15.5°C in January to +15.6°C in July. The annual mean precipitation is approximately 508 mm (Pretula and Ko, 1982). Forest, brushlands, and tree muskegs cover approximately 80 percent of the headwater region of the catchment. The deciduous, Aspen forest is the predominant vegetation type (AENR, 1977). Agriculture and woodland grazing are the main land use in the region. The rugged topography and limited access have prevented significant enroachment of agriculture development into the remaining forest areas, although the demand for grazing leases has increased substantially in recent years (AENR, 1977). The major soil group of the basin is of Hubalta series associated with Onoway and Modeste (Twardy and Lindsay, 1971) which are characterized by strongly developed Orthic Gray Wooded features. The dominant texture for such a soil type is the clay loam soil under moderately well drained conditions.

The existing stands of Aspen play an important role in controlling the amount of flood runoff, subsurface flow and sediment production from the headwater area (AENR, 1977). The catchment has a moderate hydrological response with an average land slope of 3-5%. Runoff from the undisturbed forestlands is delivered to stream channels almost entirely as sub-surface flow because the intensity of snowmelt or rainfall rarely exceeds soil infiltration rates. The portion of the lands which deliver sub-surface flow, is mainly located adjacent to the stream channels. However, these source areas for sub-surface flow vary temporally, expanding as the moisture capacity of the soil mantle is exceeded by incoming rain water and contracting between storm events when water is depleted by subsurface flow to the channel (AENR, 1977). This is based on the variable source area concept of Hewlett and Hibbert (1967).

A study of watershed management in the headwaters of the Paddle River Basin by Alberta Energy and Natural Resources (1977) for controlling flood runoff indicates three hydrological response zones: (i) the critical zone which has the greatest potential for contributing to flood runoff as a result of quick-flow from source areas; (ii) areas which have a moderate potential for contributing to flood runoff; and (iii) zones which have the lowest potential for contributing to flood runoff.

1.6 Miscellaneous

Tables and figures are presented at the end of each chapter. Appendices are included at the end of the thesis. However, the thesis is written so that to have more or less stand-alone chapters, which means that a symbol could represent different quantities in different chapters. To avoid confusion, definitions of symbols are given in appropriate places in each chapter.

References

Abbott, M. B. (1972) The use of digital computers in hydrology. *In Teaching Aids of Hydrology*, Technical papers in Hydrology 11, *UNESCO*, LC No. 72-87901.

Abbott, M. B., Bathurst, J. C., Cunge, J. A., O'Connell, P. E., and Rasmussen, J. (1986). An introduction to the European hydrological system-System hydrologique Europeen, 'SHE', 1: History and philosophy of a physically-based, distributed modeling system. *Jour. of Hydrol.*, 87(1/2), 45-59.

Alberta Energy and Natural Resources (AENR), *"A study of Watershed Management Options For Controlling Flood Runoff in the Headwaters of the Paddle River Basin,"* No. 44, pp. 1-39, 1977.

Amerman, C. R. (1965). The use of unit-source watershed data for runoff prediction. *Water Resour. Res.*, Vol. 1, No. 4, pp. 499-507.

Amorocho, J. and Orlob, G. T. (1961) Nonlinear analysis of hydrologic systems, *Water Resources Center, University of California*, Contribution No. 40, Berkeley.

Beven, K. J. and Kirkby, M. J. (1979). A physically-based variable contributing area model of basin hydrology. *Hydrol. Sci. Bull.*, 24, pp. 43-69.

Beven, K. J., Calver, A., and Morris, E. M. (1987). The Institute of Hydrology distributed model. *Institute of Hydrology Report 98*, Wallingford, UK.

Brest, C. L. and Goward, S. N. (1987). Deriving surface albedo measurements from narrow band satellite data. *Int. J. Remote Sensing*, 8, pp. 351-367.

Burnash R. J., Ferral R. L., and Mcguire R. A. (1973). A generalized stream flow simulation system, Conceptual modeling for digital computers, *U. S. NWS*, Sacramento, California.

Carroll, T. R., and Allen, M. (1988) Airborne gamma radiation snow water equivalent and soil moisture measurements and satellite areal extent of snow cover measurements. A *User's Guide*, Version 3.0, National Weather Service, NOAA, Minneapolis, MN.

Castruccio, P. A., Loats, Jr, H. L., Lloyd, D., and Newman, P. B. (1980) Cost/benefit analysis for the operational applications of satellite snow cover observations (OASSO). *Proc. Final Workshop on Operational Applications of Satellite Snow Cover Observations*, NASA CP-2116, pp. 239-254.

Chang, A. T. C., Foster, J. L., Hall, D. K., Rango, A., and Hartline, B. K. (1982) Snow Water Equivalent Estimation by Microwave Radiometry, *Cold Regions Science and Technology*, 5, pp. 259-267.

Chang, A. T. C., Foster, J. L., and Rango, A. (1991) Utilization of Surface Cover Composition to improve the Microwave Determination of Snow Water Equivalent in a Mountain Basin, *Inter. J. of Remote Sensing*, 12 (11), pp. 2311-2319.

Clark, C. O. (1945). Storage and the unit hydrograph. *Trans. Amer. Soc. Civil Eng.*, 110, pp. 1419-1488.

Crawford, N. H., and Linsley, R. K. (1966). Digital simulation in hydrology; Stanford Watershed Model IV. Dept. of Civil Eng., Stanford University, *Tech. Rept.* No. 39.

Dickinson, R. E. and Kennedy, P. J. (1991). Land surface hydrology in a general circulation model global and regional fields needed for validation. In Wood, E. F. (Ed.), Land Surface Atmospheric Interactions for Climate Modeling. *Kluwer, Dordrecht.* 115-126.

Diskin, M. H. (1964) A basic study of the Linearity of the Rainfall-Runoff Process in Watersheds. *Ph.D. Thesis*, Univ. III, Urbaba, III., 160pp.

Donald, J. R., Seglenieks, F. R., Soulis, E. D., Kouwen, N. and Mullins, D. W. (1992) Mapping of partial snowcover during melt season using C-Band SAR imagery. *Proc. 15th Canad. Symp. Remote Sensing*, Toronto, Ontario, 170-175.

Dooge, J. C. (1959). A general theory of the unit hydrograph. *J. Geophys. Res.*, 64(2), 241-256.

Dooge, J. C. (1973) Linear theory of hydrologic systems, *Tech. Bull.* No. 1468, *Agri. Res. Serv.*, pp. 117-124, October, U. S. Department of Agriculture, Washington, D. C.

Duguay, C. R., and LeDrew, E. F. (1991). Mapping surface albedo in the east slope of the Colorado Front Range, USA, with Landsat Thematic Mapper. *Arctic and Alpine Research*, 23, pp 213-223.

Eagleson, P. E., Mejia-r, R. and March, F. (1965) The Computation of optimum realizable unit hydrographs from rainfall and runoff data. *Hydrodyn. Lab. Rep.* No. 84, MIT.

Emaruchi, B. (1998) A hydrologic model for forested mountain watersheds. *Ph.D. Thesis*. Univeristy of Regina. 243.

England, C. B., and Stephenson, G. R. (1970). Response units for evaluating the hydrologic performance of rangeland watersheds. *J. Hydrol.*, 11, pp. 89-97.

Engman, E. T. (1990) Use of microwave remotely sensed soil moisture in hydrologic modeling. In: Application of Remote Sensing in Hydrology, ed. G. W. Kite and A. Wankiewicz, 279-292. *Proc. Symp. No. 5, NHRI*, Saskatoon, Canada.

Engman, E. T. and Gurney, R. J. (1991) Remote sensing in hydrology, *Chapman and Hall*, New York, USA.

Fortin, J. P., Villeneuve, J. P., Guibot, A., and Seguin, B. (1986). Development of a modular hydrological forecasting model based on remotely sensed data, for interactive utilization on a microcomputer. *Hydrologic applications of space technology*, A. I. Johnson, ed., 307-319.

Fung, A. K., Lee, Z., and Chen, K. S., Backscattering from a randomly rough dielectric surface, *IEEE Transactions on Geoscience and Remote Sensing*, 30(2), pp.356-369, 1992.

Gan, T. Y. (1996) Passive Microwave snow research in the Canadaian High Arctic. Cand. *J. of Remote Sens.*, vol. 22, No. 1, pp. 36-44.

Gan, T. Y., Biftu, G. F. (1996). Automatic calibration of conceptual rainfall-runoff models: optimization algorithms, catchment conditions, and model structure. *Water Resources Research*, American Geophysics Union, Vol. 32, No. 12, pp. 3513-3524.

Goldhirsh, J. (1988) Analysis of algorithms for the retrieval of rain-rate profiles from spaceborne dual-wavelength radar. *IEEE Trans. Geosci. Remote Sens.* GE-26,98-114.

Goodison, B. E., Walker, A. E., and Thirkettle, F. W. (1990) Determination of Snow Water Equivalent on the Canadian Prairies using near real-time Passive Microwave data, *Proceedings of the Workshop on Applications of Remote Sensing in Hydrology*, Kite and Wankiewicz (eds.), Saskatoon, pp. 297-309.

Haefner, H., Holecz, F., Meier, E., Nuesch, D. Piesbergen, J. (1994) Capabilities and limitations of ERS-1 SAR data for snowcover determination in Mountainous regions, *Proc. Second ERS-1 Symp.-Space at the service of Our Environment*, Huburg, Germany, 11-14 October, 1993, pp. 971-976.

Hall, D. K., Foster, J. L., and Chang, A. T. C. (1982) Measurement and Modeling of Microwave Emission from Forested Snowfields in Michigan, *Nordic Hydrology*, 13, pp. 129-138.

Hallikainen, M., Kurvonen, L., Jaaskelainen, V., Koskinen, J., Herland, E. A., and Perala, J. (1994) Microwave Remote Sensing of snow using radar and radiometer, *Proc. Second ERS-1 Symp.-Space at the service of Our Environment*, Huburg, Germany, 11-14 October, 1993, pp. 977-982.

Hewlett, J. D. and Hibbert, A. R. (1967) Factors affecting the response of small watersheds to precipitation in humid areas, in int. Symp. on Forest Hydrology, ed. By W. E. Sopper and H. W. Lull, Pergamon Press, Oxford, pp. 275-290.

Holroyd, E. W. III, Verdin, J. P, and Carroll, T. R. (1989) Mapping snowcover with satellite imagery: comparison of results from three sensor systems. In: *Proc. Western Snow Conference* (Ft. Collins, Colorado, USA), 59-68.

Kite, G. W. (1989) Using NOAA data for hydrological modeling. In: Quantitative Remote Sensing: An Economic Tool for the Nineties, (*Proc. IGARSS'89, IEEE*), 553-558.

Kite, G. W. (1995). Scaling of input data for macroscale hydrologic modeling. *Water Resour. Res.*, 31(11), 2769-2781.

Kite, G. W., and Kouwen, N. (1992) Watershed modeling using land classifications. *Water Resour. Res.* 28(12), 3193-3200.

Kite, G. W. and Spence, C. D. (1995) Land cover, NDVI, LAI, and evapotranspiration in hydrological modelling. In: Application of Remote Sensing in Hydrology, ed. G. W. Kite, A. Pietrniro and T. Pultz, 223-240. *Proc. Synp. No. 14, NHRI*, Saskatoon, Canada.

Kite, G. W. and Pietroniro, A. (1996) Remote sensing applications in hydrological modelling. *Hydrological Sciences Journal*, 41(4):563-591.

Kouwen, N. (1988). WATFLOOD. A micro-computer based flood forecasting system based on real- time weather radar. *Can. Water. Resour. J.*, 13(1), 62-77.

Lattenmaier, D. P., and Gan, T. Y. (1990). Hydrologic Sensitivities of the Sacramento-San Joaquin River Basin, California, to Global Warming, *Wat. Resour. Res.*, 26,69-86.

Lattenmaier, D. P., McCabe, G., Stakhiv, E. Z. (1997) Global Climate change: Effect on hydrologic cycle, Chapter 29 in Larrey W. Mays (eds.), *Handbook of Water Resources*, McGraw-Hill.

Longley, R.W., "*Climatic maps for Alberta,*" University of Alberta, 1968.

McClain, E. P., Pichel, W. G., Walton, C. C., Ahmad, Z., and Sutton, J. (1983) Multichannel improvements to satellite-derived global sea surface temperatures, *Adv. Space Res.*, 2, pp. 43-47.

Meneghini, R., Eckerman, J. and Atlas, D. (1983) Determining rain rate from a spaceborne radar usin measurements of total attenuation. *IEEE Trans. Geosci. Remote Sensing* GE-21, 34-43.

NASA (1984) Earth Observing System, vols. I and II, *NASA TM-86129*, NASA/Goddard Space Flight Center, Greenbelt, MD.

Nash, J. E. (1957). The form of the instantaneous unit hydrograph, *IASH publication* no. 45, vol. 3-4, pp. 114-121.

NOAA (1993) Nile Forecasting System, *Tech. Manual*, US Dept. of Commerce, Silver Spring, Colorado, USA.

O'Conner, K. M. (1976) A discrete linear cascade model for hydrology, *J. of Hydrology*, 29, pp. 203-242.

Pietroniro, A., Wishart, W. and Solomon, S. I. (1989) Use of remote sensing data for inventory and runoff forecast. In: *Satellite Hydrology*, 230-234. *AWRA*, Minneapolis, Minnesota, USA.

Pietroniro, A., Solomon, S. I. and Soulis, E. D. (1991) Hydrometeorological data extension for the Sudan Sahel Zone of West Africa. *IEE Trans. Geosci. Remote Sens.* 28(5).

Pietroniro, A., Soulis, E. D., Kouwen, N., Routunno, O. and Mullins, D. W. (1993) Using wide swath C-band SAR imagery for basin soil moisture mapping. *Can. J. Remote. Sens.*, Special Issue, January, 77-82.

Pietroniro, A., Prowse, T. D., and Lalonde, V. (1995) Classifying terrain in a muskeg-wetland regime for application to GRU-type distributed hydrologic modelings. In: Applications of Remote Sensing in Hydrology, ed. G. W. Kite, A. Pietroniro and T. Pults, 275-286. *Proc. Symp.* No. 14, NHRI, Saskatoon, Canada.

Pretula, B. R., and Ko, C. A., *Hydrogeology Paddle River Reservoir area near Mayerthorpe*, Alberta, Report prepared for Alberta Environment Protection (AEP), pp. 1-107, 1982.

Price, J. C. (1984) Land Surface Temperature Measurements from the Split Window channels of the NOAA 7 Advance Very High Resolution Radiometer. *J. of Geophy. Res.*, Vol. 89, No. D5, pp. 7231-7237.

Rango, A. (1980) Operational applications of satellite snowcover observations. *Wat. Resour. Bull.* 16, 1066-1073.

Rodriguez-Iturbe, I. and Valdes, J. B. (1979) The geomorphologic structure of hydrologic response. *Water Resour. Res.*, Vol. 15(6), 1409-1420.

Rott, H., Nagler, T. (1994) Capabilities of ERS-1 SAR data for snow and Glacier Monitoring in Alpine areas, *Proc. Second ERS-1 Symp.-Space at the service of Our Environment,* Huburg, Germany, 11-14 October, 1993, pp. 965-970.

Running, S. W., Patterson, D. L., Spanner, M. A., and Teuber, K. B. (1986) Remote Sensing of coniferous forest leaf area. *Ecology* 67, pp. 273-276.

Schmugge, T. J., Jackson, T. J. and McKim, H. L. (1980) Survey of methods for soil Moisture determination. *Water Resour. Res.* 16, 961-979.

Schott, J. R. and Volchok, W.J. (1985) Thematic Mapper Thermal Infrared Calibration. *Photogrammetric Engineering and Remote Sensing*, vol. 51, No. 9, pp. 1351-1357.

Scofield, R. A. (1983) Satellite-derived precipitation estimates for hydrologic applications. *IAHS Publ.* No. 145, 259-272.

Sellers, P. J., Mintz, Y., Sud, Y. C., and Dalcher, A. (1986). A simplified biosphere model (SiB) for use within general circulation models. *J. Atmos. Sci.*, 43, 305-331.

Sherman, L. K. (1932). Streamflow from rainfall by the unit graph method. *Eng. News Rec.*, 108, 501-505.

Stuttard, M. J., Hayball, J. B., Narciso, G, Suppo, M and Oroda, A. (1994) Use of GIS to assist hydrological modeling of lake basins in the Kenyan Rift Valley. *Proc. Agi 94*, 13.4.1-13.4.8, Birmingham, UK.

Snyder, W. M., (1955). Hydrograph analysis by the method of least squares, *Proc. Amer. Soc. Civ. Eng.*, vol. 81, 1-24.

Twardy, A.G., J.D. Lindsay, "*Soil Survey of the Chip Lake Area,*" Alberta Soil Survey, No. 28, pp. 1-71, 1971.

Wilheit, T. T., Rao, M. S. V., Chang, T. C., Rogers, E. B. and Theon, J. S. (1977) A satellite technique for quantitative mapping rainfall rates over the ocean. *J. Appl. Meteorol.* 16(S), 551.

WMO (1975). Intercomparison of conceptual models used in operational hydrological forecasting. *WMO operational Hydrology Rep.* No. 7, WNO no. 429.

WMO (1992). Simulated real-time Intercomparison of hydrological models. *WMO Operational Hydrology Rep.* No. 38, WNO no. 779.

Wood, E. F., Lettenmaier, D. P., and Zartarian, V. G. (1992). A land surface hydrology parameterization with sub-grid variability for general circulation models. *J. Geophys. Res.*, 97(D3), 2717-2728

Chapter 2

Semi-distributed, Physically Based, Hydrologic Modeling using Remotely Sensed data and GIS, I. Model development

2.1 Introduction

With the progress of civilization, human activities gradually intrude on the natural water environment by altering the dynamic equilibrium of the water cycle and initiating new processes and events. In recent years, environmental protection, sustainable development and climate change are becoming issues of major concern to nations all around the world. Both politicians and scientists are interested in the implications of land use changes, agricultural practices, afforestation or deforestation, building of mammoth reservoirs to our environment and to the world's water resources. These changes are first manifested through local-scale processes such as evaporation, runoff, and soil moisture but their effects are gradually felt at regional or even larger scales.

Rainfall-runoff transformation is a complex phenomenon involving the interaction of many hydrologic processes and over many scales. In the last several decades, hydrology has evolved from empiricism to a discipline of applied science, which studies hydrological processes from measurable causative factors. Applied hydrology has many engineering applications such as water resources management and planning, urban sewer design, and land reclamation drainage systems design. In particular, system theoretical models (e.g. Sharman, 1932; Clark, 1945; Snyder, 1955; Nash, 1957; Eagleson *et al.*, 1965; and Rodriguez-Iturbe and Valdes, 1979) and lumped conceptual hydrologic models (e.g., Crawford and Linsley, 1966; Burnash *et al.*, 1973) have been practical tools to quantify the amount of runoff from watersheds.

Even though lumped conceptual rainfall-runoff models have generally been very useful in simulating runoff from river basins, they are limited in assessing the effect of changes in different hydrological and meteorological variables (see Abbott, 1972; Klemes, 1988; Link, 1983; Gan *et al.*, 1997; Gan and Biftu, 1996). The necessity to consider the effects of land cover changes in watershed modeling has been recognized (Tao and Kouwen, 1989; Duchon *et al.*, 1992). Also, the space platforms provide us with spatially distributed remotely sensed data to augment our limited, ground-based, point data to monitor land use changes. Semi- and fully distributed hydrologic models, designed to take advantage of these spatially distributed data, should be able to quantify basin hydrologic processes more accurately than before.

Freeze and Harlan pioneered the development of fully distributed hydrologic models in 1969. Since then, different models ranging from fully distributed models such as SHE (Abbott *et al.*, 1986), IHDM (Beven *et al.*, 1987), MIKE SHE (Rafsgaard and Storm, 1995), and THALES (Grayson *et al.*, 1992), to small scale semi-distributed models that account for hydrologic responses on different concepts, such as TOPMODEL (Beven *et al.*, 1995), HYDROTEL (Fortin *et al.*, 1986), WATFLOOD (Kouwen, 1988), and SLURP (Kite, 1995) have been developed. Table 2.1 summarizes and compares the general characteristics of some of these distributed hydrologic models, including the DPHM-RS model developed in this study.

The rapid development of computer technology, geographical information systems, and digital terrain data has lead to the development of complex models that solve partial differential equations governing surface and subsurface flow numerically. In addition the need for distributed predictions or hydrologic predictions at different locations of a basin

(Abbott *et al.*, 1986; Bathurst and O'Connel, 1992; and Refsgaard and Abbott, 1996) enhance the development of such distributed models. Theoretically, fully distributed models (Freeze and Harlan, 1969) use spatially distributed parameters of physical relevance (possibly measurable in the field) and thus provide more accurate hydrologic predictions over lumped-parameter models. However, such models are very data intensive and so may be difficult to apply on a routine basis.

In particular, due to the heterogeneities of nature, the demand for data by fully distributed hydrologic models are usually so great that it is almost impossible to obtain the parameters required at all grid elements. Recently Beven (1996) suggested that distributed modeling should be approached with some prudence, as the process descriptions used in current distributed models may be "artificial" at grid scale. Since effective parameter values may vary within the grid scale and parameter estimations are often done at inappropriate scales, there is sufficient uncertainty in model structure and spatial discretization to hinder the practical applications of such models. Ottl'e and Vidal-Madjar (1994) pointed out that the general lack of information on the temporal and spatial variations of precipitation also hinders the application of distributed, physically based models. As a result, whether such complicated models would perform better than the simple, lumped conceptual models is questionable.

Beven (1996) also indicated that there are multiple models differing markedly in model structures or parameter values, and yet these are almost equally acceptable to represent the catchment system of interest. He argued that the future development of distributed models must be in the direction of sub-grid parameterizations based on large scale measurements rather than the traditional quest for improving the aggregation of small scale parameterizations. This implies that when developing a model for a particular scale of basin, one must find a trade-off between the attainable resolution of processes to be modeled and the accuracy required. The resolution attainable depends mainly on the types of data available and the information contained in the data. Inevitably, the building and applying of distributed models depend largely on our ability to retrieve useful hydrologic information from satellite data and limited ground-based, point measurements.

To explore the applicability of different satellite data in hydrologic modeling, a semi-distributed, physically based hydrologic model for modeling basin scale hydrologic processes using remotely sensed and ground data is developed. The model structure should provide a linked representation of the hydrology-vegetation dynamics at several scales. The scale can range from a grid-based to a sub-basin scale, depending on the details required and the input information available. In addition, the model should be able to operate from hourly to daily or even longer time scales. Basin-scale hydrologic processes are to be represented in detail (within the limitation of current scientific understanding) that is appropriate for the practical application of the model, which should be designed to maximize the applicability of hydrologic information retrievable from currently available satellite data such as Landsat TM/MSS, NOAA-AVHRR and Radarsat SAR. The distributed information useful for hydrologic modeling such as soil moisture, snow depth, vegetation index, radiative fluxes and land use classes can be retrieved from such or similar space platforms.

2.2 Model Components of DPHM-RS

The semi-distributed, physically based hydrologic model using GIS and remote sensing data, DPHM-RS is divided into seven components (see Figure 2.1). A description of each of these components is outlined below.

2.2.1 Interception

Precipitation falling from the atmosphere is partly intercepted by the canopy before it reaches the ground surface. The amount of water intercepted by the canopy and the net precipitation reaching the ground surface depend upon the type and density of vegetation. The interception loss can be substantial in the case of catchments densely covered with trees (Rutter, 1967, 1971). Furthermore, the evaporation from wet leaves in a forest can be much faster than from a water surface exposed to the same meteorological conditions

(Murphy and Knoerr, 1975; Stewart, 1977). The canopy storage is filled by the precipitation and discharged by evaporation and drainage (see Figure 2.2).

In DPHM-RS, the water balance for the canopy is described by

$$\frac{dC}{dt} = (1-\delta)p - e_{wc} - k\exp\left[b(C-S)\right] \qquad 0 \le C \le S \tag{2.1}$$

Where p is the precipitation rate, e_{wc} is the wet canopy evaporation rate, S is the canopy water storage capacity, C is the actual amount of water intercepted by canopy, k and b are Rutter drainage parameters, and δ is the free throughfall coefficient (the proportion of rain which falls to the ground without striking the canopy).

For forest vegetation k and b are typically 0.002 mm/min and 4 mm^{-1} respectively (Rutter *et al*, 1975). The method used to determine the throughfall coefficient is explained in chapter 3. The drainage parameters are estimated by Rutter *et al*, (1975) as:

b = 3.7 (mean value between 3.0-4.6)

$$k = \exp\left[\ln(0.0019 * S) - b * S\right] \tag{2.2}$$

S is evaluated from the vegetation index using Dickinson's equation (1984) as:

$$S = K_L * LAI \tag{2.3}$$

Where K_L is taken as 0.2 mm, after Dickinson (1984) who suggested K_L to be based on the range of total canopy storages quoted in Rutter (1975). The wet canopy evaporation is evaluated as:

$$e_{wc} = \min(C, \omega e_{wct}) \tag{2.4}$$

Where e_{wct} is the rate of evaporation from the entire wet canopy (see equation (2.47)), and ω is the area fraction of wet canopy, which is determined from Deardorff (1978) as:

$$\begin{aligned} \omega &= \left(\frac{C}{S}\right)^{(2/3)} && e_{wct} > 0 \\ \omega &= 1 && e_{wct} \le 0 \end{aligned} \tag{2.5}$$

As indicated by Deardorff (1978), the fractional power is specified to allow the canopy water to evaporate more rapidly with the water occupying only fraction of the leaf area during evaporation and the entire area during accumulation (condensation). The initial canopy storage can be approximated from the simple form of equation as:

$$C_o = \frac{LAI}{LAI_{\max}} S \tag{2.6}$$

with $LAI_{\max}$ = 6.0 as given by EAP (1991). However one can over-ride C_o if actual data is available.

2.2.2 Evapotranspiration

Evapotranspiration (ET) constitutes an important component of the water fluxes of the hydrosphere and the atmosphere. In DPHM-RS, the actual ET is estimated using the two-source model of Shuttleworth and Gurney (1990) based on the energy balance at 3 layers. The energy budget equation reflects the amount of energy available for the actual evaporation, modified for transport capacity and moisture availability on a catchment scale. The general form of the energy budget equation is (Brutsaert, 1982) written for the control volume shown in Figure 2.3 is

$$R_n - L_e E - H - L_p F_p - G_s - A_h = \frac{\partial W}{\partial t} \tag{2.7}$$

Where R_n is the net radiative flux density at the reference layer, L_e is the latent heat of vaporization, L_p the thermal conversion factor for the fixation of carbon dioxide, F_p the specific flux of CO_2, G_s the specific energy flux leaving the layer at the lower boundary, A_h the energy advection into the layer, and W is the energy storage per unit area. For many practical purposes, several of the above terms can be omitted and equation (2.7) can be simplified to:

$$R_n - L_e E - H - G_s = 0 \tag{2.8}$$

2.2.2.1 Net Radiation

The net radiation at the surface (Figure 2.4) is given by

$$R_n = R_s(1 - \alpha_s) + \varepsilon_s R_{ld} - R_{lu} \tag{2.9}$$

Where R_s is the short-wave radiation, α_s the albedo of the surface which can be derived from Landsat TM data for different land cover classes, R_{ld} the downward long wave or atmospheric radiation, R_{lu} the upward long wave radiation, and ε_s the surface emissivity. In Equation (2.9) the incoming fluxes are relatively independent of the surface conditions, but the outgoing fluxes are highly dependent on surface conditions.

2.2.2.1.1 Short Wave Radiation

The short wave radiation at a location is composed of direct, diffused sky and terrain reflected components. For a surface of moderately rolling topography, the short wave radiation can be measured using radiation sensors like radiometer or pyranometer. In mountainous terrain, measurements of all components of short wave irradiance require a dense network of stations due to the surface dependence of total short wave irradiance. To evaluate the surface variations of short-wave radiation, it is necessary to consider all the components.

In DPHM-RS, if measured short wave radiation is not available, the total daily incoming short wave radiation is estimated by (Brutsaert, 1982):

$$R_S = \left(a_S + b_S \frac{n}{N}\right) I_0 \tag{2.10}$$

Where I_o is the solar constant corrected for deviation of the actual sun-earth distance from its mean value, and a_s and b_s are parameters indicating the fraction of extraterrestrial radiation on overcast and clear days. The parameters a_s and b_s depend on atmospheric conditions and the solar declination and can be determined from regressing local measurements of incoming short wave radiation on overcast days and on days with bright sunshine.

2.2.2.1.2 Long Wave Radiation

The long wave radiation is the radiant flux emitted by atmospheric gases, and the land and water surfaces of the earth. More accurate methods for calculating the atmospheric radiation under clear skies require vertical profiles of humidity and temperature. Such radiosonde data are rarely available. A simpler approach to estimate the downward long wave radiation based on the air temperature is

$$R_{ld} = \varepsilon_{ac} \sigma T_a^4 \tag{2.11}$$

Where T_a is the air temperature near the ground usually taken at the shelter level, σ is the Stefan-Boltzmann constant = 5.6679×10^{-2} Wm^{-2} k^{-4} (1.354×10^{-12} cal cm^{-2} s^{-1} k^{-4}), ε_{ac} is the atmospheric emissivity under clear skies estimated from Satterlund (1979) equation as:

$$\varepsilon_{ac} = 1.08\left[1 - \exp\left(-e_a^{T_a/2016}\right)\right] \tag{2.12}$$

Where e_a is the vapor pressure of air in mb and T_a is in ^oK.

The effect of cloud cover can be adjusted by multiplying the clear sky atmospheric emissivity by an empirical coefficient τ that depends on fractional cloud cover.

$$\tau = 1 + 0.22 f_c \tag{2.13}$$

Where f_c is fractional cloud cover of the sky. If data on cloud cover are not available, the daily net long wave radiation can be corrected by assuming that the fractional cloud cover is equal to the fraction of sunshine hours.

The upward long wave irradiance is usually obtained by assuming that the ground, the canopy or the water surface under consideration is equivalent to an infinitely deep gray body of uniform temperature and emissivity ε_s, which is close to unity. This allows the following formulation.

$$R_{lu} = \varepsilon_s \sigma T_s^4 \tag{2.14}$$

Where T_s is the skin temperature, ε_s = 0.97 for water, 0.98 for melting snow, 0.98 for vegetation, and 0.90 for other surfaces (Frampton and Marks, 1980; Cogan, 1985). The skin temperature can be estimated from Landsat TM or NOAA-AVHRR data. If there are no satellite data the skin temperature T_s can be calculated iteratively using equation (2.8) (e.g., Liang, 1994).

2.2.2.2 Sensible and Latent Heat Fluxes

For surfaces covered by the vegetation, the sources of latent heat, L_eE, and sensible heat, H, fluxes are from the canopy and soil surface. To evaluate these fluxes fully, it is necessary to determine the energy budget for each source. In DPHM-RS the two-source model (Shuttleworth and Wallace, 1985; Shuttleworth and Gurney, 1990; Shuttleworth, 1991) has been adopted to evaluate the actual evaporation from land surface and transpiration from vegetation canopy separately. Shuttleworth (1991) has discussed the theoretical basis of the model in detail.

The model assumes energy balance at three layers (above canopy, within canopy, and at soil surface) as shown in Figure 2.5. The net energy received at the reference height is partitioned into net radiation on the canopy, R_{nc} and on the soil, R_{ns}, using Beer's law:

$$R_n = R_{ns} + R_{nc} \tag{2.15}$$

Where $R_{ns} = R_n \exp(-\alpha LAI)$ (2.16)

Assuming a spherical distribution of leaves exposed to sun at a solar altitude θ, the value of the attenuation coefficient, α for the direct light was estimated as (Choudhury and Monteith, 1988):

$$\alpha = 0.5\cos ec(\theta) \tag{2.17}$$

2.2.2.2.1 Energy Balance Above Canopy

Above the canopy the sensible and latent heat fluxes are given as:

$$H = \frac{\rho c_p (T_h - T_a)}{r_{aa}} \tag{2.18}$$

and

$$L_e E = \frac{\rho c_p (e_h - e_a)}{\gamma\, r_{aa}} \tag{2.19}$$

The aerodynamic resistance to heat and vapor are assumed to be the same in this case and given by (Shuttleworth, 1991):

$$r_{aa} = \frac{1}{\kappa u^*} \ln\left[\frac{(z_a - d)}{(h - d)}\right] + \frac{h}{\lambda_e K_h}\left\{\exp[\lambda(1 - Z/h)] - 1\right\} \tag{2.20}$$

Where:

$$K_h = \kappa u^*(h - d) \tag{2.21}$$

$$u^* = \frac{\kappa u}{\ln\left(\frac{(z_a - d)}{z_o}\right)} \tag{2.22}$$

$$Z = Z_o + D \tag{2.23}$$

z_a is reference height above canopy, d is the zero plane displacement height for the partial canopy, z_o is the roughness length for partial canopy, h the canopy height, Zo the roughness length for full canopy (z_o at $LAI=4.0$), D is zero plane displacement height for full canopy (d at $LAI=4.0$), λ_e is the attenuation coefficient for eddy diffusivity, and u the wind speed at reference height and κ (=0.41) the Von-Karman's constant.

The above equations are applicable under neutral atmospheric stability. Shuttleworth and Gurney (1990) suggested an iterative technique to correct for stability effects. However to avoid iterative methods which require excessive computation, the approximate analytical correction method developed by Louis (1979) is used in DPHM-RS. For unstable or stable conditions, the aerodynamic resistance obtained in Equation (2.20) is multiplied by a coefficient β, which depends on the bulk Richardson number R_{iB}.

$$\beta = \frac{1}{1.351 * F_w} \tag{2.24}$$

such that

$$F_w = 1 - \frac{9.4 \times R_{iB}}{1 + c\left|R_{iB}\right|^{1/2}} \qquad R_{iB} < 0 \tag{2.25}$$

$$F_w = \frac{1}{(1 + 4.7 \times R_{iB})} \qquad 0 \le R_{iB} \le 0.2 \tag{2.26}$$

$$R_{iB} = \frac{g \times z_r (T_a - T_h)}{T_a V_a^2} \tag{2.27}$$

g is the acceleration due to gravity, T_h is the air temperature at within-canopy source height, and z_r and V_a are the modified reference height and wind speed, and they are expressed following Smith *et al.* (1993):

$$z_r = z_a - d \tag{2.28}$$

and

$$V_a^2 = u^2 + U_c^2 \tag{2.29}$$

With U_c = 1.0 m/s for unstable conditions and U_c = 0.1 m/s for stable conditions. The parameter c in equation (2.25) is given as:

$$c = 49.82 \times \frac{\kappa^2 \left(\frac{z_a - d}{z_o}\right)^{1/2}}{\left[\ln\left(\frac{z_a - d}{z_o}\right)\right]^2} \tag{2.30}$$

The zero plane displacement height d and roughness length z_o are estimated from the equation by Shaw and Pereira (1982) as:

$$d = 1.1h \ln[1 + (0.07 LAI)^{1/4}] \tag{2.31}$$

and

$$z_o = z'_o + 0.3h(0.07 LAI)^{1/2} \qquad for \qquad LAI < 2.85 \tag{2.32}$$

$$z_o = 0.3h(1 - d / h) \qquad for \qquad LAI > 2.85 \tag{2.33}$$

Where z'_o is the roughness length of the soil.

2.2.2.2.2 Energy Balance Within Canopy Height

The latent and sensible heat within canopy height are given by (Shuttleworth, 1991):

$$H_c = \frac{\rho c_p \left(T_c - T_h\right)}{r_{ac}} \tag{2.34}$$

$$L_e E_c = \frac{\rho c_p \left(e^*(T_c) - e_h\right)}{\gamma \left(r_{ac} + r_s^c\right)} \tag{2.35}$$

The aerodynamic resistance within canopy height is given by (Choudhury and Monteith, 1988):

$$r_{ac} = r_b / 2LAI \tag{2.36}$$

$$r_b = \left(\frac{100}{n'}\right)\left\{\frac{(w_f / u_h)^{1/2}}{[1 - \exp(-n'/2)]}\right\} \tag{2.37}$$

$$u_h = \frac{u^*}{\kappa} \ln\left[\frac{(h-d)}{z_o}\right] - \psi_m \tag{2.38}$$

Where

n' = attenuation coefficient for wind speed, dimensionless

w_f = representative leaf width, m

u_h = wind speed at top of canopy, m/s

ψ_m = surface layer stability corrector for momentum, dimensionless and estimated according to Weeb(1970) for stable conditions and Dyer and Hicks (1970) for unstable conditions, respectively as:

$$\begin{aligned} \psi_m &= (1 - 5R_{iB})^{-1} \\ \psi_m &= (1 - 16R_{iB})^{-1/2} \end{aligned} \tag{2.39}$$

The Bulk stomatal resistance, r_s^c, of the canopy depends largely on the minimum resistance, the available solar energy, the availability of water in the root zone and the air temperature (Jarvis, 1976). In DPHM-RS, r_s^c is based on the work of Dickinson (1984).

$$r_s^c = \frac{r_{\min} \alpha_r \ \beta_s}{LAI \ \eta_s^4} \tag{2.40}$$

Where

$$\alpha_r = \frac{1 + f_r}{1 + r_{\min}/r_{\max}} \tag{2.41}$$

and $$f_r = \frac{1.1 R_{sc}}{R_s^{ref}\, LAI} \tag{2.42}$$

Where R_{sc} is the incoming solar radiation at the surface of canopy given by Beer's law (see Equation (2.43)) and R_s^{ref} is a reference value of the photosynthetically active part of the incoming solar flux (R_s^{ref} = 30 Wm^{-2} for trees and 100 Wm^{-2} for grassland and crops (Bougeault, 1991)).

$$R_{sc} = R_s(1 - \exp(-\alpha LAI)) \tag{2.43}$$

$r_{\min}$ is the minimum value of stomatal resistance and β_s is a soil moisture stress factor depending on the water availability in the active soil layer for agricultural and pasture land and in the transmission zone for forest land cover, written as:

$$\begin{aligned} \beta_s^{-1} &= 1 && \theta_1 \geq \theta_{cr} \\ \beta_s^{-1} &= \frac{\theta_1 - \theta_w}{\theta_{cr} - \theta_w} && \theta_w \leq \theta_1 \leq \theta_{cr} \\ \beta_s^{-1} &= 0 && \theta_1 < \theta_w \end{aligned} \tag{2.44}$$

Where θ_1 is the soil moisture content in the active layer layer (θ_2 the transmission zone soil moisture for forest land cover), θ_{cr} the critical value above which transpiration is not affected by the moisture stress in the soil, and θ_w the soil moisture content at the permanent wilting point. η_S, which accounts for the reduced activity of plants when the air temperature is very hot or very low is formulated as:

$$\eta_S = 1 - 0.0016(298.0 - T_a)^2 \tag{2.45}$$

The energy balance within the canopy height is

$$R_{nc} = H_c + L_e E_c \tag{2.46}$$

For a wet canopy there is no limit to the amount of water for evaporation. Hence, the evaporation from the entire wet canopy e_{wct} is determined by solving equation (2.34) for the temperature of the wet vegetated surface by setting z_o and d consistent with the type of wet vegetation, and setting r_s^c equal to zero. i.e.

$$e_{wct} = \frac{\rho c_p\left(e^*(T_c)-e_h\right)}{L_e\gamma\, r_{ac}} \qquad (2.47)$$

The transpiration rate from the dry canopy can be obtained as:

$$e_{dc} = (1-\omega\ )E_c \qquad (2.48)$$

Where E_c is the transpiration rate that can be obtained from equation (2.34) and ω is the area fraction of wet canopy given in equation (2.5).

2.2.2.2.3 Energy Balance at Soil Surface

The energy balance at the soil surface is given by (Shuttleworth and Gurney, 1990):

$$R_{ns} - L_e E_s - H_s - G = 0 \qquad (2.49)$$

Where:

$$L_e E_s = \frac{\rho c_p(e^*(T_s) - e_h)}{\gamma\ (r_{as} + r_s^s)} \qquad (2.50)$$

and

$$H_s = \frac{\rho c_p(T_s - T_h)}{r_{as}} \qquad (2.51)$$

The aerodynamic resistance at the soil surface is given by (Choudhury and Monteith, 1988):

$$r_{as} = \frac{h\exp(\lambda)}{\lambda_e K_h}\left[\exp(-\lambda_e z_o' / h) - \exp(-\lambda_e Z / h)\right] \qquad (2.52)$$

The actual rate of soil evaporation is taken as the minimum of a soil controlled exfiltration capacity f_e^*, or the atmospherically controlled evaporation rate, E_P,

$$E_s = \min(f_e^*, E_p) \qquad (2.53)$$

The potential evaporation from the soil surface is calculated from Priestley and Taylor (1972) equation (see Equation (A.24) in Appendix A3). The soil exfiltration capacity is given by Milly (1986) as a function of the cumulative exfiltration F_e, active zone moisture content at the start of an inter-storm period, and soil properties (see Appendix A2 for detail).

$$f_e^*(t, s_e) = \frac{1}{2} S_e\ t^{-1/2} - \alpha_v\, e_{dc} + w \qquad (2.54)$$

Where S_e is the exfilitration sorptivity of the soil, w is the rate of capillary rise (defined in section 2.3), and e_{dc} is the transpiration rate from dry the canopy.

The ground heat flux, in general, is given by Fourier's law.

$$G_s = -k_g \frac{dT}{dz} \tag{2.55}$$

If there is no measurement of ground heat flux, the soil heat flux at a given depth can, in principle, be calculated by means of Equation (2.55) from measurements of the soil temperature gradient, provided the thermal conductivity of soil, k_g is known. In our study the ground heat flux was estimated from a single thermal soil layer and average soil temperature measured at a certain depth using a thermocouple. The ground heat flux is approximated as:

$$G_s = \frac{k_g}{D_g}(T_s - T_g) \tag{2.56}$$

Where T_g is the soil temperature at depth D_g.

In addition the total sensible and latent heat fluxes of the soil-vegetation system are given as:

$$H = H_c + H_s \tag{2.57}$$

$$L_e E = L_e E_c + L_e E_s \tag{2.58}$$

Equations (2.46), (2.49), (2.53), (2.57), and (2.58) represent five simultaneous non-linear equations with seven unknowns (T_s, $e^*(T_s)$, T_h, e_h, T_c, $e^*(T_c)$, *and* r_s^s). However the saturation vapor pressure at the soil and canopy surfaces are functions of the surface/skin and canopy temperature respectively and so the number of unknowns is reduced to five. The above five non-linear equations are solved simultaneously to obtain the canopy temperature, surface temperature, air temperature at canopy height, evaporation from the soil surface, and transpiration from vegetation (see Appendix A3).

2.2.2.3 Evaporation for each Sub-Basin

The local rate of evapotranspiration, E for each sub-basin is determined by summing the total evaporation (transpiration, wet canopy evaporation, and evaporation from soil surface) from each land cover, weighted by their corresponding areal fractions α_j.

$$E = \sum_{j=1} \alpha_j (E_s + e_{dc} + e_{wc})_j \tag{2.59}$$

2.2.3 Soil Moisture Component

Soil moisture represents the temporary storage of precipitation in a shallow layer of the earth surface. In DPHM-RS the soil profile is assumed to have three homogeneous layers (the active layer, the transmission zone, and the saturated zone). The top active layer (usually range between 15 to 30 cm depth) simulates rapid changes of soil moisture content under high-frequency atmospheric forcing while the transmission zone characterizes the seasonal soil moisture behavior, which changes relatively slowly because of the overlying top active layer. Either of the two sets of simple soil water balance equations given in Section 2.2.3.1 or 2.2.3.2 will apply to each layer, depending upon the depth of the local groundwater table.

2.2.3.1 Capillary Fringe lies Within the Transmission Zone

In this case, the unsaturated zone is partitioned into an active layer of depth z_l and an underlying transmission zone. The vertical distance between the top of the capillary fringe and the base of the active layer is defined as the transmission zone of depth z_2 (see Figure 2.6).

The active layer water balance equation is

$$z_1 \frac{d\theta_1}{dt} = \sum_{j=1} \alpha_j i_v - \sum_{j=1} \alpha_j E_s - \alpha_{bs} e_{dc} - g_1 + w \tag{2.60}$$

for $\quad z - \psi_c \geq z_l \qquad \theta_r \leq \theta_l \leq \theta_s$

Where i_v is the infiltration rate into soil (Equation (2.63)), α_j is the fraction of land cover for each land use within a sub-basin, α_{bs} is the fraction of agricultural and pasture lands, g_l is the downward soil water flux from the base of the active layer, θ_l is the uniform moisture content which extends from the top of the capillary fringe to the land surface, θ_r is the residual moisture content, θ_s is the saturated soil moisture content, ψ_c is the depth of capillary fringe, and z is the depth of ground water table.

The transmission zone water balance equation is

$$z_2 \frac{d\theta_2}{dt} = g_1 - g_2 - \alpha_v e_{dc} \qquad z_2 > 0 \tag{2.61}$$

for $\quad z_2 = z - \psi_c - z_l \qquad \theta_r \le \theta_2 \le \theta_s$

Where α_v fraction of forest land covers, g_2 is the downward soil water flux from the base of the transmission zone and θ_2 is the uniform moisture content in the transmission zone.

2.2.3.2 Capillary Fringe lies Within the Active Layer

There is no transmission zone if the capillary fringe lies within the active layer.

The active layer water balance equation is

$$z_1^* \frac{d\theta_1}{dt} = \sum_{j=1} \alpha_j i_v - \sum_{j=1} \alpha_j E_s - \alpha_{bs} e_{dc} - g_1 + w \tag{2.62}$$

for $\quad z_l^* = z - \psi_c \qquad z_l > z - \psi_c \ge 0 \qquad \theta_r \le \theta_l \le \theta_s$

The actual infiltration rate into the soil is taken as the minimum of an infiltration capacity $f_i{}^*$, or the net rate of precipitation reaching the soil surface, i.e.

$$i_v = \min\left[f_i{}^*, \delta\, p + k \exp\left[b(C - S)\right]\right] \tag{2.63}$$

The infiltration capacity of a soil is given by Eagleson (1978) and Milly (1986) in terms of cumulative infiltration, F_i, soil properties, and the active layer moisture content at the start of each storm event (see Appendix A1 for detail).

$$f_i^* = A_o \left\{ 1 + \left[-1 + \left(1 + \frac{4 A_o F_i}{S_i^2} \right)^{1/2} \right]^{-1} \right\} - w \tag{2.64}$$

Where A_o is the saturated hydraulic conductivity at the rewetted moisture content, S_i is the infiltration sorptivity of the soil, and w is the rate of capillary rise.

The rate of capillary rise is based on the result of Gardner (1958) for a steady upward flow from a water table as:

$$w = m\vartheta / (z - \psi_c)^{\zeta} \tag{2.65}$$

Where the parameters m, ϑ, and ζ are functions of soil type and are given by Eagleson (1978) in terms of soil parameters of Brooks and Corey (1966) as:

$$\begin{aligned} \vartheta &= K_s(\psi_c)^{\zeta} \\ \zeta &= B \times \eta \\ m &= 1 + [1.5/(\zeta - 1)] \end{aligned} \tag{2.66}$$

Where B is the pore size distribution index. Drainage from the base of the active layer and transmission zone is assumed to proceed to gravity driven rates. These fluxes are described by (Brooks and Corey, 1966; Orlandini *et al.*, 1996):

$$g_1 = Max(K_s, f_i^*)\left[\frac{\theta_1 - \theta_r}{\theta_s - \theta_r}\right]^{\eta} \tag{2.67}$$

Where, $$\eta = \frac{2 + 3B}{B} \tag{2.68}$$

and g_2 is given by replacing θ_1 by θ_2 above.

Remotely sensed spatially distributed soil moisture data can be derived from Radarsat SAR image (see Chapter 5). This remotely sensed soil moisture information can serve as the initial soil moisture input to DPHM-RS or to update its soil moisture state variables.

2.2.4 Saturated Subsurface Flow

In modeling the unsaturated flow component, the soil water transport in the unsaturated zone is assumed vertical and non-interactive between sub-basins. The lower boundary condition of the unsaturated zone is the top of the capillary fringe controlled by the local average water table depth. As a result, the water table dynamic is useful to determine accurately the water and energy fluxes at a sub-basin scale. In DPHM-RS, the catchment scale, water table equation at a grid scale from Sivapalan *et al.* (1987) is modified for simulating the average water table for each sub-basin. The topographic-soil index of Beven (1986) is used to parameterize the spatial variability of topographic and soil properties, and thus the average water table depth for each sub-basin.

Sivapalan *et al.* (1987) derived a simple expression for the local water table depth z_i in terms of the local topographic- soil index, $\ln\left\{(aT_e)/(T_i \tan\beta_g)\right\}$ as:

$$z_i = \bar{z} - \frac{1}{f}\left\{\ln\left(\frac{aT_e}{T_i \tan\beta_g}\right) - \Lambda\right\} \tag{2.69}$$

where f is the exponential decay of saturated hydraulic conductivity per meter depth, a is the area drained through the local unit contour, T_e is the catchment average value of the saturated transmissivity coefficient (saturated hydraulic conductivity divided by f), T_i is the local value of the transmissivity coefficient, β_g is the local slope angle, Λ is the catchment average value of the topographic variable $\ln(a/\tan\beta_g)$, and $\bar{z}$ is the catchment average water table depth.

The parameter f can be determined following Beven's (1982) suggestion for various soils. The distribution of the topographic index can be calculated from the DEM or DTED data. To estimate the initial average water table depth, two procedures can be applied. If an initial base flow discharge is known, it is possible to use the inversion of the following equation with $Q_b = Q(0)$.

$$Q_b = Q_o \exp(-f\,\bar{z}) \tag{2.70}$$

Where $Q_o = AT_e \exp(-\Lambda)$

Where A is the catchment area. If the water table depth at a particular catchment grid element is known, the mean depth of the catchment's water table can be approximately estimated from Equation (2.69).

Modeling the temporal changes in $\bar{z}$ allows the spatial distribution, including the areal extent of hydrologically active saturated areas, to be updated in time. The temporal changes in average ground water table for each sub-basin have to satisfy the water balance for the whole catchment. From equation (2.69) the rate of change of the local water table depth dz_i/dt is equal to $d\bar{z}/dt$, the rate of change of the areal average water table depth. This quantity can be approximated by the overall mass balance considerations for a discretized catchment as $\Delta z / \Delta t$ (Famiglietti and Wood, 1994):

$$\frac{d\bar{z}}{dt} \approx \frac{\Delta z}{\Delta t} = \left[\sum_{j\in\Omega_1,\Omega_2} w_j + \sum_{j\in\Omega_3} Ej + Q_b / a_j - \sum_{j\in\Omega_1} g_2^j - \sum_{j\in\Omega_2} g_1^j \right] \bullet \left[\sum_{j\in\Omega_1} (\theta_s^j - \theta_2^j) + \sum_{j\in\Omega_2} (\theta_s^j - \theta_1^j) \right]^{-1} \tag{2.71}$$

Where Ω_1, Ω_2, and Ω_3 represents the regions where the top of the capillary fringe lies beneath the bottom of the active layer, within the active layer, and saturated grid elements respectively; Q_b is base flow; and a_j is the area of each sub-basin. The terms in the denominator of (2.71) represent the catchment storage deficit in the transmission and active layers respectively.

2.2.5 Surface Runoff

The runoff from each sub-basin flows through drainage paths at the surface and sub-surface layers to the nearest stream. In DPHM-RS, the surface runoff is transferred into stream flow using an average lag function characterizing the distribution of runoff for each sub-basin such as that shown in Figure 2.7. The average response function for each sub-basin is derived using the kinematic wave equation. In finding the response function in each sub-basin, a reference runoff (e.g., 1cm depth) is made available for one time step for all grid cells within the sub-basin. Then the kinematic wave equation is applied to each grid cell, which has a resolution of DTED, and the flow is routed from cell to cell based on eight possible flow directions until the total volume of water corresponding to the reference runoff for a sub-basin is completely evacuated.

Using the average response function, the actual surface runoff computed for each sub-basin would then distribute temporally at this time lag function. The resulting runoff becomes a lateral inflow to the stream channel within the sub-basin. The saturated excess runoff and infiltration excess or Horton runoff for vegetated (q_v) and bare land (q_{bs}) are computed within the model as:

$$
\begin{array}{ll}
q_{bs} = p & \text{if } \theta_1 = \theta_s \\
q_{bs} = p - f_i^* & \text{if } \theta_1 < \theta_s \text{ and } p > f_i^* \\
q_v = \delta p + k \exp[b(C-S)] & \text{if } \theta_1 = \theta_s \\
q_v = \delta p + k \exp[b(C-S)] - f_i^* & \text{if } \theta_1 < \theta_s \text{ and } \delta p + k \exp[b(C-S)] > f_i^*
\end{array}
\tag{2.72}
$$

The basic kinematic wave applied to each grid cell to derive the lag function characterizing the surface runoff from each cell to the outlet of sub-basin is defined as follows.

Continuity equation:

$$\frac{\partial R}{\partial x} + \frac{\partial y}{\partial t} = q \tag{2.73}$$

Kinematic equation:

$$y = \chi R^{\nu} \tag{2.74}$$

Where R is the surface runoff, y the flow depth, q the water available for runoff from the vertical water budget function, x the side length of each square cell, and t the time. Using Manning's equation, the coefficients ν and χ are given by

$$
\begin{gathered}
\nu = 0.6 \\
\chi = \left(\frac{n_m}{\sqrt{S_o}} \right)^{3/5}
\end{gathered}
\tag{2.75}
$$

Where n_m is Manning's roughness coefficient estimated from land -use classes, and S_o is the slope of the surface of the square. Equations (2.73) and (2.74) are solved using a non-linear kinematic wave scheme (see Chow *et al.*, 1988).

2.2.6 Channel Routing

In DPHM-RS the Muskingum-Cunge flow routing method is used to route flow through the drainage network. Though an approximate solution of a modified diffusion equation, it is one of the most effective flow routing techniques (Fread, 1985; Miller and Cunge, 1975). The recursive equation applicable to each sub-reach for each time step is

$$Q_{i+1}^{j+1} = C_1 Q_i^{j+1} + C_2 Q_i^{j} + C_3 Q_{i+1}^{j} + C_4 \tag{2.76}$$

Which is similar to the Muskingum method, but expanded to include lateral inflow (q) through the coefficient C_4. The coefficients C_1, C_2, C_3, and C_4 are given by

$$C_1 = \frac{\Delta t - 2KX}{2K(1-X)+\Delta t}$$

$$C_2 = \frac{\Delta t + 2KX}{2K(1-X)+\Delta t}$$

$$C_3 = \frac{2K(1-X) - \Delta t}{2K(1-X)+\Delta t}$$

$$C_4 = \frac{\bar{q}_l \, \Delta x \Delta t}{2K(1-X)+\Delta t} \tag{2.77}$$

In the conventional Muskingum method parameters K and X are determined from selected observed inflow and outflow hydrographs. In Muskingum-Cunge model, the storage constant, K and the coefficient expressing the relative influence of inflow on storage levels, X are defined as (Cunge, 1969):

$$K = \frac{\Delta x}{\bar{c}}$$

$$X = \frac{1}{2}\left(1 - \frac{\overline{Q}}{\overline{B}\,\bar{c}\,S_O \Delta x}\right) \tag{2.78}$$

in which $\overline{Q}$ is the discharge, $\overline{B}$ is the cross-sectional top width associated with the discharge, Δx is the reach length, S_o the bed slope, and $\bar{c}$ is the kinematic wave celerity. The bar indicates the variable is averaged over the reach and time step. In most cases these parameters are based on a certain reference $\overline{Q}$. However, Dooge (1973) showed that the assumption of constant parameters makes the solution dependent on reference values. Similarly, Ponce and Yevjevich (1978) showed that a more realistic approach, in which the parameters can be allowed to vary in space and time, will provide more accurate simulation of flood flows. As a result in DPHM-RS an iterative four-point approach is used to evaluate the variable parameters.

In addition, if there is a reservoir or lake within the catchment, the flows are routed using level-pool routing. The level-pool routing technique is based on some established stage-discharge relationships at the outlet of the lake or reservoir and assumes a horizontal water surface profile throughout the length of lake. This will provide a good approximation for unsteady flow routing in reservoirs which are not excessively long and in which the inflow hydrograph is not rapidly changing with time. The conservation of mass equation used is

$$\frac{ds}{dt} = I(t) - Q(t) + q(t) \tag{2.79}$$

Kinematically, the momentum equation can be replaced by a simple stage discharge relationship of the form:

$$Q = \phi \, y^{\varphi} \tag{2.80}$$

Where ϕ and φ are constants that depend upon geometric properties of the reservoir. For a rectangular cross-section reservoir or lake,

$$\phi = \sqrt{gL} \tag{2.81}$$

$$\varphi = 1.5$$

Where $g = 9.81$ ms^{-2} and L is the width at the outlet of the lake.

Equation (2.79) can be discretized using an iterative trapezoidal integration method as:

$$A_r(y_{t+\Delta t} - y_t) = \left[\frac{I_{i,t} + I_{i,t+\Delta t}}{2}\right]\Delta t - \left[\frac{Q_{o,t} + Q_{o,t+\Delta t}}{2}\right]\Delta t + \left[\frac{q_t + q_{t+\Delta t}}{2}\right]\Delta t \tag{2.82}$$

Where A_r is the lake or reservoir surface area; y is the stage level of the lake, I_i is the input stream flow, Q_o is the output stream flow, and q is the lateral inflow to reservoir. The above equation can also be applied for reservoirs with uncontrolled overflow spillway and gate-controlled spillway if the gate setting (height of the gate bottom above the gate sill) is a predetermined function of time.

2.2.7 Snowmelt Models

Snowmelt is an important component of the basin hydrology in countries where there is snowfall during winter season. The amount of snowmelt depends upon the energy available for melting the snow, and models ranging from the simple degree-day method to the data-intensive, surface energy method have been developed to simulate the snowmelt process. Sand (1990) applied a number of these models to both temperate and arctic regions and found that only the energy balance is applicable to all the test regions.

Douglas *et al.* (1992) applied three models (surface energy balance, degree-day temperature index, and the combined degree-day temperature/radiation index) to an Alaska watershed. They found that all three models perform very well with the energy balance model being the best. In DPHM-RS, the energy balance and the modified degree day methods developed by Riley *et al.* (1972) are incorporated to model the snowmelt process.

2.2.7.1 The Surface Energy Balance Model

The surface energy balance during snowmelt can be depicted as:

$$Q_m = R_n - L_e E - H + Q_c + Q_v - Q_{cc} \tag{2.83}$$

Where, Q_m the energy utilized for melting of the snowpack, Q_c energy flux via conduction between surface and subsurface, Q_{cc} energy deficit or cold content of the snowpack, Q_v advected energy in rainfall. In Equation (2.83), the heat transferred by snowmelt water away from the snow surface is ignored with the assumption that the quantity is small compared to others. The net radiation, latent heat, and sensible heat fluxes are given by equations (2.9), (2.48), (2.49) with the surface resistance $r_s^s = 0$ and the mean height of the roughness obstacles taken as snow depth. The advected heat in precipitation is given by

$$Q_v = c_p \rho_w p T_a \tag{2.84}$$

Where c_p is the specific heat of water, ρ_w is the density of water, p is precipitation depth, T_a is temperature of the air. In DPHM-RS the flux of heat exchange between the snowpack and the underlying ground is assumed to be negligible as compared to other magnitudes on a daily base. The cold content of the snowpack is given by

$$Q_{cc} = -\int_0^{D_s} \rho_p(z) c_s T_p(z) dz \tag{2.85}$$

Where D_s is the snowpack depth; z is the vertical coordinate, measured positively upward from ground surface; $\rho_p(z)$ is the snow pack density as a function of depth; $T_p(z)$ is the snow pack temperature profile; and c_s is the snow pack specific heat (~0.5 for all practical snow and ice densities). If the density of the snow pack and the temperature profile through out the snow depth are assumed constant, the depth averaged cold content is given by

$$Q_{cc} = -\rho_p c_s D_s T_p \tag{2.86}$$

The snowmelt model can be initiated at any time, with an input of the initial temperature and density of the snowpack to determine the cold content. However, no melting of the snow pack will occur until the snow pack is isothermal. The melt at snow surface is given by

$$h_s = \frac{Q_m}{\rho_w L_m} \tag{2.87}$$

Where h_s is the melt at snow-air interface; L_m is latent heat of freezing.

2.2.7.2 Modified Degree-Day Method

As an alternative to the energy-balance snowmelt model, the modified degree-day method developed by Riley *et al.* (1972) is also included as an option in DPHM-RS,

$$h_s = C_f \frac{R_s}{R_h}(T_a - T_{th})(1-\alpha_s) + 0.0125 p T_a \tag{2.88}$$

Where C_f the melt factor depends on land-use, R_s is the radiation index for a sloping surface (Frank and Lee, 1966), and R_h is the radiation index for a horizontal surface. During winter season for temperature around 0°C precipitation may either fall as snow or rain. For a given air temperature at the measuring station, the variation between snowfall and rainfall at each cell or within each sub-basin depends on the variation of temperature at the mean altitude of each cell or sub-basin. The change of temperature with respect to altitude depends on the lapse rate, which often varies between 0.5 to 1.0°C per 100m. Air temperature observed at the climate station is first interpolated to each cell. The threshold temperature separating between snowfall or rainfall is often assumed to be 0°C. If the simulation time step (hours) is 24 hours and there is no hourly data available, then, all precipitation is considered as solid if the maximum air temperature T_{max} is less than or equal to the threshold temperature. On the other hand, if the maximum temperature is greater than the threshold temperature, the fraction of precipitation considered as rain is given by

$$Rain = p\left(\frac{T_{\max} - T_{th}}{T_{\max} - T_{\min}}\right) \tag{2.89}$$

Where T_{th} is the threshold temperature and $T_{\min}$ is the minimum daily air temperature. When the time step is less than 24 hours, hourly values are assumed to be available and the hourly precipitation is added to either the rainfall or the snowfall total depending on the difference between the air temperature and the threshold temperature. The transformation of rainfall into snowfall takes into account the density of new snow as a function of air temperature using the following equation (Fortin *et al.* 1986).

$$\rho_p = 151 + 10.63T_a + 0.2767T_a^2 \tag{2.90}$$

2.3 Division of a River Basin into Sub-Basins

Theoretically, distributed, physically based hydrologic models should provide more accurate predictions of streamflow than lumped-parameter conceptual models. The current rapid development in computer technology increased the interest towards solving differential equations governing surface and subsurface flow over dense numerical grids. This requires the discretization of a heterogenious catchment into grid elements, which has been an on going research topic for several decades. Various methods of aggregating point scale processes at grid scale have been proposed to account for the highly heterogeneous properties of watersheds and spatial variability of hydroclimatic data.

For models operating on a grid base, Wood *et al.* (1988) proposed the concept of representative elemental area (REA) which represents the scale at which the spatial variability largely disappears in catchment runoff. However, Fan and Bras (1995) showed that the concept has limited use in catchment hydrology as REA is relative to the resolution of the model, is "artificial", and does not exist in natural environment. On the other hand, even though hydrological processes of distributed models have been discretized at the grid scale (say REA), almost all practical applications of such models experience a certain degree of compromise due to the limitation of input data. Beven (1989, 1996) even argued that, it is very difficult to estimate effective model parameter values for the current generation of fully distributed physically based hydrologic models to operate at elemental scale. Another group of researchers concentrated on the development of semi-distributed conceptual/physical models. Such models involve discretization schemes such as the hydrological response unit (HRU) or the group response unit (GRU) (Amerman, 1965; England and stephenson, 1970; Fortin *et al.* 1986; Martinec *et al.*, 1983; Kouwen, 1988; Kite, 1995). Kite and Pietroniro (1996) provided a full review of various discretization processes.

DPHM-RS accounts for the spatial variation of meteorological inputs and the effects of different land use control on different hydrological variables by dividing the catchment into a number of sub-basins drained by a defined drainage network. The hydrologic processes are evaluated for different land covers at point scale and then aggregated according to the proportions of the land cover present within the sub-basin. As a result, land use types play a part to the hydrologic response of each sub-basin to climatic forcing. Finally, the surface runoff of each sub-basin is routed to the channel network based on an average response function derived for each sub-basin. The study site, Paddle River Basin of Central Alberta (265 km^2) is divided into five sub-basins and terrain feature is the primary criterion used in the sub-division. The distribution of six land-use types considered among the five sub-basins are derived from a Landsat TM image and the details are elaborated in Chapter 3.

2.4 Calibration of Model Parameters

Traditionally the criterion of model parameter calibration is minimizing the difference between simulated and observed discharges at the outlet of the catchment. This method has also been used in distributed hydrologic models. However, lately some authors have expressed doubts about the use of such calibration criterion in fully distributed hydrologic models (e.g., Beven, 1989; Refsgaard, 1997) because of the large number of parameters involved in distributed models. The distributed nature of models cannot be fully realized by this traditional method of calibration. The calibration processes should take into account the distributed nature of internal processes within the model. In other words, a multi-objective calibration criterion should be adopted for distributed models.

In DPHM-RS, the number of parameters that can be optimized is kept as low as possible. Table 2.2 shows the parameter classes used in the model. The average (or initial) estimate for most parameters can be easily obtained from field measurement or from past values proposed by different authors. The model calibration component is elaborated in the Chapter 3.

2.5 Summary

A semi-distributed, physically based hydrologic model (called DPHM-RS) is developed. The model characterizes basin scale, hydrologic processes at sub-basin level, with each sub-basin having its own land cover types and terrain features. The hydrologic processes are evaluated for different land covers and then aggregated according to proportions of the land cover present within each sub-basin. The actual ET from each land cover is estimated using the two-source model, the soil moisture at the active soil layer and the transmission zone is estimated by a water budget approach, and the surface runoff from each sub-basin is routed to the channel network using a response function derived for each sub-basin. The runoff is then routed through the channel systems to the basin outlet using the Muskingum-Cunge model.

In order to model such hydrologic processes at sub-basin scale effectively, ground-based point measurements alone are not sufficient. Spatially distributed hydrologic data are necessary. Therefore, DPHM-RS is designed to take advantage of the spatial topographic information of DTED processed by a GIS and spatial hydrologic information of satellite data. With more and more space platforms being launched, satellite data become more readily available for hydrologic and other geophysical applications. It seems that hydrologic models that utilize satellite data may some day replace lumped conceptual models in operational hydrology. Furthermore, models such as DPHM-RS can be used for studies on the hydrologic impact of land use changes, and can become the land surface components of GCMs, or coupled with mesoscale atmospheric models for climate change studies.

References

Abbott, M. B. (1972) The use of digital computers in hydrology. In Teaching Aids of Hydrology, Technical papers in Hydrology 11, *UNESCO*, LC No. 72-87901.

Abbott, M. B., Bathurst, J. C., Cunge, J. A., O'Connell, P. E., and Rasmussen, J. (1986) An introduction to the European hydrological system-System hydrologique Europeen, 'SHE', 1: History and philosophy of a physically-based, distributed modeling system. *Jour. of Hydrol.*, 87(1/2), 45-59.

Amerman, C. R. (1965) The use of unit-source watershed data for runoff prediction. *Water Resour. Res.*, Vol. 1, No. 4, pp. 499-507.

Bathurst, J. C. and O'Connell, P. E. (1992) Future of distributed modelling: the Systeme Hydrologique Europeen. *Hydrological Processes* 6(3), 265-277.

Beven, K. J. (1982) On subsurface stormflow: an analysis of response times. *Hydrol. Sci. J.*, 27, pp. 505-521.

Beven, K. J. (1986) Runoff production and flood frequency in catchments of order n: An alternative approach, in *Scale Problems in Hydrology*, edited by V. K. Gupta *et al.*, pp. 107-131, *D.* Reidel, Norwell, Mass.

Beven, K. J. (1989) Changing ideas of hydrology: the case of physically-based models. *J. Hydrol.*, 105, 157-172.

Beven, K. J., Calver, A., and Morris, E. M. (1987) The Institute of Hydrology distributed model. *Institute of Hydrology Report 98*, Wallingford, UK.

Beven, K. J., Lamb, R., Quinn, P., Romanowicz, R. and Freer, J. (1995) TOPMODEL, in V. P. Singh (Ed.), Computer Models of watershed hydrology, *Water Resources Publications*, Colorado, 627-668.

Beven, K. J. (1996) A discussion of distrinuted hydrological modelling. In M. B. Abbott and J. C. Refsgaard (eds.), Distributed hydrological modelling, *Water Resour. Pub.*, pp.255-278.

Bougeault, P. (1991) Parameterization schemes of Land-Surface processes for mesoscale Atmospheric models. In Schmugge, T. J. and Andr'e, J. (Editors), Land Surface Evaporation. *Springer*, New York, pp. 55-92.

Brooks, R. H., and Corey, A. T. (1966) Properties of porous media affecting fluid flow. J. Irrig Drain. Div., Proc. *Amer. Soc. Civil Eng.*, 92(IR2), pp. 61-68.

Brutsaert, W. (1982) Evaporation into the Atmosphere. *D. Reidel Pub. Co.*, Dordrecht, Holland.

Burnash R. J., Ferral R. L., and Mcguire R. A. (1973) A generalized stream flow simulation system, Conceptual modeling for digital computers, *U. S. NWS, Sacramento*, California.

Choudhury, B. J. and Monteith, J. L. (1988) A four-layer model for the heat budget of homogeneous land surfaces. *Q. J. R. Meteorol. Soc.*, 114, pp. 373-398.

Chow V. T., D. R. Maidment, L. W. Mays (1988) Applied Hydrology, *McGraw-Hill International Editions*, pp. 1-572.

Clark, C. O. (1945) Storage and the unit hydrograph. *Trans. ASCE*, Vol. 110, pp. 1419-1446.

Cogan, J. L. (1985) Remote sensing of surface and near surface temperature from remotely piloted aircraft. *Applied Optics*, 24, pp. 1030-1036.

Crawford, N. H., and Linsley, R. K. (1966) Digital simulation in hydrology; Stanford Watershed Model IV. Dept. of Civil Eng., Stanford University, *Tech. Rept. No. 39*.

Cunge, J. A. (1969) On the subject of a flood propagation computation method (Muskingum method), *Journal of Hydraulic research*, Vol. 7, No. 2, pp. 205-230.

Deardorff, J. W. (1978) Efficient prediction of ground surface temperature and moisture, with inclusion of layer of vegetation. *J. Geophys. Res.*, 83, pp.1889-1903.

Dickinson, R.E. (1984) Modelling evapotranspiration for three-dimensional global Climate models, in Climate processes and Climate sensitivity, *Geophys. Monogr. Ser.*, 29, J.E. Hansen and T. Takahashi, ed., pp.58-72, AGU, Washington, D.C.

Dooge, J. C. I. (1973) Linear Theory of Hydrologic Systems. *Agricultural Research Service Technical Bulletin No. 1468.*

Douglas L. Kane, Robert E. Gieck, Gerd Wendler and Larry D. Hinzman (1992) Snowmelt at a small Alaskan Arctic Watershed 2. Energy Related Modeling results. *9th International Northern Research Basins Symposium/Workshop, Canada, NHRI Symposium No. 10,* T. D. Prowse, C.S.L. Ommanney & K.E. Ulmer (editors), P.227-247.

Duchon, C. E., Salisbury, J.M., Lee Williams, T. H., and Nicks, A. N. (1992) An example of using Landsat and GOES data in a water budget model. *Wat. Resour. Res.* 28(2), 527-538.

Dyer, A. J., Hicks, B. B. (1970) Flux-gradient relationships in the constan flux layer. *QJR Meteorol Soc* 96:715.

Eagleson, P. S., Mejia-r, R. and March, F. (1965) The Computation of optimum realizable unit hydrographs from rainfall and runoff data. *Hydrodyn. Lab. Rep.* No. 84, MIT.

Eagleson, P. S. (1978) Climate, soil, and vegetation, 3. A simplified model of soil moisture movement in the liquid phase, *Water Resour. Res.*, 14(5), pp. 722-730.

England, C. B., and Stephenson, G. R. (1970) Response units for evaluating the hydrologic performance of rangeland watersheds. *J. Hydrol.*, 11, pp. 89-97.

Environmental Protection Agency (EPA) (1991) Global ecosystems database documentation, in EPA Global Climate Research Program NOAA/NGDC Global change database program, *EPA Res. Lab.*, Corvallis, Ore.

Famiglietti, J. S., and E. F. Wood (1994) Multi-scale modeling of spatially-variable water and energy balance processes, *Water Resour. Res.*, 30(11), pp. 3061-3078.

Fan, Y. and Bras, R. (1995) On the concept of a representative elementary area in catchment runoff. *Hydrol. Processes*, Vol. 9, 821-832.

Fortin, J. P., Villeneuve, J. P., Guibot, A., and Seguin, B. (1986) Development of a modular hydrological forecasting model based on remotely sensed data, for interactive utilization on a microcomputer. *Hydrologic applications of space technology*, A. I. Johnson, ed., 307-319.

Frampton, M. and Marks, D. (1980) Mapping of snow surface temperature from thermal satellite data in the southern sierra Nevada. *Proceedings of the Western Snow Conference*, 88-96.

Frank, E. C. and Lee, R. (1966) Potential solar beam irradiation on slopes. *US Forest Service research paper RM-18*, 116 p.

Fread, D. L. (1985) Channel routing, Chap. 14 in *Hydrological Forecasting*, ed. by M.G. Anderson and T. P. Burt, *Wiley, New York*, pp. 437-503.

Freeze, R. A. and Harlan, R. L. (1969) Blueprint for a physically-based digitally-simulated hydrological response model. *Journal of Hydrology*, 9, 237-258.

Gan, T. Y., Biftu, G. F. (1996) Automatic calibration of conceptual rainfall-runoff models: optimization algorithms, catchment conditions, and model structure. *Water Resources Research*, American Geophysics Union, Vol. 32, No. 12, pp. 3513-3524.

Gan, T. Y., Dlamini, E. M., Biftu, G. F. (1997) Effects of model complexity and structure, data quality, and objective functions on hydrologic modeling. *Journal of Hydrology*, Elsevier Science, 192, pp. 81-103.

Gardner, W. R. (1958) Some steady-state solutions of the unsaturated moisture flow equation with application to evaporation from a water table. *Soil Sci.*, 85(4), pp. 228-232.

Grayson, R. B., Moore, I. D., and McHahon, T. A. (1992) Physically based hydrological modelling. 1. A terrain-based model for investigative purposes. *Water Resources Research*, 28(10), 2639-2658.

Jarvis, P. G. (1976) The interpretation of the variations in leaf water potential and stomatal conductance found in canopies in the field. *Philos. Trans. R. soc. London Ser. B 273*, pp. 593-610.

Kite, G. W. (1995) Scaling of input data for macroscale hydrologic modeling. *Water Resour. Res.*, 31(11), 2769-2781.

Kite, G. W. and Pietroniro, A. (1996) Remote sensing applications in hydrological modelling. *Hydrological Sciences Journal*, 41(4):563-591.

Klemes, V. (1988) A hydrological perspective. *Journal of Hydrology*, 100, 3-28.

Kouwen, N. (1988) WATFLOOD. A micro-computer based flood forecasting system based on real- time weather radar. *Can. Water. Resour. J.*, 13(1), 62-77.

Liang, X. (1994) A two-layer variable infiltration capacity land surface representation for general circulation models. *Water Resources Series, Technical Report No.* 140:208, University of Washington, Seattle.

Link, L. E. (1983) Compatibility of present hydrologic models with remotely sensed data. *Proc., 17th Int. Symp. on Remote Sensing of Envir.*

Louis, J. (1979) A parametric model of vertical eddy fluxes in the atmosphere, *Boundary Layer Met.* 17, pp. 187-202.

Martinec, J., Rango, A. and Major, E. (1983) The Snowmelt-Runoff Model (SRM) User's Manual, *NASA Reference Publ.* 1100. Goddard Space Flight Center, Greenbelt, Maryland, USA.

Miller, W. A. and Cunge, J. A. (1975) Simplified equations of unsteady flow. Unsteady flow in open channels, K. Mahmood and V. Yevjevich, eds., *Water Resources Publications*, Fort Collins, Colorado.

Milly, P. C. D. (1986) An event-based simulation model of moisture and energy fluxes at a bare soil surface, *Water Resour. Res.*, 22(12), pp. 1680-1692.

Murphy, C. E. Jr. and Knoerr, K. R. (1975) The evaporation of intercepted rainfall from a forest stand: An analysis by simulation, *Water Resour. Res.*, 11, pp 273-280.

Nash, J. E. (1957) The form of the instantaneous unit hydrograph. *Inter. Assoc. Sci. Hydrol.* Pub. No. 45, 3, pp. 114 -121.

Ottl'e, C., and Vidal-Madjar, D. (1994) Assimilation of soil moisture inferred from infrared sensing in a hydrological model over the HAPEX-MOBILHY region. *Journal of Hydrology*, 158, pp. 241-264.

Ponce, V. M. and Yevjevich, V. (1978) Muskingum-Cunge method with variable parameters. *Proceedings of American Society of Civil Engineers*, Vol. 104, No. HY12.

Priestley C. H. B., Taylor, R. J. (1972) On the assessment of surface heat flux and evaporation using large scale parameters. *Mon. Weather Rev.* 100:81-92.

Rafsgaard, J. C. (1997) Parameterisation, calibration, and validation of distributed hydrological models, *J. of Hydrology*, 198, pp. 69-97.

Rafsgaard, J. C. and Abbott, M. B. (1996) The role of distributed hydrological modelling in water resources management. In M. B. Abbott and J. C. Refsgaard (eds.), Distributed hydrological modelling, *Water Resources Publications,* 1-16.

Rafsgaard, J. C. and Storm, B. (1995) MIKE SHE. In V. J. Singh (Ed) Computer models in watershed hydrology. *Water Resources Publications.*

Riley, J. P., Israelsen, E. K., Eggleston, K. O. (1972) Some approaches to snowmelt prediction. Actes du Colloque de Banff sur le role de la neige et de la glace en hydrologie. *AISH Pub.*, Vol. 2, No 107, p. 956-971.

Rodriguez-Iturbe, I. and Valdes, J. B. (1979) The geomorphologic structure of hydrologic response. *Water Resour. Res.*, Vol. 15(6), pp. 1409-1420

Rutter, A. J. (1967) An analysis of evaporation from a stand of Scots Pine. In: W. E. Sopper and H. W. Lull (Editors), *Forest Hydrology*. Pergamon, Oxford, pp. 403-417.

Rutter, A. J., Kershaw, K. A., Robins, P. C., and Morton, A. J. (1971/72) A Predictive model of rain interception in forests, 1. Derivation of the model from observations in a plantation of Corsican Pine. *Agric. Meteorolo.*, 9:367-384.

Rutter, A. J., Morton, A. J., and Robins, P. C. (1975) A Predictive model of rain interception in forests, 1. Generalization of the model and comparison with observations in some coniferous and hardwood stands. *J. Appl. Ecol*, 12:364-380.

Sand, K. (1990) Modeling snowmelt runoff processes in temperate and arctic environments. University of Trondheim, *Norwegian Institute of Technology*, IVB-rapport B-2-1990-1, 176pp.

Sivapalan, M., Wood, E. F., Beven, K. J. (1987) On hydrologic similarity, 2, A scaled model of storm runoff production, *Water Resour. Res.*, 23(12), 2266-2278.

Satterlund, D. R., (1979) An improved equation for estimating long-wave radiation from the atmosphere. *Water Resour. Res.*, 11, pp. 742-744.

Sherman, L. K. (1932) Streamflow from rainfall by the unit-graph method. *Eng. News Record*, vol. 108, pp. 501-505

Shaw, R. H. and Pereira, A. R. (1982) Aerodynamic roughness of a plant canopy. A numerical experiment. *Agric. Meteorol.*, 26, pp. 51-65.

Shuttleworth, J. W. (1991) Evaporation models in hydrology. In Schmugge, T. J. and Andr'e, J. (Editors), Land Surface Evaporation. *Springer, New York*, pp. 93-120.

Shuttleworth, J. W. and Gurney, R. J. (1990) The theoretical relationship between foliage temperature and canopy resistance in sparse crops. *Q. J. R. Meteorol. Soc.*, 116, pp. 497-519.

Shuttleworth, J. W. and Wallace, J. S. (1985) Evaporation from sparse crops-an energy combination theory. *Q. J. R. Meteorol. Soc.*, 111, pp. 839-855.

Smith, E. A., Cooper, H. J., Crosson, W. L., and Wang H. (1993) Estimation of surface heat and moisture fluxes over a prairie grassland 3. Design of hybrid physical/remote sensing biosphere model, *J. Geophys. Res.*, 98(D3), pp. 4951-4978.

Stewart, J. B. (1977) Evaporation from the wet canopy of pine forest, *Water Resour. Res.*, 13, pp. 915-921.

Snyder, W. M. (1955) Hydrograph analysis by the method of least squares. *Proc. ASCE.*,, Vol. 81, 793.

Tao, T. and Kouwen, N. (1989) Remote sensing and fully distributed modeling for flood forecasting. *J. Wat. Resour. Plan. Manag. Div. ASCE* 115(6), 809-823.

Webb, E. K. (1970) Profile relationship: The log-linear range, and extension to strong stability. *Quart J. R. Meteorol. Soc.* 96:67-90.

Wood, E. F., Sivapalan, M., Beven, K. and Band, L. (1988) Effects of spatial variability and scale with implications to hydrologic modelling. *J. Hydrol.* 1020, 29-47.

List of Symbols

A	Catchment area
A_h	Advected energy into the layer
A_o	Saturated hydraulic conductivity at rewetted moisture content
A_r	Lake or reservoir surface area
a	Area drained through the local unit contour
a_s	Parameter indicating fraction of radiation on overcast day
B	Pore size distribution index
$\bar{B}$	Mean top cross-sectional width of flow
b	Rutter drainage parameter
b_s	Parameter indicating fraction of radiation on days with sunshine
C	Depth of water stored in the canopy
$\bar{c}$	Average celerity for computing storage parameters
$C1, C2, C3, C4$	Muskingum-Cunge coefficients
C_f	Melt factor depending on land use
C_o	Initial depth of water stored in the canopy
c_s	Snowpack specific heat
c_p	Specific heat at constant pressure
c	Defined by equation [30]
D	Zero plane displacement height for full canopy
d	Zero plane displacement height for partial canopy
D_e	Dimensionless desorption diffusivity
D_g	Depth at which the average soil temperature is measured
D_i	Effective infiltration diffusivity
D_s	Depth of the snowpack
E	Total evapotranspiration above Canopy
E_c	Transpiration from Canopy
E_p	Potential evaporation at soil surface.
E_s	Actual evaporation from the soil
e_a	Vapor pressure of the air above canopy
e_{dc}	Transpiration rate from dry canopy

e_h	Vapor pressure of air at within-canopy source height
e_{wc}	Wet canopy evaporation rate
e_{wct}	Rate of Evaporation from entire wet canopy
$e^*(T)$	Saturated vapor pressure at temperature T ($T= T_a, T_c, T_s$)
F_i	Cumulative infiltration
F_p	Specific flux of CO_2
F_w	Defined by equations [25] and [26]
f	Exponential decrease (with depth) parameter for K_s
f_c	Fractional cloud cover
f_i^*, f_e^*	Infiltration and exfiltration capacity of soil respectively
f_r	Defined by equation [42]
G_s	Ground heat flux
g	Gravitational acceleration
g_1	Downward soil water flux from active layer
g_2	Downward soil water flux from the base of transmission zone
g_r	Root extraction function
H, H_c, H_s	Sensible heat flux above the canopy, from the canopy, and from the soil
h	Mean canopy height
h_s	Snow water equivalent at snow-air interface
I	Input flow from upstream of channel reach
I_o	Solar constant
i_v	Infiltration rate into soil surface
K	Storage coefficient
K_h	Eddy diffusion coefficient at the top of the canopy
K_L	Constant in the relationship of S to LAI
K_s	Saturated hydraulic conductivity
k	Rutter drainage parameter
k_g	Thermal conductivity of soil
L	Width at the outlet of the lake.
LAI	Leaf Area Index
$LAI_{\max}$	Maximum leaf area index

L_e	Latent heat of vaporization
L_m	Latent heat of freezing
L_p	Thermal conversion factor for the fixation of CO_2
m	Index relating soil properties
N	Number of hours of daylight.
$NDVI$	Normalized Difference Vegetation Index
n	Number of hours of sunshine
n'	Attenuation coefficient for wind speed
n_m	Manning's roughness coefficient
p	Precipitation rate
Q	Channel flow
Q_b	Base flow from aquifer
Q_c	Energy flux via conduction between surface and subsurface
Q_{cc}	Cold content of the snow pack
Q_o	Out put flow at the end of channel reach
Q_m	Energy utilized for melting of the snowpack
Q_v	Advected energy in rainfall
$\overline{Q}$	Average discharge for computing storage parameters
q	Net lateral inflow
R	Surface runoff
R_h	Short wave radiation for a horizontal surface
R_{iB}	Bulk Richardson number
R_{ld} , R_{lu}	Downward and upward long wave radiation respectively
R_n	Net radiation at reference height
R_{nc} R_{ns}	Net radiation on the canopy and at soil respectively
R_s	Short wave radiation
R_{sc}	Incoming solar radiation at the surface of canopy
R_s^{ref}	Reference incoming solar-flux for photosynthetically active canopy.
r_{aa}	Above canopy aerodynamic resistance
r_{ac}	Bulk boundary layer resistance of the canopy

r_{as}	Aerodynamic resistance between the soil and within-canopy source height
r_b	Mean boundary layer resistance per unit area of vegetation
r_{min} , r_{max}	Minimum and Maximum canopy resistance
r_s^c , r_s^s	Bulk canopy and soil surface resistances respectively
S	Canopy water storage capacity
S_e, S_i	Exfiltration and Infiltration sorpitivity of soil respectively
S_o	Slope of the surface or channel
s	Channel storage
T_a , T_c	Air temperature near surface and Canopy temperature respectively
T_e	Catchment average saturated transmissivity coefficient
T_g	Soil temperature at depth D_g
T_h	Air temperature at within-canopy source height
T_i	Local value of transmissivity coefficient
T_{min}, T_{max}	Minimum and Maximum air temperature respectively
T_p	Snowpack temperature
T_s	Skin surface temperature
T_{th}	Threshold temperature
t	Time
U_c	Correction factor for atmospheric stability
u	Wind speed at above-canopy reference height
u_h	Wind speed at top of canopy
$u*$	Friction velocity
V_a	Modified wind speed
W	Stored energy per unit area in the layer
w_f	Leaf width
w	Rate of capillary rise
X	Storage proportion coefficient in Muskingum method
x	Grid cell size
y	Flow depth or stage
$\bar{z}$	Catchment average groundwater depth
Z_o	Roughness length for full canopy

z	Actual depth into soil profile
z_1, z_2	Depth of active soil layer and transmission zone respectively
z_a	Reference height above canopy
z_i	Local water table depth
z_o	Roughness length for sparse canopy
z'_o	Roughness length for bare soil
z_r	Modified reference height
z_1^*	Reduced depth of active layer for capillary fringe within actual active layer
α	0.5cosec(θ) (attenuation coefficient for radiation)
α_1 α_2	Coefficents as defined in equations [A.30] and [A.34] respectively.
α_{bs}	Fraction of agricultural and pasturelands
α_v	Fraction of forest land covers
α_j	Fraction of land cover for each land use within a sub-basin
α_r	Defined by equation [41]
α_s	Surface albedo
β	Coefficient for the correction of aerodynamic resistance
β_1, β_2	Coefficents as defined in equations [A.31] and [A.35] respectively.
β_g	Local slope angle of ground surface
β_s	Soil moisture stress factor
χ	Coefficient in kinematic equation
δ	Free throughfall coefficient
ε_{ac}	Atmospheric emissivity under clear skies
ε_s	Surface emissivity
ϕ	Constant that depend up on geometric properties of reservoir
γ	Psychrometric constant
η	Defined by equation [69]
η_s	Factor for reduced activity of plants for very hot or low air temperature
φ	Constant that depend up on geometric properties of reservoir
κ	Von Karman's constant = 0.41

Λ	Catchment average topographic variable
λ_e	Attenuation coefficient for eddy diffusity
ν	Coefficient in kinmatic equation
θ	Solar altitude
θ_o	Initial soil moisture content in the active layer
θ_1, θ_2	Soil moisture content in the active layer and transmission zone respectively
θ_{cr}	Critical moisture content with no effect of moisture stress for transpiration
θ_r, θ_s	Residual and saturated soil moisture content respectively
θ_w	Soil moisture content at permanent wilting point
ρ	Density of air
ρ_p	Density of snowpack
ρ_w	Density of water
σ	Stefan-Boltzmann constant $=5.6679\times10^{-2}$ Wm^{-2} k^{-4}
τ	Coefficient for correction of atmospheric emissivity for cloud effect
υ	Coefficient relating soil properties
ω	Area fraction of wet canopy
ψ_c	Depth of capillary fringe
ψ_m	Surface layer stability correction for momentum
ζ	Index relating soil properties
$\Omega_1, \Omega_2, \Omega_3$	Regions indicating where top of the capillary fringe lies

Table 2.1 Summary and comparison of the general characteristics of some distributed and semi-distributed hydrological models.

Classification	**SHE**	**TOPMODEL**	**HYDROTEL**	**WATFLOOD**	**SLURP**	**DPHM-RS**
Operation mode	REA[1]	REA	HHU[2]	GRU[3]	ASA[4]	Sub-basin
Modeling time steps	Fraction of hours	Hourly or Daily	Daily	Daily	Daily	Fraction of Hours -Days
Interception	Rutter et al.(1971/72)	Rutter et al. (1971/72)	None	Linsley et. al (1949)	Spittlehouse (1949)	Rutter et al. (1971/72)
Actual/potential Evapotranspiration	Penman-Monteith	Energy balance at soil-atmospheric interface and exfilitration capacity of soil.	Thornthwaite (1948) Linacre (1977) Monteith (1965) Priestley-Taylor (1972)	Constant value	Morton (1983) Granger (1995) Spittlehouse (1989)	Two-source model and exfilitration capacity of soil
No. of soil moisture storage zones	Depends on vertical grid resolution in solution of Richard's equation	Three: Upper zone, transmission zone, and ground water zone	Two or Three based on the choice of alternative model component	Three: Surface storage, upper zone storage, and base flow	Two: Fast store and slow store	Three: active layer, transmission zone, and ground water zone
Infilitration model	One-dimensional Richards equation	Milly (1986) equation	Darcy equation	Green & Ampt equation	Green & Ampt equation	Milly (1986) equation
Overland flow	Two- dimensional diffusion wave	None: fluxes are aggregated depending up on the proportion of vegetated and bare ground	Kinematic wave equation or response function for each HHU	Manning's Equation	Manning's equation	Response function derived using Kinematic wave theory for each sub-basin
Interflow	None			Linear reservoir	None	
Base flow	Two-dimensional saturated sub-surface flow	Groundwater level is updated based on topographic-soil index	None	Constant value	Base on non-linear reservoir	Groundwater level is updated based on topographic-soil index
Channel routing	one-dimensional diffusion wave	None	Modified kinematic wave or Diffusive wave	Storage routing	Storage routing	Muskingum-Cunge method

---

[1] Representative Elemental Area
[2] Hydrologically Homogenous Unit
[3] Group Response Unit
[4] Aggregated Simulation Area

Table 2.2 Parameters of the DPHM-RS model

Parameter	Description	Sensitivity	Remark
	Energy Flux		
a_s	fraction of radiation on overcast day	high	required for daily simulation
b_s	fraction of radiation on sunshine day	high	required for daily simulation
	Vegetation		
w_f	Leaf width	low	estimated for different vegetation type
C_o	Initial Canopy storage	low	estimated as percent of canopy capacity
λ	Attenuation coefficient for eddy diffusivity	moderate	estimated based on past research value
n'	Attenuation coefficient for wind speed	Low	Estimated based on past research value
r_{min}	minimum canopy resistance	moderate	estimated
	Soil		
z_l	depth of active soil layer	Moderate	Estimated
f	exponential decrease parameter for K_s	moderate	estimated and then calibrated
K_s	saturated hydraulic conductivity	moderate	estimated based on soil type
θ_{cr}	critical moisture content	low	estimated based on soil type
θ_w	moisture content at permanent wilting point	low	estimated based on soil type
θ_s	saturated moisture content	high	estimated based on soil type
θ_r	residual moisture content	moderate	estimated based on soil texture
B	Pore size index	moderate	estimated based on soil texture
k_g	soil thermal conductivity	low	estimated
z'_o	roughness length for bare soil	low	estimated
$\bar{z}$	Catchment average groundwater depth	moderate	estimated from surrounding well development
n_m	Manning roughness	moderate	estimated and then calibrated
	Channel		
$\bar{B}$	Mean cross-sectional top width	moderate	estimated and then calibrated
n_m	Manning roughness	moderate	estimated and then calibrated

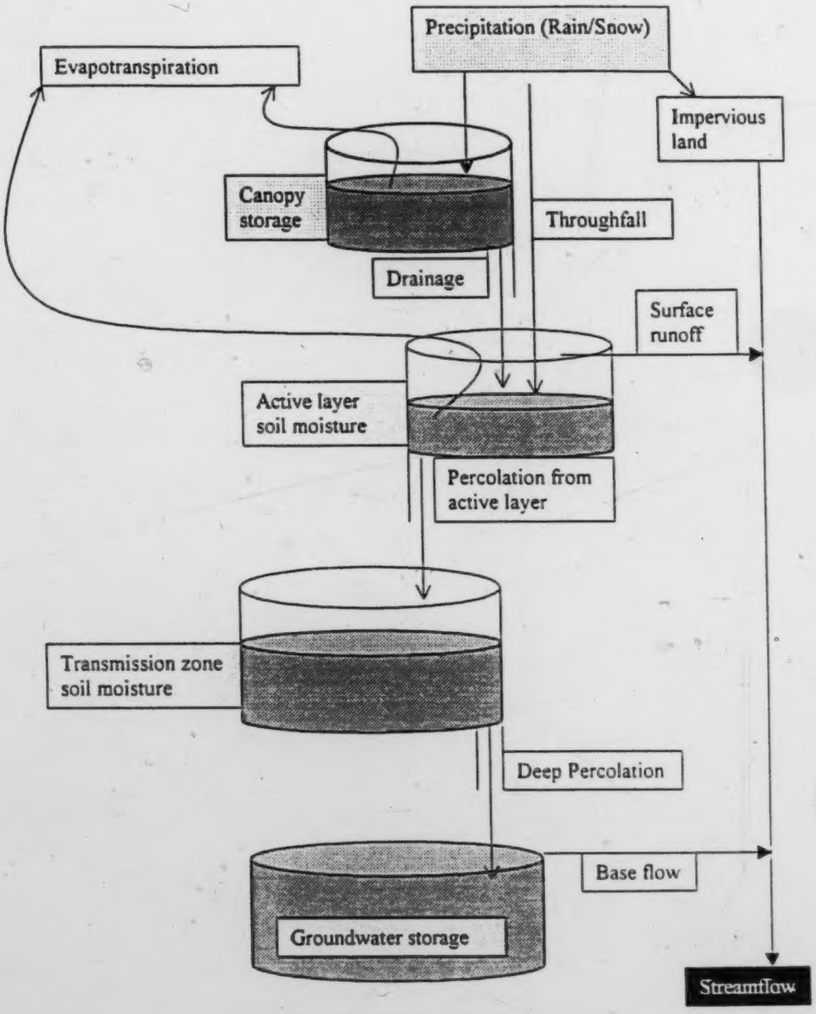
Precipitation (Rain/Snow)
Evapotranspiration
Impervious land
Canopy storage
Throughfall
Drainage
Surface runoff
Active layer soil moisture
Percolation from active layer
Transmission zone soil moisture
Deep Percolation
Base flow
Groundwater storage
Streamflow

Figure 2.1 Flow Chart of DPHM-RS model for each sub-basin

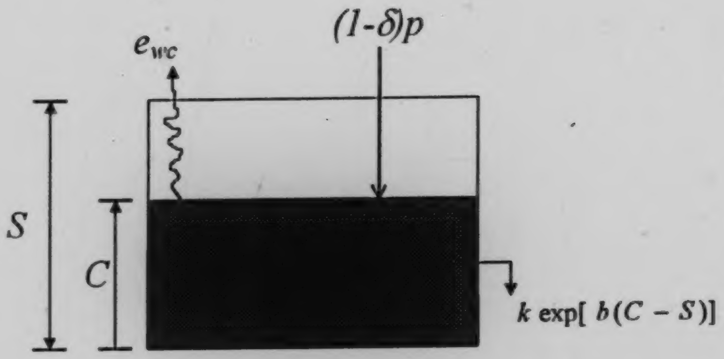
e_{wc}
$(1-\delta)p$
S
C
$k\ \exp[\ b(C - S)]$

Figure 2.2 Water balance scheme of a canopy

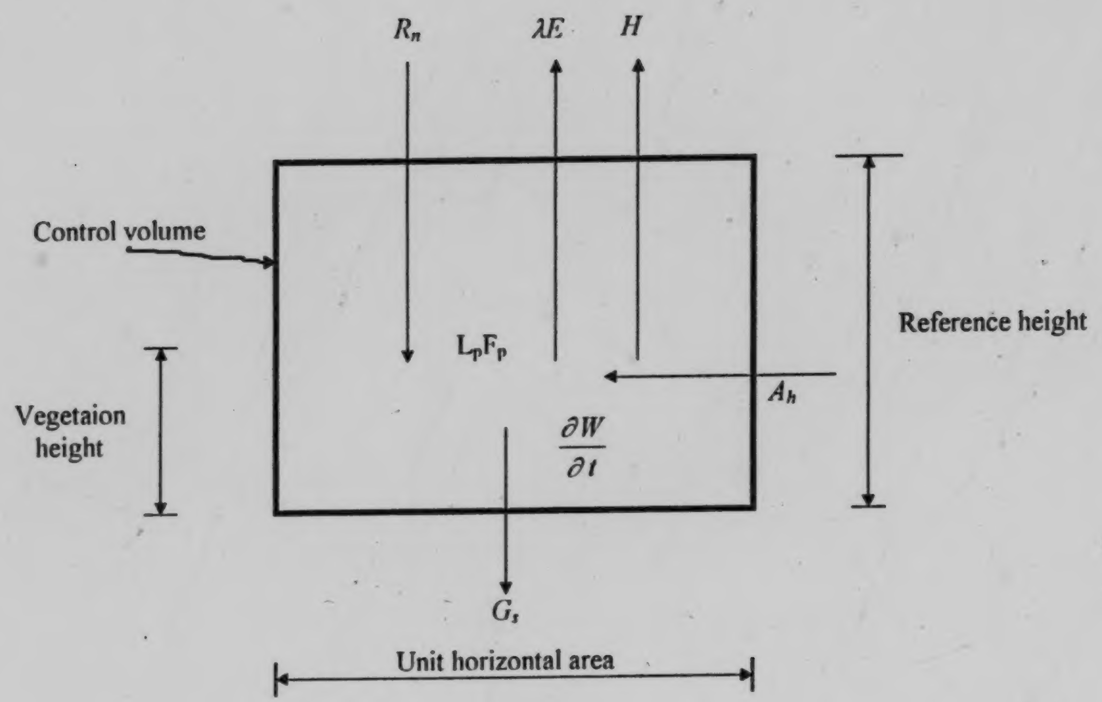
R_n
λE
H
Control volume
L_pF_p
Reference height
A_h
Vegetaion height
$\frac{\partial W}{\partial t}$
G_s
Unit horizontal area

Figure 2.3 Energy balance of the boundary layer that is at a reference height above ground.

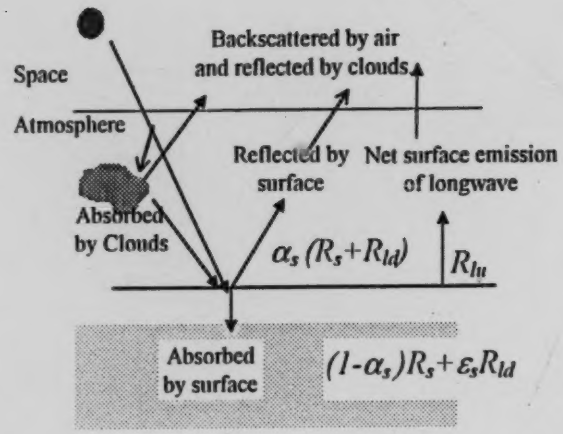
Space
Atmosphere
Backscattered by air and reflected by clouds
Absorbed by Clouds
Reflected by surface
Net surface emission of longwave
$\alpha_s (R_s+R_{ld})$
R_{lu}
Absorbed by surface
$(1-\alpha_s)R_s+\varepsilon_s R_{ld}$

Figure 2.4 Radiation balance at land surface and its air column

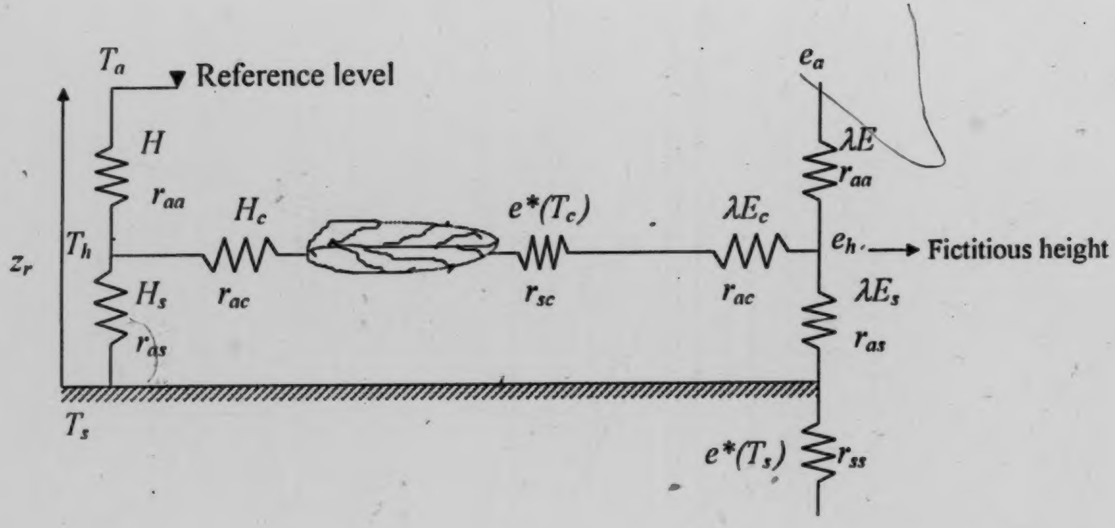
T_a
Reference level
e_a
H
r_{aa}
λE
r_{aa}
H_c
$e^*(T_c)$
λE_c
z_r
T_h
e_h
Fictitious height
H_s
r_{ac}
r_{sc}
r_{ac}
λE_s
r_{as}
r_{as}
T_s
$e^*(T_s)$
r_{ss}

Figure 2.5 A schematic diagram of the energy fluxes of the two source model for the vegetation canopy, the soil surface, and the air column above canopy (modified from Shuttleworth and Walace, 1985).

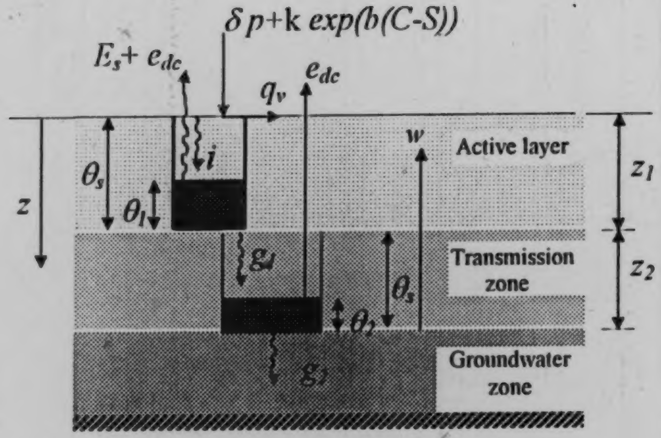
$\delta p+k\, exp(b(C-S))$
$E_s + e_{dc}$
q_v
e_{dc}
w
Active layer
Transmission zone
Groundwater zone
z
θ_s
θ_l
i
g_d
θ_s
θ_2
g_l
z_1
z_2

Figure 2.6 Conceptual representation of soil infiltration, between the active layer, transmission zone, and groundwater zone for each sub-basin.

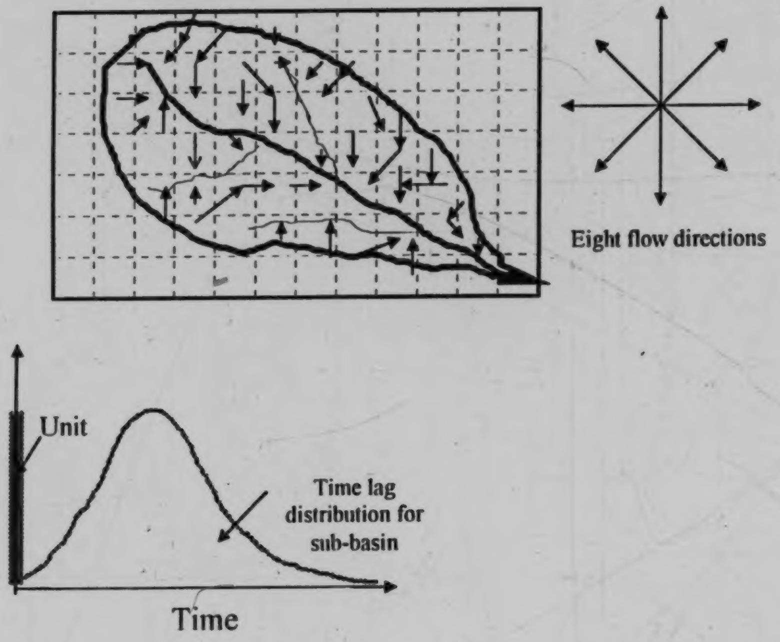
Eight flow directions
Unit
Time lag distribution for sub-basin
Time

Figure 2.7 The average response function per unit rainfall excess for a sub-basin based on the kinematic wave theory and eight flow directions.

Chapter 3

Semi-distributed, Physically Based, Hydrologic Modeling using Remotely Sensed data and GIS, II. Application to the Paddle River Basin, Alberta

3.1 Introduction

Distributed, physically based hydrologic models have been used to study the effects of land-use changes due to agricultural development, surface and subsurface water exploitation, deforestation, subsurface migration of industrial and agricultural chemicals and others. This is partly because, theoretically, with an adequate database, distributed physically based hydrologic models should be able to predict hydrologic responses of catchments under changing environment. Unfortunately, the amount of input data required by these models are not readily available.

Some researchers have discussed the practical limitations of fully distributed, physically based hydrological models, the uncertainties associated with the parameterization of such models at sub-grid levels, and the aggregation of the parameters at a higher level (e.g., Beven, 1989; Bergstrom, 1991; Tsang, 1991; Oreskes *et al.* 1994; and Refsgaard, 1996). Beven (1989, 1996) specifically discussed the limitations of such models with respect to the limitations of lumped conceptual models and concluded that the former must suffer from the same kind of problems as the latter, if not to the same degree. Example problems to the former are such as reality of model equations under a heterogeneous setting; the lack of a theory of sub-grid scale integration; practical constraints on solution methodologies; and problems of dimensionality in parameter calibration. In addition, Beven (1989) pointed out that the application of such models might best be carried out in parallel with a field measurement program for the consistency of model predictions and real world processes. Rosso (1994) summarized in detail the problems related to the initialization, calibration and validation of distributed models. Basically, the problems associated with parameterizing the hydrological and thermal characteristics of the land surface occupy the central place in applied hydrology as well as atmospheric science.

Because of the above problems, Beven (1996) argued that simpler models like TOPMODEL (Beven *et al.*, 1995) that are less data intensive can serve the same purpose equally well. Furthermore, given that simpler models are not data and/or computationally intensive, one can readily use them for the sensitivity analysis of model parameters and model limitations.

On the other hand, Grayson *et al.* (1992a, b) indicated the large amount of output information that models such as THALES can provide. Refsgaard *et al.* (1996) argued that even though simpler hydrological models are sufficient to simulate runoff under stationary catchment conditions, they can not simulate runoff in heterogeneous catchments under non-stationary conditions, e.g., land use changes, surface and subsurface water development, human interference, and modeling water quality and soil erosion.

The resolution of current models depends partly on the types of data available and the information contained in that data. Ultimately, in addition to limited ground-based, point measurements, remote sensing is the only means that can provide spatially distributed hydrologic information at a reasonable cost. In view of the problems of dealing with fully distributed models mentioned above, this chapter explores the applicability of different satellite data in a semi-distributed, physically based hydrologic model developed in the second chapter of this thesis. DPHM-RS is applied to the Paddle River Basin (265 km^2) of Central Alberta (Figure 3.1), using distributed hydrologic data such as surface albedo, land use classification, vegetation index, surface skin temperature, and near surface soil moisture derived from space platforms like NOAA-AVHRR, Landsat TM/MSS, and Radarsat SAR. Topographic information such as mean elevation, ground slope, flow directions, the delineation of Paddle River Basin into sub-basins, drainage systems, and topographic soil index were derived from digital terrain elevation data using a raster GIS.

3.2 Data Description

To apply the model to Paddle River Basin, the model parameters are derived either from remote sensing, or ground observations or model calibration. Data required to run DPHM-RS are local or areally averaged meteorological data, soil parameters, land use and topographic data, which are summarized in Table 3.1. The mechanisms used to retrieve model parameters, and hydrological variables at sub-basin scale are described in section 3.3.

3.2.1 Meteorological Data

A 10m high meteorological station was set up in the Paddle River Basin to obtain meteorological data during the summer of 1996 and 1997 (July - October) and spring to summer of 1998 (May to July). The net radiation and the solar irradiance were measured at a height of 2m using a Q-7 net radiometer and a LI-200SZ Pyranometer sensor respectively. The relative humidity and air temperature were measured at two levels (2m and 10m) using two sets of CS500 Temperature and relative Humidity probes. The wind speed was also measured at two levels (2m and 10m) using two Met-one wind speed sensors. The soil heat flux was measured using a heat flow transducer buried at a depth of 0.05m. The depth-averaged soil temperature for the top 8cm of the soil was measured using a TCAV thermocouple probe. All the data from each sensor were sampled at 1-min. interval and the averaged values over every 15-min. periods were recorded using a CR10X data logger. The average rainfall within the basin was measured using a TE525M

Tipping Bucket Rain gauge at 1-min. intervals and aggregated over 15-min. periods. Figure 3.2 (a)-(f) shows typical plots of different meteorological data for four days including that of a rainy day starting on August 2, 1996.

3.2.2 Soil Data

A map of soil types for Chip Lake Area prepared by the Soils Division (Twardy and Lindsay, 1971), Research Council of Alberta was co-registered to digital terrain elevation data for Paddle River Basin as shown in Figure 3.3. Clay loam is the dominant soil type for most of the basin. Each sub-basin is assigned with only one set of soil parameters based on its dominant soil. The soil water characteristic was specified in terms of Brooks and Corey's (1964) relationship, whose parameters were derived from the dominant soil based type's percentage of sand and clay obtained from the vertical soil profile (see Table 3.2).

3.2.3 Topographic Data

The Digital Terrain Elevation Data (DTED) of the USGS Defense Mapping Agency (DMA) of 100m resolution is used to derive different topographic information required for the model. From DTED, the mean altitude (Figure 3.4), flow directions (Figure 3.5), and the slope of each grid in the specified basin have been derived using the PCI EASE/PACE image analysis software. DTED is also used to delineate drainage network (see Figure 3.1), and the division of the Paddle River Basin into five sub-basins.

To estimate the sub-surface flow, the topographic-soil index is required to determine the local mean level and the temporal change of groundwater table for the basin. Based on the principle of multiple flow directions, Quinn et al. (1993) developed an algorithm to derive the topographic-soil index from digital terrain models. The general formulation for flows in downhill directions is given by:

$$\ln\left(\frac{a}{\tan\beta}\right) = \ln\left(A \Big/ \sum_{j=1}^{n} \tan\beta_j L_j\right) \qquad (3.1)$$

Where a is the cumulative up-slope area draining through a point (per unit contour length), $\tan\beta_j$ is the slope angle at that point, A is the total up-slope area entering a grid element, L is the contour length in the down hill direction, and n is the total number of downhill directions. In this study, the topographic soil index was first estimated, $\ln(a/\tan\beta)$, for each grid element of 100m resolution from the DTED of DMA (see Figure 3.6). Then the topographic soil index of each sub-basin for the Paddle River Basin is taken as the average value of the $\ln(a/\tan\beta)$ of all the grid elements that make up the sub-basin.

3.2.4 Vegetation Index

Satellite data have been used extensively for mapping the land use and for monitoring the seasonal change of vegetation of river basins (Running and Nemani, 1988; Pinty and Verstraete, 1992). The Normalized Difference Vegetation Index (NDVI) is commonly applied to derive the leaf area index (LAI) from channels 1 and 2 of NOAA-AVHRR data at 1-km^2 resolution. First, a raw NOAA-AVHRR image is calibrated using conversion coefficients given for the AVHRR on-board calibration (see Table 3.3). The image is then geometrically corrected and *NDVI* is obtained using the near infrared and visible spectral bands (Deering *et al*, 1975),

$$NDVI = \frac{R_{NIR} - R_{VIS}}{R_{NIR} + R_{VIS}} \tag{3.2}$$

Where R is the reflectance and the indices NIR and VIS refer to the near-IR and visible spectral bands. The NDVI derived from sixteen NOAA-AVHRR images acquired in 1996 and 1997 (eight images for each year) are shown in Figure 3.7. Table 3.4 shows the average NDVI values derived for different land use groups in the Paddle River Basin. Based on NDVI values the LAI for different land use groups are estimated using equations shown in Table 3.5.

3.2.5 Land Cover Classes

In hydrologic modeling, the heterogeneity of the land surface is usually approximated by a number of land covers identifiable from satellite images or from ground cover. From two data sets derived from Landsat-MSS and NOAA-AVHRR images, Kite (1995) found that both space platforms produce virtually the same land cover classes, except for perennial snow/ice which are difficult to detect from small patches on mountain tops by the NOAA-AVHRR data of 1-km resolution. Pietroniro *et al.* (1995) have shown that for three small basins (<2000 km^2) near Fort Simpson, Landsat images provided considerably more information than NOAA-AVHRR images.

The land cover information provides the basis for finding model parameters in DPHM-RS. For computing water and energy fluxes, DPHM-RS operates at a sub-basin level. However, each sub-basin has one or more land use classes which all exert an impact on the vertical soil moisture balance, and the amount of water exchange at the land-atmosphere interface through evapotranspiration. For the Paddle River Basin, the Landsat TM (channels 1, 2, 3, 4, 5, and 7) image acquired on August 7, 1996 was used to derive its land cover classifications using the back propagation, artificial neural network. The training area for each land cover class is obtained from field investigations. In practice, the number of land covers is limited to those that have a dominant effect on the hydrological response of the catchments. In this case, six classes have been identified to represent most of the land covers within the watershed. These classes are water and swamp, impervious areas, agricultural/crop areas, pastureland, mixed forest types, and coniferous forest (see Figure 3.8). Table 3.6 shows the percentage of each land use class in five sub-basins identified for the Paddle River Basin.

3.2.6 Surface Albedo

Surface albedo is a major determinant of the net solar energy received at the earth/atmosphere interface. Although surface albedo can be measured in the field, there are two severe limitations. First, field measurements are limited and so depends largely on the homogeneity of the terrain (Brest and Goward, 1987). Second, field measurements are not feasible for relatively inaccessible areas. Apparently, satellite measurements provide the only practical means of obtaining representative, regional/basin scale surface albedo at reasonable time resolutions (Kimes and Sellers, 1985; Kimes *et al*, 1987).

In DPHM-RS the surface albedo was derived from two Landsat TM images acquired on July 31 and August 7, 1996 during the calibration period and another two Landsat TM images acquired on July 25 and August 26, 1997 during the validation period. There are two calibration steps required to derive the surface albedo from the Landsat TM image. The first process is to convert the digital counts, D_i into values such as the sensor radiance, L_i.

For Landsat TM, the radiance in a single band can be obtained as:

$$L_i = A_o + A_1 D_i \tag{3.3}$$

Where A_o and A_1 are the offset and gain calibration coefficients for each TM band respectively (Table 3.7).

Next, the spectral reflectance of the earth-atmospheric system is converted to the corresponding surface or terrain reflectance using an atmospheric correction factor. It involves the direct measurements of the atmospheric properties and a detailed calculation based on the radiative transfer theory (Duguay and LeDrew, 1991). Duguay and LeDrew divided the surface into snow covered, vegetated, and/or non-vegetated areas. They then used a weighting scheme of the electromagnetic spectrum (Equation 3.4) to estimate the surface albedo of vegetated surfaces from the Landsat TM reflectance:

$$\alpha_{vs} = 0.526\rho_2 + 0.362\rho_4 + 0.112\rho_7 \tag{3.4}$$

Where weighting factors, 0.526, 0.362, and 0.112 represent respective portions of the incoming radiation in the visible ρ_2, near infrared ρ_4, and mid infrared ρ_7 part of the electromagnetic spectrum. For the surface covered by snow, the sensor saturation frequently occurs in TM bands 1, 2 and 3 (Duguay and LeDrew, 1991, 1992) and the weighting scheme is

$$\alpha_{ss} = 0.526(1.12\rho_4) + 0.232\rho_4 + 0.130(0.63\rho_4) + 0.112\rho_7 \qquad 3.5)$$

The albedo of all other non-vegetated surface is:

$$\alpha_{ns} = 0.526\rho_2 + 0.474\rho_4 \tag{3.6}$$

Assuming a Lambertian surface, the hemispherical reflectances near nadir TM radiance measurement is:

$$\rho_j = \frac{\pi\left[L(j) - L_p(j,z)\right]}{\left[T_v(j,z).E(j,z)\right]} \tag{3.7}$$

Where $L(j)$ is the sensor radiance for TM band j, $L_p(j,z)$ is the path radiance between the satellite sensor and the surface at altitude z, $T_v(j,z)$ is the vertical transmission from altitude z up to the sensor, and $E(j,z)$ is the total short wave irradiance for a given TM band j on an inclined surface at altitude z. The path radiance and the vertical transmission are determined using the LOWTRAN 7 atmospheric model (Kneizys *et al*, 1988). $E(j,z)$ is calculated from Equation (3.8).

In order to evaluate the surface variations of short-wave radiation, it is necessary to consider all the components of total short wave irradiance on a sloping surface. Hay's (1983) equation was used to compute $E(j,z)$

$$\begin{aligned} E(j,z) = {} & \phi S_h(j,z)(\cos(i)/\cos(i_h)) + D_h(j,z)\{k'(j,z)(\cos(i)/\cos(i_h)) \\ & + 0.5(1 - k'(j,z))(1 + \cos(s))\} + 0..5\alpha' k_h(j,z)(1 - \cos(s)) \end{aligned} \tag{3.8}$$

Where ϕ is a binary coefficient that is either set to zero (surface in shadow) or one (surface in sun); $S_h(j,z)$, $D_h(j,z)$, and $k_h(j,z)$ are the direct, diffuse sky, and total irradiances to an unobstructed horizontal surface computed from LOWTRAN 7 atmospheric model; i_h is the angle of incidence to a horizontal surface; i is the angle of incidence to a sloping surface; s is the slope of surface; $k'(j,z)$ is the anisotropy index used to separate diffuse sky irradiance into isotropic and circumsolar components (Hay, 1983); α' is the average albedo of the surrounding terrain (α' =0.60 for snow covered surface and 0.20 for all other surfaces).

The anisotropy index for any slope is defined by (Hay, 1983):

$$k'(j,z) = \frac{S_h(j,z)\cos(i)}{I_o \cos Z} \tag{3.9}$$

Where I_o is the solar constant (4.871 MJ m^{-2} h^{-1}) corrected for the deviation of the actual sun-earth distance from its mean value, and Z is the solar zenith angle. The surface albedo derived from the Landsat TM image for each land use class in the Paddle River Basin is given in Table 3.8 and its spatial distribution based on the image acquired on August 7, 1996 is shown in Figure 3.9.

3.2.7 Surface Temperature

The surface temperature derived from two satellite platforms (NOAA-AVHRR of 1-km resolution and Landsat-TM of 30 to 120m resolution) is used to evaluate the accuracy of spatial and temporal surface temperature simulated by DPHM-RS. The surface temperature, T_s from NOAA-AVHRR is derived from the brightness temperature of channel 4, T_B^4 and channel 5, T_B^5 using the split window method of Price (1984), assuming that there are no variations of emissivity of natural surfaces between channels 4 and 5.

$$T_S = T_B^4 + 3.33\left(T_B^4 - T_B^5\right) \tag{3.10}$$

The brightness temperatures are evaluated from the energy radiated at 10.8 μm and 11.9 μm for channels 4 and 5 respectively. The blackbody radiance L_λ^B at a specific wavelength λ is

$$\begin{aligned} L_\lambda^B &= \frac{c_1}{\lambda^5[\exp(c_2 / \lambda T_B) - 1]} \\ c_1 &= 2hc^2 \\ c_2 &= hc / k \end{aligned} \tag{3.11}$$

Where c is the velocity of light (3×10^8 m/s), h is the Planck's constant (6.6262×10^{-34} J/s), and k is the Boltzmann's constant (1.3806×10^{-23} $J\,K^{-1}$). By inverting equation (3.11), the brightness temperature, T_B of the body is:

$$T_B = \frac{c_2}{\lambda\left(\ln\left[\frac{c_1}{L_\lambda^B \lambda^5}+1\right]\right)} \qquad (3.12)$$

The blackbody radiance is evaluated from NOAA-AVHRR image digital number, D_i using the offset, A_o and gain factor, A_1 given in Table 3.3 for thermal bands of NOAA satellite as:

$$L_\lambda^B = A_o + A_1 D_i \qquad (3.13)$$

The surface temperature derived from sixteen NOAA-AVHRR images during the calibration and validation period of the DPHM-RS on the Paddle River Basin under different land cover condition is given in Table 3.9.

Surface temperature was also derived from Landsat-TM data using Schott and Volchok (1985) equation as:

$$T_s = \frac{k_2}{(\ln(k_1 / L(\lambda) + 1))} \qquad (3.14)$$

Where k_1 is a first constant (66.776 $mw\ cm^{-2}\ sr^{-1}\ \mu m^{-1}$ for TM-5), k_2 is a second constant (1260.56 $^o k$ for TM-5), and $L(\lambda)$ is the radiance derived from Landsat TM band 6 digital numbers ($mw\ cm^{-2}\ sr^{-1}\ \mu m^{-1}$). The surface temperature values derived from Landsat-TM images during calibration and validation of DPHM-RS are given in Table 3.10. In addition Figure 3.10 shows the spatial variation of surface temperature derived from Landsat-TM image of August 7, 1996.

3.2.8 Streamflow

The stream flow gauging station operated by Environment Canada, Water Survey of Canada is located at the Paddle River near Anselmo Hall (Latitude 53° 51', 29" N and Longitude 115° 21' 45" W). Daily stream flow measurements are available since 1980, the year the station was established. Figure 3.11(a) shows the averaged daily flow obtained from data of 1980-1993. However, hourly data obtained at the gauging station in the summer of 1996 was used to calibrate the model parameters. The stage discharge relationship (Figure 3.11(b)) established by Water Survey Canada is used to obtain the discharge from water level. Figures 3.11(c) and (d) show the hourly discharge used for the calibration and validation periods.

3.2.9 Throughfall Coefficient

The throughfall coefficient δ is necessary to estimate the percentage of precipitation reaching the surface without striking the vegetation canopy. In theory, the value of this coefficient can be obtained from field measurements of net rainfall and total precipitation for individual storms (e.g., Rutter *et al*, 1971). However, in practice, it is not possible to obtain the throughfall coefficient from field measurements. As a result there is a need to establish an alternative method to obtain this coefficient. In this study, based on past measurements of δ shown in Table 3.11, and the leaf area index, LAI, a simple regression is established to convert *LAI* to δ. The linear relationship shown in Figure 3.12 (R^2=0.97) fit very well to data obtained for different types of vegetation. As a result, δ is related to *LAI* as

$$\delta = a + mLAI \tag{3.10}$$

Where a is 0.997 and m is -0.139.

3.3 Parameter Estimation

The Paddle River Basin consists of about 50% mixed forest, 21% coniferous forest, 15% agricultural land, 11% pasture land with short grass, 2% water body and 1% relatively impervious lands. In applying DPHM-RS to Paddle River Basin, the number of parameters that were subjected to calibration was kept to a minimum (see Table 3.12). Some parameters are either directly measured from field observation or indirectly from values given in past studies conducted in other catchments. In addition, a significant number of hydrological variables and parameters have been derived from different space platforms. For the evaluation of energy fluxes the parameters required such as the eddy attenuation coefficient λ_e, the attenuation coefficient for wind speed n', the minimum and maximum canopy resistance, and the mean canopy height for different land cover types are estimated from past findings and field observation (see Table 3.12). The initial estimate of Manning's roughness for routing the surface runoff on different land cover types is based on values suggested in the literature.

DPHM-RS models the Paddle River Basin as either one or two soil layers depending on the relative location of the average ground water table within each sub-basin. Based on the mean water table observed from surrounding wells, the average local groundwater table depth was initialized at a depth of 5.5m during calibration and validation periods. The upper, active soil layer, designed to reflect the rapid changes of soil moisture to rainfall events was fixed at 20cm depth while the transmission zone is the remainder depth above the average ground water table and below the active layer. By using spatial soil moisture measurements retrieved from Radarsat data, DPHM-RS has provision to initialize or to update the state of soil moisture content for the active layer. However, this was not done in this study given that Radarsat data was obtained only on dates other than that of the calibration as well as validation periods. Based on the average field conditions observed, the initial soil moisture for the active layer and transmission zones are assumed to be, 60% of the saturated moisture content during calibration period and 80% during validation period.

Based on the percentage of different textures obtained in the vertical soil profile shown in Table 3.2, the residual moisture content, θ_r, the pore size index, B, and the bubbling pressure, ψ_c, of the dominant soil type – clay loam - are obtained from Rawls and Brakensiek's (1985) regression equation. The total porosity, ϕ (=0.464), and the saturated hydraulic conductivity $K_s = 0.024$ m/hr are based on the mean values given by Rawls and Brakensiek (1985) for clay loam soil. The critical soil moisture content, θ_{cr}, is assumed as the amount of water retained at -33 kPa and the moisture content at wilting point, θ_w, is assumed to be water retained at –1500 (see Table 3.12).

3.4 Discussion of the Results

DPHM-RS was applied to the Paddle River Basin using hourly hydroclimatic data collected from a 10-m meteorological tower set up in the basin. Since the basin is small (265 km^2), the spatial variation of meteorological inputs was assumed to be negligible. However, to check this assumption on rainfall variability, an additional rain gauge (station 2) was installed in 1997 at a location 13km away from the original rain gauge (station 1) which was installed in the summer of 1996. The hourly rainfall data at both locations are compared for some rainy days in the summer of 1997 (Figure 3.13). As one can see from Figure 3.13, differences in the rainfall events occurring over the basin are not significant even though the two rain gauges were located at different altitude and 13 km apart (Figure 3.1). From Figure 3.13 one can observe that there is a lag in time in the occurrence of rainfall at the two rain gauge locations. However, the time lag is much less than the hourly time step used. As a result, it is not necessary to consider the lag in rainfall between the two rain gauge stations.

The spatial and temporal variation of rainfall was also assessed for the study site based on daily rainfall data (1980-1990) measured at seven climatic stations, of which one is located within the basin and the others outside the basin (Figure 3.14). The daily rainfall data from different gauging stations are reasonably correlated as shown in Table 3.13. Table 3.13 shows that the correlation between stations decreases with increasing inter-station distance. For example, the meteorological station at Roman is approximately at a distance of 19km from meteorological station at Highway. Correspondingly, the correlation coefficient between these two stations is about 0.8. This shows that the spatial rainfall variation in the area is not significant, and it is generally sufficient to use rainfall data measured at one or two rain gauges for simulation of flow from the Paddle River Basin.

3.4.1 Model Calibration and Validation

Model calibration was based on hourly data collected from July 25 to August 29, 1996 and assessed using graphical plots of observed and simulated hydrographs at the basin outlet and the coefficient of efficiency of Nash and Sutcliffe (1970). The downhill simplex optimization method of Nelder and Mead (1965) is included in model code development for automatic calibration of model parameters. However, in this case manual calibration was used to investigate closely the effects of different model parameters.

The routing of the surface runoff is based on the response functions of unit rainfall excess developed for each sub-basin using the kinematic wave approach at the beginning of the simulation period. The response functions were adjusted by changing Manning's roughness parameters so as to improve the simulated peak with respect to observed peak runoffs at the basin outlet for calibration period. The response function derived for each sub-basin is shown in Figure 3.1. In the calibration process, the soil parameter *f* was adjusted to provide the proper base flow or recession curve. This resulted in a final *f* value of 1.2 m^{-1}. In simulating the water balance in the unsaturated zone, the computation time step is reduced to about 5 minute to minimize the computation error in soil water balance especially during rainfall. In channel routing, the channel roughness parameters were first estimated from field observations and refined via matching the time lag and magnitude of the peak discharge observed at the basin outlet. This resulted in a final n_m value of 0.038. Channel routing was based on Muskingum-Cunge method and it is found that the model is not too sensitive to the mean top width of the water surface at channel reaches. Therefore it should be acceptable to assume that the top width of the flow at different channel reaches is approximately the same as the channel width estimated from field measurements.

3.4.1.1 Runoff at Basin Outlet

Figure 3.15(a) shows the simulated hydrograph versus the observed counterpart at the calibration stage (July 25 – August 29, 1996). In general, simulated and observed runoff are in good agreement (R^2=85%) except in the first day of simulation because of the initialization problem of channel flows at different junctions and initial soil moisture content for the active layer. At the validation stage (July 16 to September 26, 1997), the simulated runoff still agrees well with the observed runoff especially for peak flows (see Figure 3.15(b)). However, on August 12 and 13 of 1997, the location of the gauging station is shifted 100m upstream and the continuous measurement of water level at the outlet of the catchment was interrupted. The observed hourly data for these two days were extrapolated based on one manual measurement per day (Tim Davis, 1998 personal communication). This extrapolation approach resulted in an increase in the streamflow for these two days compared to streamflow in the previous and the later days. This does not make sense since no rainfall was recorded in these two days. In other words, the simulated streamflow should be more accurate than the observed counterparts extrapolated from two measurements taken in these two days (August 12 and 13, 1997).

The model is also validated based on meteorological, hydrological, and remote sensing data obtained in the spring of 1998 (May 1 to June 30). The simulated discharge at the outlet of the catchment for this period also agrees well with observed discharge especially the peak runoff but there is some discrepancy in the recession part of the hydrograph (see Figure 3.15(c)). This could be due to initial estimate of the average ground water table depth for the catchment, which is assumed to be the same for all three years at a depth of 5.5m. In general the model is versatile to apply for different periods of the year by calibrating with sufficient information and initializing the model appropriately.

3.4.1.2 Net Radiation

In addition to assessing the model performance in terms of streamflow, the model's simulated net radiation is also compared with the net radiation collected using a Q7 net radiometer. With reference to Equation 2.9, the simulated net radiation depends on the measured short-wave radiation (R_s), surface albedo derived from Landsat TM data (α_s), observed air temperature T_a (for estimating the downward long-wave radiation), and simulated surface temperature T_s (for estimating the upward long-wave radiation).

From Figure 3.16(a) and 3.16(b), the simulated hourly net radiation (R_n) generally agrees closely with the observed counterpart. However, from the scatter plots, there is an under-simulation of the net radiation (dots above the 45° line), which mostly occurred in rainy days. This is because, there is no information on the fraction of cloud cover (f_c of Equation 2.13) needed to correct the atmospheric emissivity (ε_{ac} of Equation 2.12) and the downward long-wave radiation R_{ld} is under-simulated. The effect of cloud cover is evident from the plot of measured short wave radiation against measured net radiation. From Figure 3.17(a), we can observe that the short wave reaching the ground surface is also affected by cloud cover in a similar fashion to the simulated net radiation. During cloud cover the short wave radiation measured decreases and result in an increase in downward longwave radiation. An attempt has been made to relate the fraction of cloud cover to measured shortwave radiation based on a daily solar radiation envelope (see Figure 3.17(b) and (c)). While such a relationship can provide a good indication of the fraction of cloud cover on a daily basis (Hicks *et al.*, 1995), it is not straightforward to desegregate into hourly fraction of cloud cover required by the model. In this case the functional relationship established for fraction of cloud cover based on measured average daily short wave radiation is used to correct the effect of cloud cover on hourly basis (Figure 3.17(c)). This function is able to correct the model simulation under cloud cover condition marginally (see Figure 3.17(d)). It is apparent that the fraction of cloud cover, f_c should form part of the model input to ensure that the model simulate the net radiation accurately.

As mentioned in Section 3.6, α_s was estimated from Landsat TM images and two such images were acquired on July 31 and August 7 of 1996 while the calibration period range from July 25 to August 30. As such, it is assumed that α_s of August 7 to remain constant until August 30, 1996 of the calibration period. Apparently, the assumed α_s may be lower than the actual value, which resulted in an over-simulation of net radiation. The over-simulation is more pronounced in high R_n, which mostly occurred during mid-day hours (shown by dots on the far right falling below the 45° line in Figure 3.16(a)). In the validation period, there is no obvious over-simulation problem of R_n as in the calibration period. This is likely because α_s obtained from the two Landsat TM images acquired over one month's interval (July 25 and August 26, 1997) probably are more representative of the actual values during the validation period (July 16 to September 26, 1997). In other words, it is more reasonable to assume a constant α_s from August 26 to September 26 of 1997 (fall period) than a constant α_s from August 7 to August 30, 1996 (late summer period).

3.4.1.3 Surface Temperature

Next, the model performance was assessed by comparing its simulated surface/skin temperature with that retrieved from either NOAA-AVHRR or Landsat TM data for four types of land covers in the Paddle River Basin (see Table 3.14 and Figure 3.18). The discrepancies between simulated skin temperature and skin temperature retrieved from NOAA-AVHRR or Landsat TM data are less than 2^oK for most days except July 16, August 26, and September 8 of 1997. On these three days, the NOAA-AVHRR images were partly cloud-covered which affects the retrieval of skin temperature from the images. On these three days, the retrieved skin temperature differs from the simulated surface temperature by 4^oK, 3^oK, and 7^oK respectively, because the skin temperature of cloud-cover was lower than the skin temperature of the ground surface, and so cloud cover attenuated some of the ground emitted radiation from reaching the satellite sensor. The results show that the model generally simulates credible surface temperature.

3.4.1.4 Soil Moisture

Lastly, some qualitative discussion of the model's simulated soil moisture at the active layer and transmission zone (see Figure 2.6) is presented. From Figures 3.19(n) and 3.20(n), one can see that soil moisture in the active layer (dotted lines) responded actively to atmospheric forcing – an almost instant increase during rainfall events and gradual recessions due to evapotranspiration and percolation to the transmission zone during inter-storm periods. However, as expected, there is relatively small response from the transmission zone (solid lines) during storm and inter-storm periods.

Other than the above qualitative analysis, for three days in the validation period (August 5, 12, and 29, 1997) in which the basin wide near-surface soil moisture was estimated from three scenes of Radarsat SAR images (see Chapter 5). The amount of near-surface soil moisture in these three days were 14.4, 13.6, and 11.6 mm respectively. Compared to the corresponding daily mean soil moisture simulated by the model for the active layer for these 3 days (12.6, 14.0, and 11.8 mm), it is conclude that the model's simulated soil moisture in the active layer is realistic and reliable.

3.4.2 Effect of Land Cover on Water and Energy Fluxes

Some of the results of this study also demonstrate significant effect of land cover types on basin scale water and energy fluxes as shown in Figures 3.19(a) to 3.19(m). Considerable differences in fluxes such as evaporation, transpiration, wet canopy evaporation, surface temperature, canopy temperature, and sensible and latent heat fluxes at different layers are found among various land covers for the Paddle River Basin. There is no way to validate these results directly but intuitively the results make sense. For example, for forest cover, transpiration from vegetation canopy should be more than evaporation from soil surface but vice versa for pastureland. This makes sense because for forest cover, e.g., coniferous forest cover shown in Figure 3.19(a)-(b), the net energy reaching the soil surface for evaporation is only 25-36% of the total energy, but for pastureland, the net energy reaching the soil surface is 50 to 60% or higher (see Figure 3.19 (l) and (m)).

On the other hand, soon after each rainfall event, wet canopy evaporation dominates over transpiration through plants or evaporation from soil surface (e.g., compare fluxes at 30-40 hr in Figure 3.19(a), (b), and (c)). During day time, sensible heat flux over water surface is small compared to land surface of almost all vegetation type because the aerodynamic resistance for water surface is relatively high (see Equation 2.18 and Figure 3.19(f)). Conversely, latent heat flux over water surface is high compared to all land surface cover in the basin because evaporation gradient is proportionally higher over water surface than land surfaces (see Equation 2.19 and Figure 3.19(i)). Figure 3.19(a) to (n) represent plots for the calibration period. Similar characteristics in water and energy fluxes are also observed in the validation period (see Figure 3.20(a) to (n)).

3.5 Application of TOPMODEL to Paddle River Basin

TOPMODEL is a topography-based hydrological model developed from the variable contributing area theory at the University of Leeds (United Kingdom) with the aim of providing a physically realistic but parametrically simple rainfall runoff model that had ability to predict different types of hydrological response (Beven and Freer, 1996). The model makes use of an idea that the distribution nature of catchment responses could be indexed on the basis of an analysis of topography. This approach to hydrological modeling has attracted a great deal of attention recently due to increasing availability of digital elevation data. Beven *et al.* (1995) recently did a full review of the development of TOPMODEL and its applications.

The TOPMODEL, which requires few field measurements, has been applied widely in humid temperate regions where the variation of soil moisture content are less as compared to arid and semi-arid climate (e.g., Beven and Wood, 1983; Wood et al., 1990; Quinn et al., 1995). Application of TOPMODEL to well-studied catchments has not always been successful (e.g., Hornberger *et al.*, 1985). Two flow mechanisms are considered in TOPMODEL: a surface runoff generated by rainfall on saturated contributing areas and a subsurface down hill flow. The main assumptions used by TOPMODEL to relate the down-slope flow rate at each point and the discharge at the catchment outlet are: (1) the downhill saturated flow declines exponentially with reference to the local soil moisture deficit below saturation; and (2) the direction of the local hydraulic gradient is parallel to the local slope, i.e., the water table is parallel to the surface.

Water redistribution within the root zone at each time step was accounted for using a simple model. The soil layer is modeled as three interconnected reservoirs described by three parameters. The root zone reservoir, which receives rain and potential evaporation inputs, has a maximum storage capacity Sr_{max}. All water in excess of Sr_{max} after evapotraspiration will contribute to streamflow. Water remaining in this reservoir is therefore available only for evapotranspiration. An auxiliary temporary reservoir represents moisture intercepted by vegetation and moisture remaining in the uppermost soil layers after infiltration into an unsaturated profile. The water in this temporary storage is available for evapotranspiration at the potential rate, even if the rest of the soil profile is under water stress conditions. This auxiliary storage collapses into the main soil reservoir under wet conditions.

The third reservoir (of the unsaturated zone) has a variable capacity dependent on the local water storage deficit D_i. Water from the third reservoir in excess D_i contribute to surface runoff which is routed to the stream. The vertical gravity drainage recharging the saturated zone is assumed to be proportional to the water in this reservoir and inversely proportional to a mean residence time, $T_D D_i$, where T_D is the time delay per unit deficit. The reservoir therefore acts locally as a linear reservoir with a time constant dependent on the local deficit. Surface water routing is based on a constant overland flow velocity, R_V and a routing distance distribution determined from topographic data that varies as the contributing area expands and contracts.

TOPMODEL has been applied to simulate runoff from the Paddle River Basin of Central Alberta as a compared to the semi-distributed model (DPHM-RS) developed in this study. The inputs to the model are the hourly rainfall, hourly potential evaporation, and the topographic index derived from the digital terrain elevation data (DTED). The TOPMODEL parameters were calibrated using hourly rainfall data measured at the Paddle River hydroclimatic station in the summer of 1996 for 35 days (July 25 to August 30, 1996). The potential evaporation needed by TOPMODEL is evaluated based on Penman model (Penman, 1948) using hourly net radiation, relative humidity, and air temperature measured at the study site. The topographic index is derived from DTED at a 100m x 100m grid of surface elevations. The local storage deficit is evaluated based on an assumption that the hydraulic behavior of every part of the catchment is adequately described by this index. The outputs are the hourly average soil moisture deficits below saturation and hourly discharge.

The calibration of model parameters based on simulated and observed catchment runoff was automated by an optimization algorithm built into the model. The simulated and observed hydrograph at the calibration stage (shown in Figure 3.21(a)) are generally in good agreement (R^2=0.85). Table 3.15 provides the optimum model parameters obtained from calibration. The model is then validated using hourly data for the summer of 1997 (July 16 to September 26, 1997) and the spring of 1998 (May 1 to June 30). However, the simulated discharge during the validation stage does not agree with observed discharge (R^2= -0.65 for 1997 and R^2=-0.22 for 1998, and see Figure 3.21(b)&(c)). In general, the model over-estimated the peak flow and under- estimated the ground flow recession. The independent check at the validation stage probably indicates that model parameters were "forcibly" optimized at the calibration stage. The drastic deterioration of model performance under hydrologic conditions different from the calibration stage shows that the model parameters obtained through automatic calibration still lacks physical basis. In addition the simple nature of TOPMODEL may not be sufficient to simulate the hydrologic response of the Paddle River Basin. Specifically, the routing component of the TOPMODEL which depends on a single average velocity, R_V obtained during calibration is inadequate to simulate the complex drainage pattern of semi-arid catchments at short time steps, e.g. 1 hour.

Beven and Kirkby (1979) noted that the optimization of TOPMODEL parameters for some catchments tend to force the model to operate in a way that is not consistent with the underlying theory even though good results could be obtained at the calibration stage as shown here. Beven and Freer (1996) also argued that, to apply TOPMODEL, it is necessary to evaluate the distributed predictions of the model with the understanding gained from field observations and modifying the model accordingly. By applying TOPMODEL to a small catchment (area=0.36 km^2), Ambroise et al. (1996) concluded that by changing the model structure, which includes relaxing the assumption of an exponential transmissivity and the assumption of uniform transimissivity in the catchment using observed saturated area information, the TOPMODEL's performance for that catchmnet was significantly improved.

Our experience with TOPMODEL, good result at the calibration stage but poor result at the validation stage, likely indicates the need to reconsider the model structure and parameterization with respect to filed measurements to improve the consistency of the model. For this case it is not clear if the difficulty in simulation arises either from the model structure or due to limitations of the input data with which it is being driven. For example, during rain storms, the simulation of saturated contributing area based on topography and a homogeneous soil layer for the catchment (which is not true) might not be sufficient for Paddle River Basin.

Unlike DPHM-RS, in TOPMODEL, the spatial distribution of land cover types is not taken into consideration which have a significant impact on the estimation of water and energy fluxes from a watershed such as the Paddle River Basin. For example, the amount of evaptranspiration vary from vegetation to vegetation quite significantly and affects the runoff from the catchment. As a result, the use of spatially distributed information retrieved from remote sensing such as the vegetation index (NDVI), surface albedo, and land use types at sub-basin contribute partly to the better and consistent performance in DPHM-RS as compared to TOPMODEL. By finding the response function for surface routing for each sub-basin, in addition, DPHM-RS accounts for the individual effects of land cover types whereas TOPMODEL lumps all such effects into one parameter that primarily reflects the effect of terrain only. As a result, a more accurate surface runoff routing (kinematic wave routing) model is used in DPHM-RS which also partly contribute its better performance at the validation stage when compared to TOPMODEL.

3.6 Summary and Conclusions

A semi-distributed model, DPHM-RS, is used to simulate runoff, evapotranspiration energy fluxes and soil moisture from the Paddle River Basin of Central Alberta. In addition to meteorological data obtained from field measurements, the model was driven with distributed hydrologic data such as surface albedo, land use classification, vegetation index, surface skin temperature, and near-surface soil moisture derived from space platforms like NOAA-AVHRR, Landsat TM, and Radarsat SAR. The hourly data collected from July 25 to August 30, 1996 were used to calibrate the model which was then validated with another similar set of hourly data obtained in the summer of 1997 and spring of 1998. DPHM-RS was assessed in terms of several hydrologic variables. On a whole, the simulated runoff at the basin outlet agrees well with the observed data both during calibration and the validation periods. The simulated net radiation agrees well with the observed except for rainy days. The simulated surface/skin temperature agrees closely with skin temperature retrieved from either NOAA-AVHRR or Landsat-TM data except for those days partly covered by cloud.

Qualitatively (since it is not possible to verify them) the model also simulated realistic soil moisture for each sub-basin and realistic energy and water fluxes for all land cover types of the basin. The results demonstrated the feasibility of modeling basin-scale water and energy fluxes using the semi-distributed approach, the usefulness of spatial topographic information derived from DTED, and spatial hydrologic information retrieved from NOAA-AVHRR, Landsat-TM, and Radarsat SAR data.

The variable contributing area hydrological model TOPMODEL has been applied to Paddle River Basin as a comparison to DPHM-RS model. The result obtained by applying TOPMODEL is not encouraging for this catchment. Either the variable contributing area concept is not a dominant process for this catchment or the information used to describe the spatial distribution of contributing area based on topography is not sufficient to represent the actual process. In addition, actual evaporation in TOPMODEL is related linearly to potential evaporation based on soil moisture deficit. Further modification of the model structure by including detailed modeling of evapotranspiration and surface routing component might improve the accuracy of runoff simulation and will provide physical model parameters during calibration.

In summary, TOPMODEL compares less favorably to DPHM-RS because of the following reasons:

(1) The concept of variable contributing area may not be a dominant process for the Paddle River Basin; and

(2) In addition to topography, the effects of land cove types should be accounted for in the evapotranspiration and surface runoff routing component in order to model the basin's hydrologic response adequately.

Lastly, the simple model structure of TOPMODEL can be modified so that it can take advantage of the massive spatial hydrologic information now made available through satellite data as demonstrated in this study. More extensive studies are needed to further investigate the usefulness of satellite in basin and mesoscale hydrologic modeling.

References

Ambroise, B., Beven, K. J., and Freer, J. (1996). Application of a generalized TOPMODEL to a small Ringelbach catchment, Vosges, France, *Water. Resour. Res.*, Vol. 32, No. 7, pp. 2147-2159.

Bergstorm, S. (1991) Principles and confidence in hydrological modelling. *Nordic Hydrology*, 22, 123-156.

Beven, K. J. and Kirkby, M. J. (1979). A physically-based variable contributing area model of basin hydrology. *Hydrol. Sci. Bull.*, 24, pp. 43-69.

Beven, K. J. and Wood, E. F. (1983). Catchment geomorphlogy and the dynamics of runoff contributing areas, *J. Hydrol.*, 65, 139-158.

Beven, K. J. (1989) Changing ideas of hydrology: the case of physically-based models. *J. Hydrol.*, 105, 157-172.

Beven, K. J., Lamb, R., Quinn, P., Romanowicz, R. and Freer, J. (1995). TOPMODEL, in V. P. Singh (Ed.), Computer Models of watershed hydrology, *Water Resources Publications*, Colorado, 627-668.

Beven, K. J. (1996) A discussion of distributed hydrological modelling. In M. B. Abbott and J. C. Refsgaard (eds.), Distributed hydrological modelling, *Water Resources Publications*, 255-278.

Brest, C. L. and Goward, S. N. (1987). Deriving surface albedo measurements from narrow band satellite data. *Int. J. Remote Sensing*, 8, pp. 351-367.

Brooks, R. H., and Corey, A. T., (1964) Hydraulic properties of porous media, *Hydrology Papers*, no. 3, Colorado State Univ., Fort Collins, Colorado.

Deering, D. W., Rouse, J. W., Haas, R. H. and Schall, J. A., (1975). Measuring forage production of grass units from Landsat MSS data. *Environment, Ann Arbor, MI*, pp. 1169.

Duguay, C. R., and LeDrew, E. F. (1991). Mapping surface albedo in the east slope of the Colorado Front Range, USA, with Landsat Thematic Mapper. *Arctic and Alpine Research*, 23, pp 213-223.

Duguay, C. R., and LeDrew, E. F. (1992). Estimating surface reflectance and albedo from Landsat-5 Thematic Mapper over rugged terrain. *Photogrammetric Engineering and Remote Sensing*, 58, pp. 551-558.

Grayson, R. B., Moore, I. D., and McHahon, T. A. (1992a). Physically based hydrological modelling. 2. Is the concept realistic? *Water Resources Research*, 28(10), 2659-2666.

Grayson, R. B., Moore, I. D., and McHahon, T. A. (1992b). Physically based hydrological modelling. 1. A terrain-based model for investigative purposes. *Water Resources Research*, 28(10), 2639-2658.

Hay, J. E. (1983). Solar energy system design: the impact of the mesoscale variations in solar radiation. *Atmosphere-Ocean*, 21:138.

Hicks, F., Cui, W., and Andres, D. (1995). Forecasting break up on the Mackenzie River at the Ft. Providence ferry crossing, Water Resources Engineering Report 95-H2, University of Alberta, Department of Civil Engineering, pp. 1-105.

Hornberger, G. M., Beven, K. J., Cosby, B. J., and Sappington, D. E. (1985). Shenandoah watershed study: Calibration of a topography-based, variable contributing area hydrological model to a small forested catchment, Water Resour. Res., 21(12), pp. 1841-1850.

Kanemasu, T., Rosenthal, U. D., Raney, R. J., and Stone, L. R. (1977). Evaluation of an evapotranspiration model for Corn. *Agron. J.,* 69, pp. 461-464.

Kimes, D. S. and Sellers, P. J. (1985) Inferring hemispherical reflectance of the Earth's surface for global energy budgets from remotely sensed nadir or directional radiance values. *Remote Sensing of Environment*, 18, pp. 205-223.

Kimes, D. S., Sellers, P. J. and Diner, D. J. (1987) Extraction of spectral hemispherical reflectance (albedo) of surface from nadir and directional reflectance data. *Int. J. Remote Sensing*, Vol. 8,No. 12, pp. 1727-1746.

Kite, G. W. (1995). Scaling of input data for macroscale hydrologic modeling. *Water Resour. Res.*, 31(11), 2769-2781.

Kite, G. W. and Spence, C. D. (1995) Land cover, NDVI, LAI, and evapotranspiration in hydrological modelling. In: Application of Remote Sensing in Hydrology, ed. G. W. Kite, A. Pietrniro and T. Pultz, pp 223-240. *Proc. Synp. No. 14, NHRI*, Saskatoon, Canada.

Kneizys, F. X., Shettle, E. P., Abreu, L. W., Chetwynd, J. H., Anderson, G. P., Gallery, W. O., Selby, J. E. A., and Clough, S. A. (1988). User code to LOWTRAN 7. AFGL-*TR-88-0177 Environmental Research papers, No. 1010*, US Department of Defense, Air Force Geophysics Laboratory, Optical Physics Division, pp. 137.

Leyton, L., Reynolds, E. R. C. and Thompson, F. B. (1967). Rainfall interception in forest and moorland. *Forest Hydrology* (Ed. by W. E. Sopper and H. W. Lull), Pergamon Press, Oxford, pp. 163-168.

Nemani, R. R., and Running, S. W. (1989). Testing a theoretical climate-soil-leaf area hydrologic equilibrium of forests using satellite data and ecosystem simulation. *Agricultural and Forest meteorology,* 44: 245-260.

Oreskes, N., Shrader-Frechette, K., Belitz, K. (1994) Verification, validation and confirmation of numerical models in the earth sciences. *Science* 264, 641-646.

Penman, H. L. (1948). Natural evaporation from open water, bare soil and grass, Proc. R. Soc. London A, 193, 120-145.

Peterson, D. L., Spanner, M. L., Running, S. W., and Teuber, K. B. (1987). Relationship of thematic mapper simulator data to leaf area index of temperate coniferous forests. *Remote Sensing of Environment*, 22, pp. 323-341.

Pietroniro, A., Prowse, T. D., and Lalonde, V. (1995) Classifying terrain in a muskeg-wetland regime for application to GRU-type distributed hydrologic models. In: Applications of Remote Sensing in Hydrology, ed. G. W. Kite, A. Pietrniro and T. Pultz, pp 275-286. *Proc. Synp. No. 14, NHRI*, Saskatoon, Canada.

Pinty, B and Verstraete, M. M. (1992) GEMI: a non-linear index to monitoring global vegetation from satellite. *Vegetation* no. 101, pp. 15-20.

Price, J. C. (1984) Land Surface Temperature Measurements from the Split Window channels of the NOAA 7 Advance Very High Resolution Radiometer. *J. of Geophy. Res.*, Vol. 89, No. D5, pp. 7231-7237.

Quinn, P., Beven, K. J., Chevallier, P., and Planchon, D. (1993). Prediction of hillslope flow paths for distributed hydrological modelling using Digital Terrain Models, in K. J. Beven and I. D. Moore edition, Terrain analysis and distributed modelling in hydrology, *John Willy & Sons*, pp. 63-83.

Quinn, P.F., Beven, K. J., and Lamb, R. (1995). The ln(a/tan β) index: How to calculate it and to use it within the TOPMODEL framework, *Hydrol. Process.*, 9, 161-182.

Rawls, W. J., and Brakensiek, D. L. (1985) Prediction of Soil Water Properties for hydrologic modeling. Watershed Management in the Eighties, *ASCE*, pp. 293-299.

Rafsgaard, J. C. (1996) Terminology, Modelling protocol and classification of hydrological model. In M. B. Abbott and J. C. Refsgaard (eds.), Distributed hydrological modelling, *Water Resources Publications,* 17-39.

Rafsgaard, J. C., Storm, B. and Abbott, M. B. (1996) Comment on 'A discussion of distributed hydrological modelling' by K. Beven. In M. B. Abbott and J. C. Refsgaard (eds.), Distributed hydrological modelling, *Water Resources Publications,* 279-287.

Robins, P. C. (1969) Comparative studies of evaporation from Pinus nigra and Pseudotsuga menziesii with particular reference to air and stomatal resistances. *Ph.D. thesis*, University of London.

Robins, P. C. (1974) A method of measuring the aerodynamic resistance to the transport of water vapor from forest canopies. *J. appl. Ecol.*, 11, pp. 315-325.

Rosso, R., (1994) An introduction to spatially distributed modeling of basin response. In: Ross, R., Peano, A., Becchi, I., Bemporad, G.A. (Eds.), Advances in Distributed Hydrology. *Water Resources Publications*, pp. 3-30.

Running, S. W. and Nemani, R. R. (1988). Relating seasonal patterns of the AVHRR vegetation index to simulated photosynthesis and transpiration of forests in different climates. *Remote Sens. Environ.*, 24, pp 347-367.

Rutter, A. J., Kershaw, K. A., Robins, P. C., and Morton, A. J. (1971/72). A Predictive model of rain interception in forests, 1. Derivation of the model from observations in a plantation of Corsican Pine. *Agric. Meteorolo.*, 9:367-384.

Schott, J. R. and Volchok, W.J. (1985) Thematic Mapper Thermal Infrared Calibration. *Photogrammetric Engineering and Remote Sensing*, vol. 51, No. 9, pp. 1351-1357.

Thompson, F. B. (1972) Rainfall interception by oak coppice (Quercus robur, L.). Research paper in Forest Meteorology (Ed. by J. A. Taylor), pp. 59-74. *Cambrian News Ltd*, Aberystwyth.

Tsang, C. F. (1991) The modelling process and model validation. *Ground water* 29, 825-831.

Twardy, A. G. and Lindsay, J. D., (1971). Soil survey of the Chip Lake Area, Alberta soil survey, Report No. 28, pp. 1-71.

Wood, E. F., Sivapalan, M., and Beven, K. J. (1990). Similarity ana scale in catchmnet storm response, Rev. Geophys., 28, 1-18.

Table 3.1 Data requirements for applying DPHM-RS to the Paddle River Basin.

Data type	Data Description	Source
Topographic	Mean altitude, aspect, flow direction, slope of the surface, drainage network, and topographic-soil index.	DTED, of the USGS Defense Mapping Agency
Land use	Spatial distribution of land use classes, surface albedo, and vegetation index.	Remote sensing (Landsat TM, NOAA-AVHRR)
Soil properties	Spatial distribution of soil types, antecedent moisture content, and soil hydraulic properties.	Research Council of Alberta, and Radarsat SAR data.
Stream flow	Hourly stream flow data for all gauging stations in the catchment.	Alberta Environmental Protection
Meteorological	Minimum daily temperature, maximum daily temperature, hourly air temperature, hourly precipitation, hourly wind speed, hourly relative humidity, hourly net radiation, short-wave radiation, and ground heat flux.	Meteorological station

Table 3.2. Analysis of an Hubalta Soil Profile, the major soil group of Paddle River Basin (Source: Twardy and Lindsay, 1971)

Depth (cm)	% Sand	% Silt	% Clay	% Fine C
0-10	25	64	11	1
10-17.5	28	43	29	17
17.5-80	32	31	37	22
80-122.5	33	31	36	21
at 122.5	35	32	33	19

Table 3.3. NOAA-AVHRR radiance conversion parameters
(Source: Canadian Center for Remote Sensing, CCRS)

Band	Wave length (μm)	Gain (A_1)	offset (A_o)
1	0.580 - 0.680	0.61095	-25.0
2	0.725 - 1.100	0.40567	-15.0
3	3.550 - 3.930	-0.001475	1.504
4	10.30 - 11.30	-0.17194	170.8
5	11.50 - 12.50	-0.17973	179.1

Table 3.4. Normalized Difference Vegetation Index (NDVI) from NOAA-AVHRR data acquired in 1996 and 1997 for different land covers (averaged over the whole Paddle River Basin).

Date of data Acquisition	Land use classes					
	Water body	Coniferous forest	Mixed forest	Agricultural land	Pasture	Impervious and highways
July 28, 1996	0.353	0.367	0.370	0.379	0.389	0.382
August 1, 1996	0.425	0.413	0.441	0.407	0.413	0.403
August 11, 1996	0.395	0.390	0.410	0.391	0.406	0.396
August 22, 1996	0.382	0.381	0.400	0.390	0.406	0.391
August 25, 1996	0.366	0.364	0.359	0.355	0.368	0.363
August 30, 1996	0.338	0.341	0.358	0.362	0.365	0.358
September 12, 1996	0.238	0.247	0.252	0.265	0.274	0.270
October 12, 1996	0.068	0.081	0.055	0.099	0.111	0.102
June 26, 1997	0.210	0.267	0.283	0.344	0.335	0.307
July 9, 1997	0.408	0.414	0.411	0.428	0.413	0.418
July 19, 1997	0.406	0.414	0.416	0.427	0.416	0.420
August 3, 1997	0.406	0.412	0.411	0.418	0.410	0.410
August 26, 1997	0.150	0.163	0.172	0.176	0.174	0.181
September 8, 1997	0.323	0.330	0.329	0.339	0.326	0.333
September 23, 1997	0.124	0.138	0.140	0.147	0.141	0.138
October 5, 1997	0.074	0.082	0.088	0.102	0.089	0.082
May 10, 1998	0.220	0.202	0.199	0.190	0.191	0.188
June 10, 1998	0.086	0.160	0.200	0.211	0.215	0.165

Table 3.5. Relationship between NDVI and Leaf Area Index (LAI) for different land use classes.

	Land cover type	Equation	Reference
1.	Agriculture	$LAI = -2.5\ln(1.2 - 2NDVI)$	Kanemasu et al., 1977[#]
2.	Pasture	$LAI = 0.21\exp(NDVI / 0.264)$	Kite and Spence, 1995
3.	Mixed forest	$LAI = \left(0.52 * \left(\frac{NDVI + 1}{1 - NDVI}\right)\right)^{1.715}$	Petersen et al., 1987
4.	Coniferous forest	$LAI = 0.65 * \exp\left(\frac{NDVI}{0.34}\right)$	Nemani and Running, 1989

[#] Based on $NDVI_{min}=0.1$ and $NDVI_{max}= 0.6$.

Table 3.6. Percentage of different land cover classes for each sub-basin of Paddle River Basin

Sub-basin	Area of each sub-basin (km^2)	Land use classes					
		Water body	Coniferous forest	Mixed forest	Agricultural land	Pasture	Impervious and highways
1	55.02	2.01	17.87	59.96	11.03	8.36	0.77
2	49.91	4.45	24.77	51.85	9.79	8.47	0.67
3	56.97	0.62	20.03	27.38	26.11	22.90	2.95
4	88.68	1.55	20.57	59.79	12.28	5.10	0.71
5	11.13	0.07	22.76	17.35	27.14	29.68	3.00

Table 3.7. LANDSAT TM 5 radiance parameters (Source: Duguay and Ledrew, 1991)

Band	Wave length (μm)	Gain (A_1) (w m^{-2} sr^{-1} μm^{-1} DC^{-1})	offset (A_o) (w m^{-2} sr^{-1} μm)
TM_1	0.45 - 0.52	0.602	-1.500
TM_2	0.52 - 0.60	1.175	-2.805
TM_3	0.63 - 0.69	0.806	-1.194
TM_4	0.76 - 0.90	0.814	-1.500
TM_5	1.55 - 1.75	0.108	-0.370
TM_6	10.5 - 12.5	0.0563	1.238
TM_7	2.08 - 2.35	0.057	-0.150

Table 3.8. Surface albedo for different land cover classes in each sub-basin for August 7, 1996 and averaged for each land cover of the whole Paddle River Basin for August 7, July 31, 1996 and July 25, August 26, 1997.

Sub-catchment	Land use classes					
	Water body	Coniferous forest	Mixed forest	Agricultural land	Pasture	Impervious and highways
1	0.018	0.045	0.089	0.136	0.161	0.152
2	0.017	0.040	0.085	0.129	0.160	0.150
3	0.021	0.055	0.094	0.122	0.160	0.153
4	0.012	0.047	0.086	0.117	0.150	0.142
5	0.035	0.060	0.10	0.113	0.165	0.144
Average	0.021	0.049	0.091	0.123	0.159	0.148
July 31, 1996*	0.100	0.109	0.124	0.160	0.168	0.178
July 25, 1997*	0.103	0.186	0.100	0.290	0.253	0.189
August 26, 1997*	0.040	0.083	0.021	0.137	0.122	0.110

* Averaged surface albedo over the whole basin for different land use classes for that day.

Table 3.9. Average surface temperature derived from NOAA-AVHRR data of 1996 and 1997 for different land covers of Paddle River Basin

Date of data Acquisition	Land use classes					
	Water body	Coniferous forest	Mixed forest	Agricultural land	Pasture	Impervious and highways
July 28, 1996	297.10	297.75	297.02	298.40	298.48	298.42
August 1, 1996	295.39	296.19	295.53	297.56	297.13	296.91
August 11, 1996	295.82	296.57	295.93	297.23	297.27	296.97
August 22, 1996	293.05	293.64	292.99	294.34	294.47	294.13
August 25, 1996	296.13	296.70	296.54	296.98	297.16	296.99
August 30, 1996	298.36	299.00	298.42	299.67	299.74	299.56
September 12, 1996	292.61	292.36	292.20	292.38	292.38	292.49
October 12, 1996	280.72	281.22	281.27	282.03	282.45	282.07
July 9, 1997	285.83	286.12	286.35	286.41	286.09	286.38
July 19, 1997	283.87	283.94	284.04	283.97	283.74	284.12
August 3, 1997	286.20	286.62	286.73	286.85	286.44	286.59
August 26, 1997	298.90	301.03	301.28	301.83	301.50	302.40
September 8, 1997	276.62	276.56	276.89	276.69	276.55	276.64
September 23, 1997	283.54	283.43	283.58	283.43	283.22	283.64

Table 3.10. Surface temperature for different land cover classes in each sub-basin for August 7, 1996 and averaged for each land cover of the whole Paddle River Basin for August 7, July 31, 1996 and July 25, August 26, 1997.

Sub-catchment	Land use classes					
	Water body	Coniferous forest	Mixed forest	Agricultural land	Pasture	Impervious and highways
1	291.03	291.88	291.40	293.79	293.32	293.71
2	291.01	291.66	291.51	293.39	293.29	293.00
3	291.51	292.47	291.89	294.70	293.54	293.77
4	291.20	291.88	291.69	293.40	293.31	293.20
5	291.62	292.78	292.19	294.28	293.51	293.71
Average	291.28	292.13	291.74	293.91	293.39	293.48
July 31, 1996*	289.74	290.69	289.91	293.41	292.45	292.82
July 25, 1997*	285.50	287.56	286.61	289.77	290.03	290.30
August 26, 1997*	291.34	291.00	288.13	289.96	286.47	286.19

*Average surface temperature over the whole basin for different land use classes for that day.

Table 3.11. Throughfall coefficient δ for various land cover types (Source: Rutter et al. 1975)

Types of vegetation	Canopy storage Capacity (mm)	Throughfall coefficient δ	Source of data
Corsican pine	1.05	0.25	Robins(1969, 1974)
Douglas fir	1.2	0.09	Robins (1969, 1974)
Norway spruce	1.5	0.25	Leyton et al. (1967)
Hornbeam leafy	1.0	0.35	Leyton et al. (1967)
Hornbeam leafless	0.65	0.55	Leyton et al. (1967)
Oak(control) leafy	0.875	0.45	Thompson (1972)
Oak leafless	0.275	0.80	Thompson (1972)
Oak, defoliatd	0.175	0.85	Thompson (1972)

Table 3.12. Model parameters derived from field observations, past studies, and model calibration.

Parameters	Description	Parameter value		Remark
		Coniferous and Mixed forest	Agriculture and pasture	
w_f	Leaf width (m)	0.020	0.010	Estimated from past research
λ	Attenuation coefficient for eddy diffusivity	3.800	2.500	Estimated from past research
n'	Attenuation coefficient for wind speed	0.600	0.600	Estimated from past research
r_{min}	Minimum canopy resistance (s/m)	80.000	110.000	Estimated from past research
r_{max}	Maximum canopy resistance (s/m)	6000.000	6000.000	Estimated from past research
θ_{cr}	Critical moisture content (m/m)	0.318	0.318	Estimated based on soil type
θ_w	Moisture content at permanent wilting point(m/m)	0.197	0.197	Estimated based on soil type
θ_s	Saturated moisture content	0.390	0.390	Estimated based on soil type
θ_r	Residual moisture content	0.080	0.080	Estimated based on soil texture
B	Pore size index	0.263	0.263	Estimated based on soil texture
ψ_c	Bubbling pressure	0.688	0.688	Estimated based on soil texture
K_s	Saturated hydraulic conductivity (m/hr)	0.024	0.024	Estimated based on soil type
z'_o	Roughness length for bare soil (m)	0.010	0.010	Estimated from past research
z_a	Reference height (m)	10.000	10.000	Measured in the field
h	Mean canopy height (m)	9.00, 6.00	0.50, 0.30	Measured in the field
$f^{\#}$	Exponential decay parameter of K_s	1.200	1.200	Estimated and then calibrated
$n_m^{\#}$	Manning rougness for different land cover	0.150	0.100	Estimated and then calibrated

[#] Parameters obtained by model calibration

Table 3.13. Cross correlation coefficients of daily rainfall data at seven climatic stations located within and around the Paddle River Basin.

	Wild wood	Paddle	Whitecourt	Shining	Roman	Highway	Edson
Wild wood	1						
Paddle	0.586266	1					
Whitecourt	0.525252	0.586379	1				
Shining	0.566960	0.633776	0.622477	1			
Roman	0.628225	0.727736	0.692309	0.728104	1		
Highway	0.633602	0.695197	0.708552	0.729987	0.796475	1	
Edson	0.547851	0.503716	0.679159	0.622567	0.610077	0.591767	1

Table 3.14. Comparison of skin temperature T_s simulated by DPHM-RS against skin temperature derived from NOAA-AVHRR and Landsat TM data.

Date	1996							
	Coniferous Forest		Mixed Forest		Pasture land		Agricultural Land	
	model	Remote sensing	model	Remote sensing	Model	Remote sensing	Model	Remote sensing
July 28	298.68	297.75	300.53	297.02	299.82	298.48	297.96	298.42
July 31*	289.03	290.69	288.74	289.91	293.05	292.45	292.32	293.41
August 1	296.10	296.19	297.29	295.53	298.74	297.13	297.01	297.56
August 7*	292.18	292.13	292.90	291.74	293.29	293.39	291.84	293.91
August 11	295.33	296.57	295.97	295.93	296.92	297.27	295.34	297.23
August 22	292.80	293.05	292.65	292.99	294.05	294.47	293.06	294.34
August 25	294.87	296.70	294.71	296.54	295.66	297.16	295.31	296.98
	1997							
July 19	288.39	283.94	288.28	284.04	287.32	283.74	286.91	284.12
July 25*	289.23	287.59	289.26	286.61	289.17	290.03	288.39	290.30
August 3	288.42	286.62	288.10	286.73	287.49	286.44	287.20	286.59
August 26*	300.36	301.03	302.82	301.28	304.14	301.50	303.88	302.40
August 26	291.12	291.00	290.99	288.13	290.38	286.47	289.96	286.19
September 8	283.75	276.56	283.75	276.89	283.36	276.55	283.21	276.64
September 23	284.27	283.43	284.04	283.58	283.77	283.22	282.96	283.64

* On this 4 days, remote sensing data are that of Landsat TM. Onother days, they are NOAA-AVHRR data.

Table 3.15 Parameter sets used in TOPMODEL

Parameter	Definition	Optimized values
m, m	Exponential storage parameter (Transmissivity profile scaling)	0.0019
T_o, m^2/h	Downslope transmissivity at saturation	5.0000
T_D, h	Unsaturated zone time delay per unit storage deficit	100.000
CH_V, m/h	Main channel routing velocity	20.00
R_V, m/h	Internal subcatchment routing velocity	1100.000
Sr_{max}, m	The root zone available water capacity	0.021
K_o, m/h	Surface hydraulic conductivity at saturation	0.024
H_f, m	Wetting front suction	0.6879

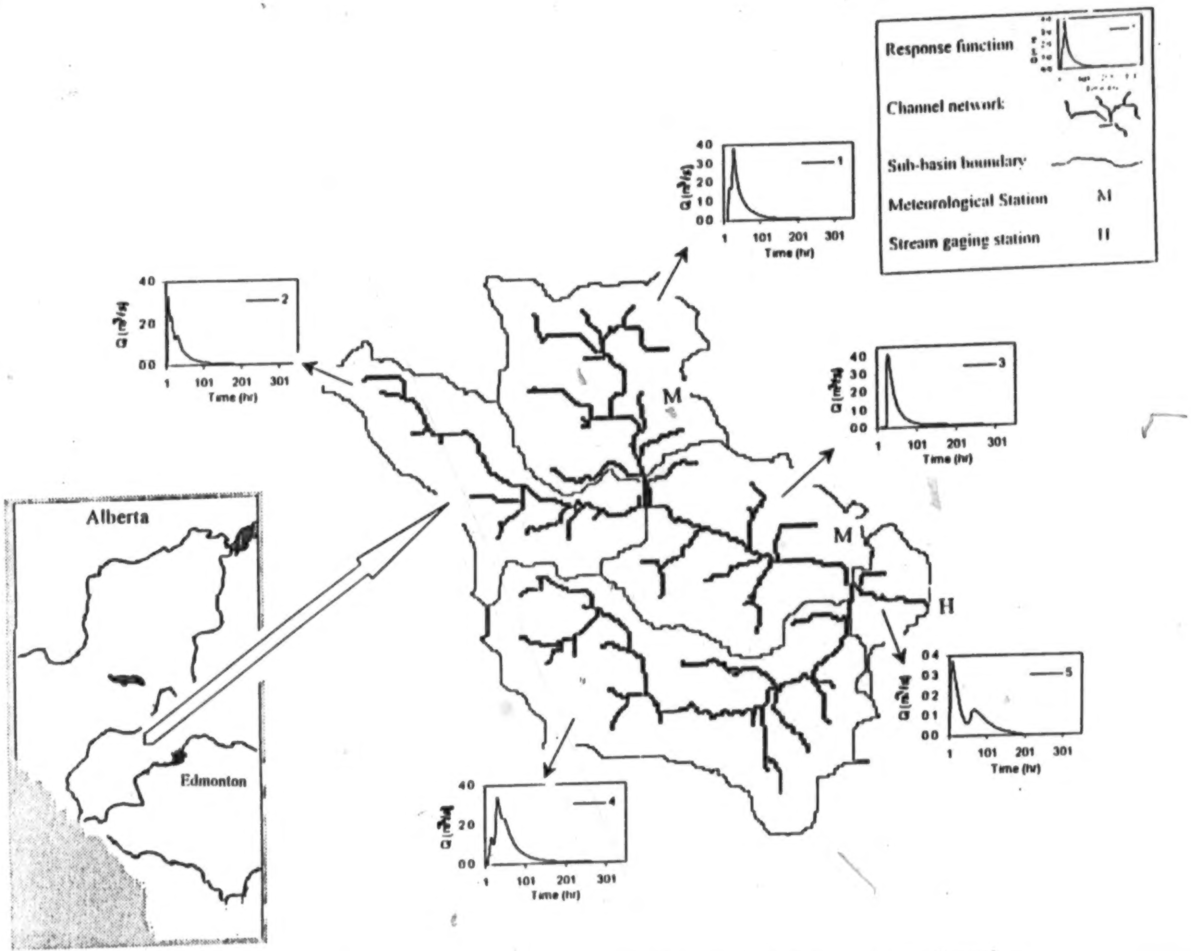
Response function
Channel network
Sub-basin boundary
Meteorological Station M
Stream gaging station H
Alberta
Edmonton
M
M
H
Q (m³/s)
Time (hr)
1 101 201 301
40 30 20 10 00
1
2
3
4
5
04 03 02 01 00

Figure 3.1 Location map, meteorological stations, stream gauging station, and the response function for each of the 5 sub-basins of the Paddle River Basin.

(a) Rainfall

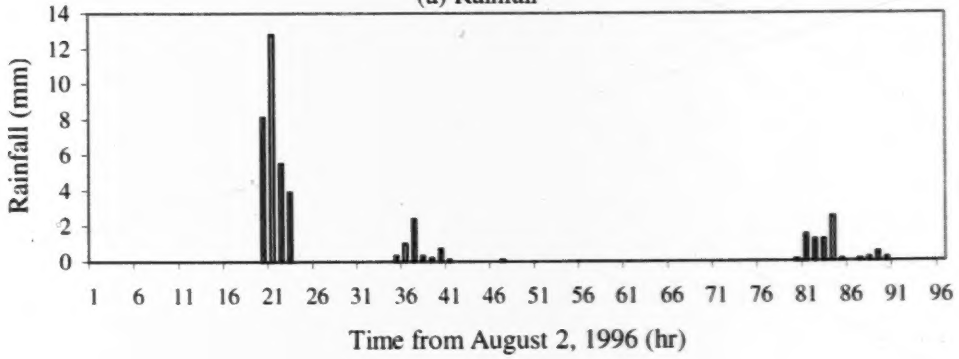

(b) Energy fluxes

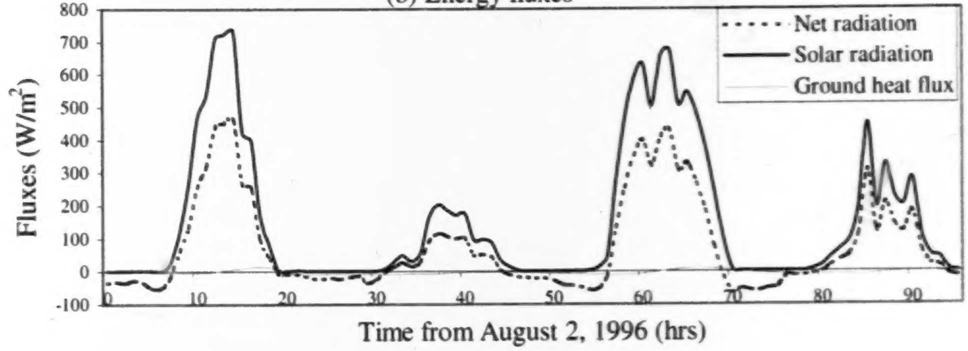

(c) Wind speed

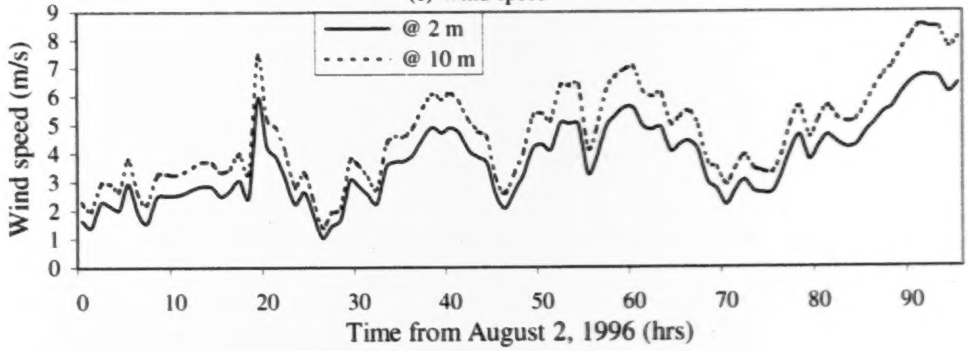

Figure 3.2 (a)-(c) Typical plots of meteorological data measured at Paddle River Basin for four days.

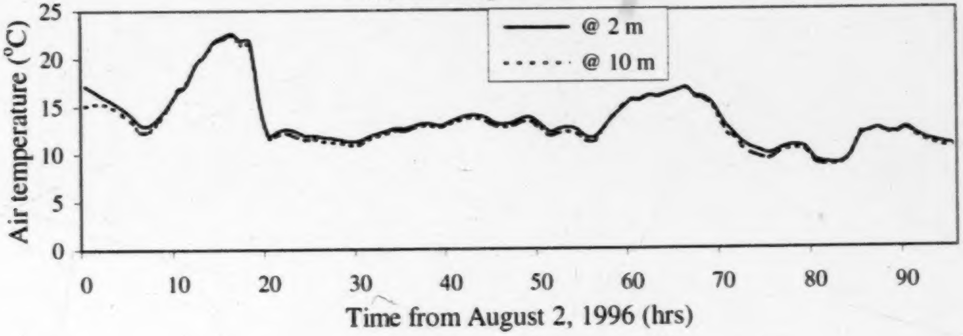
(d) Air temperature

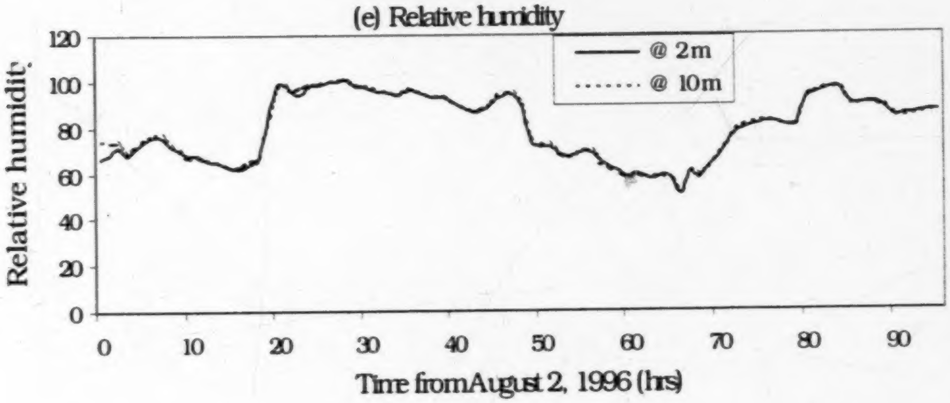
(e) Relative humidity

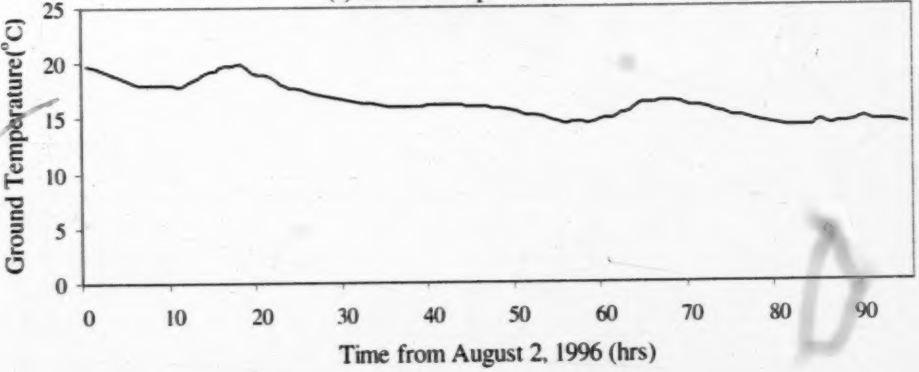
(f) Ground temperature

Figure 3.2 (d)-(f) Typical plots of meteorological data measured at Paddle River Basin for four days.

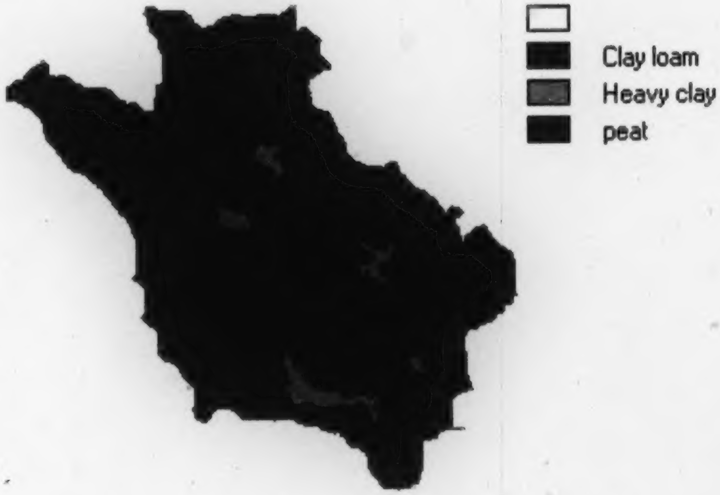
Clay loam
Heavy clay
peat

Figure 3.3 Average soil group for the Paddle River Basin

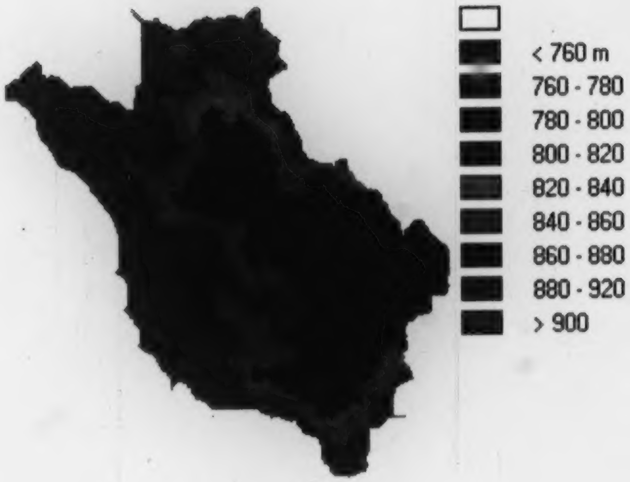
< 760 m
760 - 780
780 - 800
800 - 820
820 - 840
840 - 860
860 - 880
880 - 920
> 900

3.4 Mean elevations of Paddle River Basin derived from Digital Terrain Elevation data

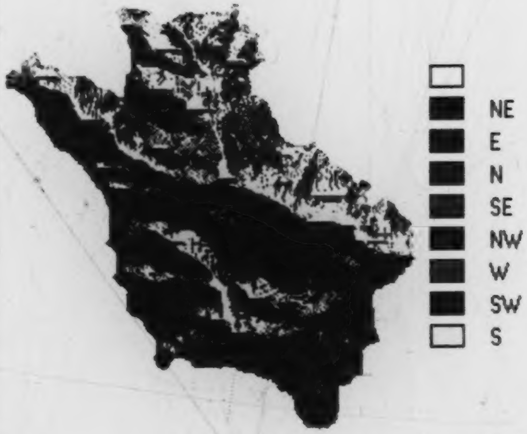
NE
E
N
SE
NW
W
SW
S

Figure 3.5 Flow direction for surface runoff from Paddle River Basin derived from Digital Terrain Elevation data

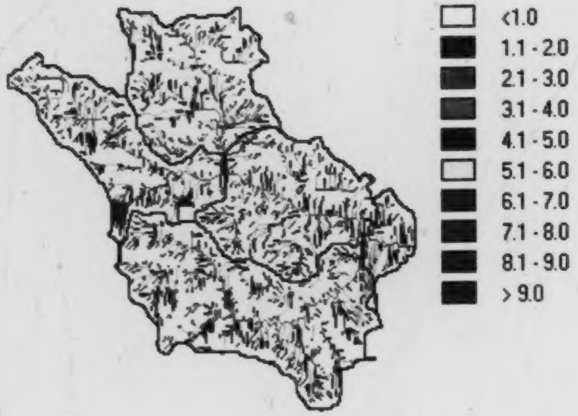
<1.0
1.1 - 2.0
2.1 - 3.0
3.1 - 4.0
4.1 - 5.0
5.1 - 6.0
6.1 - 7.0
7.1 - 8.0
8.1 - 9.0
> 9.0

Figure 3.6 Topographic-soil index for Paddle River Basin derived from Digital Terrain Elevation data

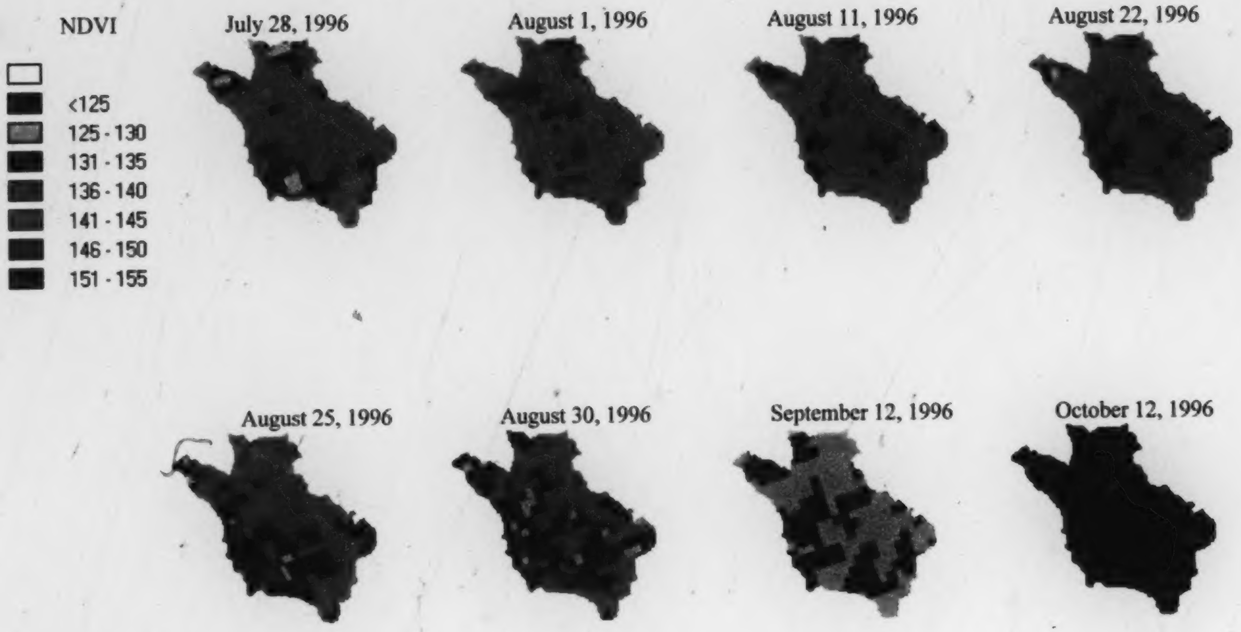
NDVI
☐
<125
125 - 130
131 - 135
136 - 140
141 - 145
146 - 150
151 - 155
July 28, 1996
August 1, 1996
August 11, 1996
August 22, 1996
August 25, 1996
August 30, 1996
September 12, 1996
October 12, 1996

Figure 3.7. Normalized Difference Vegetation Index (NDVI) derived from NOAA-AVHRR Image for Paddle River Basin (1996)

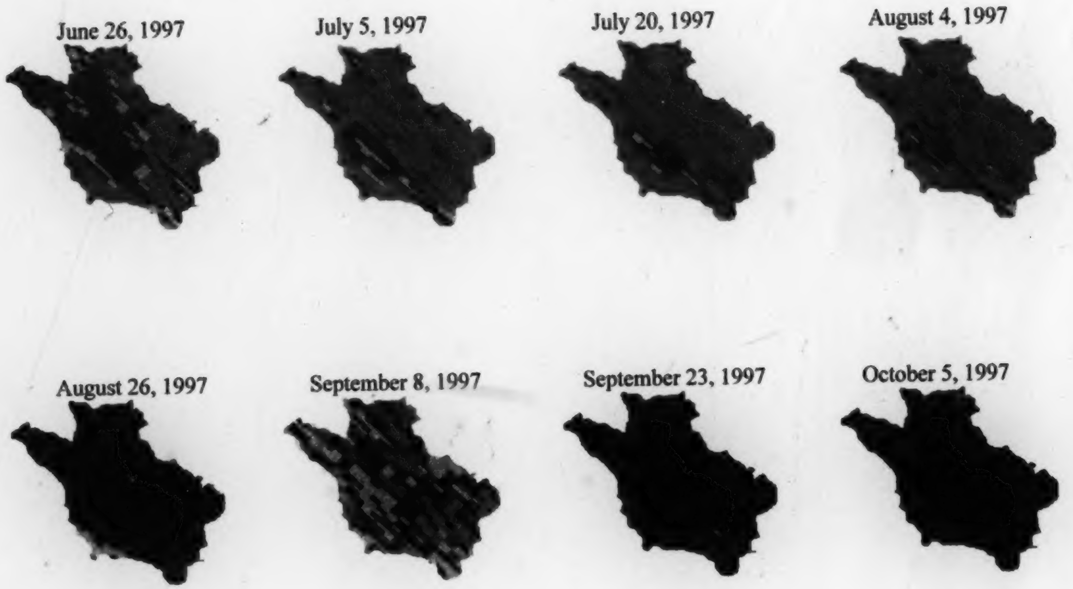
June 26, 1997
July 5, 1997
July 20, 1997
August 4, 1997
August 26, 1997
September 8, 1997
September 23, 1997
October 5, 1997

Figure 3.7. Normalized Difference Vegetation Index (NDVI) derived from NOAA-AVHRR Image for Paddle River Basin (1997)

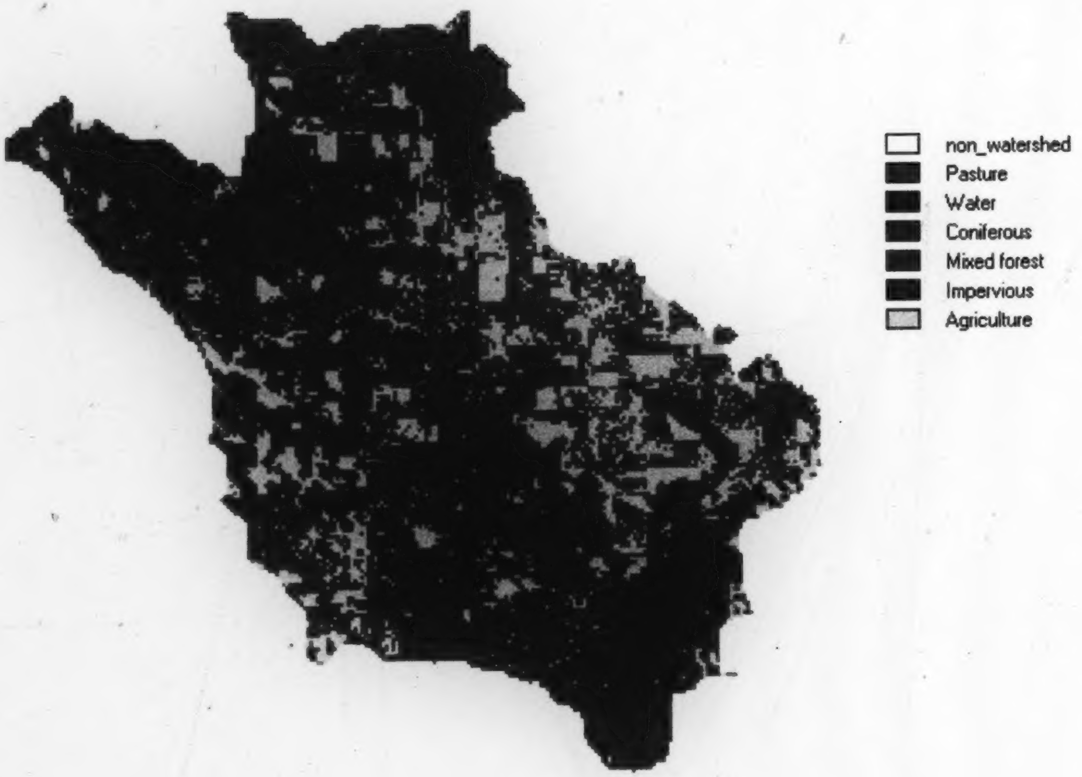
non_watershed
Pasture
Water
Coniferous
Mixed forest
Impervious
Agriculture

Figure 3.8 Land use classification for Paddle River Basin retrieved from Landsat TM image of August 7, 1996.

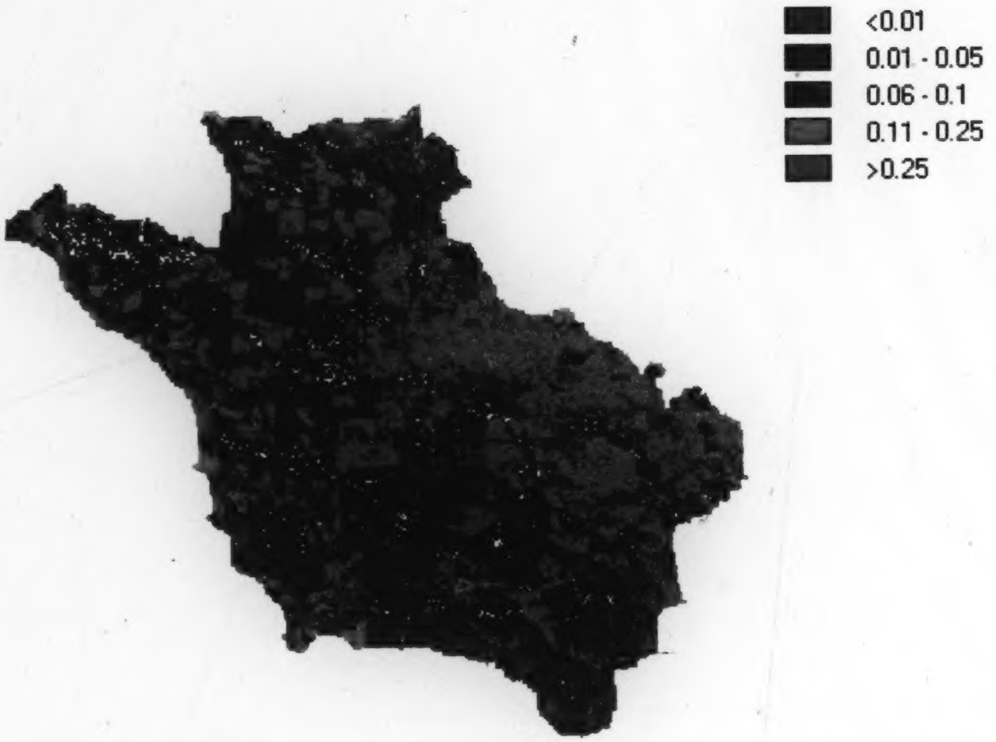
<0.01
0.01 - 0.05
0.06 - 0.1
0.11 - 0.25
>0.25

Figure 3.9 Surface Albedo for Paddle River Basin retrieved from Landsat TM image of August 7, 1996.

<15.0
15.1 - 18.0
18.1 - 19.0
19.1 - 20.0
20.1 - 25.0
> 25.0

Figure 3.10 Surface temperature for Paddle River Basin retrieved from Landsat TM image of August 7, 1996.

(a) Daily Average flow for Paddle River Basin (from 1980 to 1993 data)

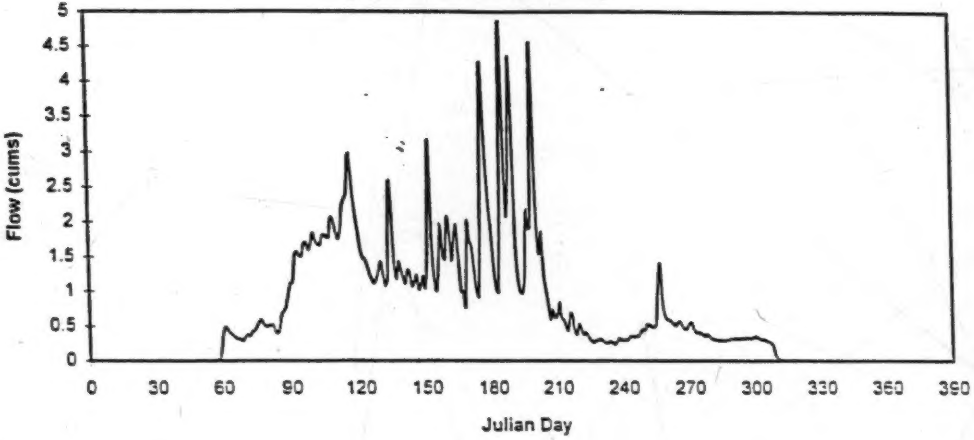

(b) Rating curve for Paddle River near Anselmo

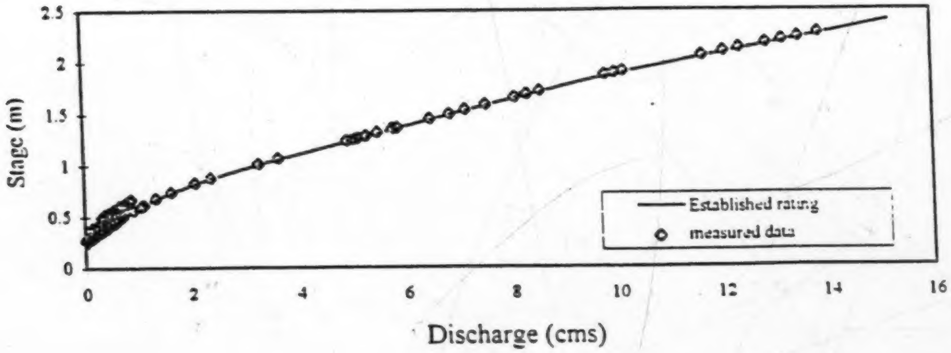

Figure 3.11 (a)-(b) Stream flow for Paddle River Basin as recorded at the stream gauging station near Anselmo (station No. 07BB011)

(a) Discharge at the basin outlet: Calibration Period

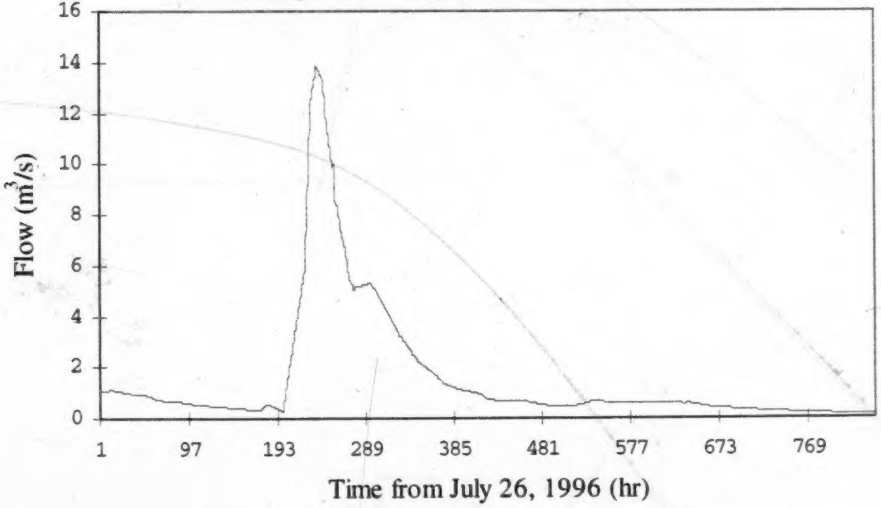

(b) Discharge at the basin outlet: Validation Period

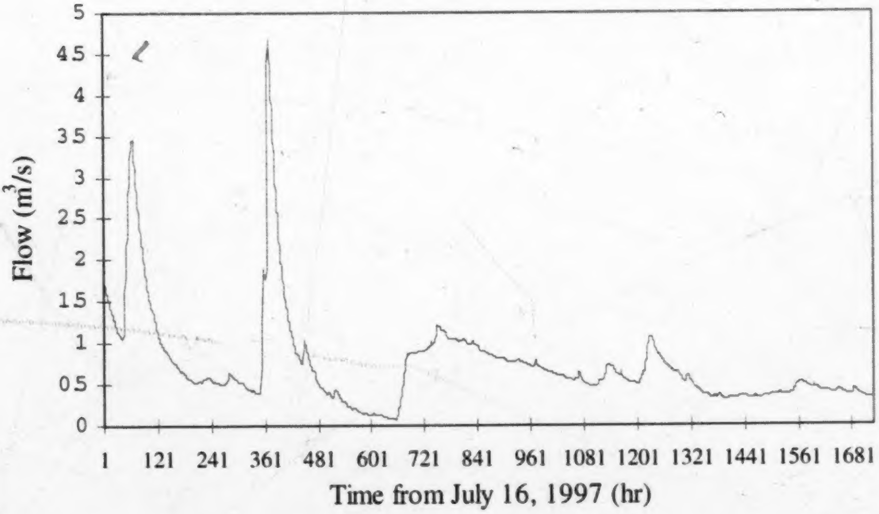

Figure 3.11 (c)-(d) Stream flow for Paddle River Basin as recorded at the stream gauging station near Anselmo (station No. 07BB011)

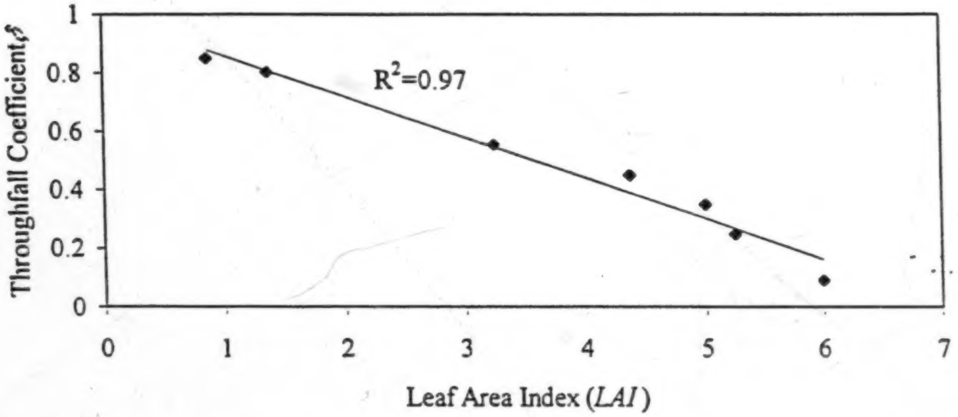

Figure 3.12. A simple regression between throughfall coefficient δ and leaf area index based on actual field measurements of several researchers.

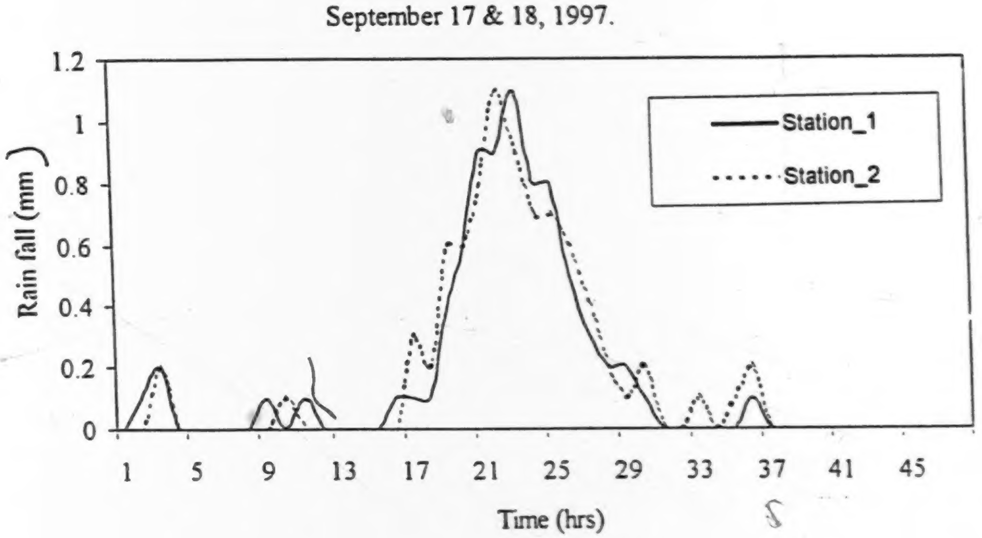

Figure 3.13 Comparison of rainfall data measured at two rain gauges installed 13 km apart in the Paddle River Basin.

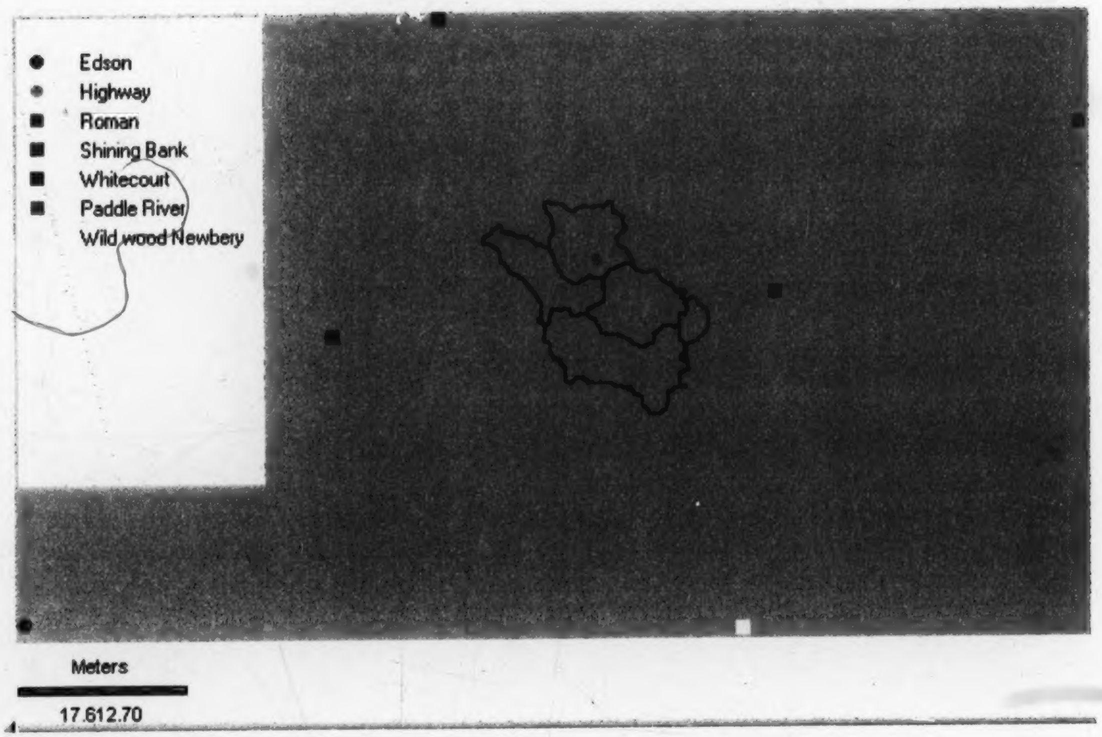
● Edson
● Highway
■ Roman
■ Shining Bank
■ Whitecourt
■ Paddle River
Wild wood Newbery
Meters
17.612.70

Figure 3.14 Location of Meteorological stations with respect to Paddle River Basin

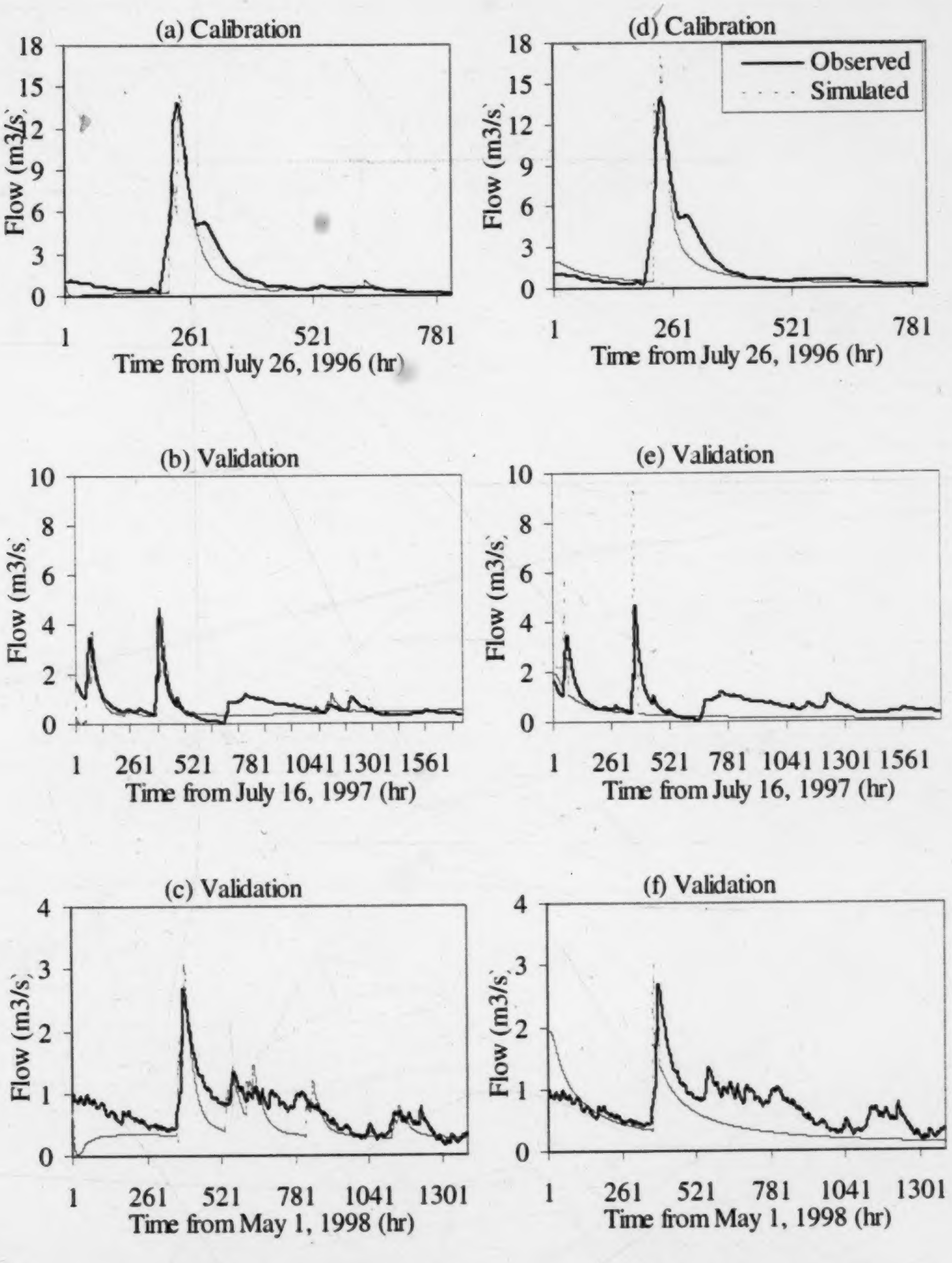

Figure 3.15 Comparison of runoff observed at the outlet of the Paddle River Basin with runoff simulated by DPHM-RS ((a)-(c)) and TOPMODEL ((d)-(f)) at both calibration and validation periods.

(a) Calibration period

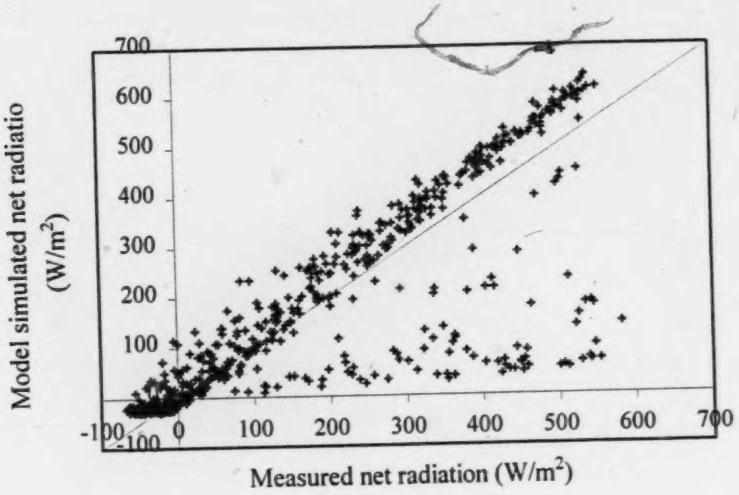

(b) Validation period

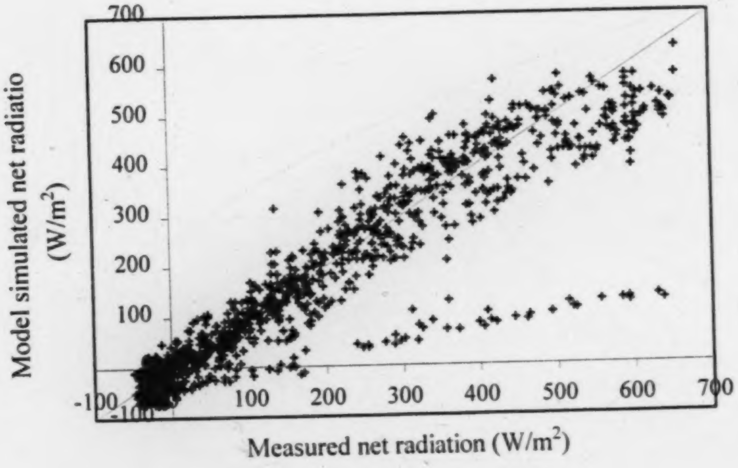

Figure 3.16 Net radiation simulated by DPHM-RS based on surface albedo retrieved from Landsat TM data, model simulated surface temperature, and measured solar radiation and air temperature for (a) calibration period of summer 1996, and (b) validation period of summer 1997.

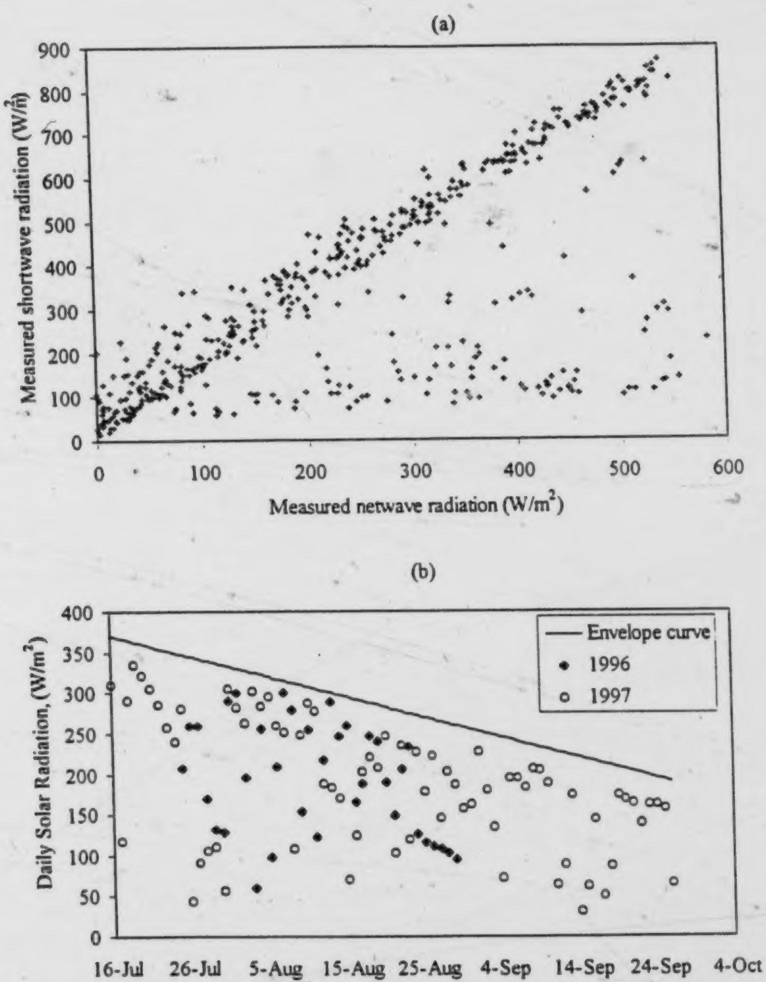

Figure 3.17 Correction for the effect of cloud cover based on the measured shortwave radiation: (a) the effect of cloud cover on the measured shortwave radiation when compared to the net radiation; (b) a proposed envelop (Rs(max)) to the daily measured short wave radiation; (c) a regression approach to compute the fraction of cloud cover; (d) Simulated net radiation after correction for cloud cover effect based on (c).

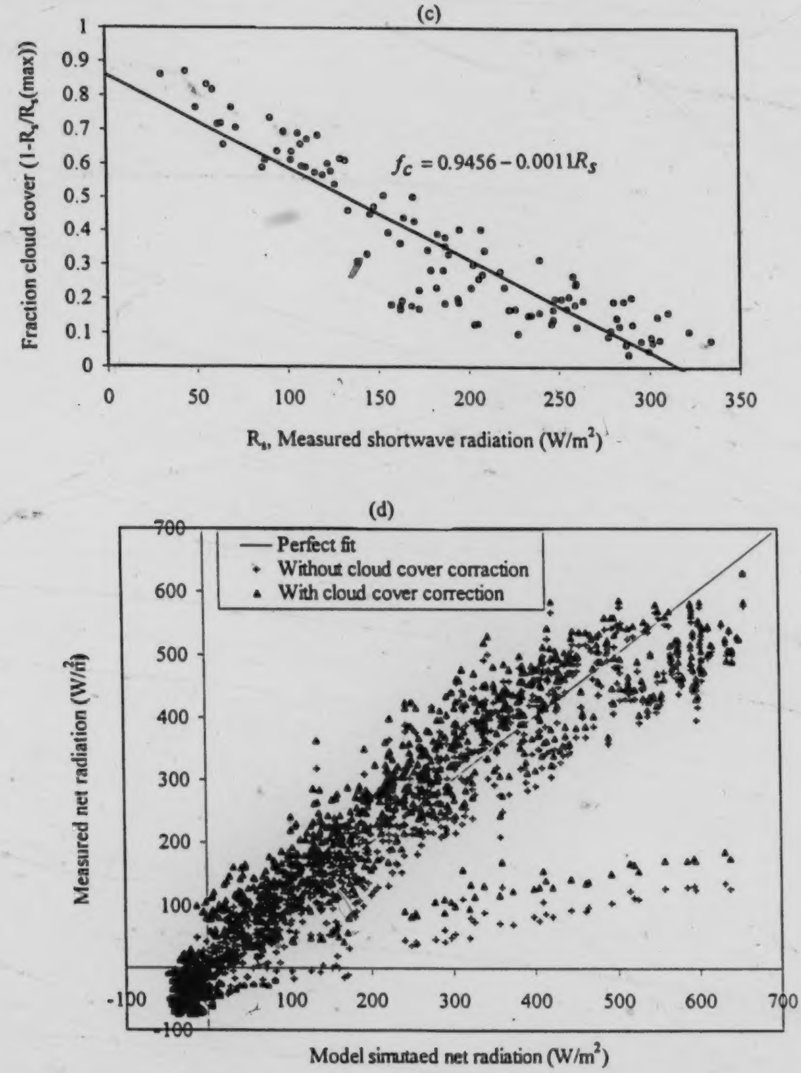

Figure 3.17 Correction for the effect of cloud cover based on the measured shortwave radiation: (a) the effect of cloud cover on the measured shortwave radiation when compared to the net radiation; (b) a proposed envelop (Rs(max)) to the daily measured short wave radiation; (c) a regression approach to compute the fraction of cloud cover; (d) Simulated net radiation after correction for cloud cover effect based on (c).

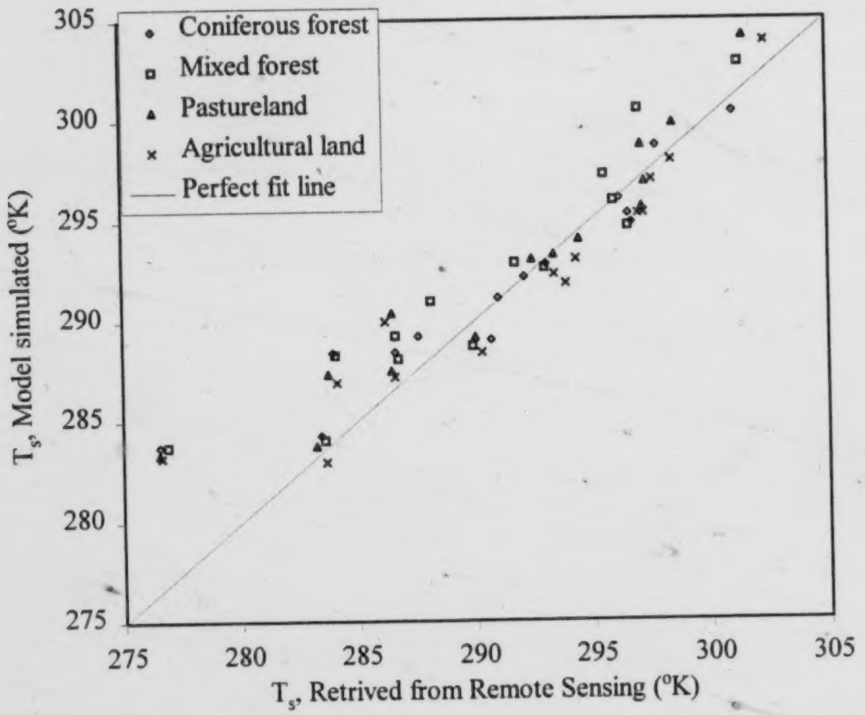

Figure 3.18 Comparison of model simulated surface temperature T_s with skin temperature retrieved from remotely sensed data (either NOAA-AVHRR or Landsat TM) for various land cover types.

(a) Actual evaporation at soil surface and water surface

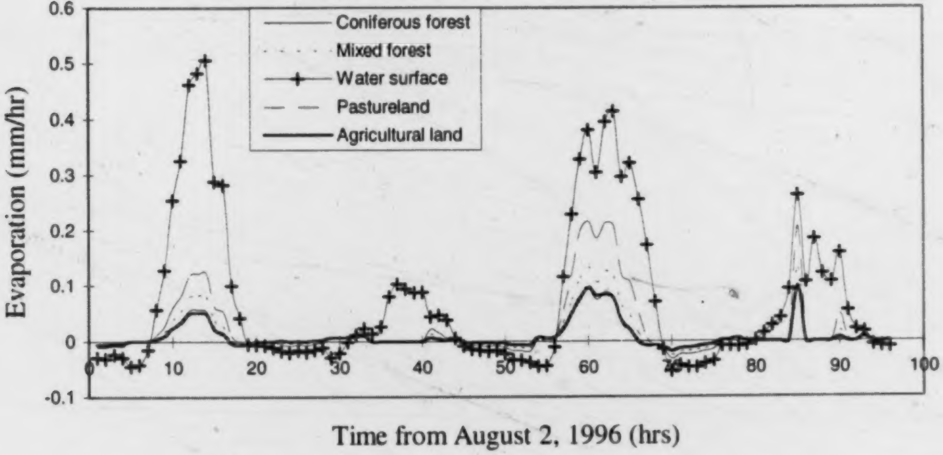

(b) Transpiration from vegetation canopy

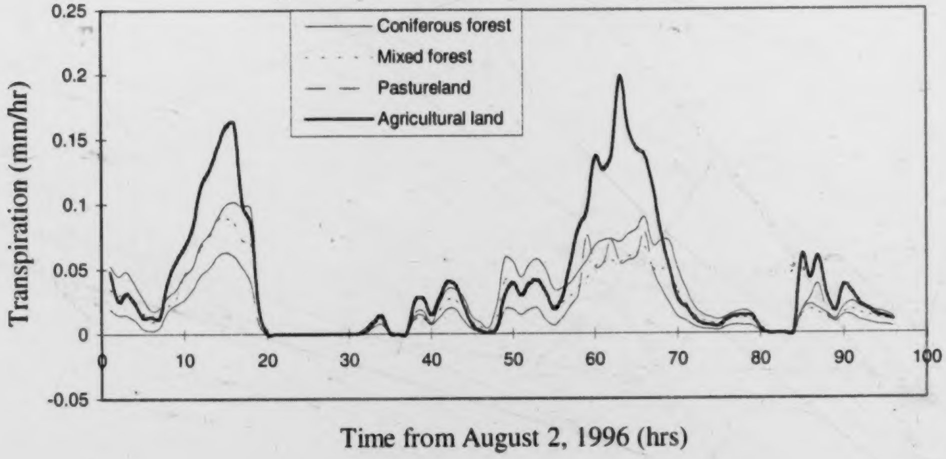

Figure 3.19 (a)-(b) Evapotranspiration, surface temperature, canopy temperature, soil moisture, and sensible and latent energy fluxes simulated by DPHM-RS during calibration period.

(c) Wet canopy evaporation

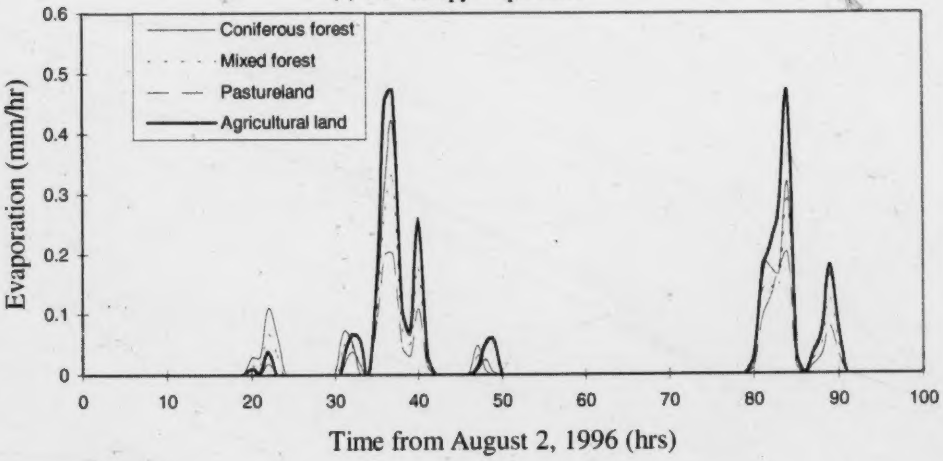

(d) Temperature at soil and water surface

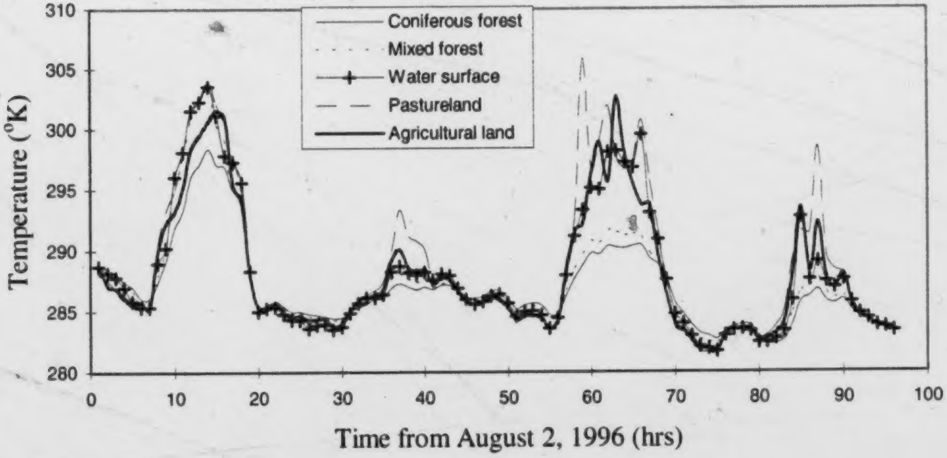

Figure 3.19 (c)-(d) Evapotranspiration, surface temperature, canopy temperature, soil moisture, and sensible and latent energy fluxes simulated by DPHM-RS during calibration period.

(e) Canopy temperature

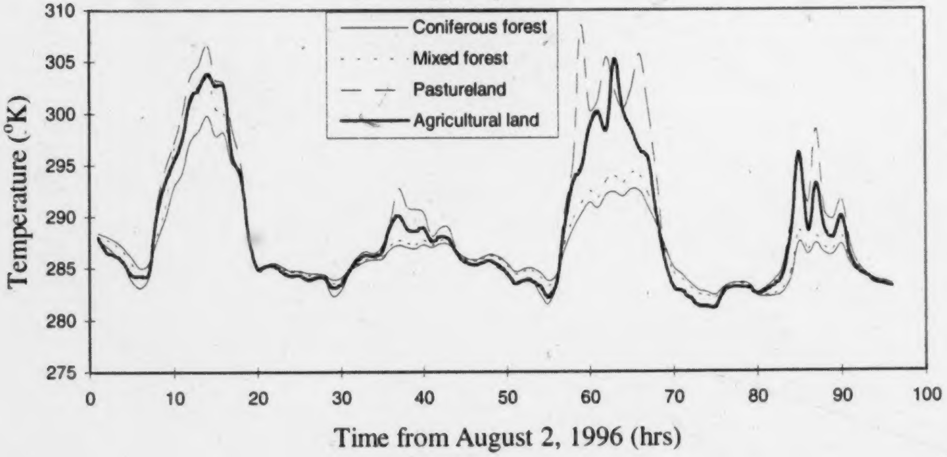

(f) Sensible heat at reference height

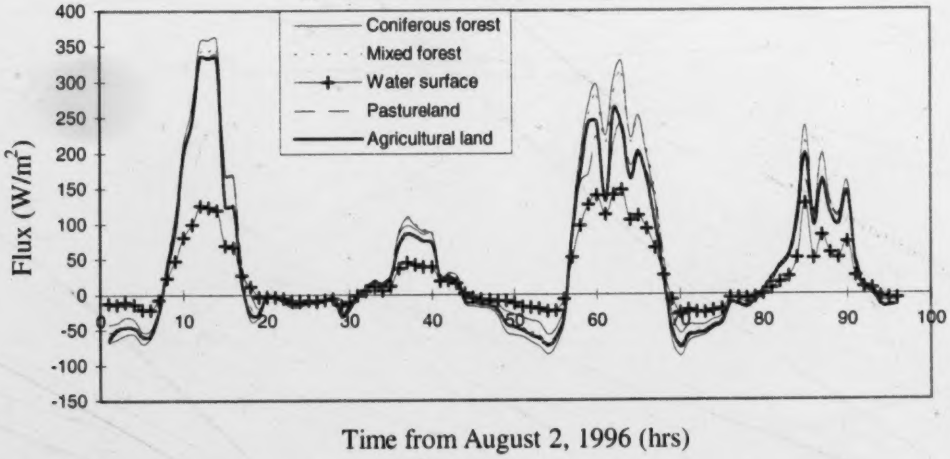

Figure 3.19 (e)-(f) Evapotranspiration, surface temperature, canopy temperature, soil moisture, and sensible and latent energy fluxes simulated by DPHM-RS during calibration period.

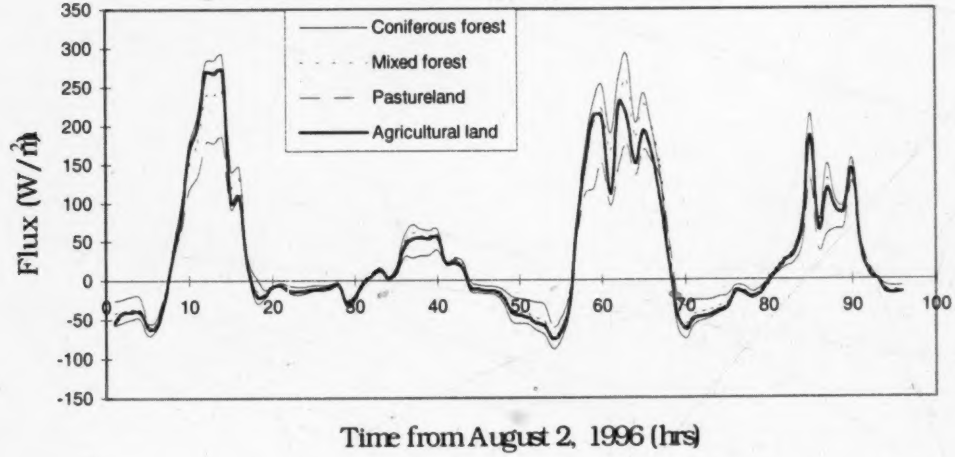

(g) Sensible heat at within canopy height (fictitious height)

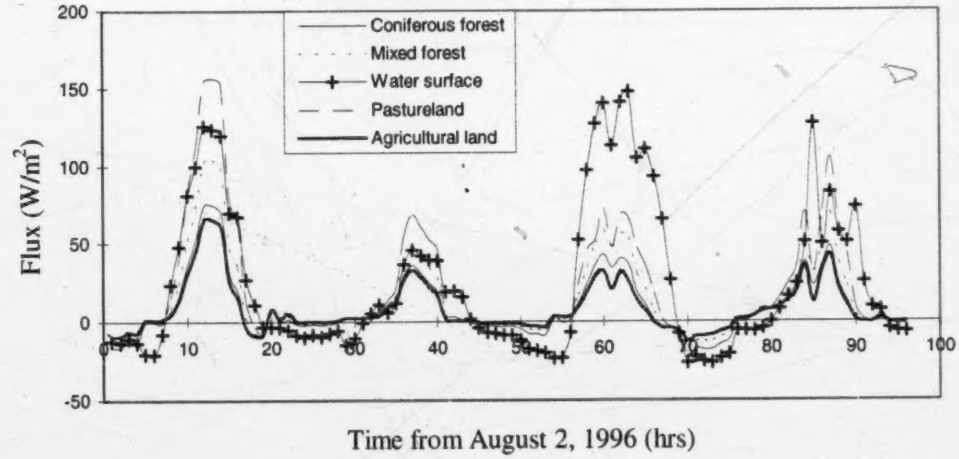

(h) Sensible heat at soil and water surface

Figure 3.19 (g)-(h) Evapotranspiration, surface temperature, canopy temperature, soil moisture, and sensible and latent energy fluxes simulated by DPHM-RS during calibration period.

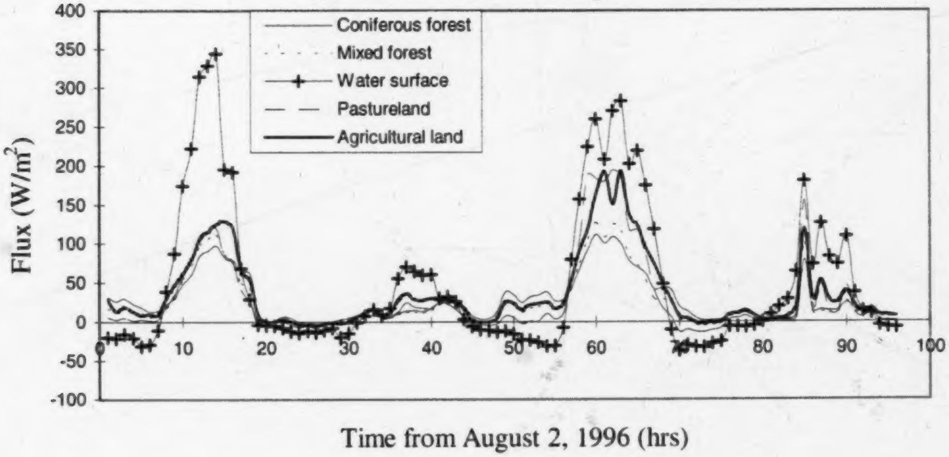

(i) Latent heat at reference height

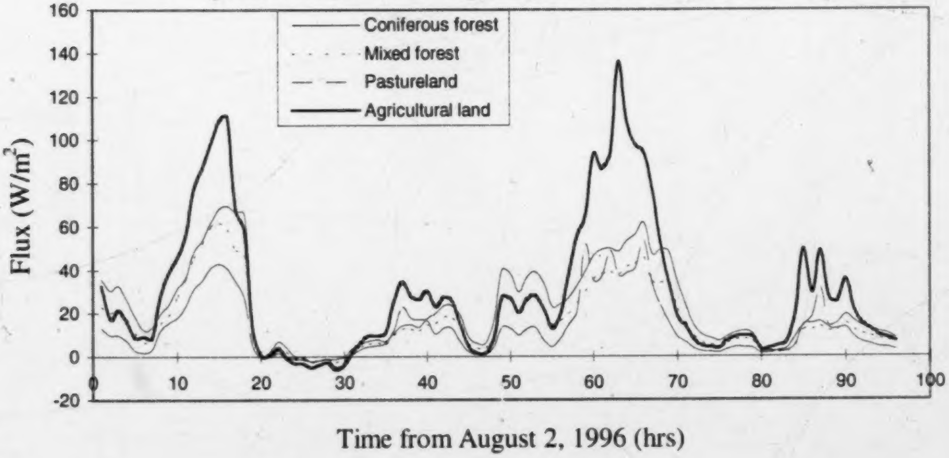

(j) latent heat at within canopy height (fictitious height)

Figure 3.19 (i)-(j) Evapotranspiration, surface temperature, canopy temperature, soil moisture, and sensible and latent energy fluxes simulated by DPHM-RS during calibration period.

(k) Latent heat at soil and water surface

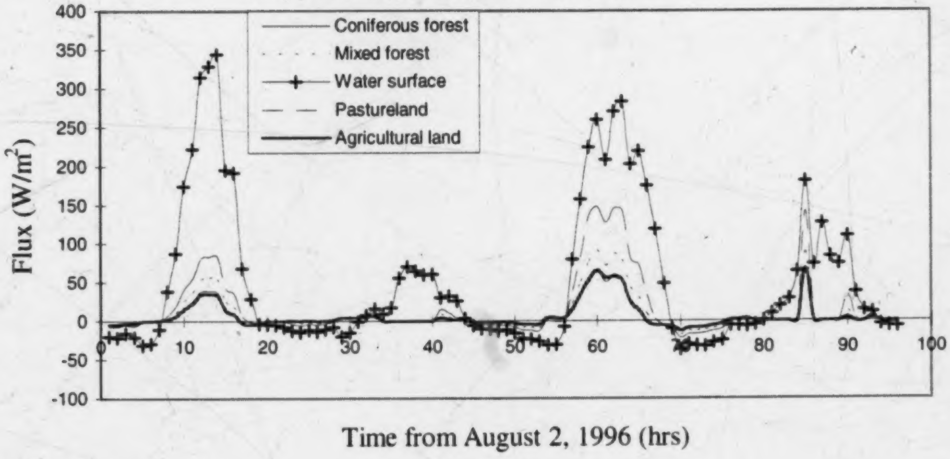

(l) Net radition at within canopy height (fictitious height)

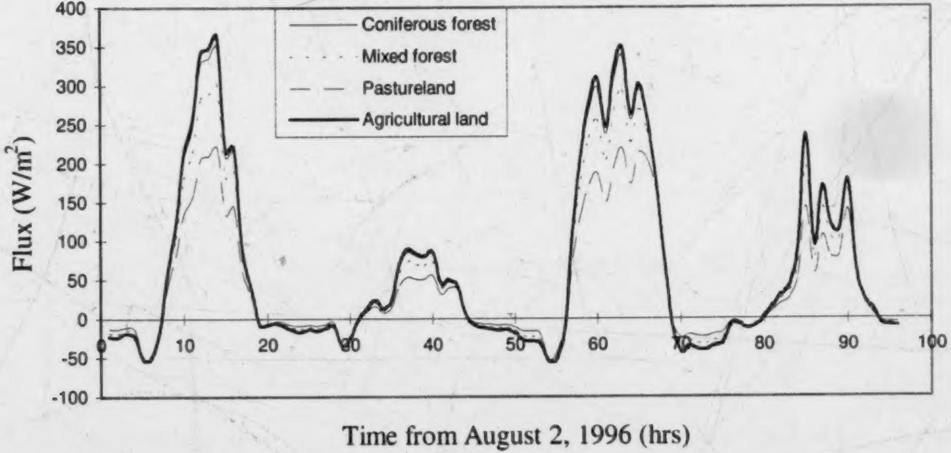

Figure 3.19 (k)-(l) Evapotranspiration, surface temperature, canopy temperature, soil moisture, and sensible and latent energy fluxes simulated by DPHM-RS during calibration period.

(m) Net radition at soil surface

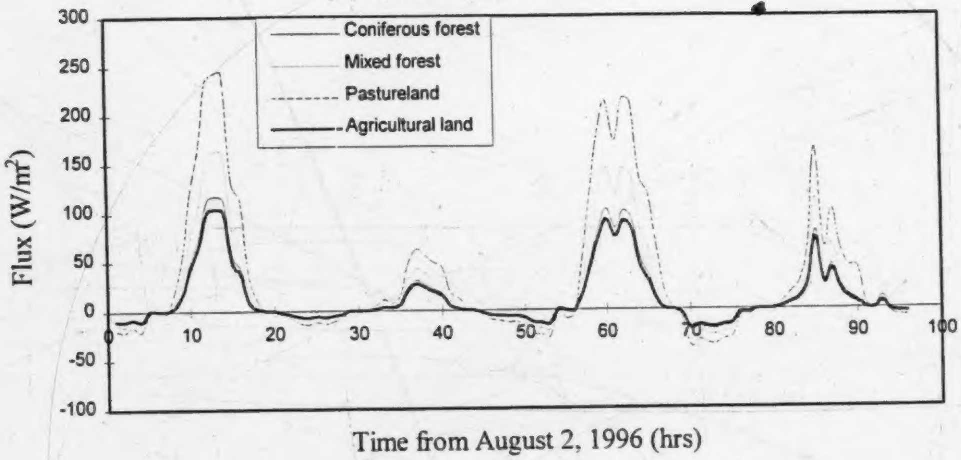

(n) Soil Moisture for one sub-basin

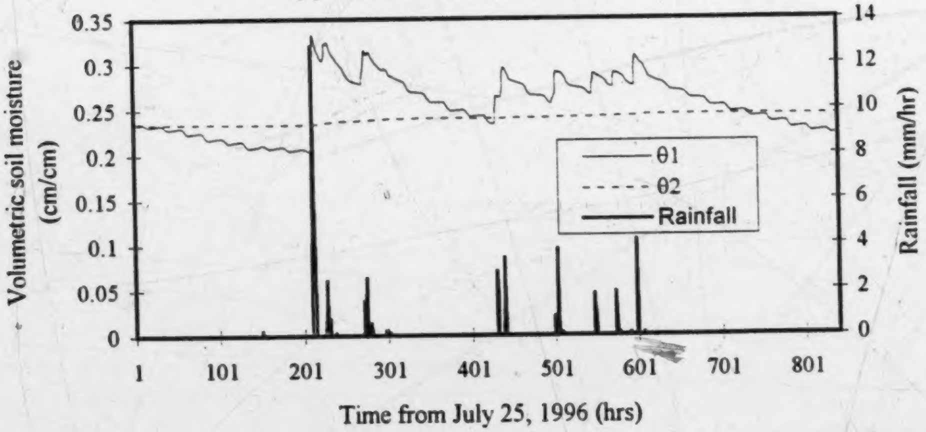

Figure 3.19 (m)-(n) Evapotranspiration, surface temperature, canopy temperature, soil moisture, and sensible and latent energy fluxes simulated by DPHM-RS during calibration period.

(a) Actual evaporation at soil surface and water surface

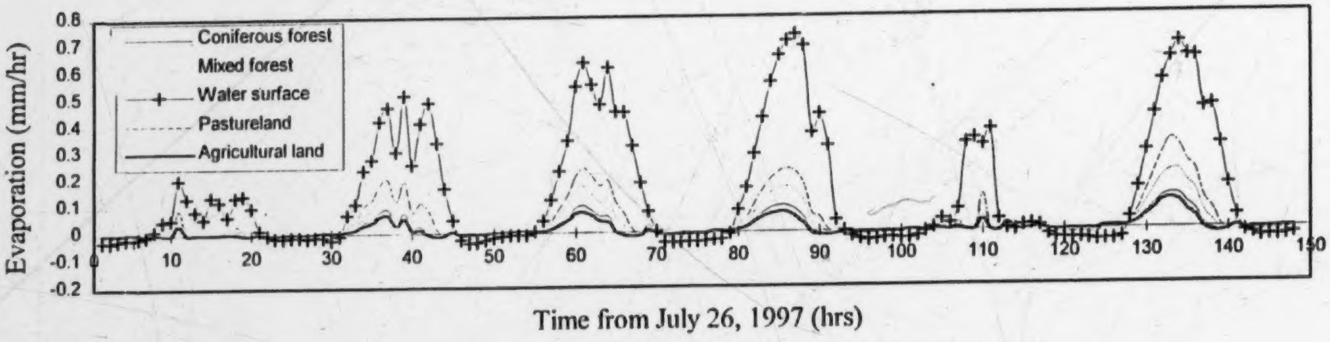

(b) Transpiration from vegetation canopy

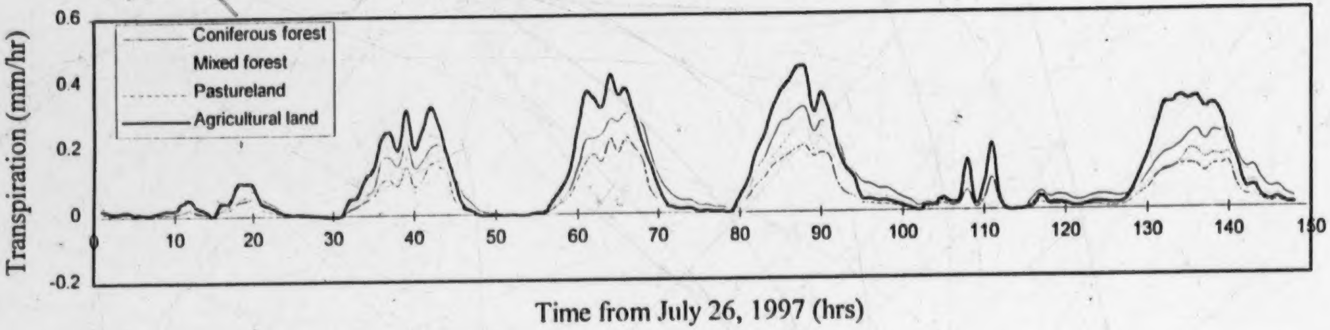

Figure 3.20 (a)-(b) Evapotranspiration, surface temperature, canopy temperature, soil moisture, and sensible and latent energy fluxes simulated by DPHM-RS during validation period.

(c) Wet canopy evaporation

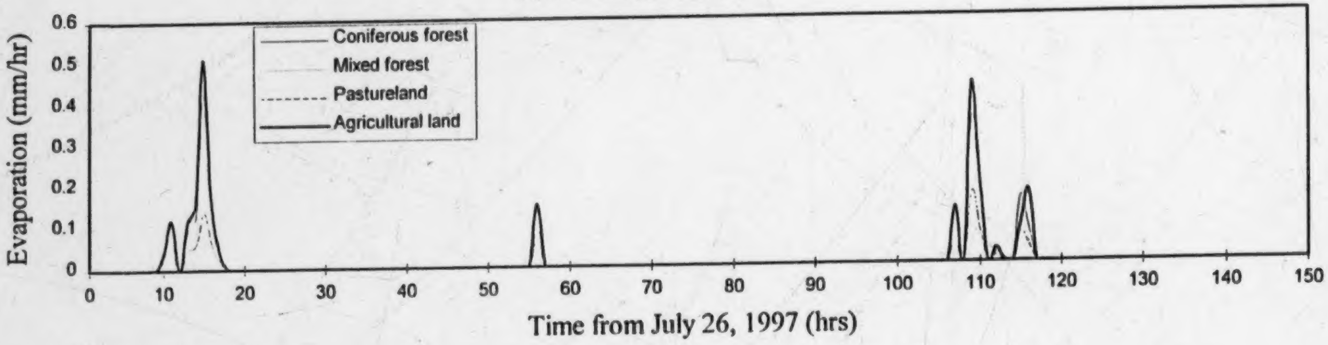

(d) Temperature at soil surface

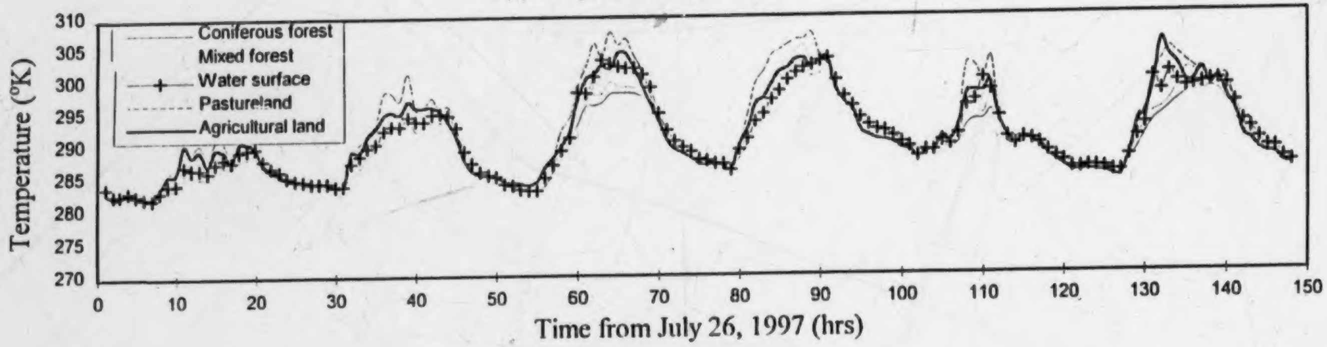

Figure 3.20 (c)-(d) Evapotranspiration, surface temperature, canopy temperature, soil moisture, and sensible and latent energy fluxes simulated by DPHM-RS during validation period.

(e) Canopy temperature

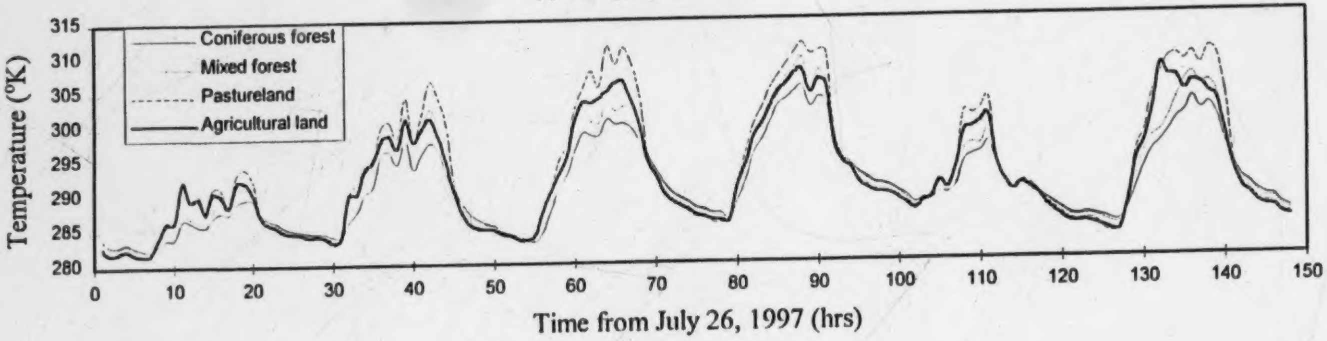

(f) Sensible heat at reference height

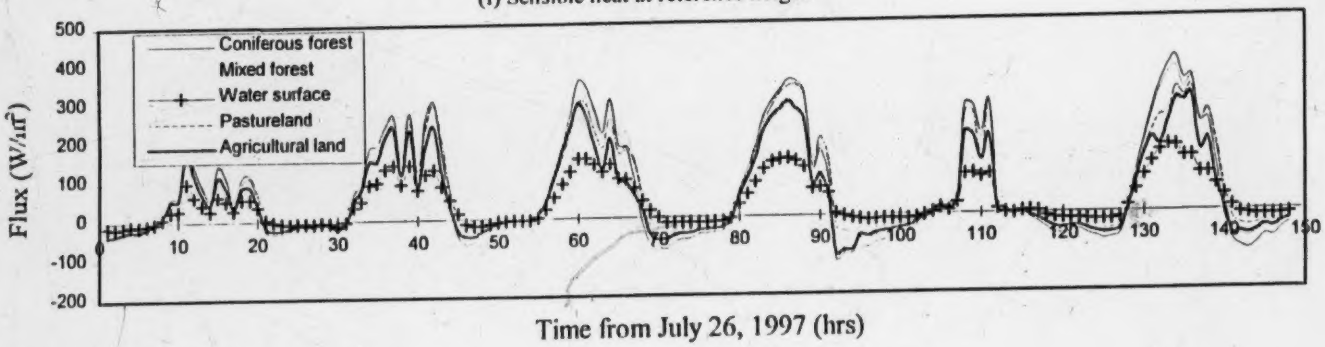

Figure 3.20 (e)-(f) Evapotranspiration, surface temperature, canopy temperature, soil moisture, and sensible and latent energy fluxes simulated by DPHM-RS during validation period.

(g) Sensible heat at within canopy height (fictitious height)

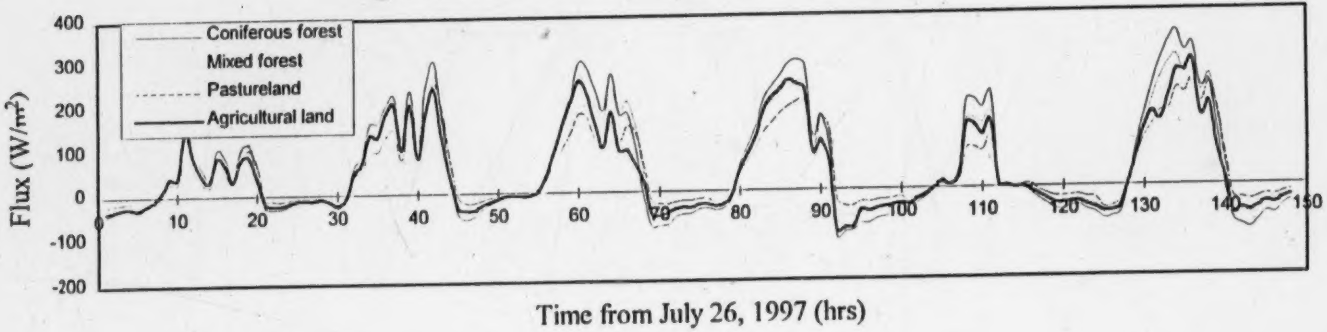

(h) Sensible heat at soil and water surface

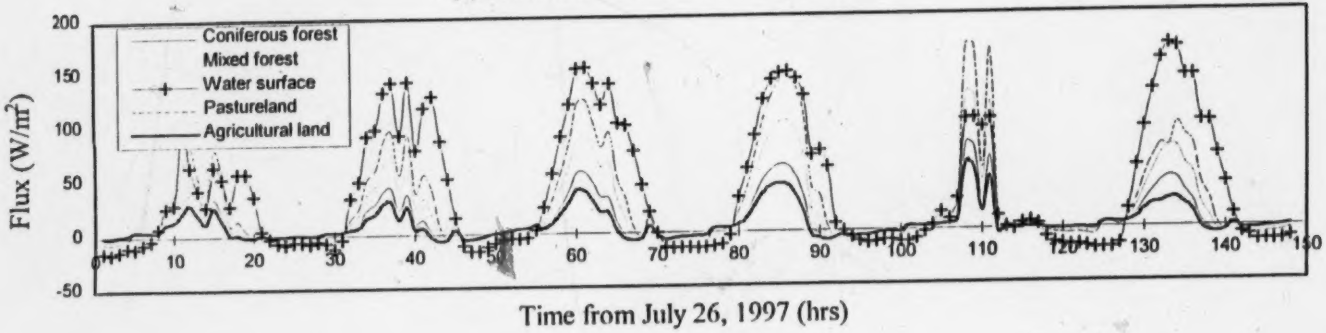

Figure 3.20 (g)-(h) Evapotranspiration, surface temperature, canopy temperature, soil moisture, and sensible and latent energy fluxes simulated by DPHM-RS during validation period.

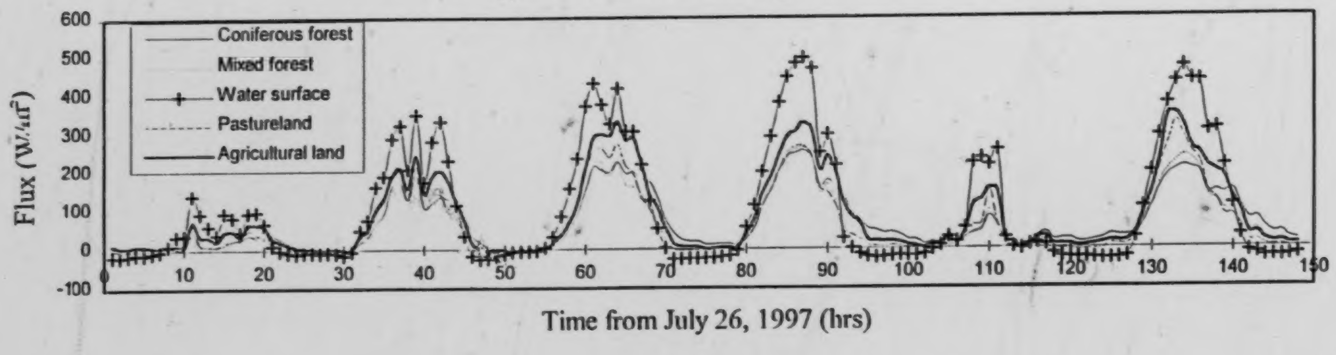

(i) Latent heat at reference height

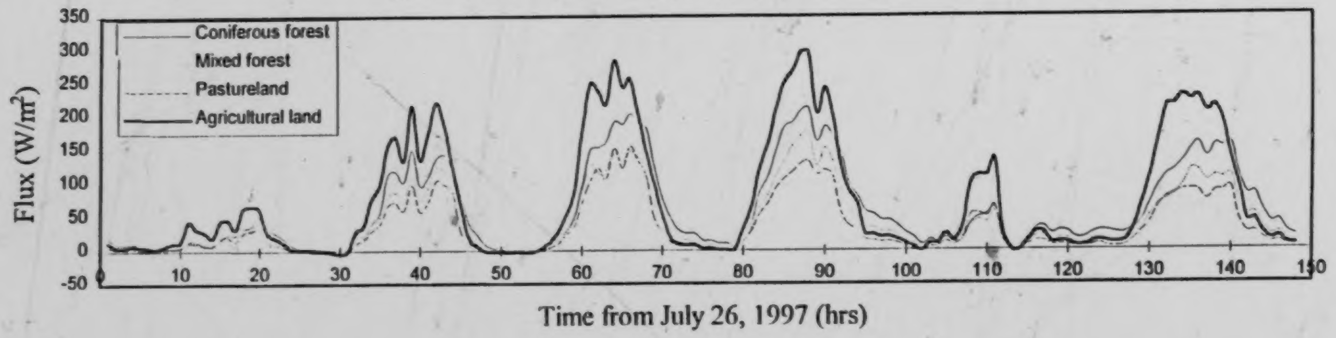

(j) Latent heat at within canopy height (fictitious height)

Figure 3.20 (i)-(j) Evapotranspiration, surface temperature, canopy temperature, soil moisture, and sensible and latent energy fluxes simulated by DPHM-RS during validation period.

(k) Latent heat at soil and water surface

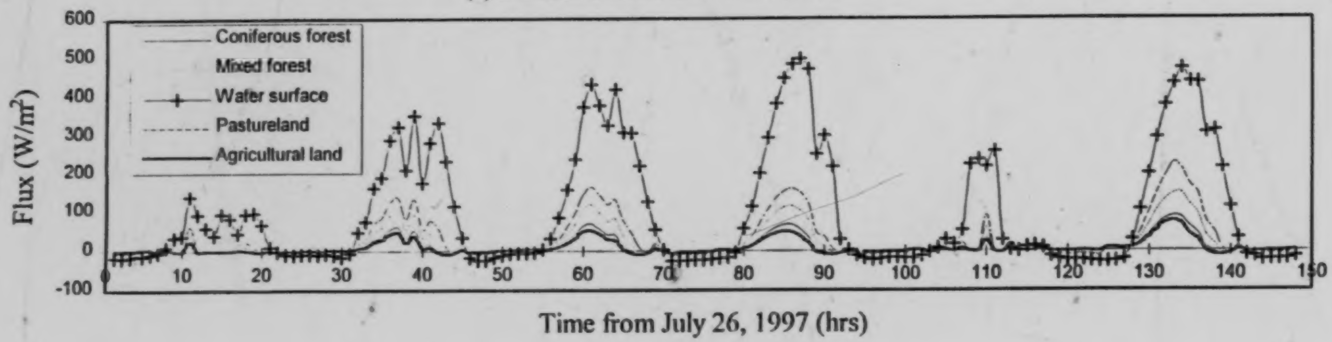

(l) Net radiation at within canopy height (fictitious height)

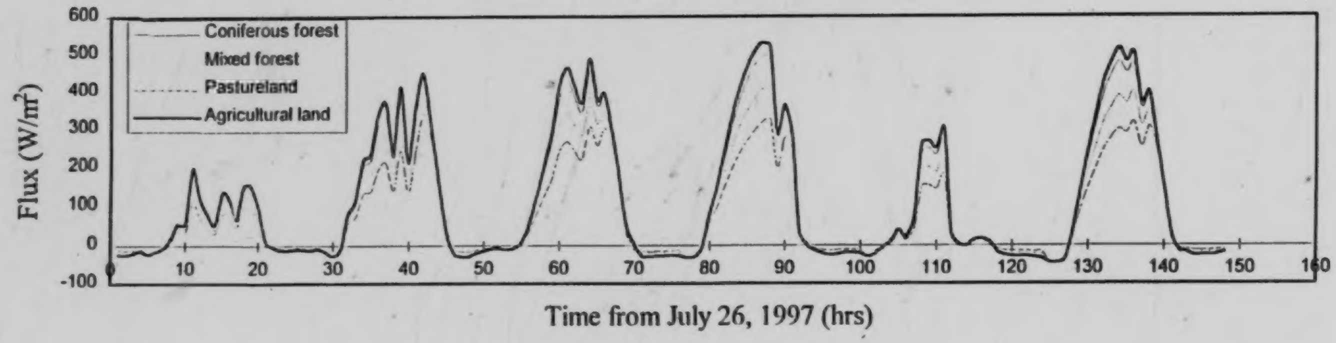

Figure 3.20 (k)-(l) Evapotranspiration, surface temperature, canopy temperature, soil moisture, and sensible and latent energy fluxes simulated by DPHM-RS during validation period.

(m) Net radiation at soil surface

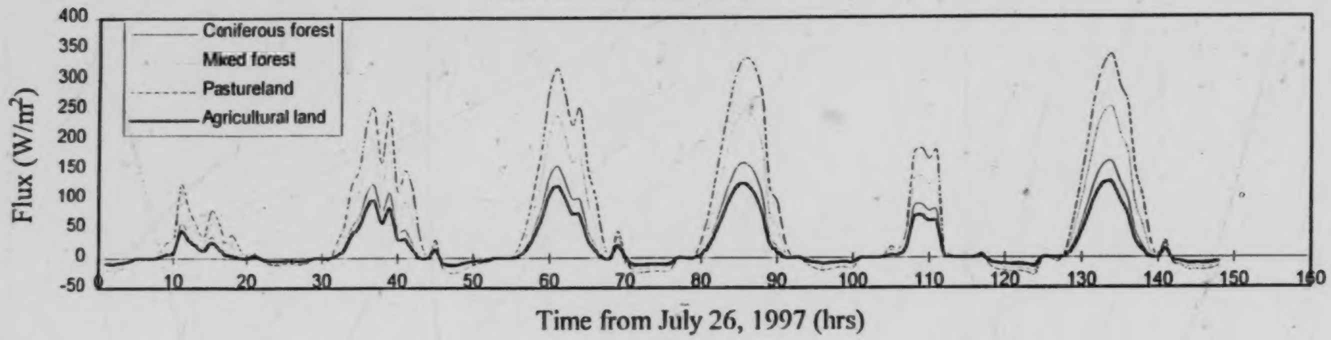

(n) Soil Moisture for one sub-basin

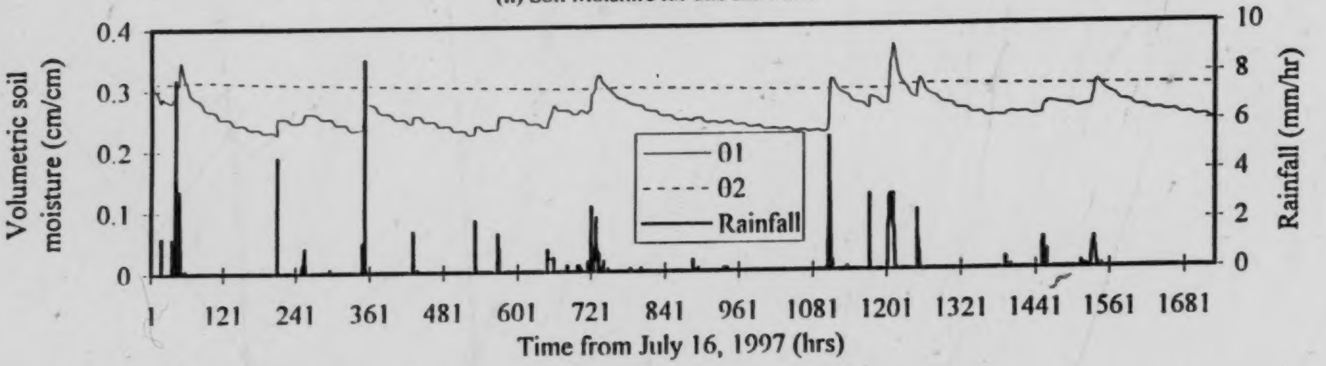

Figure 3.20 (m)-(n) Evapotranspiration, surface temperature, canopy temperature, soil moisture, and sensible and latent energy fluxes simulated by DPHM-RS during validation period.

Chapter 4

Evapotranspiration from a watershed with mixed land-use classes[*]

4.1 Introduction

Evapotranspiration (ET) constitutes an important component of the water fluxes of the hydrosphere and the atmosphere. It is the result of complex interaction between water and energy fluxes subjected to changing atmospheric, soil and vegetation conditions. The complex variations in climate, terrain features, and vegetative covers complicate our attempt to quantify the ET at a regional scale adequately. Furthermore, our quandary is further complicated by evaporative fluxes varying diurnally and seasonally.

For more than half a century, there have been many research activities in modeling evaporation and/or evapotranspiration for climatological, agronomical, and hydrological purposes (e.g., Penman, 1948; Thornthwaite, 1948; Monteith, 1965; Doorenbos and Pruitt, 1977; Calder and Newson, 1979; Shuttleworth, 1991). Despite the effort, practitioners are usually mystified and often poorly served by duplicates of models which estimate actual evaporation as a function of different conceptual rates such as potential, wet environment, reference crop ET, etc. These conceptual rates mostly reflect some measure of meteorological controls over the evaporative processes. As a result, practical applications of such evaporation models are basically limited to either a single land use class or an assumed representative land cover of uniform distribution over the scale of interest.

---

[*] Submitted for publication to Journal of Hydrology

Recently there is a growing interest in estimating evaporation and evapotranspiration for a combination of land use classes (e.g., Granger and Gray, 1989; Shuttleworth, 1991; Dunn and Mackay, 1995; Flerchinger *et al.*, 1996) and for sparsely vegetated surfaces (e.g., Shuttleworth and Wallace, 1985; Choudhury and Monteith, 1988; Smith and Choudhury, 1991; Nichols, 1992). In a heterogeneous catchment the amount of evaporation and/or transpiration taking place from different land covers depends on the respective quantity of net energy and the amount of soil moisture available for evaporation in those land covers. In particular, for sparse canopy covers, which occur seasonally in all agricultural areas and naturally throughout the year in arid and semiarid regions (Wilson and Henderson-Sellers, 1985), the estimation of ET is difficult due to different contributions from two sources, soil and plant canopy.

If we wish to credibly demonstrate the effect of land use changes on watershed hydrology, it is essential to estimate ET, a major hydrologic component, accurately. The Penman-Monteith equation (Monteith, 1965), which accounts for the influence of vegetation on evaporation, has been used frequently to model the ET flux in distributed models (e.g., Abbott *et al.*, 1986). However, this ET model mainly performs well for dense, closed canopy situations only (Thom, 1972; Shuttleworth, 1991). On the other hand, the two-source model, basically an extension of the original Penman-Monteith equation, has been tested and successfully applied for a variety of ecosystems (e.g., Kustas, 1990, Ham and Heilman, 1991; Nichols, 1992). However, the key to successfully applying the two-source model is the determination of soil surface resistance, which is a challenge when different land cover classes are involved. Different researchers have tried to establish an expression for the soil surface resistance as a function of other parameters such as soil moisture, porosity of soil, molecular diffusion coefficient for water vapor, depth of dry layer, and tortuosity (e.g., Sun, 1982; Camillo and Gurney, 1986; Choudhury and Monteith, 1988;

Massman, 1992). However, until now there is no one general expression established that is applicable to a wide variety of vegetation canopy and soil textures.

The research objectives of this paper are given in Section 4.2, details of the Penman-Monteith and the modified Penman methods are respectively given in Sections 4.3, and 4.5, data description in Section 4.6, the discussion of results in Section 4.7, and summary and conclusions in Section 4.8.

4.2 Research Objectives

This study has three primary objectives:

(1) Compare the performance of the Penman-Monteith model (Monteith, 1965) and the two-source model which is the component used in DPHM-RS for estimating hourly ET;

(2) Assess the applicability of the modified Penman model of Granger and Gray (1989) for estimating hourly evapotranspiration from different land covers; and

(3) Using the actual ET obtained from the two-source model for the Paddle River Basin, to re-establish a general expression for the relative evaporation of Granger and Gray (1989).

4.3 The Penman-Monteith Equation

The Penman-Monteith equation was modified from the Penman equation (Penman, 1948) to estimate the actual ET (Monteith, 1965) by introducing a canopy resistance to describe the influence of plants on the water flux through the roots, stems and leaves. The equation assumes that the exchange of sensible and latent heat fluxes between the canopy and the atmosphere takes place within the canopy at a fictitious height. In terms of the resistance established in the two layer, the equation is given as (Shuttleworth, 1991):

$$L_e E = \frac{\Delta \left[R_n - G_s \right] + \rho c_p \left(e_a^* - e_a \right) / (r_{aa} + r_{ac})}{\Delta + \gamma \left\{ 1 + r_{sc} / (r_{aa} + r_{ac}) \right\}} \qquad (4.1)$$

Where R_n is the net radiation, G_s is the soil heat flux, γ is the psychrometric constant, Δ is the slope of the saturation vapor pressure at the temperature of the air, c_p is the heat capacity of the air, ρ is the mean air density, e_a is the vapor pressure of the air, e_a^* is the saturated vapor pressure at air temperature, r_{aa} is the aerodynamic resistance above the canopy, r_{ac} the aerodynamic resistance within the canopy height, and r_{sc} is the bulk canopy resistance. In this study r_{aa}, r_{ac}, and r_{sc} are evaluated from the two-source model (see Chapter 2 Section 2.2.2).

4.4 The two-source Model

The two-source model determines evaporation from the soil and ET from plant canopy separately (detailed description of the two-source model is given in Section 2.2.2 of Chapter 2). An approach to separate vegetation and soil evaporative fluxes in the two-source model based on the exfilitration capacity of the soil and the potential evaporation is suggested (see Appendix A3 for detail). Based on this approach, the two-source model is used as a model component in DPHM-RS to simulate energy and water fluxes under different land cover conditions from the Paddle River Basin of central Alberta. DPHM-RS has been used successfully in simulating hourly runoff at the outlet of the basin, hourly surface temperature, hourly net radiation, and other energy and water fluxes during the calibration as well as the validation periods (see Section 3.4.1 and 3.4.2 of Chapter 3 for detail). These results also demonstrated that the two-source model (as a subset of DPHM-RS) accurately simulated evaporative fluxes from the soil and canopy covers. Therefore, the two-source model is used as the basis for evaluating of the performance of the Penman-Monteith and modified Penman models for estimating hourly ET from different land cover types in the Paddle River Basin.

4.5 Modified Penman Method

Penman (1948) derived an evaporation equation for estimating the potential evaporation, under unlimited water supply, e.g., saturated surfaces. Granger and Gray (1989) derived a modified form of Penman's equation for estimating the actual evaporation from different non-saturated land covers (see Equation 4.2). They first defined the potential evaporation as the evaporation rate that occurs for a saturated surface and constant atmospheric parameters and surface temperature. In addition, Granger (1989) showed that the same equation can be derived following the approach of Bouchet's (1963) complementary relationship.

$$E = \frac{\Delta E_R (R_n - G_s)}{(\Delta E_R + \gamma)} + \frac{\gamma E_R E_a}{(\Delta E_R + \gamma)} \tag{4.2}$$

E is the actual evaporation, E_R the relative evaporation (the ratio of actual to potential evaporation), and E_a is the drying power of the air (the evaporation due to the aerodynamic effect of wind and humidity gradient). Equation (4.2) can be rewritten in the form similar to the Penman-Monteith equation as:

$$E = \frac{\Delta (R_n - G_s) + \gamma E_a}{(\Delta + \gamma / E_R)} \tag{4.3}$$

Comparing Equation (4.3) with Equation (4.1) E_R should be a function of the aerodynamic and canopy resistances for closed canopy ET and the relative evaporation can be defined as:

$$E_R = \frac{r_{aa} + r_{ac}}{r_{aa} + r_{ac} + r_{sc}} \tag{4.4}$$

From Equation (4.4) the relative evaporation is not only a function of meteorological condition (r_{aa}) but also a function of canopy surface parameters ($r_{ac} + r_{sc}$). However, for the sparse canopy condition, canopy surface parameters should have little effect on the relative evaporation. As a result Equation (4.4) is not adequate to evaluate the relative evaporation from a sparse canopy condition. The general expression for E_R is given by (Granger and Gray, 1989):

$$E_R = \frac{\gamma E}{\Delta (R_n - G_s) + \gamma E_a - \Delta E} \tag{4.5}$$

Based on daily estimated values of actual evaporation from water balance, they used the relative drying power, D_R, given as

$$D_R = \frac{E_a}{E_a + R_n - G_s} \tag{4.6}$$

to establish an expression for E_R for different land use and vegetative cover (fallow, stubble, growing crop (wheat) and grass)

$$E_R = \frac{1}{1+0.028\exp(8.045D_R)} \tag{4.7}$$

The drying power of the air E_a is defined as:

$$E_a = f(u)(e_a^* - e_a) \tag{4.8}$$

Where $f(u)$ the wind function is given by:

$$f(u) = \frac{0.622\kappa^2 \rho u}{P \ln\left(\frac{h_1 - d}{z_o}\right) \ln\left(\frac{h_2 - d}{z_o}\right)} \tag{4.9}$$

in which P is the atmospheric pressure, u is wind speed at height h_1, h_2 is the level of relative humidity measurement, d is the zero-plane displacement, z_o is the roughness height of the surface, and κ is the Von-Karman's constant.

Granger and Gray (1989) pointed out that, due to the lack of data for wet environment (E_R>0.7), it is not possible to apply the above expression with confidence over the entire region in E_R. As a matter of fact, only four data points for E_R>0.4 are given in Figure 1 of Granger and Gray (1989). In addition their data sets do not include forest environments which generally have more transpiration than evaporation from soil surface or ET from crops. As a result it is interesting to investigate the method developed for evaporation from non-saturated surfaces on a wider range of land use classes and also for diurnal variation of meteorological inputs.

The wind function $f(u)$ defined in equation (4.9) is applicable either at daily or longer time steps or for simulation over period of short time steps under a neutral atmospheric condition. For computing hourly evaporation, the effect of stability determined by surface parameters (stable, neutral or unstable) which vary throughout the day is important. As a result, it is interesting to investigate if Equations (4.2) and (4.7) of Granger and Gray (1989) can adequately estimate hourly evaporation since they do not include stability correction.

4.6 Description of Data

The meteorological data were collected at the Paddle River Basin (53° 52' N. latitude, 115° 32' W. longitude) of Central Alberta which has a catchment area of 265 km^2. The catchment consists of about 50% mixed forest, 21% coniferous forest, 15% agricultural land, 11% pasture land with short grass, 2% water body and 1% relatively impervious lands. The annual mean precipitation is approximately 508 mm (Pretula and Ko, 1982). The major soil group of the study area is of the Hubalta series (Twardy and Lindsay, 1971) which has strongly developed Orthic Gray Wooded features. Under moderately well drained conditions, this soil type is predominantly clayey loam in texture.

During the summer of 1996 (July - October) a 10-m high meteorological station was set up within the Paddle River Basin to obtain meteorological data. Detailed description of meteorological data used in this research is given in Section 3.2.1 of Chapter 3. In addition, typical plots of different meteorological data used in this study are shown in Figure 3.2 (Chapter 3). The leaf area index LAI for different land use classes was derived from the normalized difference vegetation index NDVI of NOAA-AVHRR images (see Table 3.4 and Table 3.5 of Chapter 3). Landsat TM data obtained on August 7, 1996 was used to derive land cover using the back propagation artificial neural network (see Figure 3.8 in Chapter 3). The mean height for different land cover was obtained from field investigation. Other parameters, which are required to evaluate the models, are estimated from literature as given in Table 3.12 (Chapter 3).

4.7 Discussion of Results

4.7.1 Penman-Monteith (PM) Model versus two-source Model

The Penman-Monteith model (Equation (4.1)) was applied to evaluate hourly actual ET from four land cover classes, namely, coniferous forest, mixed forest, pasture land, and agricultural land using meteorological data obtained for 35 days in the summer of 1996. The aerodynamic resistances and the canopy resistances are evaluated based on the equations outlined in Chapter 2 (see Section 2.2.2). For coniferous forest and agricultural land covers, the total ET estimated by the Penman-Monteith method shows good agreement with the two-source model with minor under-estimation during the day time for coniferous forest (see Figure 4.1(a)&(d)). This is mostly due to our assumption in the PM model that the total energy available for ET is used at the canopy surface through the canopy system. However, in reality part of the energy will pass on to the soil for evaporation to take place from the soil surface (25-36% for coniferous forest and 22-30% for agricultural land).

However, For mixed forest and pasture land covers, the PM model under-estimates the total ET especially during mid-day hours (see Figure 4.1(b)&(c)). This indicates that the evaporation component from soil surface for such land cover is significant and so the closed canopy concept assumed in PM is not appropriate for such land cover. For pasture land the amount of energy reaching the soil surface during day time is almost 50-60% of the total energy which makes the evaporation component from the soil surface a significant contribution to the total ET. Similarly for mixed forest covers the typical daytime energy reaching the soil surface is about 38-58%. As a result it is not adequate to estimate ET from mixed forest and pasture land covers based on the original PM equation which assumes a closed canopy condition. In addition, soon after rainfall, the evaporation to the atmosphere is mainly from the wet canopy instead of transpiration through the canopy system or evaporation from soil surface. Therefore, it is important to evaluate the wet canopy evaporation based on the canopy water balance, as is done by the two-source model used in DPHM-RS. The wet canopy evaporation is significant in volume even though it persists for only a short time period (see Figure 3.18(c) and 3.19(c) in Chapter 3).

4.7.2 Modified Penman Model versus two-source Model

The modified Penman method of Granger and Gray (1989) (Equation (4.2) and (4.7)) is used to evaluate hourly ET from different land cover types without stability correction. For all land cover types considered, the modified Penman method mostly under-estimated the ET during the day time when the atmospheric condition is unstable (surface temperature is greater than air temperature) (see Figure 4.2 (a)-(d)). Specifically for pasture land covers, with respect to the two-source model, the modified Penman model under estimates the actual ET during day time but over estimates ET during early morning and late afternoon (stable atmospheric condition).

As shown in Equation (4.3), the modified Penman method of Granger and Gray (1989) is basically the same as the Penman-Monteith equation if one evaluates the relative evaporation from aerodynamic and bulk canopy resistances (Equation 4.4). In this manner the modified Penman method shares the same limitation as Penman-Monteith model. However, by establishing another expression for the relative evaporation, which accounts for the effect of soil surface parameters, in addition to meteorological condition and canopy parameters, then the modified Penman model should be applicable to various land covers including bare soil. Furthermore, the new expression for E_R should also theoretically account for stability correction so that no further stability correction is needed when one applies the modified Penman model.

Using Equation (4.5) and the actual ET simulated by the two-source model for hourly meteorological data collected in the summer of 1996, the estimated E_R was compared with the E_R relationship of Granger and Gray (1989), i.e. Equation (4.7). From Figure 4.3 (a)-(d), there are similarities and some discrepancies between the E_R data computed from Equation (4.5) and the functional relationship of E_R given by Equation (4.7). The discrepancies between Equations (4.5) and (4.7) grow when D_R decreases (e.g., E_R increases), which seems to imply that there may be more than one relationship between E_R and D_R. Equation (4.7) seems applicable to all four land cover types when the relative drying power D_R is greater than 0.9. When D_R is between 0.8 and 0.9, Equation (4.7) generally under-estimates E_R. For D_R less than 0.8, Equation (4.7) tends to over-estimate E_R. However, with the few data points exist in this case, it is difficult to conclude whether Equation (4.7) over or under-estimates E_R when D_R is less than 0.8.

Next, for each land use type and certain interval of D_R, the average E_R values were computed and plotted in the same figure (Figure 4.4). These data points exhibit similar shape as Equation (4.7) of Granger and Gray (1989) but with a discrepancy that grow with decreasing D_R. The relationship obtained out of these data points is

$$E_R = \frac{0.0951}{1+5.379\times 10^{-6}\exp(14.273D_R)} \tag{4.10}$$

Based on Equation (4.10), the ET for all land use classes was re-computed with the modified Penman's equation for the summer of 1996 and the result was compared with that of the two-source models (Figure 4.5(a)-(d)). With respect to the two-source model, there is an improvement in the ET estimated by the modified Penman model, which is not a surprise since the re-established E_R relationship given in Equation (4.10) is used for this case. The improvement is slightly more significant for ET computed for pasture and agricultural land covers (see Table 4.1).

Finally, the ET estimated by the modified Penman model with the re-established E_R relationship (Equation (4.10)) was validated with 73 days of hourly data for the summer of 1997, which are independent of the calibration data of summer 1996. Figure 4.6(a)-(d) show that the actual ET simulated by the modified Penman model agrees well with that of the two-source model at the validation stage (R^2=0.77 for coniferous forest, 0.87 for mixed forest, 0.90 for pasture land, and 0.81 for agricultural land).

4.7.2.1 A Further Look at Relative Evaporation

The general expression for relative evaporation E_R, Equation (4.5) is derived by defining E_R as:

$$E_R = \frac{E}{E_p} \tag{4.11}$$

Where $E_p = f(u)(e_s^* - e_a)$ (4.12)

In deriving the modified Penman model, Granger and Gray (1989) used the Dalton-type bulk transfer equation for actual (E) and potential evaporation (E_p). Using the surface temperature simulated by DPHM-RS (see Chapter 3) the potential evaporation is computed from Equation (4.12) for the data of summer 1997. The relative evaporation E_R is then evaluated from Equation (4.11) and compared to E_R computed based on Equation (4.5) and Equation (4.7). A close look to the values of E_R derived from the three expressions indicated that the relationship between E_R and D_R is not unique under the wet environment (either near saturation vapor pressure of air or wet surface).

For near saturated vapor pressure of air (e.g., soon after a rainfall event), the drying power, E_a, and the relative drying power, D_R, approaches zero. As a result, E_R computed based on Granger and Gray (1989) equation (Equation (4.7)) approaches unity. However, the relative evaporation obtained using Equation (4.5) is much less than unity when $(R_n-G_S) >> 0$. As $(e_s^* - e_a)$ approaches zero, E_p, also approaches zero but, due to availability of energy, there is some evaporation taking place from the wet surface. As a result, the actual evaporation is greater than the potential evaporation derived from Equation (4.12). This means that E_R computed from Equation (4.11) is greater than unity which does not make much sense.

E_R computed from Equation (4.7) indicates that the relative evaporation is very small even for an average D_R value of say 0.6. However, using Equation (4.5) and if $\{\Delta(R_n-G_S)+\gamma E_a-\Delta E\}$ is of the order of γE, E_R approaches unity and E_R computed based on Equation (4.11) indicates an average value between Equation (4.5) and Equation (4.7). This means that under a wet environment one could end up with a wide range of E_R, depending on which equation used. Therefore, it is concluded that the general expression established for E_R based on D_R for wet environment is less reliable and further investigation is necessary to establish an expression that one can use with confidence. Unfortunately the data for this study mostly represent relatively dry environments and it was not possible to establish a proper relationship for E_R under wet environment.

4.8 Summary and Conclusions

In this study three ET models – the Penman-Monteith equation, the modified Penman equation for non-saturated surface, and the two-source model – were used to estimate evapotranspiration from different land cover classes of the Paddle River Basin of central Alberta. The Penman-Monteith (PM) equation estimates hourly, actual evapotranspiration by assuming a closed canopy condition for all land covers (e.g., coniferous forest, mixed forest, agricultural, and pasture lands). The actual ET estimated by the PM equation shows good agreement with the two-source model when the land covers are coniferous forest and agricultural land, but poor agreement when the land covers are mixed forest and pasture land. This means that the closed canopy assumption is not valid for the two latter land covers because in addition to plant transpiration the proportion of evaporation from bare soil surface is also significant.

Using the relative evaporation relationship of Granger and Gray (1989), E_R, the modified Penman model for a non-saturated surface was used to simulate hourly ET for different land cover types without any stability correction. Compared to the two-source model, the modified Penman model mostly under-simulated the actual ET during mid-day hours but over-simulated the actual ET under stable atmospheric conditions during early morning and late afternoon. By re-establishing a new expression for E_R based on the actual ET computed using the two-source model, it is found that the result is significantly improved especially for the actual ET estimated for pasture and agricultural land covers. Even for the summer of 1997 data which was not used to establish the new relationship for E_R, the actual ET simulated by modified Penman model still agrees well with that of the two-source model.

The above results are based on the environment of Canadian Prairies which are relatively dry. In other words, the relationship between E_R and D_R by Granger and Gray (1989) is generally applicable for dry environment. The same relationship of E_R, however, is not quite applicable under a wet environment. This is because Dalton's transfer equation used to establish E_R only considers the aerodynamic component of evaporation, which is very insignificant compared to evaporation due to solar energy when the environment is wet.

In general, the two-source model is likely one of the most comprehensive ET models to use in hydrologic modeling. The modified Penman model is preferred over the PM for river basins in the Canadian Prairies since it is relatively simple yet estimates the actual ET of the Paddle River Basin accurately. PM is as data-intensive as the two-source model but only estimates the actual ET reasonably well if the closed canopy condition is valid such as in dense forest and agricultural land.

References

Abbott, M. B., Bathurst, J. C., Cunge, J. A., O'Connell, P. E., and Rasmussen, J. (1986). An introduction to the European hydrological system-System hydrologique Europeen, 'SHE', 1: History and philosophy of a physically-based, distributed modeling system. *Jour. of Hydrol.*, 87(1/2), 45-59.

Bouchet, R. J. (1963). Evaporation reelle et potentielle, signification climatique, in General Assembly Barkeley, Int. Assoc. of Sci. Hydrol., Gentbrugge, Belgium, vol. 62, pp. 134-142.

Calder, I. R. and Newson, M. D. (1979) Land use and upland water resources in Britain-a stratagic look. Water Resour. Bull., 15(6), 1628-1639.

Camilo P. J., Gurney R. J. (1986) A resistance parameter for bare-soil evaporation models. *Soil Sci.* 141(2): 95-105.

Choudhury, B. J. and Monteith, J. L. (1988). A four-layer model for the heat budget of homogeneous land surfaces. Q. J. R. Meteorol. Soc., 114, pp. 373-398.

Doorenbos, J. and Pruitt, W. O. (1977) Crop Water Requirements. FAO Irrigation and Drainage Paper 24. FAO, Rome, 144 pp.

Dunn, S. M., and Mackay, R. (1995). Spatial variation in evapotranspiration and the influenece of land use on catchment hydrology, J. Hydrol., 171, 49-73.

Flerchinger, G. N., Hanson, C. L., and Wight, J. L. (1996). Modeling evapotranspiration and surface energy budgets across a watershed, Water Resour. Res., vol. 32, No. 8, pp. 2539-2548.

Granger, R. J. and Gray, D. M. (1989). Evaporation from natural non-saturated surface, J. Hydrol., 111, 21-29.

Granger, R. J. (1989) A complimentary relationship approach for evaporation from non-saturated surface, J. Hydrol., 111, 31-38.

Ham, J. M. and Heilman, J. L. (1991). Aerodynamic and surface resistances affecting energy transport in a sparse crop. Agric. For. Meteorol., 53, 267-284.

Kustas, W. P. (1990) Estimates of evapotranspiration with a one- and two-dimensional model of heat transfer over partial canopy cover. J. Appl. Meteorol., 29, 704-715.

Massman, W. J. (1992). A surface energy balance method for partitioning evpotranspiration data into plant and soil components for a surface with partial canopy cover, Water, Resour. Res., 28(6), 1723-1732.

Monteith, J. L. (1965). The heat balance of soil beneath crops. In Proceedings symposium on climate and microclimate. Canberra, UNESCO, Arid Zone Research, vol. 11.

Nichols, W. D., (1992). Energy budgets and resistances to energy transport in sparsely vegetated rangeland. Agric. For. Meteorol., 60, pp. 221-247.

Penman, H. L. (1948). Natural evaporation from open water, bare soil and grass, Proc. R. Soc. London A, 193, 120-145.

Pretula, B. R. and Ko, C. A. (1982). Hydrogeology of Paddle River Reservior area near Mayerthorpe, Alberta, *Report prepared for Alberta Environment Protection* (AEP), pp.1-107.

Shuttleworth, J. W. (1991). Evaporation models in hydrology. In Schmugge, T. J. and Andr'e, J. (Editors), Land Surface Evaporation. Springer, New York, pp. 93-120.

Shuttleworth, J. W. and Wallace, J. S. (1985). Evaporation from sparse crops-an energy combination theory. Q. J. R. Meteorol. Soc., 111, pp. 839-855.

Smith, R. C. G. and Choudhury, B. J. (1991). Analysis of Normalized difference and surface temperature observations over southeastern Australia. Int. J. Remote sensing, Vol. 12, No. 10, pp. 2021-2044.

Sun, S. F. (1982) Moisture and heat transport in a soil layer forced by atmospheric conditions, M.Sc. Thesis, Univ. of Connecticut.

Thom, A. S. (1972). Momentum, mass and heat exchange of vegetation. *Q. J. R. Meteorol. Soc.* 98: 124-134.

Thornthwaite, C. W. (1948). An approach toward a rational classification of climate. Geogr. Rev., 38, 55-94.

Twardy, A. G. and Lindsay, J. D., (1971). Soil survey of the Chip Lake Area, *Alberta soil survey*, Report No. 28, pp. 1-71.

Wilson, M. F. and Henderson-Sellers, A. (1985). A global archive of land cover and soils data for use in general circulation climate models, J. Climatol., 5, 119-143.

Table 4.1 Statistics of regressions between the Penman-Monteith and the modified Penman equation with the two-source model for different land cover types.

Model type		Land cover types			
		Coniferous forest	Mixed forest	Pasture land	Agricultural land
Penman-Monteith Versus two-source	Slope	1.118	1.220	1.398	0.954
	Intercept	-0.0003	0.0016	0.0040	0.0037
	R^2	0.94	0.90	0.85	0.96
Modified Penman^1 Versus two-source	Slope	1.039	1.215	1.382	1.162
	Intercept	0.0040	-0.0080	-0.0210	-0.0070
	R^2	0.81	0.88	0.88	0.83
Modified Penman^2 Versus two-source(Calibration)	Slope	0.922	1.033	1.192	1.099
	Intercept	0.0060	-0.0040	-0.0180	-0.0070
	R^2	0.83	0.90	0.92	0.88
Modified Penman^3 Versus two-source (Validation)	Slope	0.795	0.951	1.151	1.031
	Intercept	0.0106	0.0004	-0.0105	-0.0049
	R^2	0.77	0.88	0.90	0.81

[1] Using Equation (4.7) for relative evaporation.

[2] Using Equation (4.10) for relative evaporation (1996 data).

[3] Using Equation (4.10) for relative evaporation (1997 data).

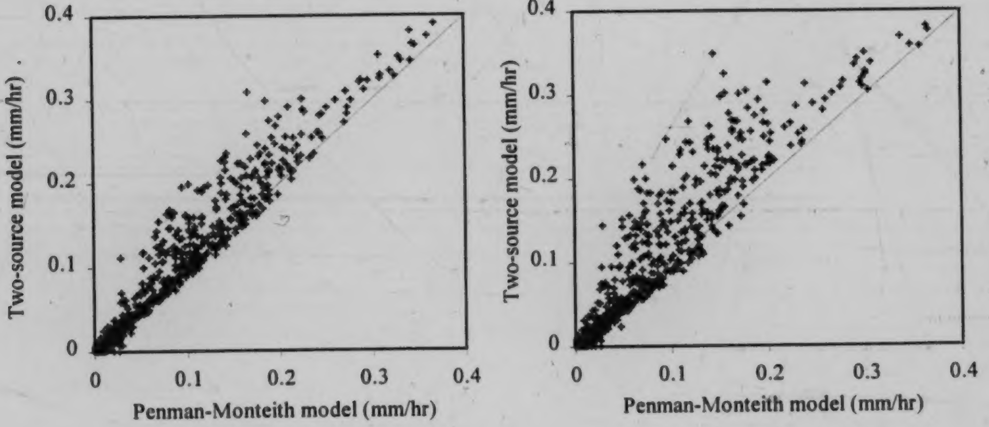
(a) Coniferous forest

(b) Mixed forest

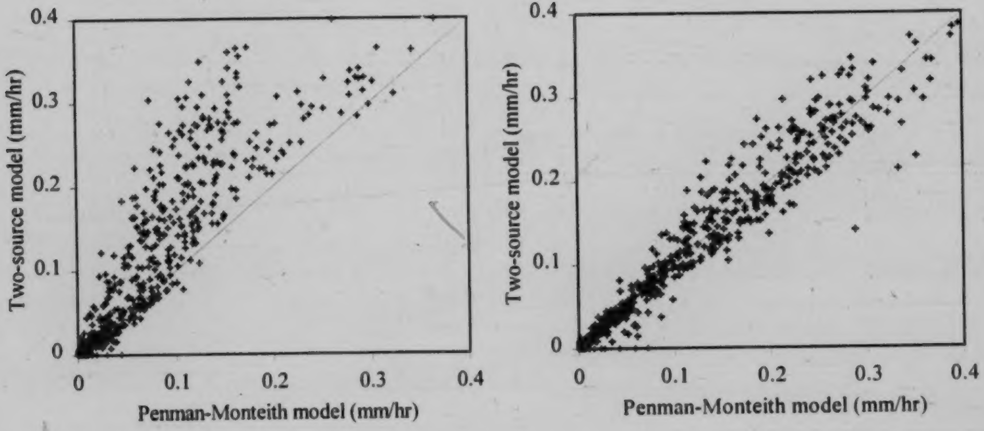
(c) Pasture land

(d) Agricultural land

Figure 4.1 (a)-(d) Comparison of actual evapotranspiration estimated by two-source and Penman-Monteith models.

(a) Coniferous forest

(b) Mixed forest

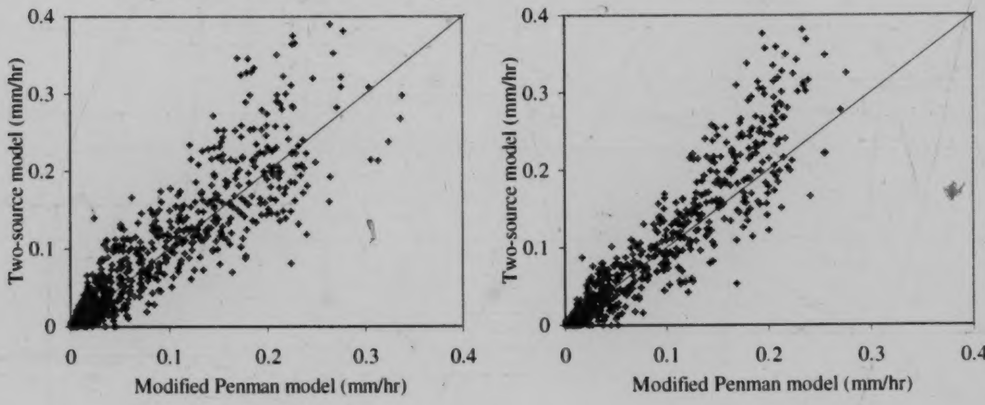

(c) Pasture land

(d) Agricultural land

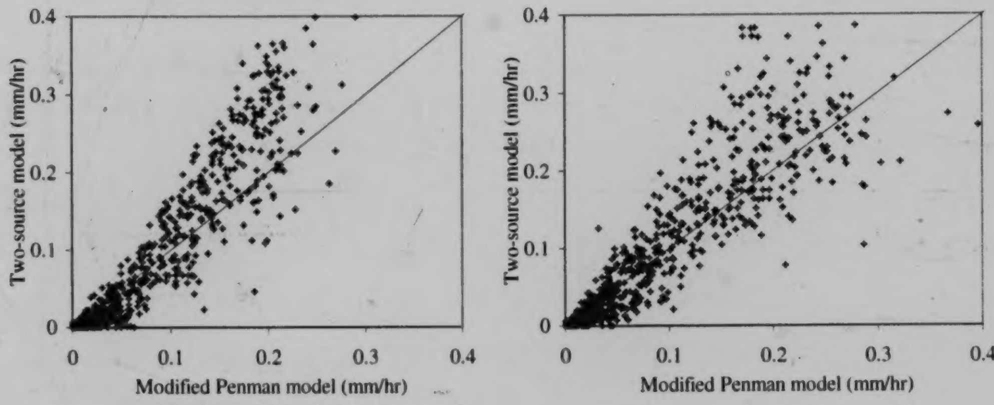

Figure 4.2 (a)-(d) Comparison of actual evapotranspiration estimated by two-source and modified Penman models with relative evaporation computed using expression established by Granger and Gray (1989) (Equation (4.7)).

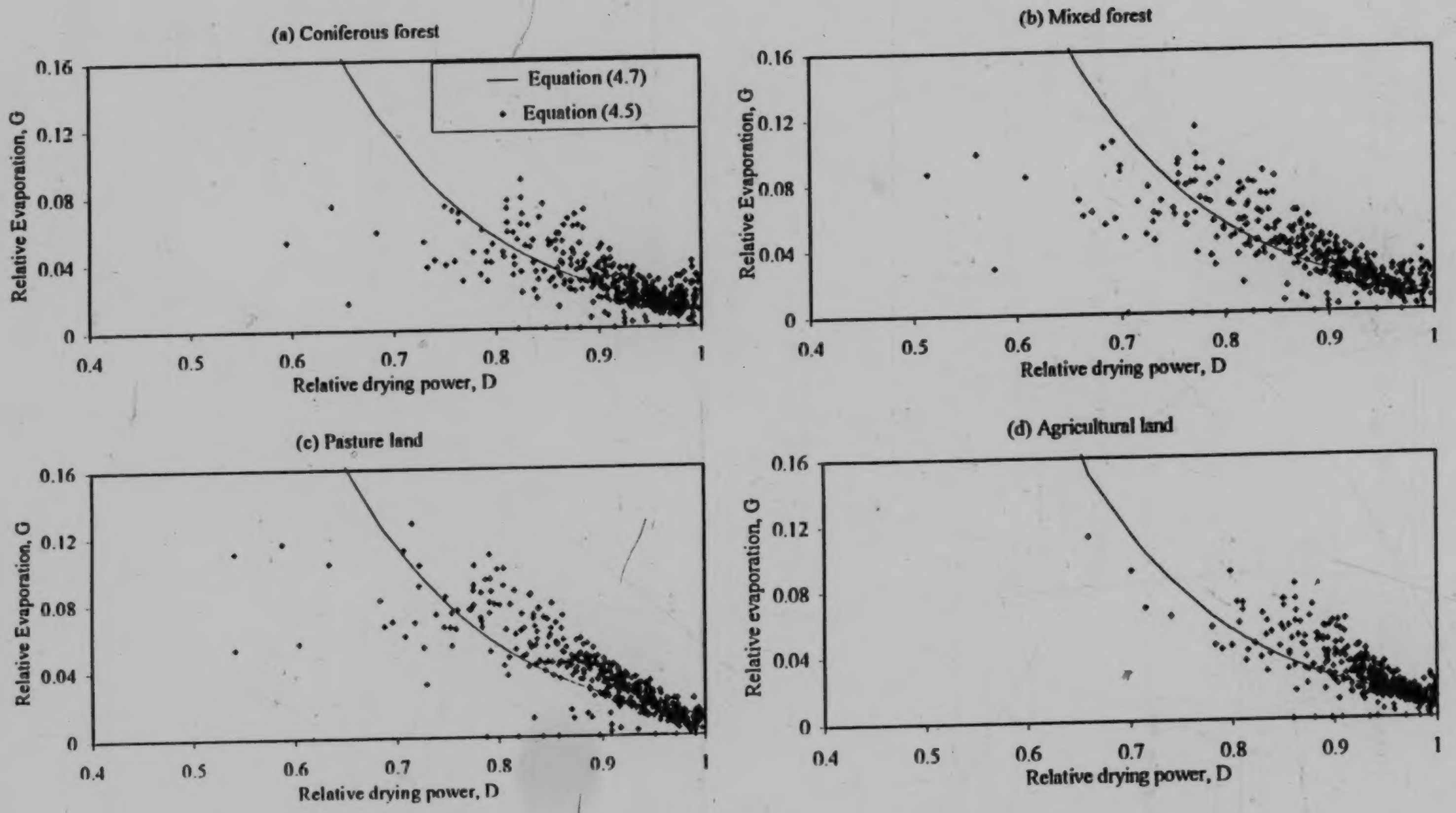

Figure 4.3 (a)-(d) Plot of relative evaporation against relative drying power derived from two-source model output data using Equation (4.5) versus Granger and Gray (1989) equation (Equation (4.7).

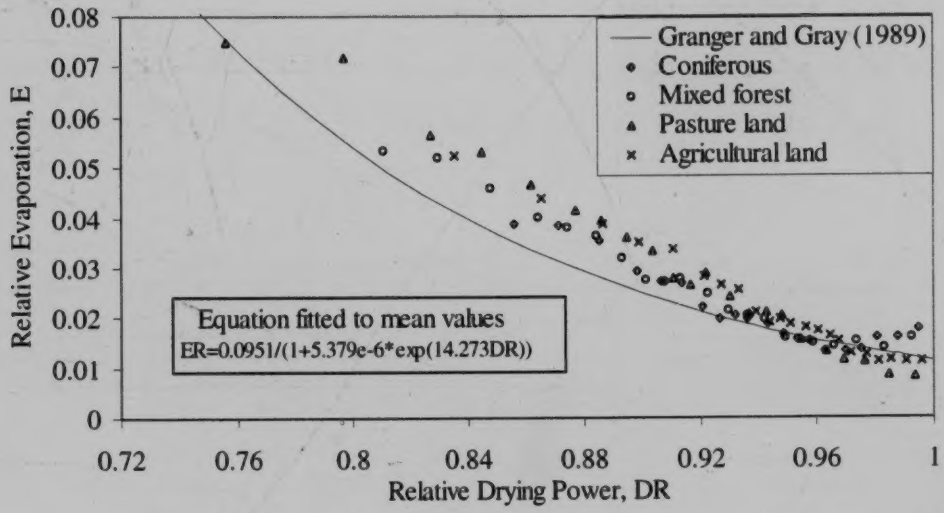

Figure 4.4 Relationship between relative evaporation, E_R and relative drying power, D_R derived based on actual evaporation simulated by two-source model for hourly data of summer of 1996 and the corresponding curve derived by Granger and Gray (1989) using daily water balance.

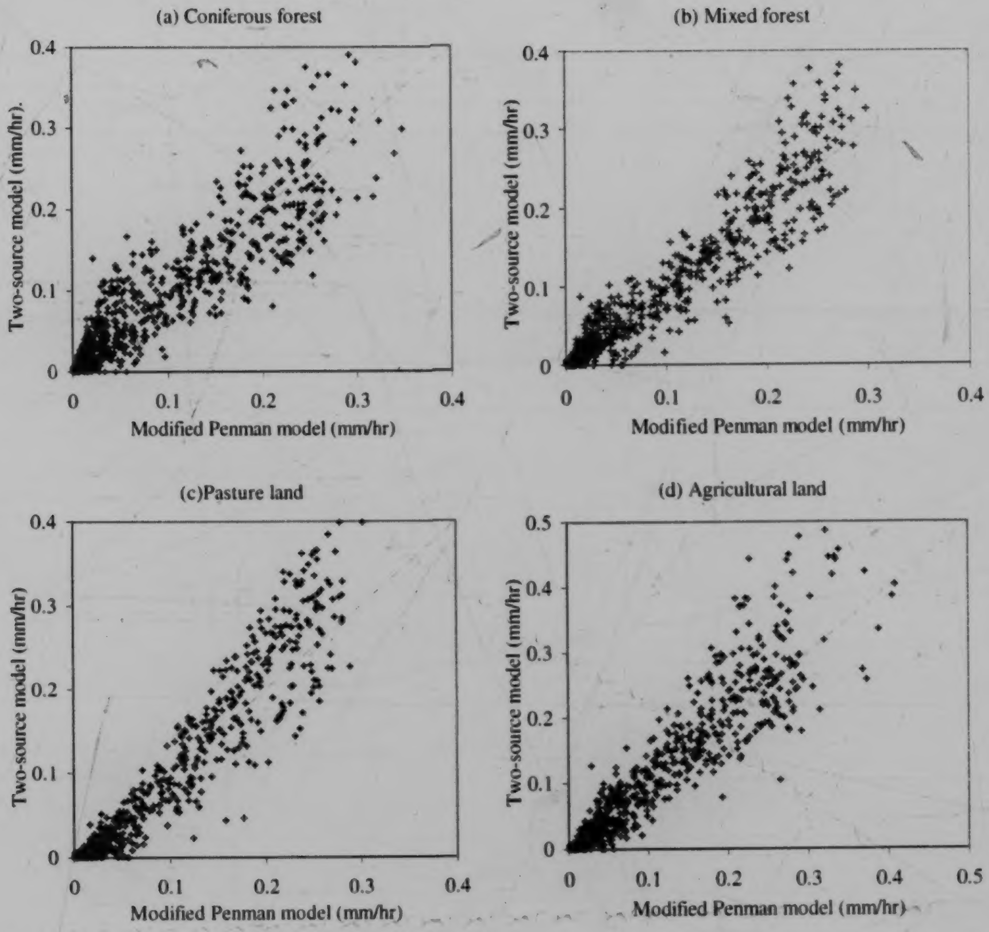

Figure 4.5. (a)-(d) Comparison of actual evapotranspiration estimated by two-source and modified Penman models with relative evaporation computed using Equation (4.10) (Calibration period).

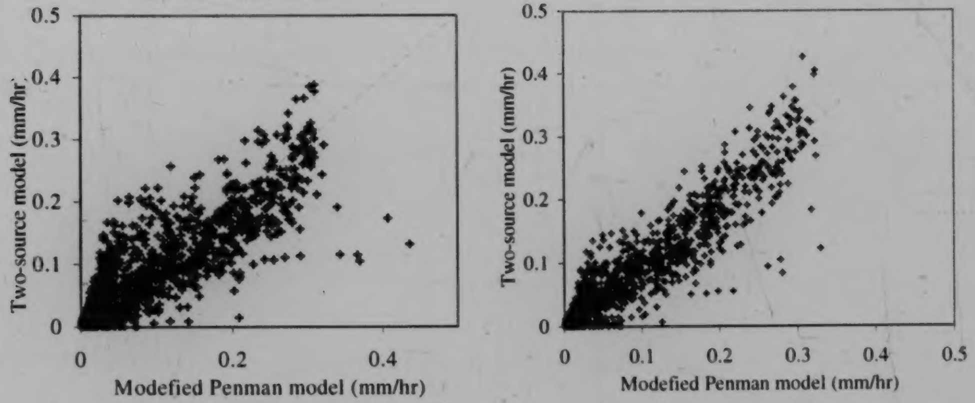
(a) Coniferous forest

(b) Mixed forest

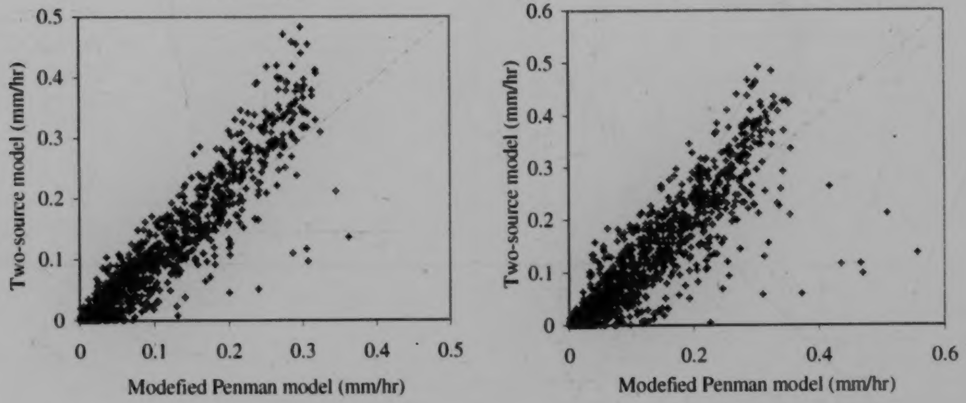
(c) Pasture land

(d) Agricultural land

Figure 4.6 (a)- (d) Actual evapotranspiration simulated by modified Penman model as compared to two-source model during validation period using hourly data of summer of 1997.

Chapter 5

Retrieving near-surface soil Moisture from Radarsat SAR Data[*]

5.1 Introduction

Soil moisture is the part of precipitation temporarily stored in a shallow topsoil layer of the earth surface. Albeit on a global basis soil moisture represents only 0.05% of the world's fresh water (Chow *et al.*, 1988), the amount of soil moisture is important for crop development, plant stress and yields (e.g., Dobson and Ulaby, 1986; Brown *et al.*, 1993; Lindsey *et al.*, 1992). The regional status of soil moisture is an important criterion for irrigation management and for the selection of crop types (O'Brien, 1992). Soil moisture also plays a major and interactive role with other hydrologic processes such as streamflow, infiltration, evaporation and groundwater recharge. Unfortunately it is difficult to assess the status of soil moisture on a regional scale accurately because it is highly variable spatially and temporally, and ground measurements that are time consuming and expensive to collect are always limited.

Research on the use of remote sensing techniques to retrieve soil moisture from microwave sensors over large areas has been ongoing for more than two decades (Ulaby *et al.*, 1978, 1979; Dobson and Ulaby, 1986). It has been demonstrated that this is possible with active microwave under a variety of topographic and land cover conditions

---

[*] Submitted for publication to Water Resources Research, AGU

(e.g., Bernard *et al.*, 1982; Crevier *et al.*, 1996). Relationships between radar backscattering echoes and surface soil moisture for bare ground or agricultural land have been established (e.g., Ulaby *et al.* 1982, 1986; Schmugge, 1985). Studies show that a C-band radar operating in VV and HH polarizations at 10°-20° incidence angle would be ideal for estimating soil moisture because such radar configurations minimize the effects of surface roughness and vegetation cover on the radar echoes (Ulaby *et al.*, 1978, 1979; Dobson and Ulaby, 1981; Bernard *et al.* 1982; Mohan *et al.* 1990; Le Toan, 1982).

Preliminary results obtained from ERS-1 (C-band) and JERS (L-band) data indicated the possibility of obtaining continuous soil moisture status over large areas of different land uses (e.g., Mohan *et al.*, 1990; Rotunno Filho *et al.*, 1996; Altese *et al.*, 1996). Lately, the Canadian Radarsat satellite carrying a C-band, synthetic aperture radar (SAR) has been designed with optimum radar parameters for monitoring near-surface soil moisture at HH polarization and beam modes operating at 10°-60° incidence angle, 10-100m resolution, and 50-500km ground swaths (Brown *et al.*, 1993). Also, by covering most parts of Canada once every 3 days, Radarsat (see Parashar et al. (1993) for full technical details) provides an opportunity to monitor the dynamics of soil moisture change in Canada and other parts of the world. Soil moisture retrieved from Radarsat data can be compared with field scatterometer results and soil moisture estimated from air-borne radar and other space platforms. Subsequent sections of this chapter include the research objectives (Section 5.2), research methodology (Section 5.3), discussion of results (Section 5.4), and summary and conclusions (Section 5.5).

5.2 Research Objectives

The primary objective of this study is to assess the feasibility of retrieving near-surface (5-10cm deep) soil moisture content of agricultural/ranch lands in the Canadian Prairies from Radarsat SAR data using an empirical and a theoretical model. The secondry objective is to examine the spatial variability of near-surface soil moisture using a semi-variogram and the homogeneity assumption (spatial correlation as a function of distance-lag only) used for spatially interpolating soil moisture with techniques such as universal kriging. The site chosen for this study is the Paddle River Basin of central Alberta in the Canadian Prairies (see Section 1.5 of Chapter 1 for detailed description of the study site).

The major soil group of the study area is of Hubalta series associated with Onoway and Modeste (Twardy and Lindsay, 1971) which are characterized by strongly developed Orthic Gray Wooded features. The dominant texture for such soil type is the clay loam soil under moderately well drained conditions (see Figure 3.3 of chapter 3). Table 3.2 of chapter 3 indicates typical particle size distributions of the Hubalta series at different depths found in the basin. The field sites chosen for soil sampling within the catchment include pasture lands (with short grasses of height generally less than 5cm), agricultural lands under post-harvest condition only (covered with short weeds), and herbaceous lands which have a mixture of grass, weeds, and some low growing brush (see Figure 5.1 and Figure 5.2).

5.3 Research Methodology

The research methodology involved collecting soil moisture data, processing and analyzing satellite images, establishing two functional relationships between SAR backscatter and soil moisture values, and examining the homogeneity assumption used in most spatial interpolation algorithms (such as universal kriging) to interpolate soil moisture data. Near-surface soil moisture measurements were made on six selected days when the Radarsat satellite passed over the Paddle River Basin -September 3, 10 and 27 of 1996 and August 5, 12 and 29 of 1997. These six days were chosen because the satellite path was such that it was possible to acquire SAR images at standard beam modes S1 or S2 that are of relatively low incident angles desirable for retrieving near-surface soil moisture (see Table 5.1). Figure 5.3 shows the six raw SAR images. The satellite passed by the study site at approximately 14:11 local time and at descending orbit.

5.3.1 Soil Moisture Data Collection

On the selected days on which Radarsat passed over the Paddle River Basin, intensive soil moisture samples were collected at nine carefully selected field sites (Figure 5.1). The nine field sites represent agricultural lands (sites 5 and 7), pasture lands (sites 1, 8, and 9), and herbaceous lands (sites 2, 3, 4, and 6) with inter-site distances ranging from 1 to 13 km. At each site, 25 soil samples, each taken at a depth of 5-10 cm, were collected per day at sampling points located approximately 50m from each other. These soil samples were analyzed for gravimetric and volumetric soil moisture in the laboratory. Field data were collected between approximately 10:00 am and 5:00 pm each day. The detailed soil moisture data with respect to three land uses for September 3, 10, and 27, 1996 are shown in Figure 5.4 while the overall mean soil moisture for the nine sites on August 5, 12, and 29, 1997 are shown in Figure 5.5. Based on field measurements, the average saturation level (volumetric moisture content/soil porosity) for the Paddle River Basin for the three days of 1996 were 68, 82, and 75%, and for the three days of 1997 were 72, 68, and 58% respectively.

5.3.2 Satellite Data Processing and Analysis

The calibration of the Radarsat SAR data involves two components. The internal component, known as radiometric calibration, requires knowledge of the transmitted power, the received power and processing gains, range and antenna gain (which depend on the angular quantity). The data obtained for our study site was calibrated radiometrically by the Canadian Center for Remote Sensing (CCRS) into a 16-bit product, SAR path image plus (SGX). The external calibration included geometric correction, change of the digital number to image intensity (brightness) and backscattering value using the EASI/PACE PCI software. To derive the backscattering values from the image digital number (DN), the following parameters were estimated (Shepherm and Associates, 1996):

I. Incidence angles for each column of the image pixel. First calculate the orbit altitude h

$$h = eph\_orb(1) * 1000 - r \tag{5.1}$$

$$r = a * 1000\sqrt{\left(\frac{\left(1+(\tan(\gamma))^2\right)}{(a/b)^2+(\tan(\gamma))^2}\right)} \tag{5.2}$$

r is the radius of the earth at the image center (m), γ is the platform geodetic latitude (radians), a and b are the semi-minor (polar) and semi-major (equatorial) axis of an ellipsoidal earth in km respectively, and *eph_orb*(1) is the first of the equinoctial orbit elements (e.g., the orbit semi-major axis for September 3, 1996 data is 7.1670955x10^6 km). a, b, and γ are normally obtained from the SAR header data summary and *eph_orb* (1) from the Canadian Earth Observation System (CEOS) parameters.

Then the slant range (*RS(i)*) for each given image column offset *i*

$$\begin{aligned} RS(i) &= SRGR(1)+(i*dRg)*SRGR(2)+(i*dRg)^2*SRGR(3) \\ &+(i*dRg)^3*SRGR(4)+(i*dRg)^4*SRGR(5) \\ &+(i*dRg)^5*SRGR(6) \end{aligned} \tag{5.3}$$

SRGR( ) is the slant range/ground range coefficients given in the CEOS header file, *dRg* is the pixel width (m) obtained from CEOS data summary file (I ranges from 0 to number of columns in the image minus one). For the Paddle River Basin and at a resolution of 8×8m, each image has about 12500 lines and 14300 columns.

Finally the incidence angle (I_j) at column j is

$$I_j = \cos^{-1}\left((h^2-(RS(i))^2+2*r*h)/(2*RS(i)*r)\right)*180/\pi \tag{5.4}$$

Where $i = j-1$

II. Radar brightness (β_{kj}) for scanline *k*, column *j*

$$\beta_{kj} = 10*\log_{10}((DN^2+Ao)/Aj) \tag{5.5}$$

DN is the image digital number, A_o is the gain offset, and A_j is the expanded gain scaling table value for column *j*. A_o and A_j are given as a segment with each SAR image data.

III. Radar backscatter (σ^o_{kj}) for scanline k, column j

$$\sigma^o_{kj} = \beta_{kj} + 10 * \log_{10}(\sin(I_j)) \qquad (5.6)$$

The six Radarsat SAR images were first subjected to speckle suppression filters using a 5 × 5 median filtering technique of the PCI EASI/PACE software. Then the images were co-registered to a Landsat TM image acquired on August 7, 1996 using a second order polynomial which requires a minimum of 7 ground control points. By applying many ground control points uniformly distributed across the whole image, we achieved accurate registration with an average error that is much less than the pixel resolution. The original images at a resolution of 8 × 8 m were then re-sampled to pixels of 25 × 25m resolution using the nearest neighbor method. From the Landsat TM image classified into six land cover classes (water bodies, coniferous and mixed forest, pasture and agricultural land, and roads or less permeable lands), locations of the soil sampling sites were identified.

Then a statistical and a theoretical functional relationship were established between Radarsat SAR backscatters and field soil moisture data for the Paddle River Basin. The former is a basin-dependent regression relationship primarily meant for the Paddle River Basin only. In this approach, the mean soil moisture values (averaged from 25 samples per site collected on a given day) for the nine field sites were regressed against their corresponding mean Radarsat SAR backscatter values (averaged from 64 pixels of 25m resolution each). This strategy of matching the average of sets of 25 soil samples with the average of sets of 64 pixels of Radarsat backscatter is to filter out the data noise as much as possible. The mean backscattering value was obtained with minimum noise by averaging along the row direction and then applying a moving average of 4 pixels along the azimuthal direction to eliminate pixels radically different from the mean.

In contrast to the regression model, the theoretical, integral equation model (IEM) of Fung *et al.* (1992) provides a site-independent relationship applicable to different radar configurations (frequency, polarization, and incidence angle) and surface parameters. The general theoretical model, IEM, includes the small perturbation model (applicable for slightly rough surface), the standard Kirchhoff model (applicable for large surface height and small surface slope), and the geometric optic solution (applicable for large surface slope with multiple scattering terms). This model has been applied over a wide range of roughness conditions and radar configuration to retrieve soil moisture from radar backscattering values (e.g., Le Toan *et al.*, 1993; Altese *et al.* 1996). However, the inversion of such a model to retrieve soil moisture requires information about the surface roughness and correlation length. In this study, based on the Gaussian and exponential correlation functions, IEM was first used to study the sensitivity of surface parameters with respect to the satellite configuration of Radarsat. Second, based on measured field soil moisture and radar backscatter values obtained from Radarsat SAR data, the surface parameters (surface rms height σ, and correlation length L) of IEM were automatically calibrated using the simplex algorithm of Nelder and Mead (1965). Lastly, using these optimized surface parameters, IEM was inverted to obtain volumetric soil moisture for the study site from Radarsat SAR backscattering values (see section 5.4.2).

5.4 Discussion of Results

The relationship between Radar backscattering echoes and soil moisture content is affected by variables such as the mean roughness height, roughness correlation length, and land cover type. Using ground based and air-borne radars, previous researchers (e.g., Ulaby *et al.*, 1978, 1982; Mohan *et al.*, 1990) showed that the effect of such variables is minimum at C-band (5.3 Ghz) and near nadir incidence angles. To by-pass the effects of these surface parameters, one practical approach is to relate radar backscatters (dB) with soil moisture data via a linear regression model as discussed below.

5.4.1 Regression Analysis

A simple linear regression (Equation 5.7) was established between Radarsat SAR backscatter (σ^0) and volumetric soil moisture (θ) data collected from 9 sites of agricultural and ranch lands located in the Paddle River Basin.

$$\sigma^0 = \alpha + \beta\theta \tag{5.7}$$

Regression parameters α and β are obtained through calibration. The regression results for each of the six days and for the three combined days in 1996 and 1997 are given in Figure 5.6(a)-(h). The regression plots of Figure 5.6 show a fairly strong dependence of radar backscatter on volumetric soil moisture. The best result obtained was for August 12, and 29 of 1997 (R=0.92) which were also the driest (with an overall basin saturation of 68% and 58% respectively) among the six days. Apparently, the assumption of a linear relationship between Radarsat SAR and field soil moisture works best when the soil is relatively dry. Near saturation, radar backscatter levels off and becomes less sensitive to an increase in the soil water content (Dobson and Ulaby, 1986). Radar backscatter would fall quickly when soil saturation is exceeded and surface ponding appears (Brun *et al.*, 1990). Therefore the deterioration of R with an increase in soil water does not come as a surprise, e.g., R=0.71 for September 10, 1996 when the average basin saturation levels were 82%. Brun *et al.* (1990) and Altese *et al.* (1996) obtained similar results.

The statistical model (Equation 5.7) developed was cross-validated using soil moisture and Radarsat SAR data that were not used to calibrate α and β. Figure 5.7(a) shows that the regression model calibrated from the 1996 data over-simulated soil moisture during the validation period of 1997. It seems that this is partly caused by the calibration data being "wetter" than the validation data because by calibrating the model with 1997 data and validating it with 1996 data, the reverse result was obtained, e.g., the model under-simulated the 1996 validation data (Figure 5.7(b)). This implies that regression model parameters would be better established with calibration data that represent a wide range of soil moisture conditions, and we would expect poorer results when retrieving soil moisture from radar backscatter under relatively wet than dry conditions. In other words, if the basin is nearly saturated, the degree of radar backscattering becomes less sensitive to increasing water content, as evident in the generally poorer agreement between the fitted regression model and observed data when the calibration period was extended to both 1996 and 1997 (Figure 5.7(c)).

5.4.2. The Integral Equation Model

The following integral equation model for radar backscatter is expressed in terms of the Radarsat satellite configuration.

$$\sigma^o = 0.5k^2 \exp(-2k_z^2\sigma^2) \sum_{n=1}^{\infty} \sigma^{2n} \left|I^n\right|^2 \frac{W^n(-2k_x,0)}{n!} \tag{5.8}$$

$$I^n = (2k_z)^n f \exp(-\sigma^2 k_z^2) + 0.5k_z^n \left[F(-k_x,0) + F(k_x,0)\right] \tag{5.9}$$

$$F(-k_x,0) + F(k_x,0) = \frac{2\sin^2\phi(1+R_\perp)^2}{\cos\phi}\left[\left(1-\frac{1}{\mu}\right) + \frac{\mu\varepsilon - \sin^2\phi - \mu\cos^2\phi}{\mu^2\cos^2\phi}\right] \tag{5.10}$$

$$f = \frac{-2R_\perp}{\cos\phi} \tag{5.11}$$

$$R_\perp = \frac{1-\sqrt{\varepsilon}}{1+\sqrt{\varepsilon}} \tag{5.12}$$

Where

σ^o = radar backscattering
σ = surface rms height
ε = dielectric constant
$R_\perp$ = Frensel reflection coefficient
μ = magnetic permeability
ϕ = incidence angle
k = wave number
$k_z = k\ cos\phi$
$k_x = k\ sin\phi$

The roughness spectrum $W^n(u,0)$ of the surface based on the nth power of the surface correlation function $\rho(\xi)$ and the Fourier transform is given by:

$$W^n(u,0) = \frac{1}{2\pi}\int \rho^n(\xi)\exp(-ju\xi)d\xi \tag{5.13}$$

In the evaluation of the roughness spectrum we assumed that the surface correlation function is isotropic and can be represented either by a Gaussian, $\rho(\xi) = \exp\left[\frac{\xi^2}{L^2}\right]$, or an exponential, $\rho(\xi) = \exp\left[-\frac{|\xi|}{L}\right]$, model where L is the correlation length.

For the Radarsat satellite configuration, by assuming the increase of the real part of the dielectric constant ε is much higher than the increase of the imaginary part at 5.3 Ghz, we only need to consider the real part of ε (see Ulaby *et al.*, 1986; Schmugge, 1985; Hallikainen *et al.*, 1985). The relationship between ε and volumetric soil moisture θ that we used was derived by Topp et al. (1980) and has been validated for a wide range of mineral soils under different conditions (Topp *et al.*, 1985; Ansoult *et al.*, 1985; Altese *et al.*, 1996).

$$\theta = (-530 + 292\varepsilon - 5.5\varepsilon^2 + 0.043\varepsilon^3) \times 10^{-4} \qquad (5.14)$$

We used equations (5.8) to (5.12) to study the sensitivity of radar backscattering σ^0 to surface parameters (σ and L) under Radarsat's configurations (C-band, HH polarization) operating at the standard beam mode (S1 and S2). The roughness parameters used in the sensitivity analysis are the most commonly encountered in agricultural land, pasturelands, and range lands. Figure 5.8(a)-(d) shows that σ^{o} is not too sensitive to ε, but more sensitive to surface rms height σ especially under the Gaussian than the exponential correlation functions, and when σ is low. Figure 5.8(b) shows that using the Gaussian correlation function at the S2 beam mode of Radarsat, σ^{o} changes by as much as 44 (dB) for only an increase of 0.3 cm in σ. Similarly σ^{o} is more sensitive to the correlation length L for the Gaussian than the exponential correlation functions (Figure 5.9(a)-(d)) for large correlation length (e.g., L>4cm). Altese *et al.* (1996) obtained similar results for ERS-1 radar configuration (VV polarization, C-band, and ϕ of 23°) and concluded that the behavior of the model is highly dependent on the choice of the correlation function. So by using an exponential correlation function we can reduce the sensitivity of σ^{o} to changes in surface parameters and then minimize their effect on volumetric soil moisture derived from backscatter values. Besides, for three relatively smooth surfaces (rms height σ = 0.32, 0.4, and 1.12), Oh *et al.* (1992) found that the measured autocorrelation function is closer in shape to an exponential function than to a Gaussian function. Similarly, Wegmuller *et al.* (1994) found that the exponential correlation function provides a better fit to the observed correlation than Gaussian models for agricultural land uses. Since our study site represents a relatively smooth surface such as agricultural, pasture and herbaceous lands, we used an exponential correlation function for further analysis with IEM.

Under natural conditions, surface parameters measured in the field are highly variable spatially and thus are not isotropic as assumed in many correlation functions. There has been extensive research on either isolating or quantifying the effects of surface parameters on radar backscattering σ^0 (e.g., Fung, 1994; Engman and Wang, 1987; Autret *et al.*, 1989; Altese *et al.*, 1996). Unfortunately, none of the above efforts lead to a method that can retrieve soil moisture from backscattering data without the surface roughness parameter. For truck-mounted or air-borne radar experiments, it is possible to collect multi-polarized data, which allow us to solve for soil moisture and surface parameters simultaneously. However, this multi-polarization technique is not possible with our current space platforms that have single frequency and polarization sensors. We need other means to estimate the surface parameters. Recently, Jackson et al. (1997) suggested a first order, rainfall-dependent, correction for the surface roughness from the land cover database established through numerous soil erosion studies. Nonetheless, due to the high sensitivity of soil moisture models to surface roughness, they suggested field measurements to increase the precision of the roughness estimate.

We first obtained a range of surface roughness parameter values for agricultural and range land covers from the literature (e.g., Jackson et al., 1997) and then optimized them with respect to the Radarsat backscattering values and soil moisture using the simplex optimization method (Nelder and Mead, 1965). Then we input the 1997 Radarsat σ^0 (August 5, 12, and 29) and surface roughness parameters calibrated from the 1996 data

(September 3, 10, and 27) to IEM and simulated the corresponding soil moisture θ for 1997, which we validated against field measurements (Figure 5.7(a)). We also did the same using 1997 as the calibration data and 1996 as the validation data (Figure 5.7(b)). The results indicated that IEM performed consistently better than the statistical model (see Figure 5.7 (a)-(b) and Table 5.2). However, as with the statistical model, IEM generally over-estimated the basin soil moisture when calibrated with the 1996 data that were "wetter" than the validation data of 1997. For the same reason, when 1997 was the calibration period, the reverse situation of the statistical model was also found in that IEM under-estimated the 1996 validation data.

Just like the statistical model, we also calibrated IEM using the whole data set of 1996 and 1997 that covers a wider range of soil moisture conditions than data of individual years. Unfortunately we could not validate the third case. Instead, we averaged the model parameters obtained from the first two cases and re-ran the statistical model and IEM using both years of Radarsat data (Figure 5.7(d)). Differences between the simulated and observed volumetric soil moisture are similar to those of the third case. In all four cases, both the statistical model and IEM's performance were poorer for relatively wet condition (75% and 82% saturation), with an average simulation error of ± 10% in soil moisture.

5.4.3 Spatial Variability of Soil Moisture

We also investigated whether the homogeneity assumption (spatial correlation as a function of distance lag only) used in spatial interpolation techniques such as universal kriging is applicable to the spatial distribution of soil moisture in the Paddle River Basin. The semi-variogram function, defined as (Journel and Huijbregts, 1978)

$$2\gamma(x,h) = E\left\{\left[z(x) - z(x+h)\right]^2\right\} \tag{5.15}$$

Where $z(x)$ and $z(x+h)$ are two numerical values (either volumetric soil moisture or backscatter coefficient) at two points x and $x+h$ separated by the distance h, was used to study the spatial correlation of the measured soil moisture, or Radarsat SAR backscatter with respect to inter-site distances (called distance lag). The classical estimator of the semi-variogram based on sampled data is defined as:

$$\gamma^* = \frac{1}{2N(h)} \sum_{i=1}^{N(h)} \left[z(x_i) - z(x_i + h)\right]^2 \tag{5.16}$$

Where N(h) is the number of pair of measurements.

The semi-variogram of all the measured soil moisture data collected in September 3, 10, and 27 of 1996 shows virtually no correlation with inter-site distances (Figure 5.10(a)) that vary from 1 to 13km. Similar result has been obtained for backscattering values derived from Radarsat SAR data. However, for a particular land cover type such as agricultural land, field measured soil moisture and Radarsat backscatter values have a definite spatial correlation with inter-site distance up to about 200-275m (Figure 5.10(b)). Beyond this distance, the spread of data points grows so much that no more meaningful correlation can be identified from the semi-variogram.

In conclusion, at field scales larger than plot sizes, besides the inter-site distance, the combined influence of local topography, vegetation cover, and other factors play a significant part in determining the spatial correlation of soil moisture or radar backscatter values. Our result agrees with that of Rotunno Filho *et al.* (1996) who found that the cross correlation of soil moisture in pasture lands breaks down at an inter-site distance of 150 to 450m. Rotunno Filho (1996) also found similar results using soil moisture data of bare field and ERS-1 satellite images. It seems that regardless of the land cover type, for deriving soil moisture maps from either satellite or field soil moisture data, the homogeneity assumption of spatial interpolation - correlation as a function of distance lag only - is only applicable for inter-site distances of order 150 to 400m.

5.5 Summary and Conclusions

On six selected days of September 1996 and August 1997, about 1350 soil samples were collected from nine sites of the Paddle River Basin (265 km^2) of central Alberta. Twenty-five soil samples per day were collected at each site (agricultural or ranch land) to characterize the average soil moisture of the site for each day. The samples were later analyzed for the volumetric soil moisture content in a laboratory. On these six days we also acquired Radarsat SAR images of standard beam modes S1 or S2 which have low incidence angles of 20-27° for the basin.

The parameters of a simple regression model were calibrated from the average of 25 observed soil moisture values per site of the nine sites against the corresponding average backscatter values of 64 pixels per site from Radarsat SAR images. This strategy of matching sets of 25 soil samples with about 64 pixels of Radarsat backscatter is to filter out the data noise as much as possible. The best calibration result obtained for the regression model has a R=0.92 for August 12 and 29 of 1997 when the basin was relatively dry, with overall saturation levels of 68 and 58% respectively.

Using the integral equation model (IEM) of Fung et al. (1992), we studied the sensitivity of radar backscattering σ^o to surface parameters based on the Radarsat satellite's configurations. We found that σ^o is highly sensitive to surface rms height especially for a relatively smooth surface and a Gaussian correlation function. Then, using the same sets of Radarsat and soil moisture data, we optimized the surface parameters of IEM by the simplex algorithm and used them to invert the IEM to retrieve soil moisture from Radarsat σ^o. IEM consistently performed better than the regression model but the performance of both models generally deteriorates as the basin soil moisture level approaches saturation level (e.g., R=0.71 for the regression model on September 10, 1996 with a basin saturation of 82%). Apparently when near saturation, radar backscatter levels off and becomes less sensitive to an increase in the soil water content.

Lastly, from the semi-variograms of measured soil moisture and radar backscatters with inter-site distance, we found that the homogeneity assumption of spatial interpolation - correlation as a function of distance lag only – breaks down at inter-site distances of about 200-275m. Apparently, spatial interpolation methods such as the universal kriging are only applicable to interpolate soil moisture from plots several hundred meters in size and of a particular land cover type.

References

Alberta Energy and Natural Resources (AENR), 1977, "*A study of Watershed Management Options For Controlling Flood Runoff in the Headwaters of the Paddle River Basin*," No. 44, pp. 1-39.

Altese, E., O. Bolognani, M. Mancini, and P.T. Troch, 1996, "Retrieving soil moisture over bare soil from ERS-1 Synthetic Aperture Radar data: Sensitivity analysis based on a theoretical surface scattering model and field data," *Water Resources Research*, Vol. 32, No. 3, 653-661.

Ansoult, M., DE Backer, L. W., and Delercq, M, 1985, Statistical relationship between apparent dielectric constant and water content in porous media, *Soil Sci. Am. J.*, 49, 45-50.

Autret, M., Bernard, R., and Vidal-Madjar, D., 1989, Theoretical study of the sensitivity of the microwave backscattering coefficient to the soil surface parameters. *Int. J. Remote Sensing*, vol. 10,171-179.

Bernard, R., D. Vidal-Madjar, F. Baudin, and G. Laurent, 1982, "C-Band Radar for Determining Surface Soil Moisture," *Remote Sensing of Environment*, 12, 189-200.

Brown, R.J., B. Brisco, R. Leconte, D.J. Major, J.A. Fischer, G. Reichert, K.D. Korporal, P.R. Bullock, H. Pokrant, and J. Culley, 1993, "Potential Applications of RADARSAT Data to Agriculture and Hydrology," *Canadian Journal of Remote Sensing*, Vol. 19, 317-329.

Brun, C., R. Bernard, D. Vital-Majar, C. Gascule-Odoux, P. Merot, J. Duchesne, and H. Nicolas, 1990, "Mapping Saturated Areas with Helicopter-borne C-band Scatterometer," *Water Resources Research*, Vol. 26, No. 5, 945-955.

Chow V.T., D.R. Maidment, L.W. Mays, 1988, "*Applied Hydrology*," McGraw-Hill International Editions.

Crevier Y., T.J. Pultz, T.I. Lukowski, T. Toutin, 1996, "Temporal Analysis of ERS-1 SAR Backscatter for Hydrology Applications," *Canadian Journal of Remote Sensing*, Vol. 22, No. 1, 65-76.

Dobson, M.C. and F.T. Ulaby, 1981, Microwave backscatter dependence on surface roughness, soil moisture, and soil texture: Part III- Soil tension, *IEEE Transactions on Geoscience and Remote Sensing*, Vol. GE-19, pp. 51-61.

Dobson, M.C. and F.T. Ulaby, 1986, "Active Microwave Soil Moisture Research," *IEEE Transactions on Geoscience and Remote Sensing*, Vol. GE-24, pp. 23-36.

Engman, E.T. and Wang, J. R., 1987, Evaluating roughness models of radar backscatter. *IEEE Trans. Geoscience and Remote Sensing*, vol. GRS-25, pp. 709-713.

Fung, A. K., Lee, Z., and Chen, K. S., 1992, Backscattering from a randomly rough dielectric surface, *IEEE Transactions on Geoscience and Remote Sensing*, 30(2), pp.356-369.

Fung, A. K., 1994, *Microwave scattering and emission models and their applications.* Norwood, MA: Artech House.

Hallikainen, M. T., Ulaby, F. T., Dobson, M. C., El-Rayes, M. A., and Wu, L. K., 1985, Microwave dielectric behavior of wet soil. Part I: Empirical models and experimental observations. *IEEE Transactions on Geoscience and Remote Sensing*, 23, pp.25-34.

Jackson, T. J., McNairn, H, Weltz, M.A., Brisco, B., and Brown, R., 1997, First Order surface Roughness correction of Active Microwave Observations for Estimating Soil Moisture. *IEEE Transactions on Geosci. and Remote Sensing*, vol. 35, No. 4, pp.1065-1069.

Journel, A.G. and C.J. Huijbregts, 1978, "*Mining Geostatistics*," San Diego, California: Academic Press.

Le Toan, T. (1982). Active microwave signatures of soil and crops: significant results of three years of experiments, *Proceeding Symposium IGARSS'82*, Munich, RFA, 1-4 June 1982.

Le Toan, T., Smachia, P., Souyris, J., Beaudoin, A., Merdas, M., Wooding, M., and Lichteneger, J., 1993, On the retrieval of soil moisture from ERS-1 SAR data. *Proceedings Second ERS-1 Symposium*, Hamburg, Germany, 11-14 October 1993. pp. 883-888.

Lindsey, S.D., R.W. Gunderson, and J.P. Riley, 1992, "Spatial Distribution of Point Soil Moisture Estimates Using Landsat TM Data and Fuzzy-C Classification," *Water Resource Bulletin*, Vol. 28, 865-875.

Longley, R.W., 1968, "*Climatic maps for Alberta*," University of Alberta.

Mohan S., N.S. Mehta, R.L. Mehta, P. Patel, V.H. Bora, K.K. Sule, S.P. Purohit, S. Rai, H.P. Singh, and Ramakrishnay, 1990, "Radar Response to Soil Moisture of Sandy Soil," *Scientific note*, SAC/RAC/RSAG/ERS-1/SN/ 01/90.

Nelder, J. A., and Mead R., 1965, A simplex method for functional minimization. *The Computer Journal*, 9: 308-313.

O'Brien, E.G., 1992, "An Agricultural Applications of Regional Scale Soil Moisture Modelling and Monitoring," *Proceedings of the NHRC Symposium*, No. 9, March 9-10, pp. 13-20.

Oh, Y., Sarabandi, K., and Ulaby, F. T., 1992, An emprical model and an inversion technique for radar scattering from bare soil surfaces, *IEEE Transactions on Geosci. and Remote Sensing*, 30(2), pp. 370-381.

Parashar, S., Langham, E., McNally, J., and Ahmed, S., 1993, "RADARSAT Mission Requirements and concepts." *Canadian Journal of Remote Sensing*, vol. 19, 280-288.

Pretula, B. R., and Ko, C. A., 1982, *Hydrogeology Paddle River Reservoir area near Mayerthorpe*, Alberta, Report prepared for Alberta Environment Protection (AEP), pp. 1-107.

Rotunno Filho O.C., 1996, "*Soil Moisture Mapping Using Remote sensing and Geostatistics Applied to Rainfall-Runoff Models*," Ph.D Thesis, Department of Civil Engineering, University of Waterloo, 396 pp.

Rotunno Filho O.C., E.D. Soulis, N. Kouwen, A. Abdeh-Kolahchi, T.J. Pultz, Y. Crevier, 1996, "Soil Moisture in Pasture Fields using ERS-1 SAR data: Preliminary Results," *Canadian Journal of Remote Sensing*, Vol. 22, No. 1, 95-107.

Shepherm, N.W. and associates, 1996, "*CDPF output Data Calibration*," Technical note, No.4.2.

Schmugge, T., 1985, "Remote Sensing of Soil Moisture," in *Hydrological Forecasting*, John Wiley, New York, Chap. 5, pp. 101-124.

Topp, G. C., J. L. Davis, and Annan, A. P., 1980, Electromagnetic determination of soil water content: Measurement in coaxial transmission lines, *Water Resour. Res.*, 16, 574-582.

Topp, G. C., and Davis, J. L., 1985, Measurements of soil water content using time domain reflectometry: A field evaluation, *Soil Sci. Am. J.*, 49, 19-24.

Twardy, A.G., J.D. Lindsay, 1971, "*Soil Survey of the Chip Lake Area*," Alberta Soil Survey, No. 28, pp. 1-71.

Ulaby, F. T, P.P. Batlivala, and M.C. Dobson, 1978, "Microwave Backscatter Dependence on surface Roughness, Soil Moisture, and Soil Texture: Part I - Bare Soil," *IEEE Transactions on Geoscience Electronics*, Vol. GE-16, pp. 286-295.

Ulaby, F. T, G.A. Bradley, and M.C. Dobson, 1979, "Microwave Backscatter Dependence on surface Roughness, Soil Moisture, and Soil Texture: Part II - Vegetation covered soil," *IEEE Transactions on Geoscience Electronics*, Vol. GE-17, pp. 33-40.

Ulaby, F.T., R.K. Moore, and A.K. Fung, 1982, "*Microwave Remote Sensing: Active and Passive*," Vol. II, Artech House, Norwood, Mass.

Ulaby, F.T., R.K. Moore, and A.K. Fung, 1986, "*Microwave Remote Sensing: Active and Passive*," Vol. III, Artech House, Norwood, Mass.

Wegmuller, U., Matzler, C., Huppi, R., and Schanda, E., 1994, Active and passive microwave signature catalogue on bare soil (2-12 Ghz), *IEEE Transactions on Geoscience Electronics*, 32(3), pp. 698-702.

Table 5.1 Description of the six Radarsat SAR images acquired at approximately 14:11 local time and at descending orbit over the Paddle River Basin.

Date	Beam type	Angle of incidence (°)	Scene center	
			latitude	longitude
9/3/96	S1	23.296	53°56'	115° 31'
9/10/96	S2	27.685	53°55'	115° 30'
9/27/96	S1	23.268	53°55	115° 34'
8/5/97	S1	23.303	53°36'	115° 39'
8/12/97	S2	27.663	53°40'	115° 34'
8/29/97	S1	23.311	53°35	115° 39'

Table 5.2 Summary of calibration and validation results of the regression model and IEM given in Figure 7.

Cases	Regression model				Integral Equation model (IEM)			
	Calibration		Validation		Calibration		Validation	
	R	SE	R	SE	R	SE	R	SE
Figure 5.7(a)	0.67	0.0517	0.83	0.0348	0.85	0.0295	0.90	0.0237
Figure 5.7(b)	0.83	0.0320	0.67	0.0474	0.92	0.0200	0.80	0.0360
Figure 5.7(c)	0.69	0.0450	-	-	0.79	0.0338	-	-

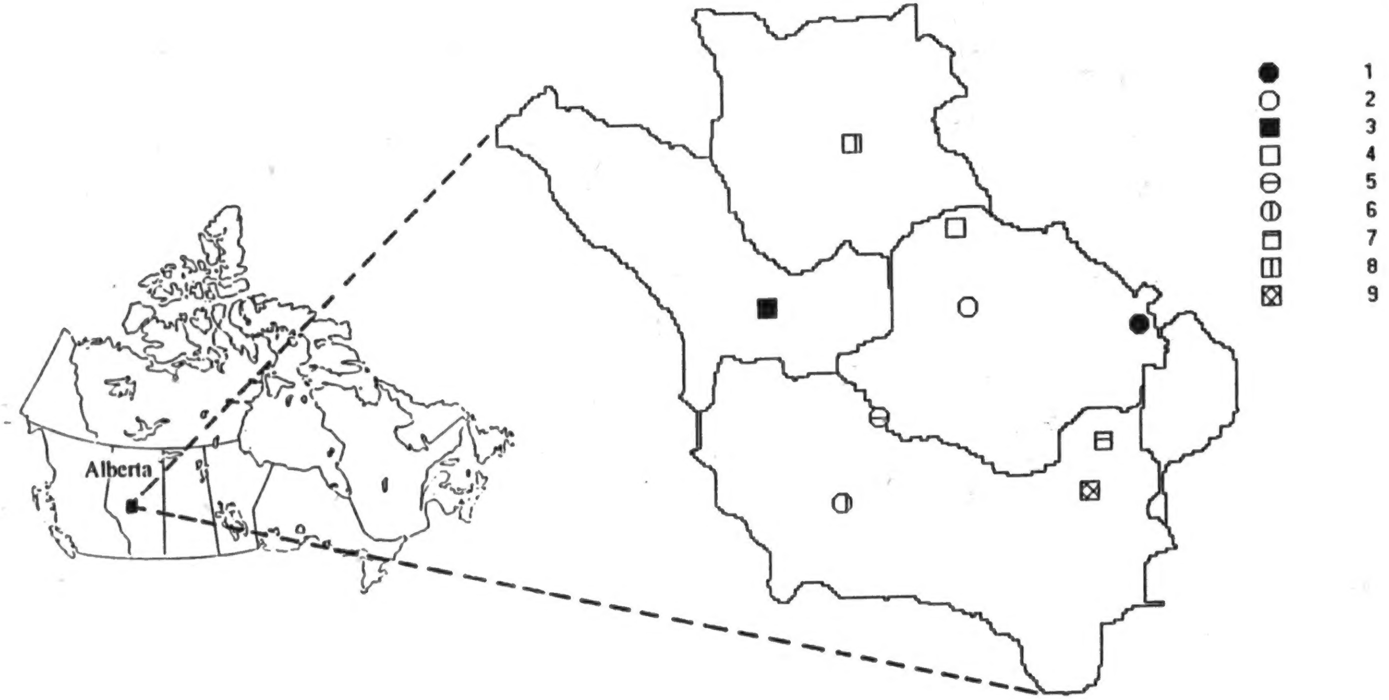
Alberta
● 1
○ 2
■ 3
□ 4
⊖ 5
⦶ 6
7
◫ 8
⊠ 9

Figure 5.1 Location map and field soil sampling sites of Paddle River Basin, Alberta.

Pasture land

Agricultural land

Herbaceous land

Figure 5.2 Photographs of three land cover types of Paddle River Basin from which soil moisture data was collected

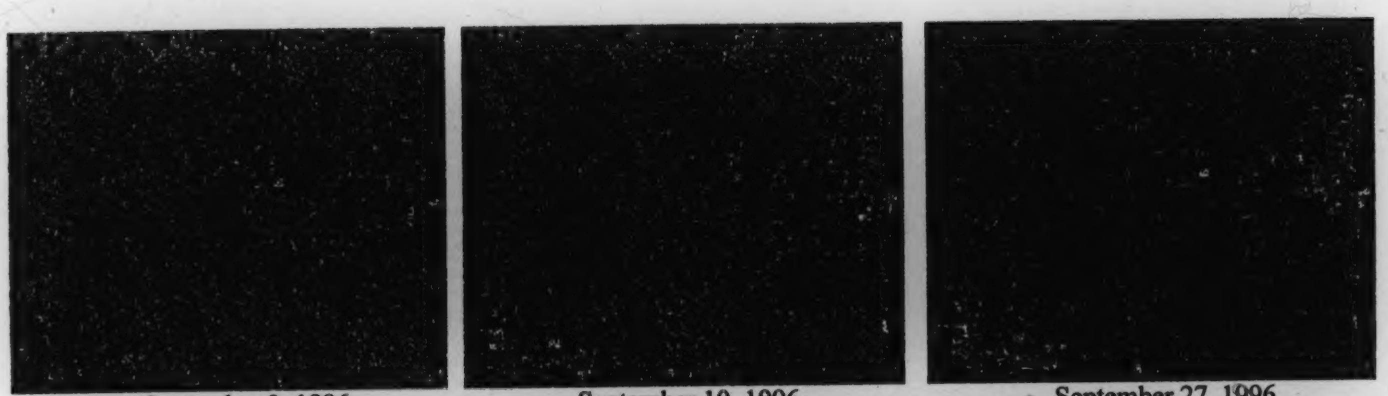

September 3, 1996

September 10, 1996

September 27, 1996

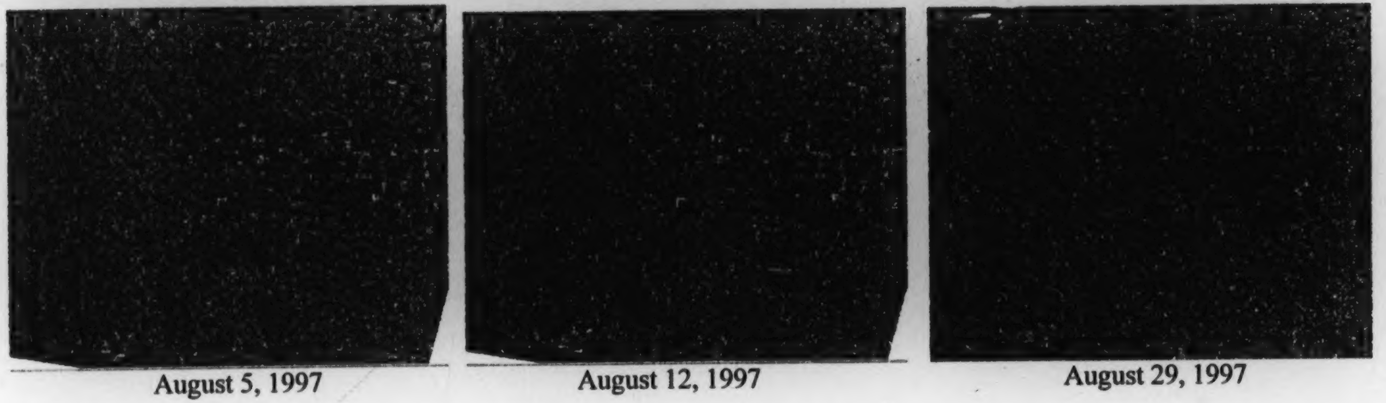

August 5, 1997

August 12, 1997

August 29, 1997

Figure 5.3 The six raw Rdarasat SAR images aquired for Paddle River Basin, Alberta

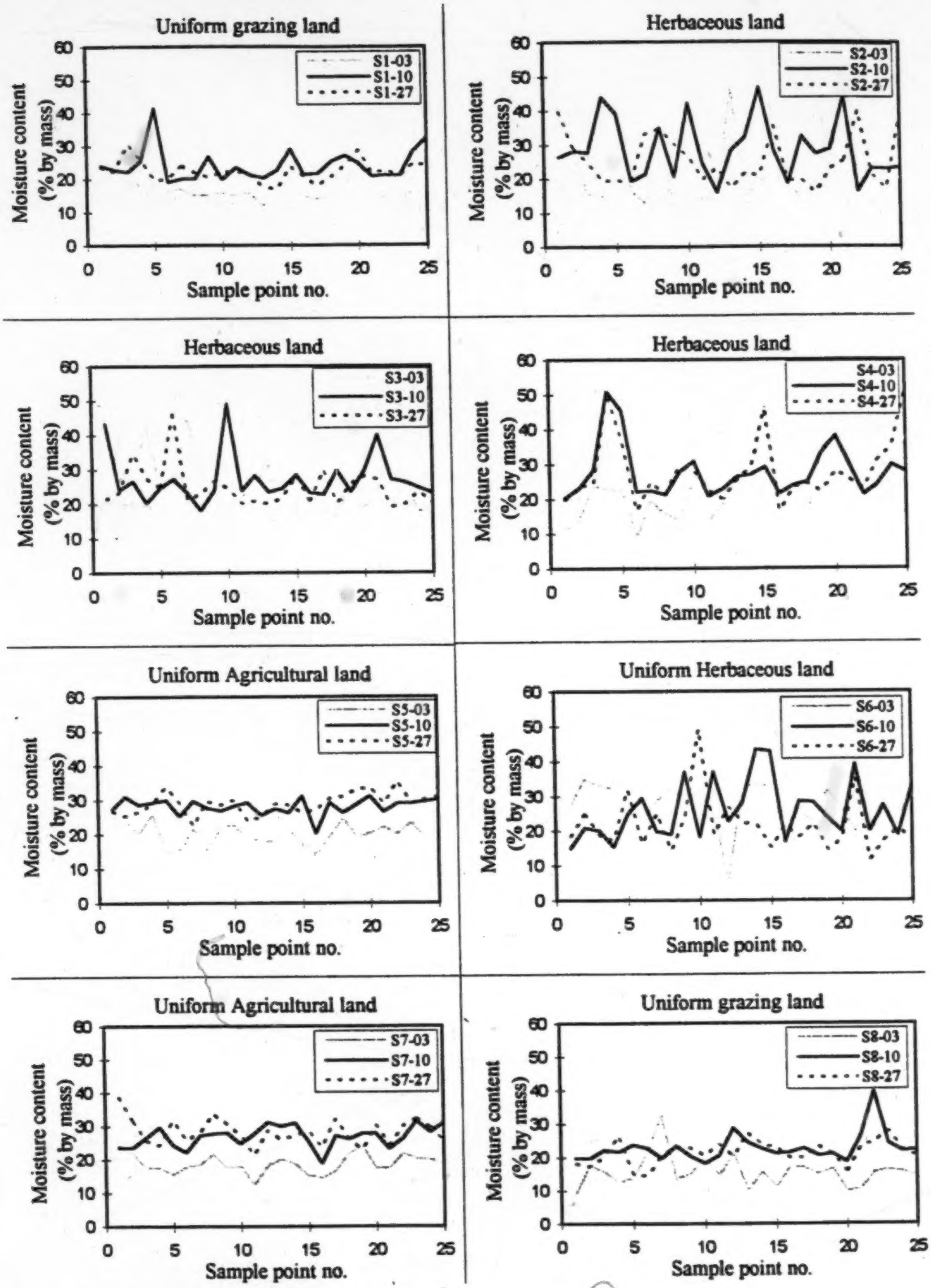

Figure 5.4 Field measured soil moisture data collected from different land cover types for September of 1996.

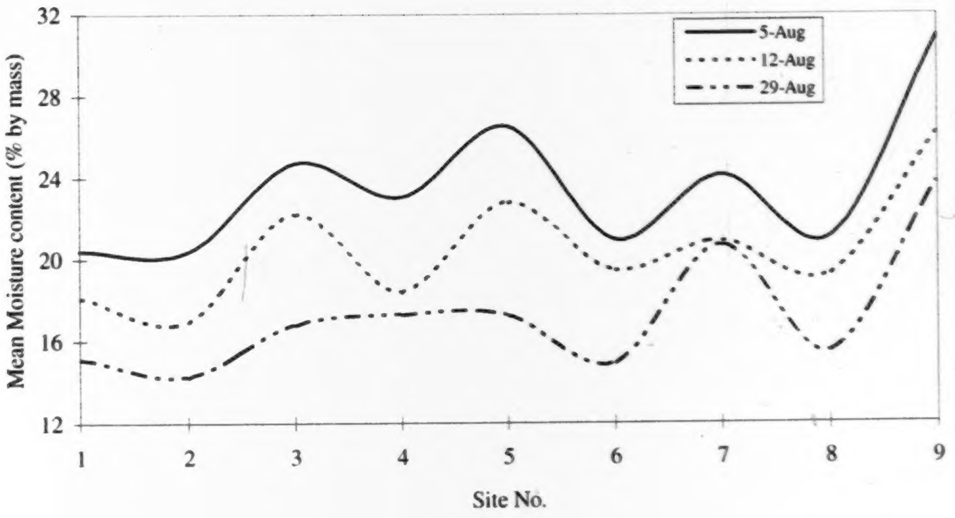

Figure 5.5 Variation of average soil moisture content among sites for three days of August 1997.

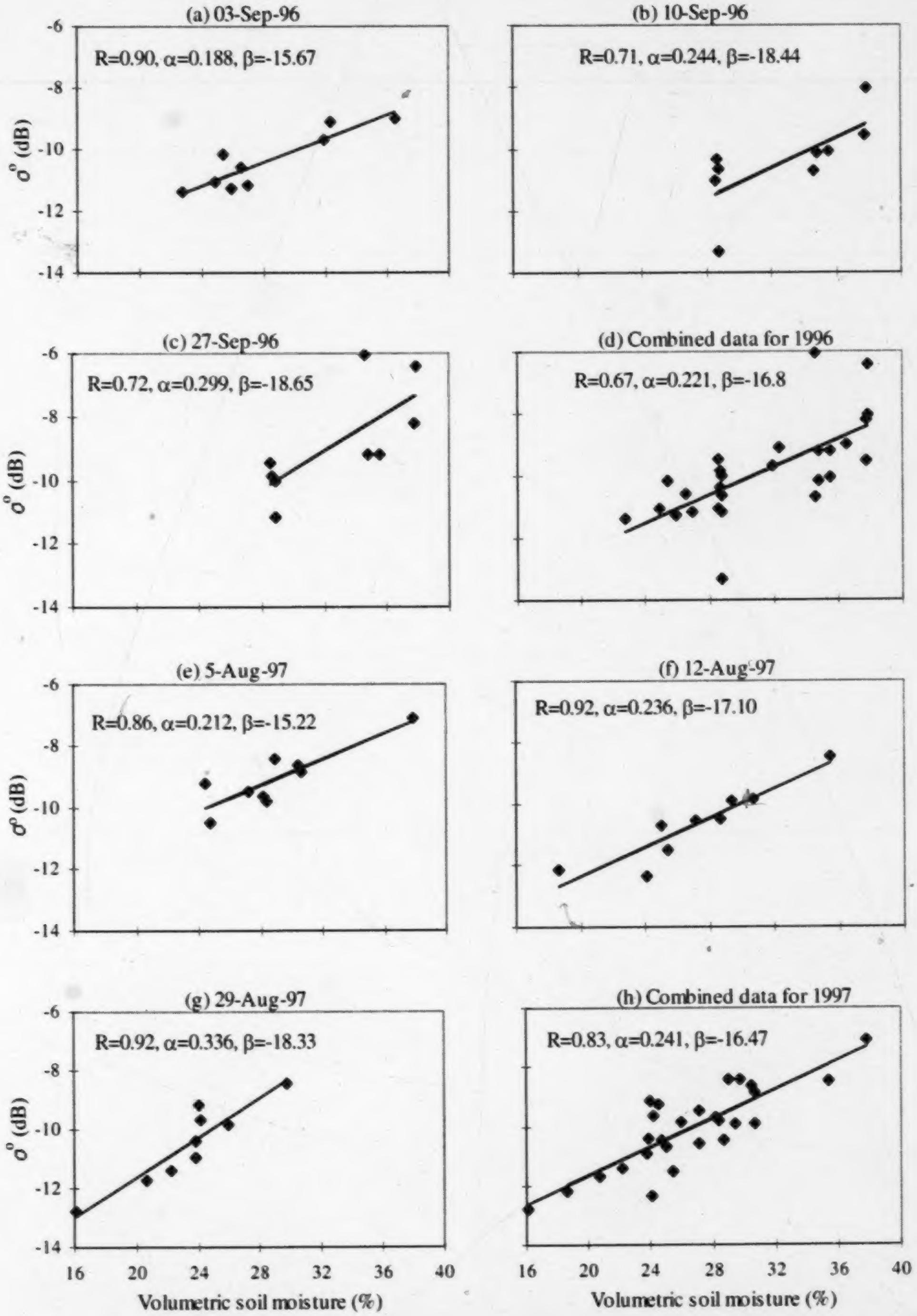

Figure 5.6 Regression relations of observed soil moisture data and Radarsat SAR backscattering values for all the six days and for the combined data.

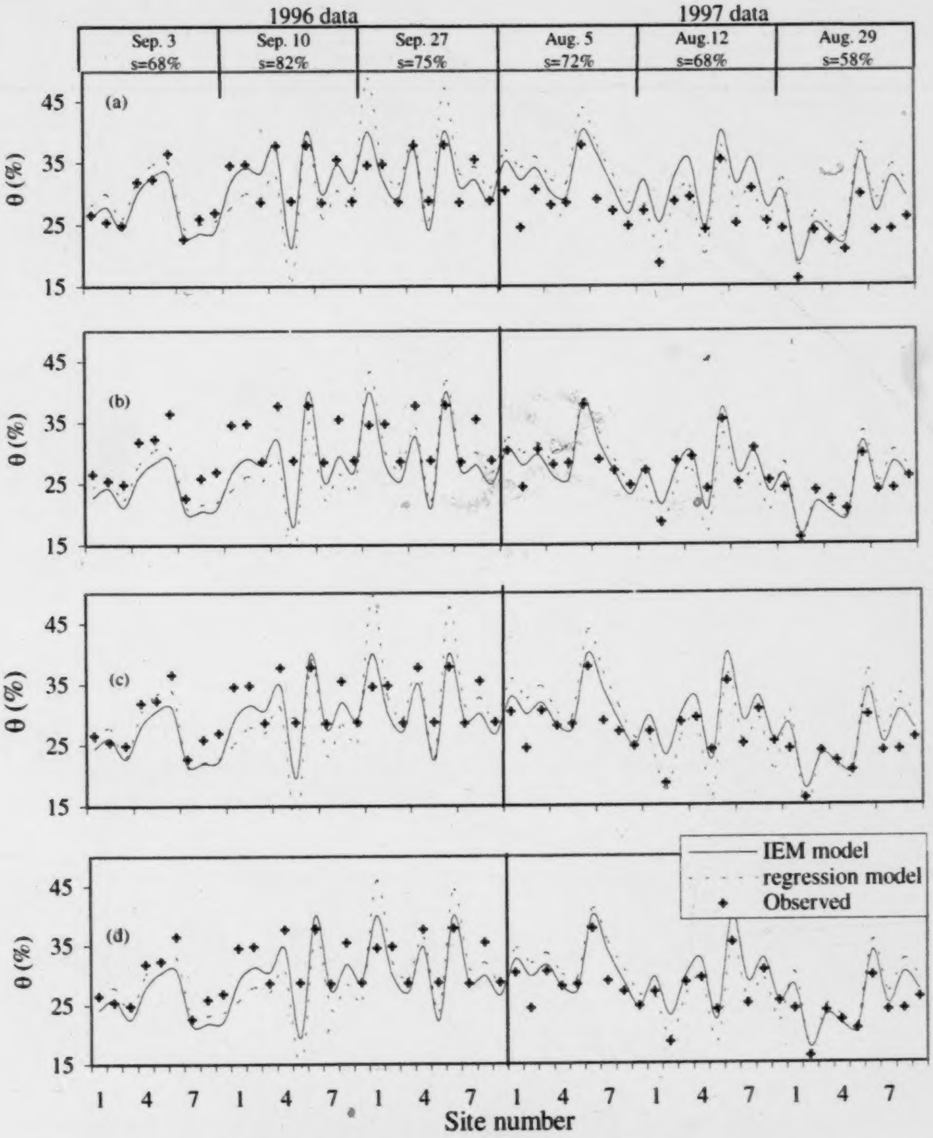

[s]Figure 5.7 Four sets of calibration and validation results for the regression model and IEM comparing the retrieved (based on Radarsat SAR data) versus observed soil moisture: (a)1996 data used for calibration and 1997 data for validation; (b) 1997 data used for calibration and 1996 data for validation; (c) Both 1996 and 1997 data used for calibration, no validation; and (d) Average values of model parameters obtained in (a) and (b) used for retrieving soil moisture from backscatter values for 1996 and 1997.

---

s = overall basin saturation level

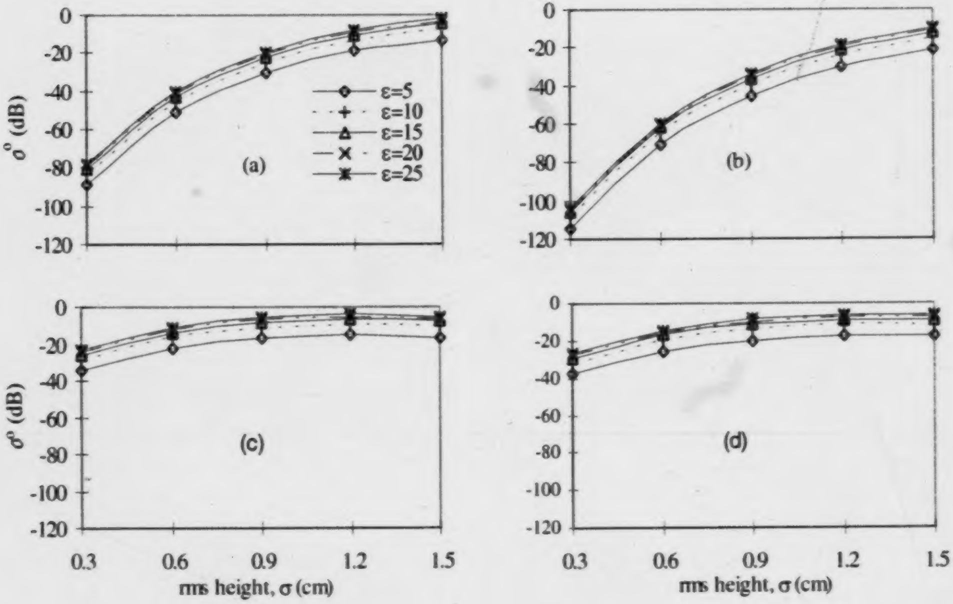

Figure 5.8 Sensitivity of the backscattering coefficient, σ^o to the surface rms height σ for Radarsat satellite configuration (set correlation length L=10), using (a) Gaussian correlation function and S1 beam (ϕ=23.3°), (b) Gaussian correlation function and S2 beam (ϕ=27.7°), (c) exponential correlation function and S1 beam (ϕ=23.3°), (d) exponential correlation function and S2 beam

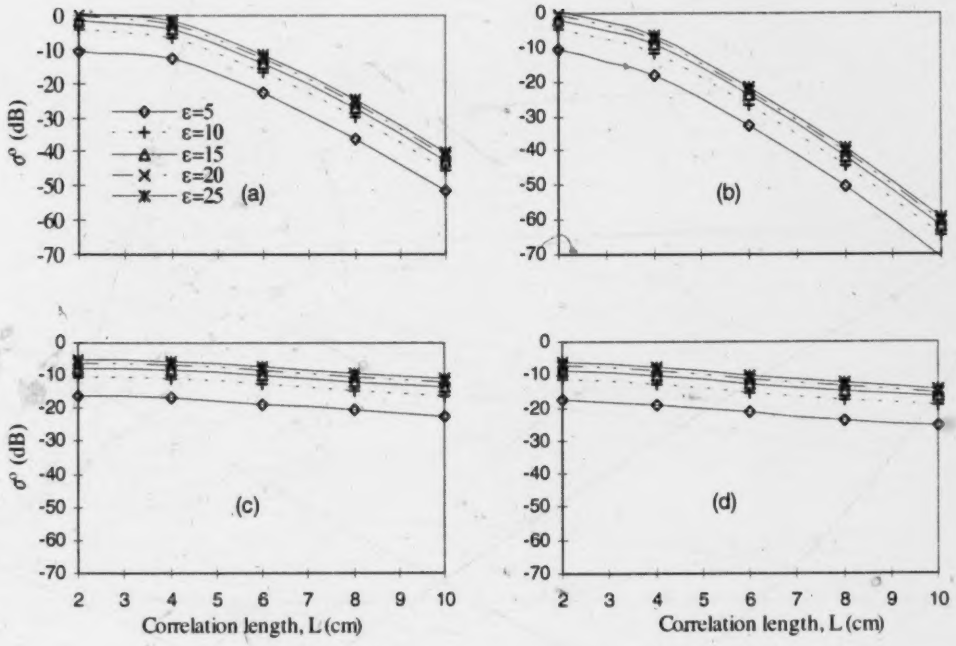

Figure 5.9 Sensitivity of the backscattering coefficient, σ^o to the correlation length L for Radarsat satellite configuration (set rms height σ=0.6), using (a) Gaussian correlation function and S1 beam (ϕ=23.3°), (b) Gaussian correlation function and S2 beam (ϕ=27.7°), (c) exponential correlation function and S1 beam ϕ=23.3°), (d) exponential correlation function and S2 beam (ϕ=27.7°).

(a) Measured soil moisture for different land covers.

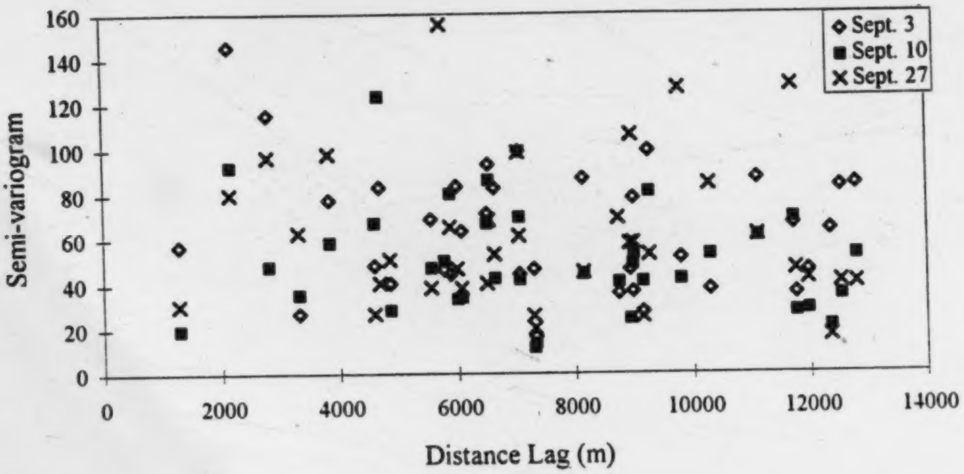

(b) Radarsat SAR image – September 3, 1996 (Agricultural field).

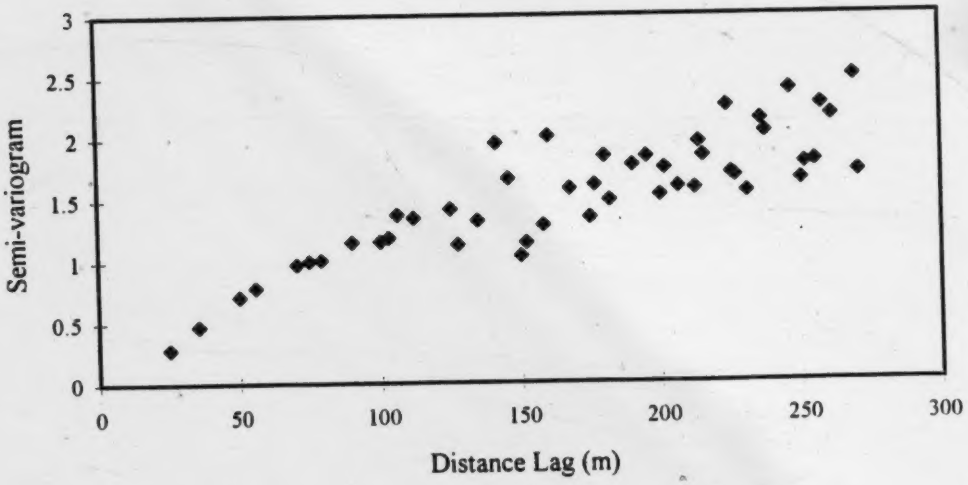

Figure 5.10 Spatial semi-variogram of (a) 1996 measured soil moisture of all 9 sites, and (b) Radarsat backscatters of so for one agricultural site of Paddle River Basin.

Chapter 6

Summary, Conclusions and Recommendations for Future Work

A semi-distributed, physically based hydrologic model (called DPHM-RS), developed to model basin scale hydrologic processes, is designed to take advantage of distributed hydrologic information retrieved from various space platforms and topographic information processed from Digital Terrain Elevation Data (DTED) using a geographic information system (GIS). DPHM-RS accounts for the spatial variation of meteorological inputs and the hydrologic effects of different land uses at a sub-basin level. Interception, evapotranspiration, and infiltration are evaluated for various land covers of each sub-basin while soil moisture is evaluated by the water balance approach at the sub-basin level. Using an average response function derived for each sub-basin, the surface runoff of each sub-basin is first routed to the channel network and then to the basin outlet using the Muskingum-Cunge method.

DPHM-RS is applied to the Paddle River Basin of central Alberta which was characterized by 5 sub-basins, drained by a network of stream channels, and with each sub-basin having its own land cover types and terrain features. Input data to the model included meteorological data collected from 2 meteorological towers set up at the study site, field soil moisture data, topographic information such as mean elevation, ground slope, flow direction, and topographic-soil index derived from DTED, and distributed hydrologic information such as surface albedo, land use classification, vegetation index, soil moisture, and surface skin temperature retrieved from NOAA-AVHRR, Landsat-TM, and Radarsat SAR data. DPHM-RS is calibrated using hourly data collected from July 25 to August 29 of 1996 and validated with 73 days (July 16 to September 26) of hourly data collected in the summer of 1997.

The simulated runoff agrees well with observed runoff especially for peak flows both during calibration and validation periods. In addition, simulated hourly net radiation also agree well with observed data. The discrepancy between simulated surface temperature and skin/surface temperature retrieved from NOAA-AVHRR and Landsat TM is less than 2^{o}K for 11 days out of the 14 days. The above results demonstrated that DPHM-RS is capable of modeling basin-scale hydrologic processes adequately. This is further confirmed by logical differences in the actual evapotranspiration (ET) and other energy fluxes simulated for different land covers and by reasonable temporal variations of soil moisture simulated for each sub-basin.

Given that in many aspects the performance of DPHM-RS is creditable, we also used its ET component (the two-source model) to assess two popular ET models, the Penman-Menteith equation and the modified Penman equation of Granger and Gray (1989) for non-saturated surface. Based on the ET simulated for several land use classes, it seems that the closed canopy assumption of Penman-Menteith is applicable to coniferous forest and agricultural lands but not to mixed forest and pasturelands of the Canadian Prairies. This is because for the two latter land covers, the proportion of bare soil evaporation is even higher than transpiration through canopy since the amount of energy reaching the soil surface is almost 50-60% of the total energy during day time.

The modified Penman model is used to evaluate hourly ET from different land cover types without stability correction. Using a new expression we established for the relative evaporation in the Penman model, we found that this model is generally applicable under dry environment but could estimate ET that is biased under cloudy, rainy days and wet environment.

From 6 scenes of Radarsat SAR images acquired for the Paddle River Basin, and 1350 soil moisture samples collected in the same days from 9 selected sites of the Basin, we demonstrated the feasibility of retrieving near-surface soil moisture from Radarsat SAR images. Soil moisture retrieval from Radarsat SAR data was achieved using a linear regression and the theoretical integration equation model (IEM) of Fung et al. (1992). Such distributed soil moisture data have many applications, such as to initialize or to update the soil moisture state of DPHM-RS or similar hydrologic models, and to provide regional soil moisture maps. From these data, we also found that for a single land use, the relationship between the cross-correlation of soil moisture and inter-site distance breaks down at a distance of about 250 m.

We have tested DPHM-RS with a relatively small flat catchment in Alberta – the Paddle River Basin. Some modifications may be needed to apply DPHM-RS to mountainous catchments or large catchments of different climatic regimes and highly variable climatic conditions.

We have not included the snow hydrology component in our study, which is important to Canada where winter can range from four to ten months in the high Arctic. Therefore, a logical extension is to expand the snow accumulation and ablation component in DPHM-RS, including snow sublimation and blowing snow phenomenon that are fairly common in the Prairies. Information on snow cover, snow depth, and snow water equivalent can be retrieved from space platforms such as SSM/I, NOAA-AVHRR, Landsat-TM and others. Lately, fractals and chaos theory has also been used to replace the standard areal depletion curve in modeling the snowmelt process (Shook and Gray, 1997).

Lastly, DPHM-RS can also be used used for impact studies of land use changes and can be further developed to a land surface component of GCMs, or coupled with mesoscale atmospheric models for climate change studies.

References

Shook, K. and Gray, D. M. (1997) Synthesizing shallow seasonal snow covers, Water Resour. Res., vol. 33, No. 3, pp. 419.426.

Appendix

A1 Infiltration Capacity

During wet surface (storm periods) the penetration of moisture into soil is caused by the effects of capillarity and gravity. According to Philip (1960), the total increase of moisture content in the semi-finite column during infiltration is given as:

$$\int_{0}^{\infty}(\theta-\theta_o)dz = \int_{\theta_o}^{\theta_1} z\,d\theta = F_i(t) - K(\theta_o)t \tag{A.1}$$

Where $F_i\ (t)$ is the cumulative infiltration. Equation (A.1) assumes that the extraction of soil moisture by vegetation through transpiration is negligible during storm periods. The integral on the left hand side of Equation (A.1) is represented by Philip (1960) in terms of expansion

$$z(\theta,t) = \phi_1 t^{1/2} + \phi_2 t + \phi_3 t^{3/2} + \ldots \tag{A.2}$$

Using Equation (A.1) into Equation (A.2) and differentiating, we have the velocity of infiltration as:

$$f_i(t) = \tfrac{1}{2} A_1 t^{-1/2} + A_2 + K(\theta_o) + \tfrac{3}{2} A_3 t^{1/2} + \ldots. \tag{A.3}$$

Where,

$$A_n = \int_{\theta_o}^{\theta_1} \phi_n\, d\theta \tag{A.4}$$

Philip (1960) rewrote the governing Richards equation in the form

$$-\frac{\partial}{\partial t}\int_{\theta_o}^{\theta} z\,d\theta = D\frac{\partial \theta}{\partial z} - \left[K(\theta) - K(\theta_o)\right] \tag{A.5}$$

Using Equation (A.2) and the simple initial and boundary conditions Philip (1960) found that

$$A_1 = S_i = 2(\theta_1 - \theta_o)[{}^{D_i}\!/\!{}_{\pi}]^{1/2} \tag{A.6}$$

Where S_i is the infiltration sorptivity, D_i is the effective infiltration diffusivity over the range (θ_l - θ_o). This makes the first term of Equation (A.3) identical with the well-known solution for linearized sorption (i.e. zero gravity infiltration). For short times Philip showed that

$$A_2 = \tfrac{1}{2}[K(\theta_1) - K(\theta_o)] \tag{A.7}$$

Neglecting higher order terms, we have the infiltration velocity as:

$$f_i(t) = \tfrac{1}{2}S_i t^{-1/2} + \tfrac{1}{2}[K(\theta_1) + K(\theta_o)] \tag{A.8}$$

and the cumulative infiltration as

$$F_i(t) = S_i t^{1/2} + \tfrac{1}{2}[K(\theta_1) + K(\theta_o)]t \tag{A.9}$$

For the boundary condition specified the infiltration rate and the infiltration capacity are identical by definition. By equating f_i to f_i^* and eliminating time between infiltration rate and cumulative infiltration Milly (1986) found that

$$f_i^* = A_o\left\{1 + \left[-1 + \left(1 + \frac{4A_oF_i}{S_i^2}\right)^{1/2}\right]^{-1}\right\} \tag{A.10}$$

Where

$$A_o = \tfrac{1}{2}\{K(\theta_u) + K(\theta_o)\}$$

For the sorption under analogous boundary and initial conditions and in a medium for which $D(\theta)$ increases monotonically with θ, *Crank* [1956, p.256] found that D_i is approximated well by

$$D_i = \tfrac{5}{3}(\theta_1 - \theta_o)^{-5/3}\int_{\theta_o}^{\theta_1}(\theta - \theta_o)^{2/3}D(\theta)\,d\theta \tag{A.11}$$

Changing variables, the dimensionless sorption diffusivity is given by Eagleson (1978)

$$\frac{3BnD_i}{5K_s\psi_s} = \phi_i(d, s_o) = (1 - s_o)^{-5/3}\int_{s_o}^{1}s^d(s - s_o)^{2/3}\,ds \tag{A.12}$$

For integer d values (Eagleson (1978))

$$\phi_i(d, s_o) = (1 - s_o)^d\left[\frac{1}{d + 5/3} + \sum_{m=1}^{d}\frac{1}{d + 5/3 - m}\binom{d}{m}\left(\frac{s_o}{1 - s_o}\right)^m\right] \tag{A.13}$$

Where,

$$d = \eta - \left(\frac{1}{B}\right) - 1$$

$$\eta = (2 + 3B)/B$$

B is the pore size index. If d is not integer, we can obtain the dimensionless diffusivity by interpolation. In evaluating sorptivity, θ_l should be replaced by θ_u (the rewetted moisture content) i.e. porosity θ_s minus entrapped air fraction.

A2 Exfiltration Capacity

During inter-storm periods we have similar relationship as Equation (A.1).

$$\int_0^{\infty}(\theta_o-\theta)dz=\int_{\theta_1}^{\theta_o}z\,d\theta=F_e(t)+[K(\theta_o)+f_v\,e_{dc}]t \qquad \text{(A.14)}$$

Where $F_e(t)$ is the cumulative exfiltration, f_v is the fraction of the surface which is vegetated, and e_{dc} is the rate of transpiration by vegetation. Here we assume that the rate of moisture extraction by roots is in equilibrium with the transpiration rate by the leaves. For exfiltration we use Equation (A.2) into Equation (A.14) and differentiate to obtain the exifltration velocity as

$$f_e(t)=\tfrac{1}{2}A_1t^{-1/2}+A_2-K(\theta_o)-f_ve_{dc}+\tfrac{3}{2}A_3t^{1/2}+.... \qquad \text{(A.15)}$$

Following Philip (1960), we can rewrite the governing differential Equation (A.5) as

$$-\frac{\partial}{\partial t}\int_{\theta_o}^{\theta}z\,d\theta=D\frac{\partial\theta}{\partial z}-\left[K(\theta)-K(\theta_o)\right]-\int_{\theta_o}^{\theta}g_r(z,\theta)\frac{\partial z}{\partial\theta}d\theta \qquad \text{(A.16)}$$

To obtain the coefficients A_n in Equation (A.15), we need a series solution of equation (A.16) under simple initial and boundary conditions. This in turn requires specification of the root extraction function $g_r(z,\theta)$, which opens the whole issue of plant physiology. For desorption (i.e. zero-gravity exfiltration) and with a steady sink of strength $(\alpha_v\,e_{dc})/z_r$ distributed uniformly over the root zone $0\leq z\leq z_r$, the desorption rate is given (Carslaw and Jaeger, 1958, p.80) by

$$f_e=\tfrac{1}{2}S_e\,t^{-1/2}-\left[2\frac{\alpha_v\,e_{dc}}{z_r}\right]\left[\frac{D_e\,t}{\pi}\right]^{1/2} \qquad \text{(A.17)}$$

Where $$S_e=2(\theta_o-\theta_1)\left[\frac{D_e}{\pi}\right]^{1/2} \qquad \text{(A.18)}$$

S_e is the exfiltration sorptivity and D_e is the effective exfiltration diffusivity over the range $(\theta_o - \theta_1)$. For reasonable values of the variables and parameters of Equation (A.17), the first term is of the order 10^{-6} cm/s, and the second term is of the order 10^{-8} cm/s. The last term is thus negligible.

By analogy with the similarities in the sorption and infiltration solutions we compare Equation (A.15) and Equation (A.16) and by analogy with the infiltration solution (allowing for the opposite sense of the surface flux) for short times we assume

$$A_2 = \tfrac{1}{2}[K(\theta_o) - K(\theta_1)]$$

The approximate exfiltration rate is

$$f_e(t) = \tfrac{1}{2} S_e t^{-1/2} - \tfrac{1}{2}[K(\theta_1) + K(\theta_o)] - f_e\, e_{dc} \tag{A.19}$$

and

$$D_e = 1.85(\theta_o - \theta_1)^{-1.85} \int_{\theta_1}^{\theta_o} (\theta_o - \theta)^{0.85} D(\theta)\, d\theta \tag{A.20}$$

The dimensionless desorption diffusivity

$$\frac{BnD_e}{K_s \psi_s} = s_o^d \phi_e(d) = 1.85(s_o)^{-1.85} \int_{s_o}^{s_o} s^d (s_o - s)^{0.85} ds \tag{A.21}$$

which becomes, for integer d, only,

$$\phi_e(d) = \left[1 + 1.85 \sum_{m=1}^{d} (-1)^m \binom{d}{m} \frac{1}{1.85 + m} \right] \tag{A.22}$$

Hence, the exfiltration capacity is given by

$$f_e^*(t, s_o) = K_s\, s_o^{1+d/2} \left[\frac{n \psi_s \phi_e(d)}{\pi\, Bt K_s} \right]^{1/2} - \alpha_v\, e_{dc} \tag{A.23}$$

A3 Solution of Evaporation Equations

Similar solution method proposed by Smith and Choudhury (1991) was used to solve the nonlinear simultaneous equation. However, in this case the latent heat flux at soil surface is obtained as the minimum of soil controlled exfiltration capacity or atmospherically controlled potential rate (see equation (2.53) in Chapter 2). The atmospherically controlled potential rate is estimated based on Priestley and Taylor (1972) equation as:

$$E_p = (1 + \alpha_e) \frac{\Delta}{\Delta + \gamma} (R_{ns} - G_s) \tag{A.24}$$

Where α_e is assumed to be 0.26. The sensible heat flux at soil surface is then given by:

$$H_s = R_{ns} - G_s - L_e E_s \tag{A.25}$$

The canopy temperature is solved from Equation (2.46) by substituting for canopy saturation vapor pressure as follows

$$e^*(T_c) = e^*(T_a) + \Delta\,(T_c - T_a) \tag{A.26}$$

Hence substituting in to Equation (2.46) and rearranging to give

$$T_c = Q_1\left(\frac{r_{ac}R_{nc}}{\rho c_p} - \frac{e^*(T_a) - \Delta T_a - e_h}{\hat{\gamma}} + T_a\right) \tag{A.27}$$

where $\hat{\gamma} = \gamma\,(1 + r_{sc}/r_{ac})$ and $Q_1 = \hat{\gamma}/(\hat{\gamma} + \Delta)$

From Equation (2.57), T_h is solved by substituting Equation (A.27) for T_c and rearranging to give

$$T_h = \alpha_1 + \beta_1 e_h \tag{A.28}$$

Where $$\alpha_1 = \frac{r_{ac}Q_2}{r_{ac} - Q_1Q_2}\left(\frac{T_a}{r_{aa}} + \frac{H_s}{\rho c_p} + \frac{Q_1R_{nc}}{\rho c_p} - \frac{Q_1(e^*(T_a) - \Delta T_a)}{r_{ac}\hat{\gamma}}\right) \tag{A.29}$$

$$\beta_1 = \frac{Q_1Q_2}{(r_{ac} - Q_1Q_2)\hat{\gamma}} \tag{A.30}$$

$$Q_2 = (r_{aa}r_{ac})/(r_{aa} + r_{ac}) \tag{A.31}$$

By substituting Equations (A.26) and (A.27) into Equation (2.58) the vapor pressure within canopy height can be evaluated as

$$e_h = \alpha_2 + \beta_2 T_h \tag{A.32}$$

Where

$$\alpha_2 = Q_3Q_4\left(\frac{e^*(T_a) - \Delta T_a}{r_{ac} + r_{sc}} + \frac{\gamma\,L_eE_s}{\rho c_p} + \frac{e_a}{r_{aa}}\right) + \frac{Q_1Q_3Q_4\Delta}{(r_{ac} + r_{sc})}\left(\frac{r_{ac}R_{sc}}{\rho c_p} - \frac{(e^*(T_a) - \Delta T_a)}{\hat{\gamma}}\right) \tag{A.33}$$

$$\beta_2 = \frac{Q_1Q_3Q_4\Delta}{r_{ac} + r_{sc}} \tag{A.34}$$

$$Q_3 = \frac{r_{aa}(r_{sc} + r_{ac})}{r_{aa} + r_{ac} + r_{sc}} \tag{A.35}$$

$$Q_4 = \frac{\hat{\gamma}\,(r_{sc} + r_{ac})}{\hat{\gamma}\,(r_{sc} + r_{ac}) - Q_1Q_3\Delta} \tag{A.36}$$

Equations (A.28) and (A.32) were solved simultaneously to give within canopy air temperature and vapor pressure. Then the values are substituted back to Equation (A.27) and Equation (49) to solve for the canopy temperature, surface temperature and soil surface resistance respectively.

References

Carslaw, H. S. and Jaeger, J. C. (1959) Conduction of heat in solids, 2nd ed., Oxford University Press, NewYork.

Crank, J. (1956) The mathematics of diffusion, Oxford University Press, NewYork.

Eagleson, P. S. (1978). Climate, soil, and vegetation, 3. A simplified model of soil moisture movement in the liquid phase, *Water Resour. Res.*, 14(5), pp. 722-730.

Milly, P. C. D. (1986). An event-based simulation model of moisture and energy fluxes at a bare soil surface, *Water Resour. Res.*, 22(12), pp. 1680-1692.

Philip, J. R. (1960) The theory of infiltration, in Advances in Hydroscience, edited by V. T. Chow, Academic, Orlando, Fla., vol. 5, pp. 215-296.

Priestley C. H. B., Taylor, R. J. (1972). On the assessment of surface heat flux and evaporation using large scale parameters. Mon. Weather Rev. 100:81-92.

Smith, R. C. G. and Choudhury, B. J. (1991). Analysis of Normalized difference and surface temperature observations over southeastern Australia. Int. J. Remote sensing, Vol. 12, No. 10, pp. 2021-2044.